Fall 2009

Freeze casting of bioactive glass and ceramic scaffolds for bone tissue engineering

Qiang Fu

Department: Materials Science and Engineering

FREEZE CASTING OF BIOACTIVE GLASS AND CERAMIC SCAFFOLDS FOR BONE TISSUE ENGINEERING

by

QIANG FU

A DISSERTATION

Presented to the Faculty of the Graduate School of the

MISSOURI UNIVERSITY OF SCIENCE AND TECHNOLOGY

In Partial Fulfillment of the Requirements for the Degree

DOCTOR OF PHILOSOPHY

in

CERAMIC ENGINEERING

2009

Approved by

Mohamed N. Rahaman, Advisor

Roger F. Brown

Delbert E. Day

B. Sonny Bal

PUBLICATION DISSERTATION OPTION

The Introduction and Background sections of this dissertation provide information about the research topic, and a review of the literature. The body of this dissertation has been compiled in the format for publication in peer-reviewed journals. Seven papers have been included in the following order. The first paper, "Freeze Casting of Porous Hydroxyapatite Scaffolds - I. Processing and General Microstructure," was published in *Journal of Biomedical Materials Research Part B Applied Biomaterials* in July 2008 in Volume 86 Issue 1 pages 25-58. The second paper, "Freeze Casting of Porous Hydroxyapatite Scaffolds - II. Sintering, Microstructure, and Mechanical Behavior," was published in *Journal of Biomedical Materials Research Part B Applied Biomaterials* in August 2008 in Volume 86 Issue 2 pages 59-88. The third paper, "Freeze-cast Hydroxyapatite Scaffolds for Bone Tissue Engineering Applications," was published in *Biomedical Materials* in June 2008 in Volume 3 Issue 2 pages 89-109. This paper was selected by the editors as one of the highlights of the papers published in *Biomedical Materials* in 2008. The fourth paper, "Proliferation and Function of MC3T3-E1 Cells on Freeze-cast Hydroxyapatite Scaffolds with Oriented Pore Architectures," was published in *Journal of Materials Science: Materials in Medicine* in May 2009 Volume 20 Issue 5 pages 110-128. The fifth paper, "*In vitro* Cellular Response to Hydroxyapatite Scaffolds with Oriented Pore Architectures," was accepted by *Materials Science and Engineering C* in April 2009 pages 129-154. The sixth paper, "Preparation and *In vitro* Evaluation of Bioactive Glass (13-93) Scaffolds with Oriented Microstructures for Repair and Regeneration of Load-Bearing Bones," was accepted by *Journal of Biomedical Materials Research Part A* in July 2009 page 155-187. The seventh paper, "*In vivo* evaluation of

13-93 bioactive glass scaffolds with trabecular and oriented microstructures in a subcutaneous rat implantation model," was prepared for submission to *Acta Biomaterialia* page 188-213.

Three papers related to the present research, but not included in the main body of this dissertation, are given in the appendix. The first manuscript, "Possible Toughening Mechanisms in Unidirectional Hydroxyapatite Scaffolds Prepared by Freeze Casting," was prepared to provide supplemental information to the body text. The second paper, "Preparation and Bioactive Characteristics of a Porous 13-93 Glass, and Fabrication into the Articulating Surface of a Proximal Tibia," was published in *Journal of Biomedical Materials Research Part A* in July 2007 Volume 82 Issue 1 pages 231-256. The third paper, "Mechanical and *In vitro* Performance of 13-93 Bioactive Glass Scaffolds Prepared by a Polymer Foam Replication Technique," was published in *Acta Biomaterialia* in November 2008 Volume 4 Issue 6 pages 257-293.

ABSTRACT

The main objectives of this dissertation were to explore the production of bioactive ceramic and glass scaffolds with oriented pore architectures by unidirectional freezing of suspensions, and to characterize the mechanical and biological performance of the scaffolds. Freezing of aqueous suspensions of hydroxyapatite (HA) or bioactive 13-93 glass particles resulted in the formation of scaffolds with a lamellar-type microstructure (pore width = 5–30 μm). The addition of polar organic solvents (such as 60 wt% dioxane) to the aqueous suspensions markedly changed the morphology and size of the oriented pores, giving scaffolds with a columnar-type microstructure and larger pore width (90–110 μm). The scaffolds showed a unique 'elastic–plastic' mechanical response in compression along the orientation direction, with large strain for failure (>20%) and strain rate sensitivity. For a similar porosity, the bioactive glass scaffolds had a higher strength than the HA scaffolds, presumably because of better sintering characteristics. Columnar bioactive glass scaffolds (porosity = 55–60%) had a compressive strength of 25 ± 3 MPa. The columnar scaffolds with the larger pore width showed better ability than the lamellar scaffolds to support the proliferation and function of murine osteoblastic cells (MLO-A5 or MC3T3-E1). Subcutaneous implantation in the dorsum of rats showed abundant tissue ingrowth into the pores of the columnar scaffolds and integration of the scaffolds with surrounding tissue. The results indicate that bioactive 13-93 glass scaffolds with the columnar microstructure could be used for the repair of segmental defects in load-bearing bones.

ACKNOWLEDGMENTS

I am grateful to my advisor, Dr. Mohamed N. Rahaman, for his advice, encouragement and guidance through the course of my study. His time, effort and commitment have been invaluable to me. I would also like to thank my co-advisor, Dr. Fatih Dogan, for introducing me to the "freeze-processing" field, and for his guidance and helpful discussion during this study.

I sincerely appreciate Dr. Roger F. Brown for his assistance with *in vitro* and *in vivo* experiments, and for helpful discussions. I would like to thank the rest of my committee, Drs. B. Sonny Bal and Delbert E. Day for their constructive suggestions for my study and for reviewing this dissertation. Sincere thanks also go to Dr. Wenhai Huang at Tongji University for introducing me to the idea of studying in the USA, and giving me good encouragement.

All of my friends and colleagues deserve many thanks as well. Working and learning with you have brought a lot of fun to my life. Thank you Yadong Li in Suzhou University, Dr. Shi-Chang Zhang, Dr. Tieshu Huang, Dr. Sumin Zhu, Sheng Chao, Xuhui Lv, Hailuo Fu, Xin Liu, Steven Jung, and Vernon Modglin.

Thank you to all my friends who have helped me enjoy staying four years in a small town as Rolla.

Last but not the least thanks to those who made this possible: my parents, Changlai Fu and Zhengling Cai, and my wife, Liying Zhang. It is their love, belief and bearing that kept me moving forward with my research.

TABLE OF CONTENTS

LIST OF ILLUSTRATIONS

Page

BACKGROUND

PAPER 1

PAPER 6

LIST OF TABLES

Page

PAPER 7

APPENDIX B

1. PURPOSE OF THIS DISSERTATION

The main purpose of this Ph.D. research was to develop porous three-dimensional bioactive glass and ceramic scaffolds using a freeze casting method for potential applications in bone repair and regeneration.

Both HA and 13-93 glass belong to the family of materials know as bioactive ceramics, which are desirable scaffold materials for use in bone tissue engineering because of their ability to enhance bone formation and bond to surrounding tissue. HA is the main inorganic component in human bone. It is biocompatible, osteoconductive and produce no systemic toxicity or immunological reactions. The glass designated 13-93 (composition in wt%: 53 SiO_2, 6 Na_2O, 12 K_2O; 5 MgO, 20 CaO and 4 P_2O_5) is a silicate-based bioactive glass with a modified 45S5 composition. In addition to its bioactivity and biocompatibility, the glass has more facile viscous flow behavior and less tendency to crystallize than 45S5. HA and 13-93 glass have been formed into three-dimensional scaffolds for potential use in bone tissue engineering applications.

This first phase of these studies was meant to fabricate porous HA and 13-93 glass scaffolds with a unidirectional structure by a freeze casting technique. The relationship between the process parameters, microstructure and mechanical properties of hydroxyapatite (HA) and bioactive 13-93 glass scaffolds was investigated. Once the scaffolds were successfully fabricated, the goal was to evaluate their *in vitro* cellular response using murine MC3T3-E1 or MLO-A5 cells, an osteoblastic cell line, and their *in vivo* performance using a subcutaneous rat implantation model.

2. BACKGROUND

2.1. SCAFFOLDS FOR BONE TISSUE ENGINEERING

Each year, millions of patients in the United States suffer tissue loss or end-stage organ failure, with a total national healthcare cost of over $400 billion [1]. Traditional treatments of organ or tissue loss include transplanting organs from one individual to another, performing surgical reconstruction, and using mechanical devices [2-4]. Despite the fact that they have saved and improved the lives of patients, these traditional therapies suffer from limitations, such as shortage of donors, long-term problems with the surgical reconstruction, and limited functions of the mechanical devices [1, 5].

Tissue engineering, an interdisciplinary field based on the principles of engineering and the life sciences toward the creation of new biological substitutes to restore, maintain, or improve tissue function, has emerged as a promising approach for the regeneration of lost or damaged tissues [1, 6]. The creation of tissues and organs for medical use is already a fact, although to a limited extent, in hospitals across the US [7]. These groundbreaking applications involve engineered skin [8], cartilage [9,10], bone [11, 12], ligament [13, 14], nervous system [15, 16] and periodontal tissues [17, 18]. The market for tissue-engineered products reached nearly $4 billion in 1999, and it was projected to expand at ~20% per year [19].

A major area of emphasis for future tissue engineering research is the development of new, more advanced biomaterials to replace the loss of hard and soft tissues due to age-related attrition or degeneration, disease, or trauma. The traditional techniques for treating bone defects include autografting and allografting cancellous

bone, applying vascularized grafts of the fibula and iliac crest, and using other bone transplantation. However, the use of autografts is constrained by limited donor sites, and associated infection, pain, and hematoma in the donor sites [20-22]. The use of allografts results in possible disease transmission and infections, and possible reduction or complete loss of the bone inductive factors [23]. Bone tissue engineering, which involves use of a scaffolding material to either induce formation of bone from the surrounding tissue, or to act as a carrier or template for implanted bone cells or other agents, may potentially provide alternative solutions for bone repair and regeneration.

The key components of this approach (Figure 1) are a suitable supply of cells, environmental factors such as growth and differentiation supplements, and three dimensional biomaterial scaffolds that can guide the growth of new tissue *in vitro* and *in vivo* [24-28]. The scaffold serves as an initial biomechanical substrate on which seeded cells can organize and develop into the desired organ or tissue prior to implantation. The scaffold is either degraded or metabolized during the formation, deposition, and organization of the newly generated matrix, which eventually leaves a vital organ or tissue. Scaffold materials for tissue engineering applications must be biocompatible and are designed to meet both nutritional and biological needs for the specific cell population involved in tissue formation [29].

In addition to being biocompatible, an ideal scaffold for bone tissue engineering should fulfill a number of criteria [12, 19, 24, 29, 31, 32]: (1) three-dimensional and highly porous structure with an interconnected pore network for cell growth, and flow transport of nutrients and metabolic waste; (2) bioactive, or biodegradable at a rate to match cell/tissue growth *in vitro* and/or *in vivo*; (3) suitable surface chemistry for cell

attachment, proliferation and function; (4) mechanical competence to provide mechanical stability in load bearing sites; (5) near-net-shape fabrication and scalability for cost-effective industrial manufacturing.

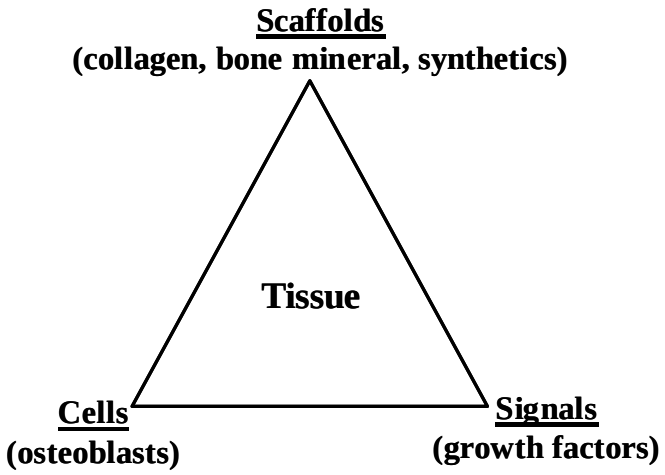

Figure 2.1. Key components in tissue engineering

As the scaffolds for bone tissue engineering are in contact with bone, it is important to understand the structure and properties of bones in the body. Bone is a living material composed of cells and a blood supply encased in a strong, interwoven composite structure. Three major components are: collagen, which is flexible and tough; hydroxyapatite bone mineral, which is the reinforcing phase of the composite; and the bone matrix or ground substance, which is a three dimensional system that has maximum strength and toughness along the lines of applied stress [33].

As shown in Figure 2, bone is generally classified into two types: cortical bone, also referred to as compact bone, and trabecular bone, also referred to as cancellous or spongy bone. Cortical bone, found primarily in the shaft of long bones and as the outer shell around cancellous bone, is much denser, with a porosity of 5–10% [27]. Trabecular

bone, found at the end of long bones, in vertebrae, and in flat bones such as the pelvis, is much more porous, with porosity in the range 50–90% [28].

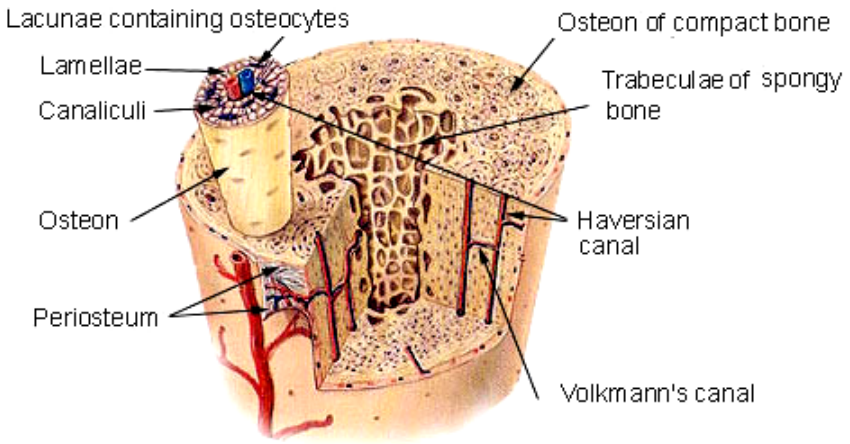

Figure 2.2. Illustration of cortical and trabecular bone

The mechanical properties of bone vary between subjects, from one bone to another, and within different regions of the same bone. The mechanical properties are also highly anisotropic, as a result of the oriented microstructure. The Young's modulus and the tensile and compressive strength in the longitudinal direction are approximately 2 and 1.5 times higher than those in the radial or tangential direction, respectively. Also, the mechanical behavior of bone shows a high strain rate sensitivity. The Young's modulus, ultimate compressive strength, and yield strength increase with increasing rate of loading. However, based on the testing of large specimens, the compressive strength and elastic modulus of cortical bone has been reported in the range 100–150 MPa and 10–20 GPa in the direction parallel to the orientation (long axis) axis [34-36]. The strength and modulus in the direction perpendicular to the long axis are typically 1.5 to 2

times lower. A wide range has been reported for the Young's modulus (0.1–5 GPa) and compressive strength (2–12 MPa) of cancellous bone [35, 36].

So far, several scaffold materials have been investigated for bone tissue engineering applications. Natural or synthetic polymers such as poly(lactic acid), PLA, poly(glycolic acid), PGA, copolymers of PLA and PGA, known as poly(lactic co-glycolic acid), PLGA, and collagen are biodegradable, so the scaffold can be gradually replaced by new bone matrix synthesized by tissue-forming cells [37-40]. The chemical properties of the saturated poly-α-hydroxy esters, such as PLA, PGA and PLGA, allow hydrolytic degradation through de-esterification. The body has highly regulated mechanisms to completely remove the degraded monomer components of each polymer through a natural pathway. PLA and PGA have been approved by the US Food and Drug Administration (FDA) to use in products and devices such as degradable sutures [41]. However, the bulk erosion process of these polymers may result in the failure of the scaffolds prematurely. Rapid release of the acidic degradation products may also cause a strong inflammatory response [42, 43].

The application of biodegradable polymers in the repair of load-bearing bones is limited because of their low mechanical strength [37]. Although the strength of dense polymers matches cancellous bone properties and approach cortical bone properties, the strength of the porous scaffolds are at least one order of magnitude lower than that of cancellous bone, and orders of magnitude lower than that of the cortical bone [31]. To improve the load-bearing properties of biodegradable polymer scaffolds, attempts have been made to reinforce the polymers with particles or short fibers. The use of reinforcing materials such as hydroxyapatite, $Ca_{10}(PO_4)_6(OH)_2$, HA, and bioactive glass provides

scaffolds that are biodegradable as well as bioactive [44-46]. However, the increase in the strength is small, due mainly to the lack of interfacial bonding strength between the ceramic phase and the polymer matrix [31].

Certain compositions of glasses, glass-ceramics, and ceramics, referred to as 'bioactive ceramics', have been widely investigated for healing bone defects, due to their ability to enhance bone formation and to bond to surrounding tissue [47]. Certain glass compositions with excellent biocompatibility as well as the ability to bond to bone were first discovered by Hench et al. in 1971 [48]. The basic components of most bioactive glasses are SiO_2, Na_2O, CaO and P_2O_5. The bioactive glass designated 45S5 (composition in wt%: 45 SiO_2, 24.5 Na_2O, 24.5 CaO, 6 P_2O_5) and other silicate bioactive glasses based on the 45S5 composition [49], such as the glass designated 13-93 (composition in wt%: 53 SiO_2, 6 Na_2O, 12 K_2O, 5 MgO, 20 CaO, 4 P_2O_5) [50], have been widely studied for biomedical applications [51].

A common characteristic of bioactive glasses and ceramics is a time-dependent modification of the surface that occurs upon implantation. The formation of a biologically active hydroxyl-carbonate apatite (HCA) layer on the surface provides the bonding interface with the tissues. The equivalence in chemical properties and structure of the HCA phase with that of the mineral phase in bone is believed to be responsible for the interfacial bonding [49]. Although some details still remain unclear, it is widely accepted that a layer of biologically active HCA must form for the bonding with bone to occur, and that HCA is the only common feature of all the known bioactive implant materials [47].

As the main mineral constituent of bone, HA has been widely investigated as a scaffold material for bone tissue engineering. Scaffolds of HA, both synthetic and natural, are biocompatible as well as osteoconductive. They produce no systemic toxicity or immunological reactions, and show biological affinity to bony tissues [49]. A disadvantage of HA is its brittleness, which limits the scaffolds to applications subjected to mainly compressive loading. One approach to this mechanical limitation is the use of HA as the bioactive phase in composites, mainly polymer matrix composites [49, 52]. By stiffening a compliant biocompatible synthetic polymer such as polyethylene (PE) with HA particles (40 vol %), composites with mechanical properties comparable to those of cortical bone, coupled with bone-bonding ability due to the HA phase, have been developed [52]. Besides bioactive glass, HA and related calcium phosphates, such as α- and β-tricalcium phosphate (α-TCP and β-TCP), also show excellent ability to bond to bone. However, the low mechanical strength and relative long degradation time, typically on the order of months or even years, of the crystalline calcium phosphates limit their application in engineering new bone tissue [31].

Several methods have been used to produce porous scaffolds for bone repair and regeneration, including solvent-casting and particulate-leaching [53, 54], polymer foam replication [55, 56], solid free-form fabrication [12, 57, 58], and the use of foaming agents [59-61]. These methods commonly provide an isotropic microstructure, as shown in Figure 3. The strength of these scaffolds varies with the composition of the scaffold and the fabrication method. Typically, the compressive strength of bioactive ceramic scaffolds prepared by these methods is comparable to that of trabecular bone (2–12 MPa).

A brief review of these fabrication techniques is presented in the following paragraphs to give a general idea of the methodology.

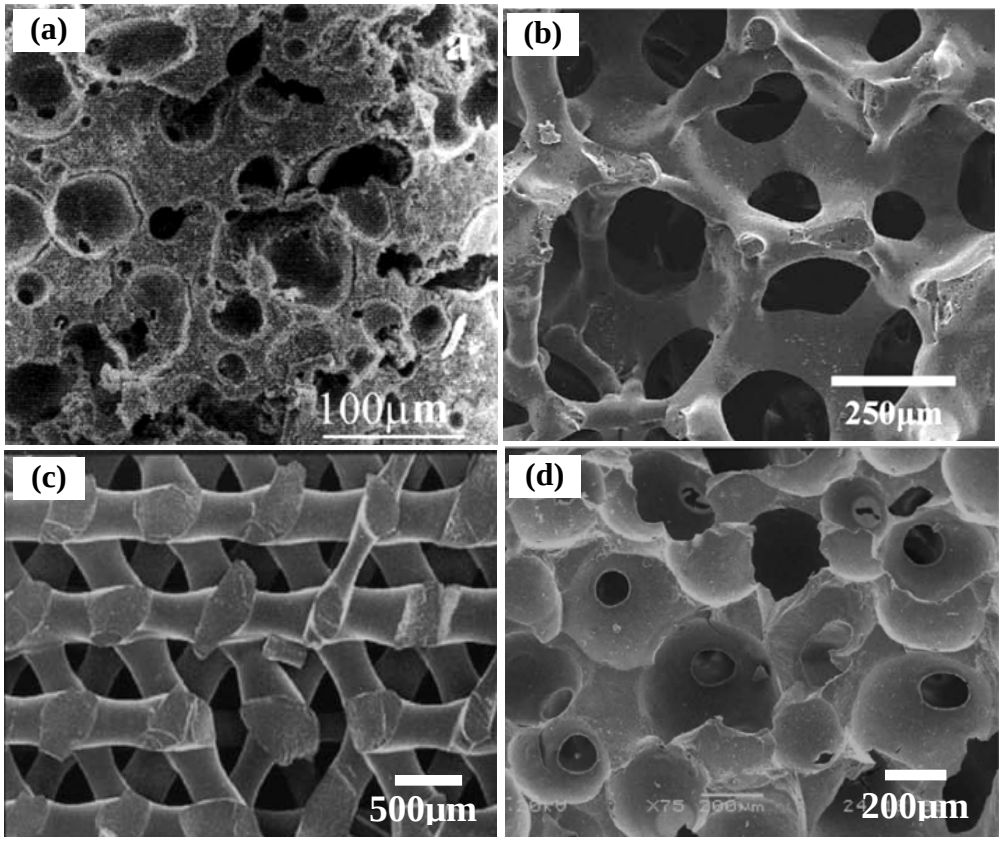

Figure 2.3. Typical structures of porous scaffolds: (a) hydroxyapatite scaffold fabricated by solvent-casting and particulate-leaching [54], (b) bioactive 13-93 glass scaffold fabricated by polymer foam replication[56], (c) solid freeform fabrication[12] and (d) bioactive 70S30C glass fabricated by a foaming method[61]. The scaffolds show an isotropic structure.

The solvent-casting and particulate-leaching method was first developed by Mikos et al. in 1993 to show that biodegradable polymers could be processed into various

cell foams by using sodium chloride particles as a porogen [53]. The method involves the combination of a suitable porogen with a solution of polymer in an appropriate mold to manufacture solid polymer-porogen constructs. The porogen is then leached out to form porous polymer sponges for the bone tissue engineering applications. Porogens such as sodium chloride [53] and starch [54] are not soluble in the organic solvents typically used to dissolve biodegradable polymers. The main advantage of the technique is the ease of the scaffold fabrication without the need for complex machinery. The primary disadvantages of the solvent casting method are: (1) poor pore interconnectivity at low porogen loading; (2) limited number of polymers and solvents that are compatible with the process; (3) the possible retention of toxic solvent within the scaffold; (4) the degradation of polymer due to the long duration of the leaching process in water. There has been limited work done on producing ceramic or polymer/ceramic composite scaffolds using the solvent leaching process.

The polymer foam replication method was first used to produce macroporous ceramics by Schwartzwalder and Somer [62]. They used polymeric sponges as templates to prepare cellular ceramic structures of different pore sizes, porosity and chemical compositions. In this method, a synthetic (e.g. polyurethane, PU) or natural (e.g. coral; wood) foam is initially soaked in a ceramic suspension to obtain a uniform coating on the foam struts. After drying of the coating, the polymer template and organic binders are burned out through careful heat treatment between 300-600 ºC. The densification of the ceramic struts is done by sintering at temperatures between 1000 to 15000 ºC, depending on the ceramic material. The main advantage of this method is the production of highly porous ceramics with open and interconnected porosity in the range 40-95%. One

disadvantage of the method is the presence of a triangular void in the center of the struts resulting from the removal of the polymer skeleton on heating, which significantly reduces the mechanical strength of the porous ceramics. However, the use of the glass with a proper thermal behavior has been show to effectively fill the void by the viscous flow sintering of glass particles [56].

Solid freeform fabrication (SFF), also referred to as rapid prototyping, is a term to describe a group of techniques that can be used to manufacture objects in a layer-by-layer fashion from a computer-aided design (CAD) file, without the use of traditional tools such as dies or molds. The SFF techniques differs significantly in the way they build parts, but they all employ three steps in their process: data input, data file preparation, and object building. Several SFF techniques have been used for scaffold fabrication, including: three-dimensional printing (3DP), fused deposition modeling (FDM), ink-jet printing and indirect casting (IC), stereolithography (SL), and selective laser sintering (SLS) [63]. Scaffolds with controlled internal architecture and interconnectivity are made with SFF from a variety of biomaterials. Polycaprolactone and HA scaffolds with fully interconnected porous networks have been fabricated by the SFF technique [57, 58]. A limitation of the method lies in the needs to improve the resolution at the micro scale.

In general, the methods mentioned above produce porous scaffolds with an isotropic microstructure. Considering the complexity of the structure of bones, the mechanical behavior varies from site to site. The mechanical properties of bone are highly anisotropic due to its oriented microstructure. It would be beneficial to develop scaffolds with oriented microstructure to fulfill the needs of different defect sites. Unidirectional freezing of suspensions has been used to produce porous polymer

constructs with oriented microstructure [64-66], and the method has been applied recently to the production of porous bioceramics [67-70].

2.2. FREEZE CASTING OF POROUS GLASS AND CERAMIC SCAFFOLDS

For the production of porous ceramic scaffolds, the freeze casting route involves rapid freezing of a colloidally-stable suspension of ceramic particles in a nonporous mold, and sublimation of the frozen solvent under cold temperatures in a vacuum, as shown in Figure 4 [71].

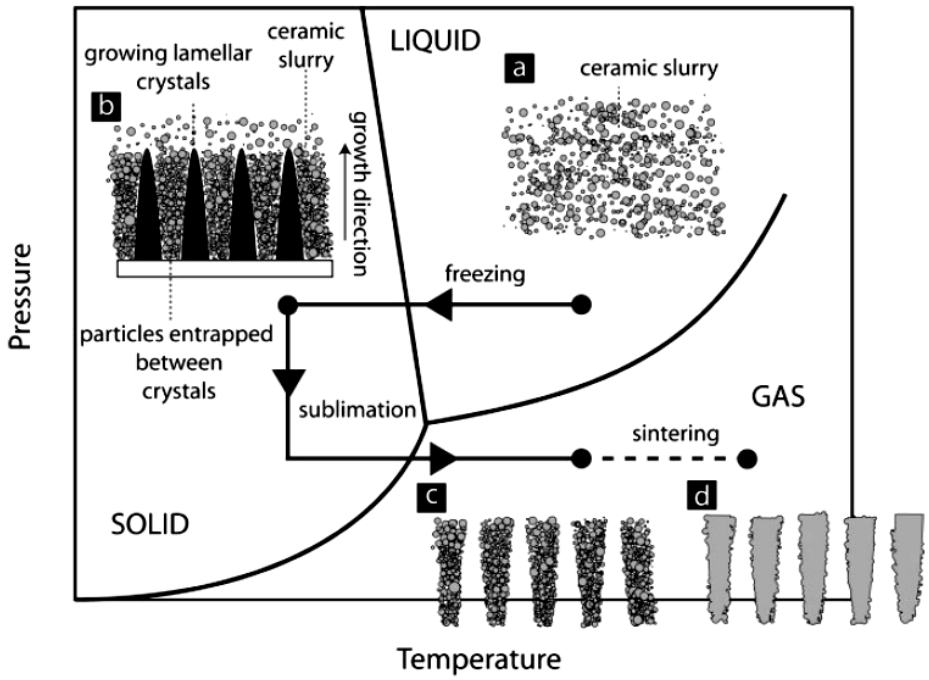

Figure 2.4. Processing steps in freeze casting: slurry preparation, solidification, sublimation and sintering[71].

After drying, the porous green samples are sintered to improve their mechanical strength. The porosity in the constructs is a replica of the frozen solvent. During the

freezing process, crystals of the solidified solvent are formed, and they grow into the ceramic suspension, while the ceramic particles are rejected by the moving solidification front, concentrated and entrapped between the solvent crystals. The microstructure and, hence, the properties of the final sintered body are determined essentially by the suspension parameters (such as particle size, particle concentration, and colloid stability of the suspension), the freezing conditions (rate and direction of freezing), and the sintering conditions (temperature and time).

2.2.1. Formation of the Structure. To obtain porous ceramic structures using the unidirectional freezing technique, two requirements must be met [71]:

(1) The ceramic particles in the suspension must be assembled within the ice template by rejection from the growing ice crystals. Figure 5 shows a schematic diagram of the interaction of the particle with the advancing solid–liquid interface of the growing ice crystal front. The interaction determines the engulfment or rejection of the particles by the solidification front. Thermodynamically, a particle is rejected when the interfacial energy between the particle and the solid phase, σ_{sp}, is larger than the sum of the energies for the solid–liquid, σ_{sl}, and liquid–particle, σ_{lp}, interfaces:

$$\Delta\sigma_0 = \sigma_{sp} - (\sigma_{sl} + \sigma_{lp}) > 0 \qquad (1)$$

Based on the thermodynamic condition in Eq. (1), the balance of the repulsive force and attractive drag force of a spherical particle moving close to a solidification front gives the critical solidification front velocity for particle engulfment [72, 73]:

$$v_c = \frac{\Delta\sigma_0 d}{3\eta r}\left(\frac{a_0}{d}\right)^n \qquad (2)$$

where r is the particle radius, a_0 is the average intermolecular distance, d is the distance between the particle and the solidification front, η is the solution viscosity, and n is an exponent that varies from 1 to 4 depending on the specific model. The critical velocity can be estimated by making assumptions that the disjoining force is negligible, (in which case $n = 1$), and using the reported values[27] for $\Delta\sigma_0 \approx 10^{-2}$ J m^{-2} and $a_0 \approx 10^{-8}$ m. Then the critical velocity can be obtained once the particle size and the viscosity of the solution are determined. For the freezing of HA suspensions, the critical velocity is determined to be $v_c = 0.01–0.1$ m s^{-1} for a particle size of ~1 μm, and the viscosity of the suspensions, of $10^{-2}–10^{-3}$ Pa s.

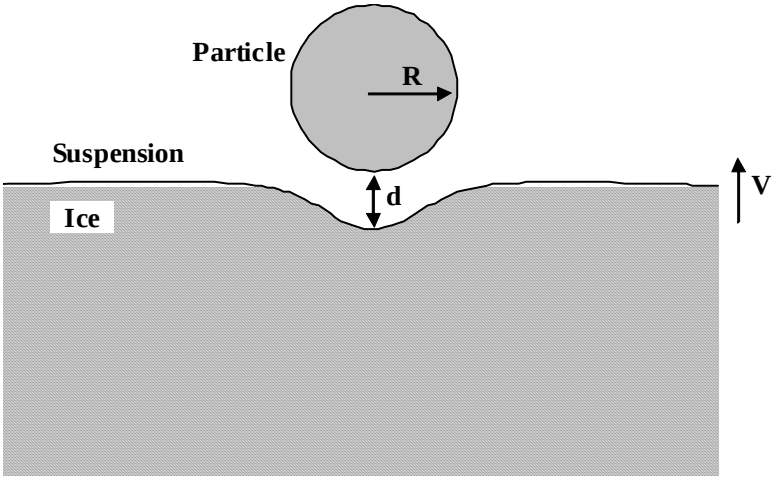

Figure 2.5. Schematic graph of the particle motion at the solidification front

(2) The ice crystals must grow into a non-planar morphology. If the ice front is planar and the ceramic particles are rejected, all the particles are pushed to one side of the sample after the solidification resulting into a dense packed cast body. The ceramic particles must be rejected from the ice front and redistributed between the gaps of the

solidification front to form porous structures. The eventual architecture of the ceramic constructs is determined essentially by the morphology of the solidification front.

2.2.2. Microstructure Development. The morphology of the growing crystals of the frozen solvent determines the pore morphology (a replica of the solidified crystals) of the sintered materials. Figure 6 shows that the pore morphology varies from lamellar, to rectangular, to columnar types. Depending on the processing parameters, including the solvent composition, slurry formulation, and solidification conditions, the pore morphology changes drastically. The freezing of suspensions containing water, water-dioxane mixture, and camphene solvents have resulted in the formation of lamellar, columnar, and dendritic pores, respectively. The unidirectional freezing results in the preferential orientation of the porosity, leading to anisotropic microstructure and properties.

Freezing of aqueous suspensions is a traditional approach which utilizes ice as a template to fabricate porous inorganic and polymeric structures. Lamellar-type pores with the pore width of 10-40 μm were formed in the sintered HA constructs [67-69]. This type of pore is a result of the crystallographic and crystal growth characteristics of ice. By unidirectional freezing of the aqueous suspension, the ice front velocity parallel to the crystallographic c axis is 100 to 1000 times lower than perpendicular to this axis (a or b axis), which results in ice platelets of a large anisotropy [71]. The fast growth of the ice crystals along the a or b axis, and slow along the c axis result in the formation of long vertical lamellar crystals, which is evidenced by the oriented architecture in the sintered ceramic constructs [67-69]. The structures developed by freezing aqueous suspensions

have been confined to the production of lamellar–type microstructures due to the hexagonal crystal structure of ice.

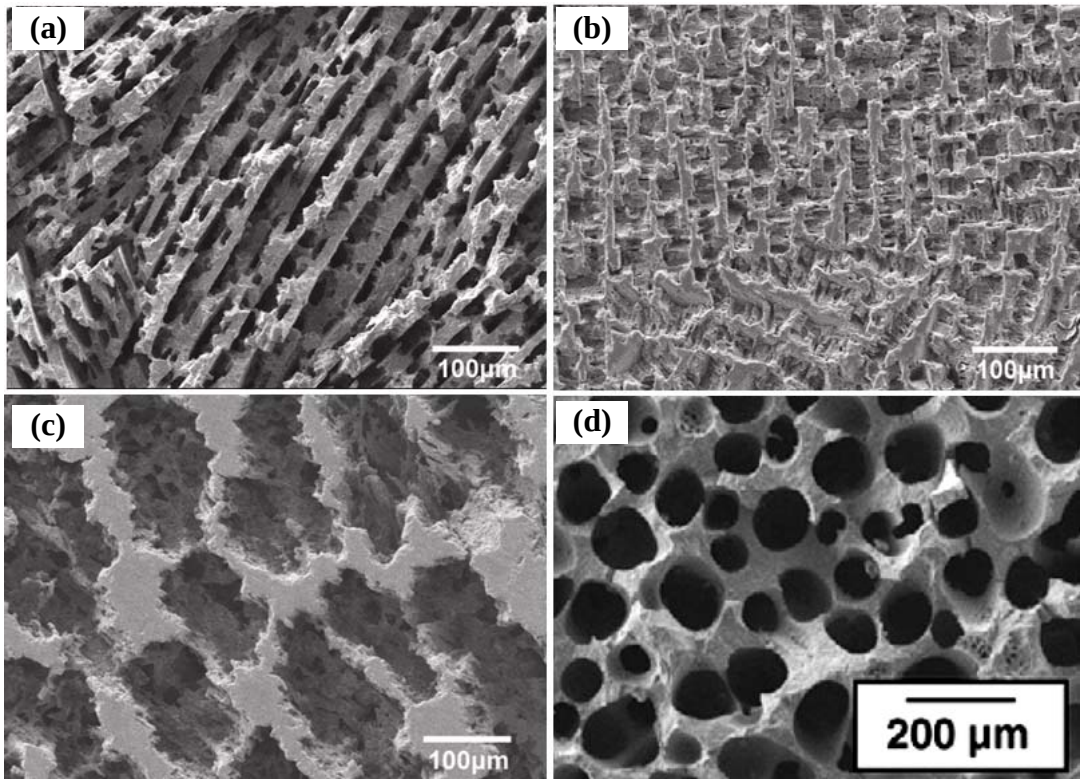

Figure 2.6. Typical porous scaffolds obtained by unidirectional freezing of suspensions: (a) hydroxyapatite using water as a solvent[69], (b) hydroxyapatite using water/glycerol (20 wt% glycerol) as a solvent[69], (c) hydroxyapatite using waster/dioxane (60 wt% dioxane) as a solvent[69], (d) calcium phosphate using camphene as a solvent[77].

Manipulation of the lamellar pore morphology resulting from the freezing of aqueous suspension was investigated by adding different polar organic solvent to the suspension prior to solidification. Certain liquids, such as glycerol and dioxane are miscible with water, and when added to water modify the local structure of the aqueous

liquid. As a result, they modify the nucleation and growth of the ice crystals, thereby modifying the freezing behavior of the aqueous liquid. Glycerol effectively binds to water molecules and disrupts the complete crystallization of ice. This leads to a localized structure, resulting in a reduced size of the growing ice crystals and inhibiting solute rejection [74]. The addition of glycerol (10–30 wt%) to the aqueous solvent reduced the viscosity of Al_2O_3 suspensions stabilized with an anionic dispersant, ammonium polymethacrylate, and produced more homogeneous microstructures after freeze casting and sintering [74]. The effects were explained in terms of the ability of glycerol to both enhance the colloidal stability of the suspensions and modify the freezing behavior of water.

Dioxane is miscible with water at any composition under ambient conditions. A study of the local solvent structure of dioxane–water mixtures [75] indicated that the structure changed at three specific compositions when the mole fraction (χ) of dioxane in the mixture was 0.13, 0.3, and 0.7. For $\chi < 0.13$, the mixture consisted mainly of water molecules with some water–dioxane complexes. For $0.13 < \chi < 0.3$, the system consisted mainly of small clusters of water–dioxane molecules, whereas for $\chi > 0.3$, the water-dioxane clusters gradually disappeared and the mixture evolved gradually to the inherent solvent structure of pure dioxane. Lamellar-, columnar-, and rectangular-type microstructures with a wider range of pore widths (10–100 μm) were obtained, depending on the composition and the concentration of the organic liquid in the mixture.

Unidirectional freezing of suspensions containing organic solvents only, such as camphene, also results in the formation of aligned pore architectures [76]. Camphene dendrites were observed to grow preferentially along the <100> direction from the

bottom to the top of the cast body. Large aligned pores were obtained by the continuous overgrowth in the direction normal to the <100> direction [77]. Columnar pores of size 122 to 166 μm were obtained by the incubation of the cast body at 32ºC for various times.

The nature of the solvent defines its crystallographic properties in the solid state which determines the main pore morphology of the cast body. The choice of solvent with different crystal structures may result in the different morphologies of the final ceramic constructs.

2.2.3. Mechanical Properties. The compressive strength of the freeze-cast ceramics is one of the most important properties, which has been widely investigated. Marked improvements in the compressive strength of HA scaffolds were reported for scaffolds formed by unidirectional freezing of aqueous suspensions. Compressive strengths as high as 65 MPa (56% porosity) and 147 MPa (47% porosity) in the direction parallel to the freezing direction were obtained (Figure 7). These strengths are well above those for scaffolds obtained by more conventional methods such as foaming and polymer foam replication. The strength of the porous HA is close to that of compact bone. The high strength is attributed to the high anisotropy of the structure in the direction of loading and the presence of inorganic bridges between the ceramic layers, which prevents Euler buckling of the ceramic layers. The high strength makes it possible to use these porous HA constructs for load-bearing applications. However, the strengths of freeze-cast ceramics are shown to be highly dependent on the morphology of the pores. Ceramics with columnar-type pores prepared by freezing of suspensions containing camphene and water-dioxane solvents have shown strength close to usual cellular ceramics [70, 76, 77].

HA constructs prepared from water-dioxane mixtures (60 wt% dioxane) with columnar pores have a compressive strength of 7.5 MPa (porosity 65%, pore size 90-110 μm) [70]. Calcium phosphate scaffolds with the similar pore morphology and porosity (65%) but larger pore size (122-166 μm) have a strength of 5-11 MPa [77].

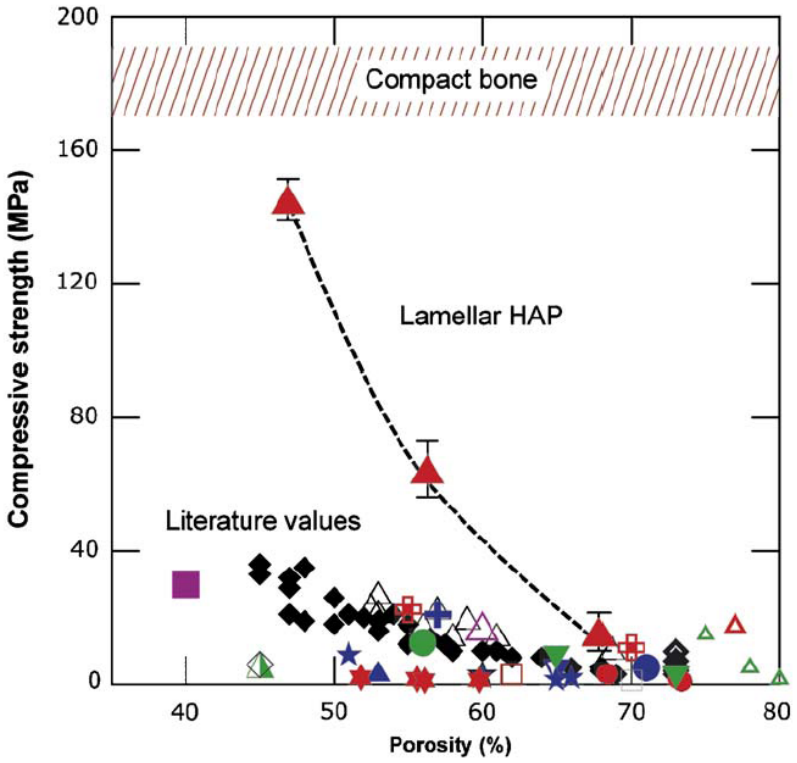

Figure 2.7. Compressive strength vs. porosity of freeze-cast hydroxyapatite constructs. Comparison with compact bone and literature values of porous HA for tissue engineering[67].

2.2.4. Physical Limits. In the case of the freeze casting of aqueous suspensions, the limits of the technique are essentially dependent on the physics of ice. The ceramic particle concentration in the suspension determines the final porosity of the ceramic constructs. At lower particle concentration, the green body is too weak to handle after sublimation of the solvent. Above a certain particle concentration, the solid/liquid

interface moves into the interparticle space before the particle redistribution occurs, and results in the entrapment of the particles within the ice.

The pore size of the final ceramic constructs is defined by the size of the crystals, which is determined by several experimental parameters including the freezing rate, the concentration of the suspension and the interaction between the solidification front and the ceramic particles. By adjusting these parameters the pore size can be controlled to some extent, but so far the freezing of the aqueous suspension results in the pore width of only 10 - 40 μm [67, 69]. For the application of the porous ceramics in bone tissue engineering, interconnected or unidirectional pores with a mean diameter (or width) of 100 μm or greater, and open porosity of >50% are generally considered to be the minimum requirements to permit tissue ingrowth and function in porous scaffolds [25, 26]

2.3. REFERENCES

1. Langer R, Vacanti JP. Tissue engineering. Science 1993;260:920-926
2. Kolff WJ, Berk HTS. The artificial kidney: a dialyzer with a great area. Acta Med Scand 1944;177:121-134
3. Murray JE, Merrill JP, Harrison JH. Renal homotransplantations in identical twins. Surg Forum 1955;6:432-436
4. Thomas ED, Storb R, Clift RA, Fefer A, Johnson FL, Neiman PE, Lerner KG, Glucksberg H, Buckner CD. Bone-marrow transplantation. N Eng J Med 1975;292:832-843, 895-902
5. Kusama K, Donegan WI, Samter TG. An investigation of colon cancer associated with urinary diversion. Dis Colon Rectum 1989;32:694-697
6. Nerem RM. Cellular engineering. Ann Biomed Eng 1991; 19:529–545.
7. Mooney DJ, Mikos AG. Growing new organs. Sci Am 1999;280:60-65.
8. MacNeil S. Progress and opportunities for tissue-engineered skin. Nature 2007;445:874-880
9. Ma PX, Schloo B, Mooney D, Langer R. Development of biomechanical properties and morphogenesis of *in vitro* tissue engineered cartilage. J Biomed Mater Res 1995;29:1587-1595
10. Stading M, Langer R. Mechanical shear properties of cell-polymer cartilage constructs. Tissue Eng 1999;5:241-250
11. Crane GM, Ishaug SL, Mikos AG. Bone tissue engineering. Nature Med 1995:1:1322-1324
12. Hutmacher D W. Scaffolds in tissue engineering bone and cartilage. Biomaterials 2000;21:2529-2543
13. Louie IVY, Hsu HP, Spector M. Healing of tendon defects implanted with a porous collagen-GAG matrix: histological evaluation. Tissue Eng 1997;3:187-195
14. Altman GH, Horan RL, Lu HH, Moreau J, Martin I, Richmond JC, Kaplan DL. Silk matrix for tissue engineered anterior cruciate ligaments. Biomaterials 2002;23:4131-4141
15. Bellamkonda R, Aebischer P. Review: tissue engineering in the nervous system. Biotechnol Bioeng 1994:43:543-554
16. Borkenhagen M, Aebischer P. Tissue-engineering approaches for central and peripheral nervous-system regeneration. MRS Bull 1996:21:59-61
17. Somerman MJ, Quyang HJ, Berry JE, Saygin NE, Strayhorn CL, D'Errico JA, Hullinger T, Giannobile WV. Evolution of periodontal regeneration: from the roots' point of view. J Periodontal Res 1999;34:420-424
18. Zhao M, Jin QM, Berry JE, Nociti FHJ, Giannobile WV, Somerman M. Periodontal tissue engineering by cementaoblastic cell therapy. J Periodontal 2004;75:154-161
19. Langer R, Vacanti JP. Tissue engineering: The challenges ahead. Sci Am 1999;280:86–89.
20. Coventry MB, Tapper EM. Pelvic instability. J Bone Jt Surg Am 1972;54-A:83-101
21. Summers BN, Eisenstein SM. Donor site pain from the ilium. J Bone Jt Surg Br 1989;71-B:677-680
22. Younger EM, Chapman MW. Morbidity at bone graft donor site. J Orthop Trauma 1989;3:192-195

23. Bostrom RD, Mikos AG. Tissue engineering of bone. In: Atala A, Mooney D, Vacanti JP, Langer R, editors. Synthetic biodegradable polymer scaffolds. Boston: Birkhäuser, 1997. p.215-234
24. Vats A, Tolley NS, Polak JM, Gough JE. Scaffolds and biomaterials for tissue engineering: A review of clinical applications. Clin Otolaryngol 2003;28:165–172.
25. Hollinger JO, Leong K. Poly(a-hydroxy acids): Carriers for bone morphogenetic proteins. Biomaterials 1996;17:187–194.
26. Hu YH, Grainger DW, Winn SR, Hollinger JO. Fabrication of poly(a-hydroxy acid) foam scaffolds using multiple solvent systems. J Biomed Mater Res 2002;59:563–572.
27. Martin RB, Burr DB, Sharkey NA. Skeletal Tissue Mechanics. New York: Springer-Verlag; 1998.
28. Goldstein SA. The mechanical properties of trabecular bone: Dependence on anatomic location and function. J Biomech 1987;20:1055–1062.
29. Stock UA, Vacanti JP. Tissue engineering: Current state and prospects. Annu Rev Med 2001;52:443–451.
30. Vacanti JP, Langer R. Tissue engineering: The design and fabrication of living replacement devices for surgical reconstruction and transplantation. Lancet 1999;354 (Suppl 1):32–34.
31. Rezwan K, Chen QZ, Blaker JJ, Boccaccinic AR. Biodegradable and bioactive porous polymer/inorganic composite scaffolds for bone tissue engineering. Biomaterials 2006;27:3413-3431
32. Yunos DM, Bretcanu O, Boccaccini. Polymer-bioceramic composites for tissue engineering scaffolds. J Mater Sci 2008;43:4433-4442
33. Ham AW. Histology. J. B. Lippincott Co., Philadelphia, PA, 1969
34. Reilly DT, Burstein AH, Frankel VH. The elastic modulus of bone. J Biomech 1974;7:271–275.
35. Rho JY, Hobatho MC, Ashman RB. Relations of density and CT numbers to mechanical properties for human cortical and cancellous bone. Med Eng Phys 1995;17:347–355.
36. Fung YC. Biomechanics: Mechanical Properties of Living Tissues. New York: Springer; 1993. p 500. 1
37. Goldstein SA, Patil PV, Moalli MR. Perspectives on tissue engineering of bone. Clin Orthop 1999;357suppl:S419–S423.
38. Kneser U, Schaefer DJ, Munder B, Klemt C, Andree C, Stark GB. Tissue engineering of bone. Min Invas Ther Alllied Technol 2002;11:107–116.
39. Griffith LG. Polymeric biomaterials. Acta Mater 2000;48: 263–277.
40. Borden M, El-Almin SF, Attawia M, Laurencin CT. Structural and human cellular assessment of a novel microsphere-based tissue engineered scaffold for bone repair. Biomaterials 2003;24:597–609.
41. Mano JF, Sousa RA, Boesel LF, Neves NM, Reis RL. Bioinert, biodegradable and injectable polymeric matrix composites for hard tissue replacement: state of art and recent developments. Compos Sci Technol 2004;64:789-817
42. Bergsma EJ, Rozema FR, Bos RRM, Debruijn WC. Foreign body reaction to resorbable poly(L-lactide) bone plates and screws used for the fixation of unstable zygomatic fractures. J Oral Maxillofac Surg 1993;51:666-670
43. Martin C, Winet H, Bao JY. Acidity near eroding polylactide-polyglycolide *in vitro* and *in vivo* in rabbit tibia bone chambers. Biomaterials 1996;17:2373-2380

44. Zhang R, Ma PX. Poly(a-hydroxyl acids)/hydroxyapatite porous composites for bone-tissue engineering. I. Preparation and morphology. J Biomed Mater Res 1999;44:446–455.
45. Thomson RC, Yaszemski MJ, Powers JM, Mikos AG. Hydroxyapatite fiber-reinforced poly(a-hydroxy ester) foams for bone regeneration. Biomaterials 1998;19:1935–1943.
46. Roether JA, Gough JE, Boccaccini AR, Hench LL, Maquet V, Jerôme R. Novel bioresorbable and bioactive composites based on bioactive glass and polylactide foams for bone tissue engineering. J Mater Sci Mater Med 2002;13:1207–1214.
47. Hench LL, Wilson J. Surface active biomaterials. Science 1984;226:630–636.
48. Hench LL, Splinter RJ, Alien WC, Greenlee. Bonding mechanisms at the interface of ceramic prosthetic materials. 1971;5:117-141
49. Hench LL. Bioceramics: from concept to clinic. J Am Ceram Soc 1991:74:1487-1510
50. Brink M, Turunen T, Happonen RP, Yli-Urpo A. Compositional dependence of bioactivity of glasses in the system Na_2O-K_2O-MgO-CaO-B_2O_3-P_2O_5-SiO_2. J Biomed Mater Res 1997;37:114-121
51. Rahaman MN, Brown R, Bal BS, Day DE. Bioactive glasses for non-bearing applications in total joint replacement. Semin. Arthroplasty 2006;17:102-112
52. Huang J, DiSilvio L, Wang M, Tanner KE, Bonfield W. *In vitro* mechanical and biological assessment of hydroxyapatite-reinforced polyethylene composite. J Mater Sci Mater Med 1997;8:775–779.
53. Mikos AG, Sarakinos G, Leite SM, Vacanti JP, Langer R. Laminated three-dimensional biodegradable foams for use in tissue engineering. Biomaterials 1993;14:323–330.
54. Rodríguez-Lorenzo LM, Vallet-Regí M, Ferreira JMF. Fabrication of porous hydroxyapatite bodies by a new direct consolidation method: starch consolidation. J Biomed Mater Res 2002;60:232–240.
55. Chen QZ, Thompson ID, Boccaccini AR. 45S5 Bioglass®-derived glass-ceramic scaffolds for bone tissue engineering. Biomaterials 2006;27:2414-25
56. Fu Q, Rahaman MN, Bal BS, Brown RF, Day DE. Mechanical and *in vitro* performance of 13-93 bioactive glass scaffolds prepared by a polymer foam replication technique. Acta Biomater 2008;4:1854-64
57. Hutmacher DW, Schantz T, Zein I, Ng KW, Teoh SH, Tan KC. Mechanical properties and cell cultural response of polycaprolactone scaffolds designed and fabricated via fused deposition modeling. J Biomed Mater Res 2001;55:203–216.
58. Chu T-MG, Oron DG, Hollister SJ, Feinberg SE, Halloran JW. Mechanical and *in vivo* performance of hydroxyapatite implants with controlled architectures. Biomaterials 2002;23:1283–1293.
59. Yuan H, De Bruijn JD, Zhang X, Van Bitterswijk CA, De Groot K. Bone induction by porous glass ceramic made from Bioglass® (45S5). J Biomed Mater Res 2001;58:270-6
60. Gough JE, Jones JR, Hench LL. Nodule formation and minerlisation of human primary osteoblasts cultured on a porous bioactive glass scaffold. Biomaterials 2004;25:2039-46
61. Jone JR, Ehrenfried, Hench LL. Optimising bioactive glass scaffolds for bone tissue engineering. Biomaterials 2006;27:964-73
62. Schwarzwalder K, Somers AV. Methods of making porous ceramic articles. US Pat 3090094, 1963.

63. Chu TMG. Solid freeform fabrication of tissue engineering scaffolds. In: Scaffolding in tissue engineering. Edited by Ma PX, Elisseeff J, CRC press Taylor & Francis Group, Boca Raton, FL 2006
64. Schoof H, Bruns L, Fischer A, Heschel I, Rau G. Dendritic ice morphology in unidirectionally solidified collagen suspensions. J Cryst Growth 2000; 209;122–29.
65. Schoof H, Apel J, Heschel I, Rau G. Control of pore structure and size in freeze-dried collagen sponges. J Biomed Mater Res Appl Biomater 2002;58:352–57.
66. Zhang H, Hussain I, Brust M, Butler MF, Rannard SP, Cooper AI. Aligned two- and three-dimensional structures by directional freezing of polymers and nanoparticles. Nature Mater 2005;4:787–93.
67. Deville S, Saiz E, Tomsia AP. Freeze casting of hydroxyapatite scaffolds for bone tissue engineering. Biomaterials 2006;27:5480–9.
68. Deville S, Saiz E, Nalla RK, Tomsia AP. Freezing as a path to build complex composites. Science 2006;311,515–8.
69. Fu Q, Rahaman MN, Dogan F, Bal BS. Freeze casting of porous hydroxyapatite scaffolds - I. Processing and general microstructure. J Biomed Mater Res Part B: Appl Biomater 2008;86B: 125–35.
70. Fu Q, Rahaman MN, Dogan F, Bal BS. Freeze casting of porous hydroxyapatite scaffolds - II. Sintering, microstructure, and mechanical properties. J Biomed Mater Res Part B: Appl Biomater 2008;86B:514–22.
71. Deville S. Freeze-casting of porous ceramics: a review of current achievements and issues. Adv Eng Mater 2008;10:155-169
72. Uhlmann DR, Chalmers B, Jackson KA. Interaction between particles and a moving ice-liquid interface. J Appl Phys 1964;35:2986-93.
73. Kőrber C, Rau G, Cosman MD, Cravalho EG. Interaction of particles and a moving ice-liquid interface. J. Cryst. Growth 1985;72:649-62.
74. Sofie SW, Dogan F. Freeze casting of aqueous alumina slurries with glycerol. J Am Ceram Soc 2001;84:1459-1464.
75. Wu YG, Tabata M, Takamuku T. A local solvent structure study on 1,4-dioxane-water binary mixtures by total isotropic Rayleigh light scattering method. J Mol Liq 2001;94:273-282.
76. Yoo BH, Choi WY, Kim HE, Kim JH, Koh YH. Aligned porous alumina ceramics with high compressive strengths for bone tissue engineering. Scrip Mater 2008;58:537-40
77. Soon YM, Shin KH, Koh YH, Lee JH, Kim HE. Compressive strength and processing of camphene-based freeze cast calcium phosphate scaffolds with aligned pores. Mater Lett 2009;63:1548-50

PAPER

1. FREEZE CASTING OF POROUS HYDROXYAPATITE – I. PROCESSING AND MICROSTRUCTURE

Qiang Fu[1], Mohamed N. Rahaman[1*], Fatih Dogan[1], and B. Sonny Bal[2]

[1]University of Missouri-Rolla, Department of Materials Science and Engineering, Rolla, Missouri 65409

[2]B. Sonny Bal, University of Missouri-Columbia, Department of Orthopaedic Surgery, Columbia, Missouri 65212

1.1. ABSTRACT

Freeze casting of aqueous suspensions on a cold substrate was investigated as a method for preparing hydroxyapatite (HA) scaffolds with unidirectional porosity. In the present paper, we report on the ability to manipulate the microstructure of freeze-cast constructs by controlling the processing parameters. Constructs prepared from aqueous suspensions (5–20 volume percent particles) on a steel substrate at –20°C had a lamellar-type microstructure, consisting of plate-like HA and unidirectional pores oriented in the direction of freezing. Sintering for 3 h at 1350°C produced constructs with dense HA lamellas, porosity of ~50%, and inter-lamellar pore widths of 5–30 μm. The thickness of the HA lamellas decreased but the width of the pores increased with decreasing particle concentration. Decreasing the cold substrate temperature from –20°C to –196°C produced a finer lamellar microstructure. The use of water–glycerol mixtures (20 wt% glycerol) as the solvent in the suspension resulted in the production of finer pores (1–10

* Correspondence to: M. N. Rahaman (rahaman@mst.edu)

μm) and a larger number of dendritic growth connecting the HA lamellas. On the other hand, the use of water–dioxane mixtures (60 wt% dioxane) produced a cellular-type microstructure with larger pores (90–100 μm). The ability to produce a uniaxial microstructure and its manipulation by controlling the processing parameters indicate the potential of the present freeze casting route for the production of scaffolds for bone tissue engineering applications.

Keywords: biomaterials; scaffolds; hydroxyapatite; freeze casting; porous ceramics

1.2. INTRODUCION

The development of new scaffolds and their processing into structures that have properties tailored for specific applications, such as the repair of large defects in load-bearing bones are becoming increasingly important. In addition to the scaffold having adequate mechanical properties for supporting physiological loads, tissue infiltration and facile integration of the scaffold with surrounding tissue are required for ultimate clinical application.

Certain synthetic and natural polymers, such as poly(lactic acid), PLA, poly(glycolic acid), PGA, copolymers of PLA and PGA, and collagen are biodegradable, so the scaffold can be gradually replaced by new bone matrix synthesized by tissue-forming cells [1-4]. However, the use of degradable polymers for replacing load-bearing bones is often challenging because of their relatively weak mechanical strength [1]. To improve the load-bearing properties of biodegradable polymer scaffolds, attempts have been made to reinforce the polymers with particles or short fibers. The use of reinforcing

materials such as hydroxyapatite (HA) and bioactive glass provides scaffolds that are biodegradable as well as bioactive [5-7].

Certain compositions of glasses, glass-ceramics, and ceramics, referred to as bioactive ceramics, have been widely investigated for healing bone defects, due to their ability to enhance bone formation and to bond to surrounding tissue [8]. Cell-seeded bioactive ceramics are also of interest as potential scaffolds for bone tissue engineering because they are osteoconductive as well as osteoinductive, and have the potential for providing higher mechanical strength than the aforementioned polymers. As the main mineral constituent of bone, hydroxyapatite (HA) has been widely investigated as a scaffold material for bone tissue engineering. Scaffolds of HA, both synthetic and natural, are biocompatible and osteoconductive. They produce no systemic toxicity or immunological reactions, and show biological affinity for bony tissues [9]. A disadvantage of HA is its brittleness, which limits the scaffolds to applications subjected to mainly compressive loading. One approach to this mechanical limitation is the use of HA as the bioactive phase in composites, mainly polymer composites [9, 10]. By stiffening a compliant biocompatible synthetic polymer such as polyethylene (PE) with HA particles (40 vol %), composites with mechanical properties comparable to those of cortical bone, coupled with bone-bonding ability due to the HA phase, have been developed [10].

A variety of methods have been used to produce porous scaffolds for bone repair and regeneration, including consolidation with a pore-producing fugitive phase such as starch or PVA [11, 12], the use of foaming agents [13,14],and solid freeform fabrication [15,16].Freeze casting is a technique which has been used to produce polymeric and

ceramic parts [17–25].It has been applied to the production of synthetic and natural polymer scaffolds for tissue engineering applications[17–19],and its application to the production of porous bioceramic scaffolds is now receiving some interest [26–29]. For the production of porous bioceramic scaffolds, such as HA, the freeze casting route involves rapid freezing of a colloidally stable suspension of HA particles in a nonporous mold, and sublimation of the frozen solvent under cold temperatures in a vacuum. After drying, the porous green samples are sintered to improve their mechanical strength. The microstructure and, hence, the properties of the final sintered body are determined essentially by the suspension parameters (such as particle size, particle concentration, and colloid stability of the suspension), the freezing conditions (rate and direction of freezing), and the sintering conditions (temperature and time). By controlling the growth direction of the ice crystals during freezing, it is possible to achieve preferential orientation of the porosity, leading to anisotropic microstructure and properties, mimicking the structural characteristics of natural materials such as bone.

Recent investigations have explored how the processing conditions, such as suspension concentration, freezing rate, and sintering conditions, influence the microstructure and compressive strength of HA scaffolds [28]. Directional freezing of aqueous HA suspensions in a cylindrical mold placed on a cold substrate produced porous constructs with three distinct zones, each characterized by a different shape and dimensions of the pores, described as fully dense, cellular, and lamellar. In the lamellar region, which formed the major portion of the construct, an increase in the freezing rate of the suspension, from 1ºC/min to 10ºC/min resulted in a reduction of the pore width from ~40 μm to ~10 μm.

A way to further manipulate the microstructure of the freeze cast construct is to control the freezing (or solidification) behavior of the liquid in the suspension, but this has received little attention. Certain liquids, such as glycerol and 1,4-dioxane (referred to hereafter simply as dioxane), are miscible with water, and when added to water modify the local structure of the aqueous liquid. As a result, they modify the nucleation and growth of the ice crystals, thereby modifying the freezing behavior of the aqueous liquid. Glycerol effectively binds to water molecules and disrupts the complete crystallization of ice. This leads to a localized structure, resulting in a reduced size of the growing ice crystals and inhibiting solute rejection [30, 31].The addition of glycerol (10–30 wt %) to the aqueous solvent reduced the viscosity of Al_2O_3 suspensions stabilized with an anionic dispersant, ammonium polymethacrylate, and produced more homogeneous microstructures after freeze casting and sintering [23].The effects were explained in terms of the ability of glycerol to both enhance the colloidal stability of the suspensions and modify the freezing behavior of water. Dioxane is miscible with water at any composition under ambient conditions. A study of the local solvent structure of dioxane-water mixtures [32] indicated that the structure changed at three specific compositions when the mole fraction (χ) of dioxane in the mixture was 0.13, 0.3, and 0.7. For $\chi < 0.13$, the mixture consisted mainly of water molecules with some water-dioxane complexes. For $0.13 < \chi < 0.3$, the system consisted mainly of small clusters of water-dioxane molecules, whereas for $\chi > 0.3$, the water-dioxane clusters gradually disappeared and the mixture evolved gradually to the inherent solvent structure of pure dioxane.

The objective of the present work was to explore the microstructural manipulation of freeze-cast HA constructs by controlling the processing parameters. Using aqueous

suspensions as the basic system, the effects of particle concentration and temperature of the cold substrate on the microstructure were studied. Further manipulation of the microstructure was explored by controlling the freezing (solidification) of the liquid in the suspension through the use of water–glycerol and water–dioxane mixtures. In Part II, the microstructure of the sintered constructs and its effect on the mechanical behavior are described. An understanding of the relationship between the processing parameters and the resulting microstructure is useful for manipulating the microstructure and properties of scaffolds for bone repair and replacement.

1.3. MATERIALS AND METHODS

1.3.1. Processing of HA Suspensions. HA powder (Alfa Aesar, Haverhill, MA) with the particle size less than 0.5 μm, determined by a laser diffraction particle size analyzer (Model LS 13 320; Beckman Coulter Inc., Fullerton, CA), was used in the present work. Aqueous suspensions were prepared by dispersing HA powder in deionized water containing a dispersant and an organic binder to improve the rheological behavior. Four anionic and one nonionic dispersants were investigated in an attempt to determine an effective dispersant for the HA particles used in the present work. The anionic dispersants were: ammonium polymethacrylate (Darvan C, molecular weigh MW = 10,000–16,000; R.T. Vanderbilt Co., Norwalk, CT), sodium polyacrylate (Darvan 811, MW = 5000; R.T. Vanderbilt Co.), ammonium polyacrylate (Darvan 821A, MW = 3500; R.T. Vanderbilt Co.), ammonium polycarbonate (Targon 1128, MW = 13000-15000; BK Ladenburg GmbH, Ladenburg, Germany). The nonionic dispersant was an ethoxylated acetylenic diol surfactant (Dynol 604, Air Products & Chemicals Inc., Allentown, PA). The effectiveness of the dispersants for stabilizing the suspension against flocculation

was investigated by measuring the viscosity of the suspensions as a function of dispersant concentration, HA particle concentration, and shear rate using a rotating cylinder viscometer (Model VT500; Haake Inc., Paramus, NJ).

Based on the viscosity data, suspensions containing 0.75 wt% of Dynol 604 and 1.5 weight percent (wt%) of an organic binder poly(vinyl alcohol), PVA, (DuPont Elvanol® 90-50, DuPont, DE), based on the dry weight of the HA powder, and 5–20 vol% HA particles were prepared by ball-milling for 48 h in polypropylene containers using Al_2O_3 grinding media. The suspensions were de-aired by ball-milling at a low speed prior to freeze casting.

To explore the effects of a modifier on the solidification of the solvent during freeze casting, aqueous suspensions containing 5–20 wt% of glycerol (Fisher Scientific, Pittsburg, PA) or 40–70 wt% dioxane (Fisher Scientific), were also prepared using the same procedure.

1.3.2. Freeze Casting of Suspensions. Freeze casting was performed by pouring the suspensions into polyvinyl chloride (PVC) tubes (~10 mm internal diameter × 20 mm long) placed on a cold steel substrate kept at a fixed temperature using a freeze dryer (Genesis 25 SQ Freeze Dryer, VirTis Co., Gardiner, NY) or cooled by liquid nitrogen. Polyurethane foam was used to cover the PVC tubes to reduce heat transfer from the surrounding environment to the slurry, ensuring optimum directional freezing of the system. The arrangement did not provide a method for providing a fixed cooling rate. Instead, it allowed the substrate to be kept at a fixed temperature. Three substrate temperatures were used in the experiments: –196°C, –50°C and –20°C. The frozen constructs were subjected to a vacuum of 4 Pa for 48 h in a freeze dryer (Genesis 25 SQ

Freeze Dryer) to cause sublimation of the frozen solvent. The green bodies were sintered in air for 3 h at temperatures between 1250°C and 1375°C, with a heating and cooling rate of 3°C/min.

1.3.3. Microstructural Characterization of Porous HA Constructs. The microstructure of the cross-sections of the green and sintered constructs, in the microstructure of the cross-sections of the green and sintered constructs, in the planes parallel to and perpendicular to the direction of freezing, was observed using scanning electron microscopy, SEM (Hitachi S-4700, Hitachi Co., Tokyo, Japan). Since the green bodies (after sublimation of the frozen liquid) were too weak for handling, most of the characterization experiments were carried out on the sintered samples. The volume of open porosity in the sintered samples was measured using the Archimedes method. In addition, the porosity and pore size distribution of open pores were measured using mercury intrusion porosimetry (Poremaster, Quantachrome, Boynton Beach, FL).

The width of the pores and the thickness of the HA lamellas in the sintered constructs were determined from SEM micrographs of cross-sections in the plane parallel to the direction of freezing. For each construct, at least 5 SEM micrographs were taken at random positions of the cross-section, and at least 10 measurements of the pore width and lamella thickness were made on each micrograph, to provide a mean value and a standard deviation.

1.4. RESULTS

1.4.1. Rheological Behavior of HA Suspensions Used for Freeze Casting.

Figure 1 shows data for the viscosity as a function of shear rate for aqueous HA suspensions (20 vol% particles) stabilized with the dispersants Darvan 811, Darvan 821A, Darvan C, Targon 1128, and Dynol 604. The concentration of each dispersant was 1.0 wt%, based on the dry mass of the particles. At a given shear rate, and particularly at shear rates < 100 s–1, Darvan 821A and Dynol 604 reduced the viscosity of the suspension more effectively, indicating their ability to better stabilize the particles against flocculation. As with other suspension-based forming methods, the colloidal stability of the suspension is important for producing homogeneous green microstructures. In the directional freeze casting route used in the present work, a high rate of flocculation can lead to zones with different microstructures from the bottom to the top of the sample.

The optimum concentration of Darvan 821A or Dynol 604 required to stabilize the HA particles was determined from data for the viscosity of the suspension (20 vol% particles) as a function of the dispersant concentration at a constant shear rate of 100 s^{-1} (Figure 2). The data indicated a minimum viscosity at ~0.75 wt% Dynol 604 and at ~1.0 wt% Darvan 821A. Furthermore, at these minima, the viscosity of the suspension stabilized with Dynol 604 was almost 3 times lower than the viscosity for the suspension stabilized with Darvan 821A. Similar trends were found for suspensions containing 5–15 vol% particles, but the data are omitted for the sake of brevity. The data in Figure 2 indicated that the viscosity of the suspensions was reduced more effectively using Dynol 604, allowing the incorporation of a higher concentration of particles for the same given

viscosity. Unless stated otherwise, henceforth the suspensions described are those stabilized with 0.75 wt% Dynol 604.

Data for the relative viscosity of the suspensions (shear rate = 100 s^{-1}) as a function of HA particle concentration are shown in Figure 3. The particle concentration had a limited effect on the viscosity for volume fractions lower than ~30 vol% but above this value, the viscosity started to increase steeply. The data can be well fitted by a modified Krieger-Dougherty equation [33, 34] of the form:

$$\eta_r = \left(1 - \frac{\phi}{\phi_m}\right)^{-n} \qquad (1)$$

with η_r, the relative viscosity, is defined as the viscosity of the suspension, η, divided by the viscosity of the solvent (water) η_L, ϕ is the volume fraction of the particles, ϕ_m is the volume fraction of particles at which the viscosity becomes practically infinite, and *n* is a fitting parameter. The maximum HA particle concentration predicted by this model was ϕ_m = 45 vol%, with *n* = 3.5. In the present experiments, the suspensions became difficult to pour for particle volume fractions greater than ~25 vol%. As a result, the highest particle concentration used was 20 vol% (equal to 45 wt%).

1.4.2. Microstructure of Freeze-Cast HA Constructs

1.4.2.1 Constructs Prepared from Aqueous Suspensions. After freeze casting and sintering, the constructs maintained a uniform cylindrical shape (Figure 4). The green constructs, after sublimation of the frozen liquid, were too weak for handling, so most of the microstructural characterization studies were performed on constructs after they were sintered. As described later (Part II), sintering at temperatures between 1250°C

and 1350°C produced an increase in the density of the HA phase of the constructs, but did not alter the general features of the microstructure. The microstructural features are therefore described for constructs sintered under the same sintering conditions (3 h at 1350 °C).

Figure 5 shows SEM images of constructs prepared from suspensions with 20 vol% HA particles on a substrate at –20°C. A uniform lamellar-type microstructure was observed throughout the whole construct, with the pores oriented in the direction of freezing. This lamellar-type microstructure is quite similar to the microstructures of polymeric materials such as collagen prepared for tissue engineering applications [19, 20]. For the present system, the plate-like HA lamellas and the inter-lamellar macropores were oriented in the direction of freezing. The HA lamellas had a thickness of 25±5 μm and a length of 100–250 μm in cross section (Figure 5(a, b)) and extended from the bottom of the construct to the top (Figure 5(c-d)). The average pore width, determined from SEM micrographs, was 15±10 μm. Dendritic structures were present on the surfaces of the HA lamellas, and in some cases, they formed bridges between adjacent HA lamellas.

Mercury porosimetry data (Figure 6) for HA scaffolds sintered for 3 h at 1350ºC showed a narrow pore size distribution, with pore widths in the range 5–30μm, in good agreement with the pore widths found in the SEM images (Figure 5). From the total volume of pores intruded, the open porosity was ~55%, in good agreement with the porosity (52%) found by the Archimedes method. The data showed that almost all the open pores in the sample were in this narrow range, indicating the good homogeneity of the microstructure produced by the present freeze casting process.

A reduction of the particle concentration of the suspension or the temperature of the cold substrate did not change the general lamellar-type microstructure, but produced changes in the thickness of the HA lamellas, the porosity, and the pore width. With decreasing particle concentration (from 20 vol% to 10 vol% and 5 vol%), the HA lamellas became thicker, the porosity was higher, and the pore width increased (Figure 7). Decreasing the substrate temperature during freezing from –20°C to –50°C and –196°C resulted in pores with finer cross sections (Figure 8). The lamellar thickness, porosity, and pore width, determined from SEM micrographs of the sample cross-sections, are summarized in Table I.

1.4.2.2 Constructs Prepared from Suspensions with Water-Glycerol and Water-Dioxane Mixtures. Figure 9 shows the microstructure of sintered HA constructs formed from suspensions (20 vol% HA particles) in which the solvent constructs formed from suspensions (20 vol% HA particles) in which the solvent consisted of a mixture of water with 5 and 20 wt% of glycerol. The freeze-cast green bodies were sintered for 3 h at 1350°C. Compared to the constructs prepared without glycerol addition (Figure 5), the presence of 5 wt% glycerol in the suspensions had the effect of thickening the cross-section of the HA lamellas and reducing the homogeneity of the microstructure (Figure 9(a, b)). With higher additions of glycerol, the microstructure became finer and more uniform. In general, the glycerol additions had the effect of increasing the number of dendritic bridges between the HA lamellas. This increased to such an extent that the cross-section of the pores changed from a plate-like morphology to a more rectangular shape. Consequently, with the increasing concentration of glycerol in the aqueous solvent, the microstructure became more uniform, the pores

became smaller, and the number of dendritic bridges between the HA lamellas increased (Figure 9(c, d)). Mercury porosimetry data (Figure 10) of the construct prepared from suspensions with 20 wt% glycerol confirmed the narrow size distribution of the pores. The pore widths were in the range 1–10 μm, compared to values 5–30 μm for similar constructs prepared without glycerol (Figure 6).

Microstructures of constructs prepared from suspensions (10 vol% particles) in which the solvent consisted of water with 30 wt% and 60 wt% dioxane are shown in Figure 11. With 30 wt% dioxane [Figure 11(a, b)], a coarse lamellar-type microstructure is obtained. However, the microstructure changed with increasing dioxane concentration, giving a cellular type microstructure [Figure 11(c, d)], with pore diameters of 100±10 μm, much larger than the pore width of constructs prepared from aqueous suspensions (i.e., 100% water). Increasing the dioxane concentration to 70 wt% did not change the general cellular microstructure, but the pore diameter decreased substantially, to 50±5 μm. Table II summarizes the microstructural parameters of the constructs prepared from suspensions with aqueous solvent (100% water), water–glycerol mixtures, and water–dioxane mixtures.

1.5. DISCUSSION

For freeze-cast constructs prepared from aqueous suspensions (no glycerol or dioxane additions), the present work showed the ability to achieve a uniform lamellar-type microstructure throughout the whole construct, with the lamellas oriented in the direction of freezing. Compared to the recent work of Deville et al. [28], in which three microstructural zones were observed from the bottom to the top of the sample (described

as fully dense, cellular, and lamellar), no fully dense or cellular zones were observed. A number of factors may be responsible for the difference in microstructure observed in this study and the work of Deville et al. They include differences in the freeze casting method and the colloidal properties of the HA suspensions used in the two investigations. For example, in the present work, the freezing of the suspension was determined by the temperature of the cold substrate, whereas Deville et al. used an arrangement that allowed greater control of the freezing rate. The HA particle size in the present study (< 0.5 μm) was much finer than that (2.4 μm) used by Deville et al., and a different dispersant was used to achieve a stable suspension [35]. The finer particle size used in the present work, coupled with the stable suspension, presumably reduced the tendency for particle settling and improved the ease with which particles were expelled from the frozen liquid during the freeze casting step, giving a homogeneous microstructure throughout the construct. It should be noted that a homogenous microstructure, such as that obtained in the present work, is desirable in many applications because it generally leads to more reliable and controllable properties of the construct.

The results also showed the ability to manipulate the microstructure of the freeze cast constructs by changing the processing conditions. For aqueous suspensions, lower particle concentration resulted in the production of constructs with higher porosity, larger pore width, and thinner HA lamellas (Table I). A lower HA particle concentration allows larger separation distances between the HA lamellas since the dentritic growth of ice crystals is relatively less hindered as the particles are pushed at the solidification front. Particles in more dilute suspensions travel longer distances and become immobilized when the highest particle packing density is achieved between two growing dentritic

crystals. The lower HA particle concentration also resulted in the fewer particles rejected by the ice lamella, leading to thinner lamellas in the sintered HA sample. From a thermodynamic point of view, a lower substrate temperature means a larger driving force for the nucleation of ice crystals, which results in the formation of a larger number of ice nuclei and an increased growth rate of the formed ice crystals. The data indicate that by adjusting the particle concentration and substrate temperature, changes in the scale of the microstructural features can be achieved without drastically altering the general lamellar-type microstructure.

Far greater changes in the microstructure of the constructs were obtained by modifying the freezing (or solidification) behavior of the solvent through the use liquid mixtures. Glycerol, with the ability to form hydrogen bonds, have been found to influence the freezing behavior of aqueous suspension by destroying the molecular order in water and reducing the size of ice crystals during freezing process [30]. Glycerol, acting as a cryoprotectant, effectively binds to natural water molecules and disrupts the complete crystallization of ice, which leads to a localized amorphous structure, resulting in the reduced size of growing ice crystals and inhibiting solute rejection [23, 31]. A small amount (5 wt%) of glycerol addition to the suspension was capable of reducing the size of ice crystals and, hence, the pore diameter in the sintered construct, which in turn resulted in the thickening of the HA lamellas [Figure 9(a, b)]. With increasing glycerol addition, more localized ice crystals were formed with less solute rejection during the solidification process. The large lamellar ice crystals eventually disappeared due to the formation of the localized ice crystals and smaller crystals produced in the frozen samples, which corresponded to fine dendritic pores in the sintered HA samples [Figure

9(c, d)]. Furthermore, the well-dispersed HA suspension enabled the formation of the uniform ice crystals in the frozen sample and, hence, the homogenous pore structure in the sintered body.

Dioxane has been shown the break the hydrogen bonds in water [36, 37], forming stable dioxane (Diox)–water (H_2O) complexes $(Diox)_m•(H_2O)_n$ [38, 39]. According to studies of the local structure [32], the these complexes are more prevalent when the mole fraction of dioxane χ is between ~0.13 and ~0.30 (~40–70 wt%). The change in microstructure of the freeze-cast constructs may be attributed to the presence of these complexes. Below 40 wt% dioxane, the structure of the solvent was dominated by hydrogen-bonded water molecules, leading to a *lamellar-type* microstructure [Figures 11(a,b)], not drastically different from the microstructure observed for aqueous solvents. For the suspension with 60 wt% dioxane, the freezing of the $(Diox)_m•(H_2O)_n$ complexes resulted in a *cellular* microstructure with pore diameters of 100±10 μm.

The microstructures obtained in the present work for HA are similar in nature to those observed in porous constructs prepared by unidirectional freezing of collagen suspensions [17-19], solutions of biodegradable polymers, such as poly(lactic acid), PLA, poly(glycolic acid), PGA, and their copolymers, PLGA [5], and suspensions of polymers and particles, such as collagen and HA [20, 26 40]. The use of suspensions with a low concentration of collagen (typically < 5 wt %) commonly resulted in lamellar or cellular microstructures such as those shown in Figure 7 and Figure 11(c,d), but with higher porosity (typically > 80–85%). Pore sizes (diameter or width) in the range 50–500 lm have been reported, depending on the freezing rate [18, 41]. Unidirectional microstructures with tubular pores were obtained using a thermally induced phase

separation (TIPS) technique during freezing of PLA and PLGA solutions [5]. Constructs with porosity of 88–97% and average pore diameter of 30–115 μm were produced, depending on the concentration of the polymer solution (2.5–10 wt %) and the freezing rate. To mimic the microstructure and mineral composition of bone, the production of unidirectional composites of HA with collagen or a biodegradable polymer (PLA, PGA, or PLGA) has also been investigated [20, 26, 40]. Typically, these composite scaffolds have microstructures similar to those of the unreinforced polymer constructs.

Scaffolds intended for the repair and regeneration of large defects in load-bearing bones must not only have sufficient strength to serve a mechanical function, but they must also support tissue ingrowth into the pores. In Part II [42], the mechanical behavior of the constructs prepared in the present work is reported. The microstructural parameters that influence tissue ingrowth include the porosity, the pore diameter, the pore shape and the pore interconnectivity. Interconnected pores with a mean diameter or width of 100 μm or greater, and open porosity of > 50% are generally considered the minimum requirements to permit tissue ingrowth and function in porous scaffolds [43, 44]. For constructs prepared from aqueous suspensions (5–20 vol % particles), the mean pore widths obtained in the present work and by Deville et al [28], are <40 μm. The ability to produce larger pores (100 ± 10 μm), by modifying the freezing behavior of the liquid, as demonstrated in this work for water-dioxane mixtures (Table II), provides an important approach for the production of HA scaffolds with the requisite microstructure forbone repair and regeneration.

1.6. CONCLUSIONS

Freeze casting of aqueous suspension of HA particles on a cold substrate produced porous constructs with a uniform, lamellar-type microstructure in which plate-like HA lamellas were oriented in the direction of freezing. Changes in the particle concentration of the suspension and temperature of the cold substrate did not drastically alter the lamellar-type microstructure but changed the porosity, the pore width, and thickness of the HA lamellas. With increasing particle concentration in the suspension (5–20 vol%), the porosity and pore cross section decreased, but the thickness of the HA lamellas increased. A decrease in the temperature of the cold substrate (–20°C to –196°C) caused a reduction in the size of the HA lamellas and the pore cross section. The addition of glycerol (~20 wt%) to the aqueous solvent used in the suspensions produced finer pores and a larger number of dendritic structures connecting the HA lamellas. On the other hand, the addition of 60 wt% dioxane produced a cellular microstructure with much larger pores.

1.7. REFERENCES

1. Goldstein SA, Patil PV, Moalli MR. Perspectives on tissue engineering of bone. Clin Orthop 1999;357S:S419-S423.
2. Kneser U, Schaefer DJ, Munder B, Klemt C, Andree C, Stark GB. Tissue engineering of bone. Min Invas Ther & Alllied Technol 2002;11:107-116.
3. Griffith LG. Polymeric biomaterials. Acta Mater 2000;48:263-277.
4. Borden M, El-Almin SF, Attawia M, Laurencin CT. Structural and human cellular assessment of a novel microsphere-based tissue engineered scaffold for bone repair. Biomaterials 2003;24:597-609.
5. Zhang R, Ma PX. Poly(α-hydroxyl acids)/hydroxyapatite porous composites for bone-tissue engineering. I. Preparation and morphology. J Biomed Mater Res 1999;44:446-455.
6. Thomson RC, Yaszemski MJ, Powers JM, Mikos AG. Hydroxyapatite fiber-reinforced poly(α-hydroxy ester) foams for bone regeneration. Biomaterials 1998;19:1935-1943.
7. Roether JA, Gough JE, Boccaccini AR, Hench LL, Maquet V, Jerôme R. Novel bioresorbable and bioactive composites based on bioactive glass and polylactide foams for bone tissue engineering. J Mater Sci Mater Med 2002;13:1207–1214.
8. Hench LL, Wilson J. Surface active biomaterials. Science 1984;226:630-636.
9. Hench LL. Bioceramics. J Am Ceram Soc 1998;81:1705-1728.
10. Huang J, DiSilvio L, Wang M, Tanner KE, Bonfield W. *In vitro* mechanical and biological assessment of hydroxyapatite-reinforced polyethylene composite. J Mater Sci Mater Med 1997;8:775–779.
11. Rodríguez-Lorenzo LM, Vallet-Regí M, Ferreira JMF. Fabrication of porous hydroxyapatite bodies by a new direct consolidation method: starch consolidation. J Biomed Mater Res 2002;60:232-240.
12. Li SH, De Wijn JR, Layrolle P, De Groot K. Synthesis of macroporous hydroxyapatite scaffolds for bone tissue engineering. J Biomed Mater Res 2002;61:109-120.
13. Sepulveda P, Binner JG, Rogero SO, Higa OZ, Bressiani JC. Production of porous hydroxyapatite by the gel-casting of foams and cytotoxic evaluation. J Biomed Mater Res 2000;50:27–34.
14. Tamai N, Myoui A, Tomita T, Nakase T, Tanaka J, Ochi T, Yoshikawa H. Novel hydroxyapatite ceramics with an interconnective porous structure exhibit superior osteoconduction *in vivo*. J Biomed Mater Res 2002;59:110 –117.
15. Roy TD, Simon JL, Ricci JL, Rekow ED, Thompson VP, Parsons JR. Performance of hydroxyapatite bone repair scaffolds created via three-dimensional fabrication techniques. J Biomed Mater Res 2003;67A:1228-1237.
16. Wilson CE, de Bruijn JD, van Blitterswijk CA, Verbout AJ, Dhert WJA. Design and fabrication of standardized hydroxyapatite scaffolds with a defined macro-architecture by rapid prototyping for bone-tissue-engineering research. J Biomed Mater Res 2004;68A:123-132.
17. Wang HW, Tabata Y, Ikada Y. Fabrication of porous gelatin scaffolds for tissue engineering. Biomaterials. 1999;20:1339-1344.

18. Schoof H, Bruns L, Fischer A, Heschel I, Rau G. Dendritic ice morphology in unidirectionally solidified collagen suspensions. J Cryst Growth 2000;209:122-129.
19. Schoof H, Apel J, Heschel I, Rau G. Control of pore structure and size in freeze-dried collagen sponges. J Biomed Mater Res Appl Biomater 2001;58:352-357.
20. Zhang H, Hussain I, Brust M, Butler MF, Rannard S, Cooper AI. Aligned two- and three-dimensional structures by directional freezing of polymers and nanoparticles. Nature Mater 2005;4:787-793.
21. Fukasawa T, Ando M, Ohji T, Kanzaki S. Synthesis of porous ceramics with complex pore structure by freeze-dry processing. J Am Ceram Soc 2001;84:230-232.
22. Dogan F, Hausner H. The role of freeze drying in ceramic processing. In: Ceramic Powder Science II, Ceramic Transactions, Vol. 1. Messing GL, Fuller ER, Hausner H, eds. Westerville, OH, The American Ceramic Society, 1988; 127-134.
23. Sofie SW, Dogan F. Freeze casting of aqueous alumina slurries with glycerol. J Am Ceram Soc 2001;84:1459-1464.
24. Araki K, Halloran JW. Porous ceramic bodies with interconnected pore channels by a novel freeze casting technique. J Am Ceram Soc 2005;88:1108-1114.
25. Halloran JW. Making better ceramic composites with ice. Science 2006;311: 479-480.
26. Yunoki S, Ikoma T, Tsuchiya A, Monkawa A, Ohta K, Sotome S, Shinomiya K, Tanaka J. Fabrication and mechanical and tissue ingrowth properties of unidirectionally porous hydroxyapatite/collagen composite. J Biomed Mater Res Appl Biomater 2007;80B:166-173.
27. Song JH, Koh YH, Kim HE. Fabrication of a porous bioactive glass-ceramic using room-temperature freeze casting. J Am Ceram Soc 2006;89:2649-2653.
28. Deville S, Saiz E, Tomsia A. Freeze casting of hydroxyapatite scaffolds for bone tissue engineering. Biomaterials 2006;27:5480-5489.
29. Deville S, Saiz E, Nalla RK, Tomsia A. Freezing as a path to build complex composites. Science 2006;311:515–518.
30. Miner CS, Dalton NN. Glycerol. New York: Reinhold; 1953:270-284.
31. Dogan F, Sofie SW. Microstructural Control of Complex-Shaped Ceramics Processed by Freeze Casting. cfi/Ber. DKG 2002;79:E35–E38.
32. Wu YG, Tabata M, Takamuku T. A local solvent structure study on 1,4-dioxane-water binary mixtures by total isotropic Rayleigh light scattering method. J Mol Liq 2001;94:273-282.
33. Krieger IM, Dougherty M. A mechanism for non-newtonian flow in suspensions of rigid spheres. Trans Soc Rheol 1959;3:137–152.
34. Bergström L. Shear thinning and shear thickening of concentrated ceramic suspensions. Colloids Surf A: Physicochem Eng Aspects 1998;133:151–155.
35. Rao RR, Kannan TS. Dispersion and slip casting of hydroxyapatite. J Am Ceram Soc 2001;84:1710-1716.
36. Reakins D, O'Neill RD, Waghorne WE.Washburn numbers. Part 5.—Relative solvent transport numbers for ion constituents in the dioxan + water and dimethylsulphoxide + water systems. J Chem Soc Faraday Trans 1 1983;79:2289-2298.
37. Mazurkiewicz J, Tomsasik P. Whay 1,4-dioxane is a water-structure breaker. J Mol Liq 2006;126:111-116

38. Zoidis E, Yarwood J, Tassing T, Danten Y, Besnard M. Vibrational spectroscopic studies on the state of aggregation of water in carbon tetrachloride, in dioxane and in the mixed solvent. J Mol Liq 1995;64:197-210
39. Buzko VY, Sukhno IV, Panytushkin VT, Ramazanova. Theoretical investigation of 1,4-dioxane complexes with water in the chair conformation by semiempiric MNDO/PM3 method. J Struct Chem 2005;46:596-602.
39. Hulbert SF, Young FA, Mathews RS, Klawitter JJ, Talbert CD, Stelling FH. Potential of ceramic materials as permanently implantable skeletal prostheses. J Biomed Mater Res 1970;4:433–456
40. Wei G, Ma PX. Structure and properties of nano-hydroxyapatite/polymer composite scaffolds for bone tissue engineering. Biomaterials 2004;25:4749–4757.
41. Buttafoco L, Engers-Buijtenhuijs P, Poot AA, Dijkstra PJ, Daamen WF, van Kuppevelt TH, Vermes I, Feijen J. First steps towards tissue engineering of small-diameter blood vessels: preparation of flat scaffolds of collagen and elastin by means of freeze drying. J Biomed Mater Res B Appl Biomater 2006;77:357–368.
42. Fu Q, Rahaman MN, Dogan F, Bal BS. Freeze casting of porous hydroxyapatite scaffolds. II. Sintering, microstructure, and mechanical behavior. J Biomed Mater Res B Appl Biomater 2007. Submitted for publication.
43. Hulbert SF, Young FA, Mathews RS, Klawitter JJ, Talbert CD, Stelling FH. Potential of ceramic materials as permanently implantable skeletal prostheses. J Biomed Mater Res 1970;4:433–456.
44. Hollinger JO, Brekke J, Gruskin E, Lee D. Role of bone substitutes. Clin Orthop Relat Res 1996;324:55–65.

Table I: Summary of lamellar thickness, porosity, and pore width for constructs prepared from aqueous suspensions with 5, 10, and 20 wt% particles.

HA concentration (vol %)	Lamellar thickness (μm)	Porosity (%)	Pore width (μm)
5	8±2	85±2	50±10
10	15±5	70±5	25±5
20	25±5	55±2	15±10

Table II: Comparison of porosity and pore widths for constructs prepared from aqueous suspensions, suspensions with glycerol, and suspensions with dioxane.

Solvent composition	HA concentration (vol%)	Pore width (μm)	Porosity (%)	General microstructure
Aqueous	10	25±5	70±5	Lamellar
	20	15±10	55±2	Lamellar
Water-Glycerol (20 wt%)	10	10±5	67±2	Rectangular
	20	4±2	46±2	Rectangular
Water-1,4-dioxane (60 wt%)	10	100±10	65±2	Cellular
	20	90±10	37±2	Cellular

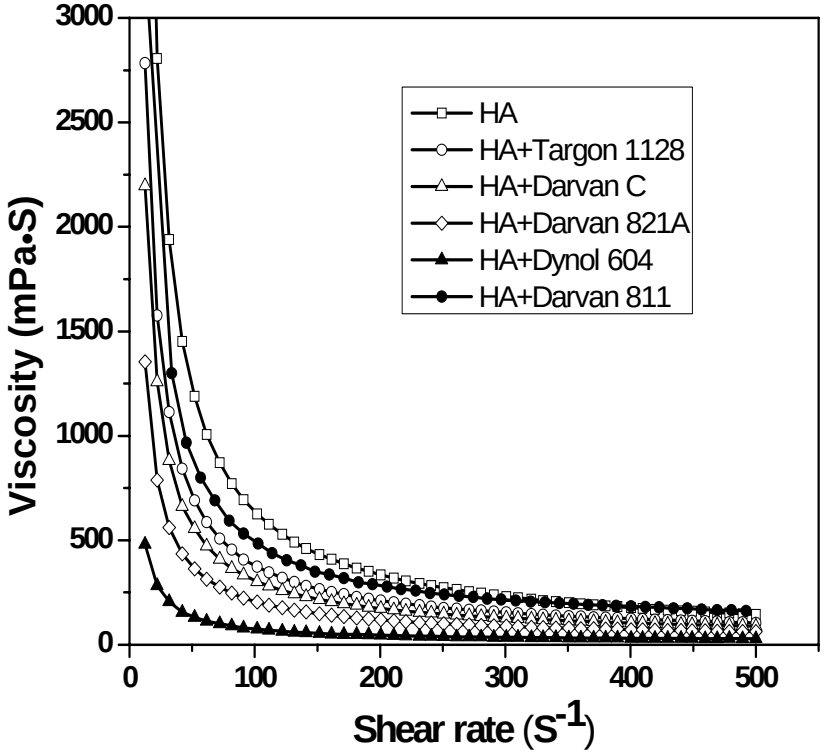

Figure 1. Viscosity of aqueous HA suspension (20 vol%) as a function of shear rate for different dispersants.

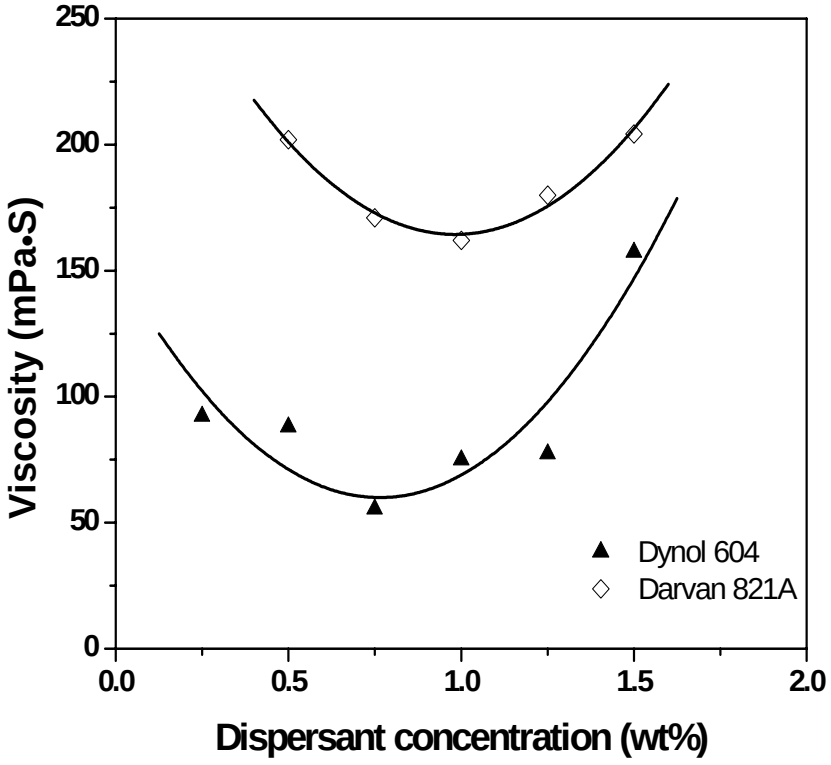

Figure 2. Viscosity of aqueous HA suspension (20 vol%) as a function of dispersant concentration for a shear rate of 100 s^{-1}.

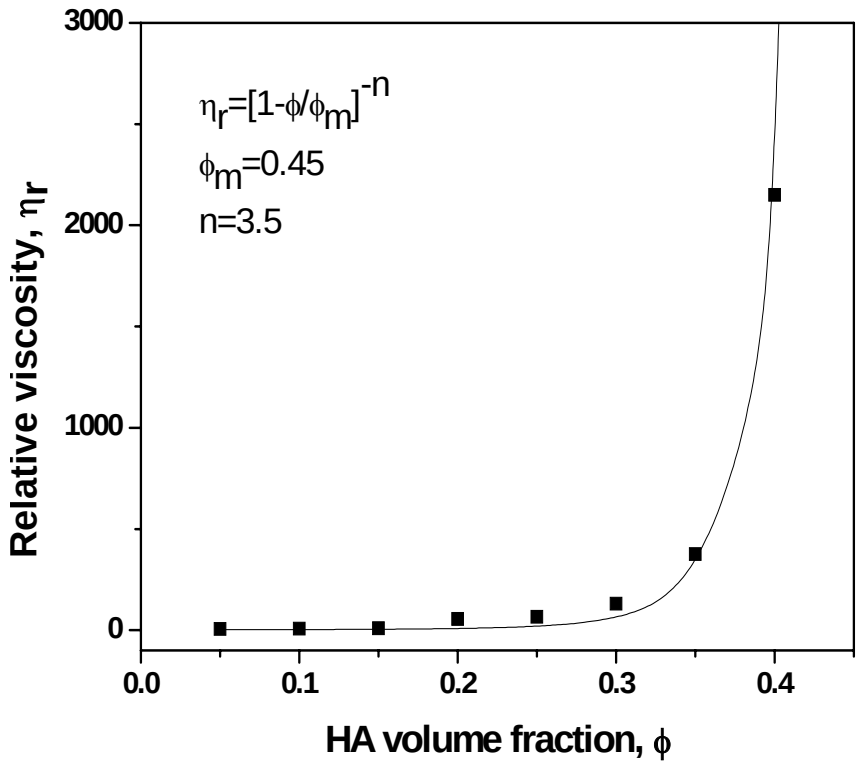

Figure 3. Relative viscosity at a shear rate of 100 s^{-1} versus volume fraction of HA particles stabilized by Dynol 604.

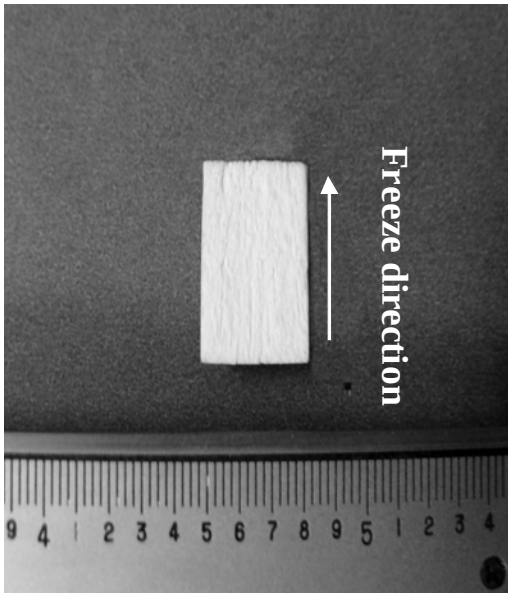

Figure 4. Optical image of a sintered HA sample, showing the shape uniformity. (Scale is in inches.)

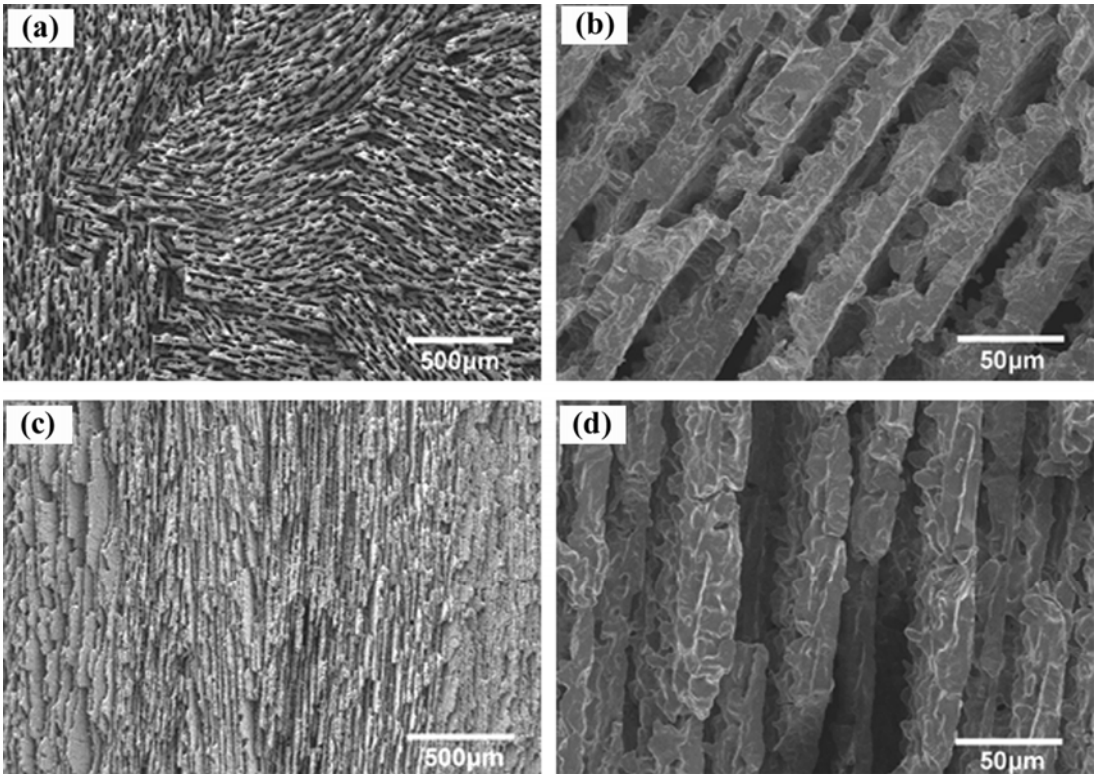

Figure 5. SEM images of the HA sample cross section perpendicular (a, b) and parallel (c, d) to the freezing direction. The sample was sintered for 3 h at 1350°C.

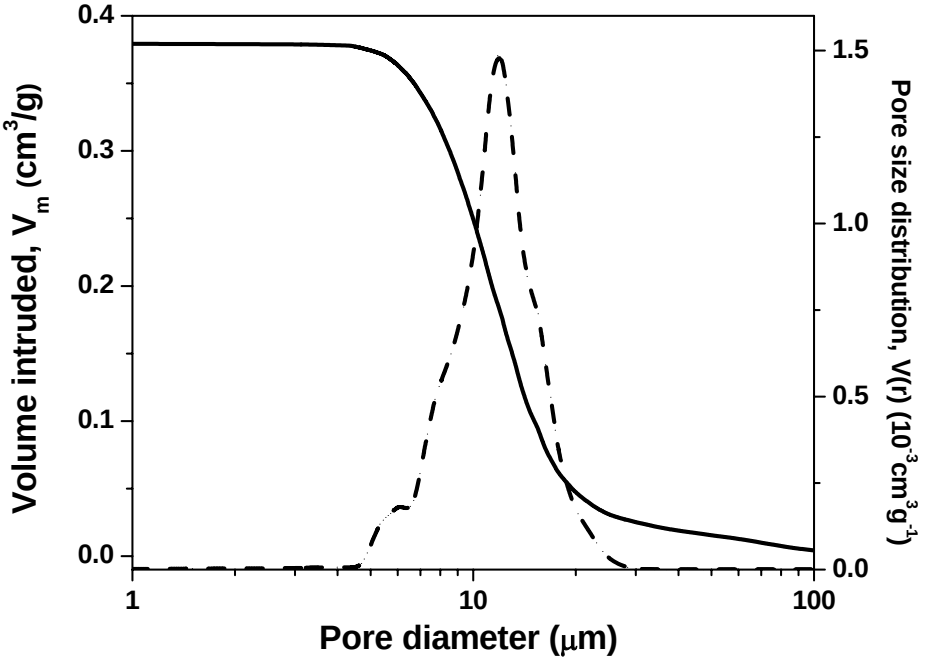

Figure 6. Mercury porosimetry data for the sintered HA sample, showing the pore volume and the pore size distribution as functions of the pore diameter.

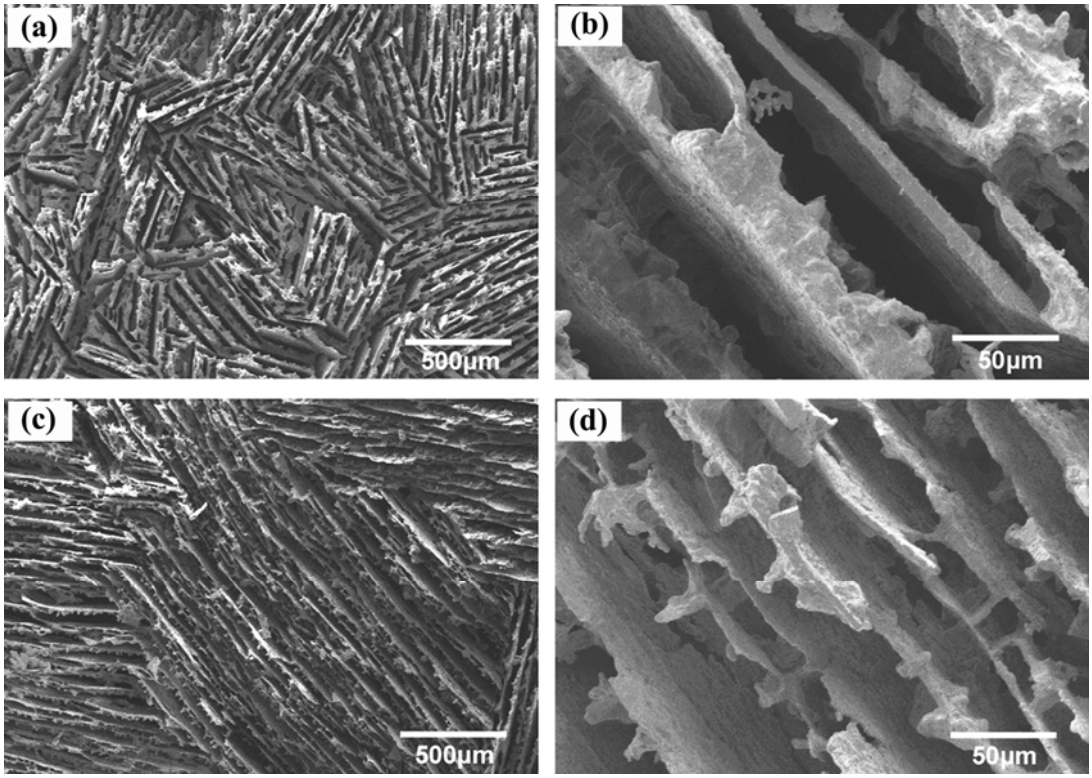

Figure 7. SEM images of the sintered HA sample fabricated from suspensions with different particle concentrations: (a), (b), 10 vol%; (c), (d), 5 vol%. (The cross section is perpendicular to the freezing direction.)

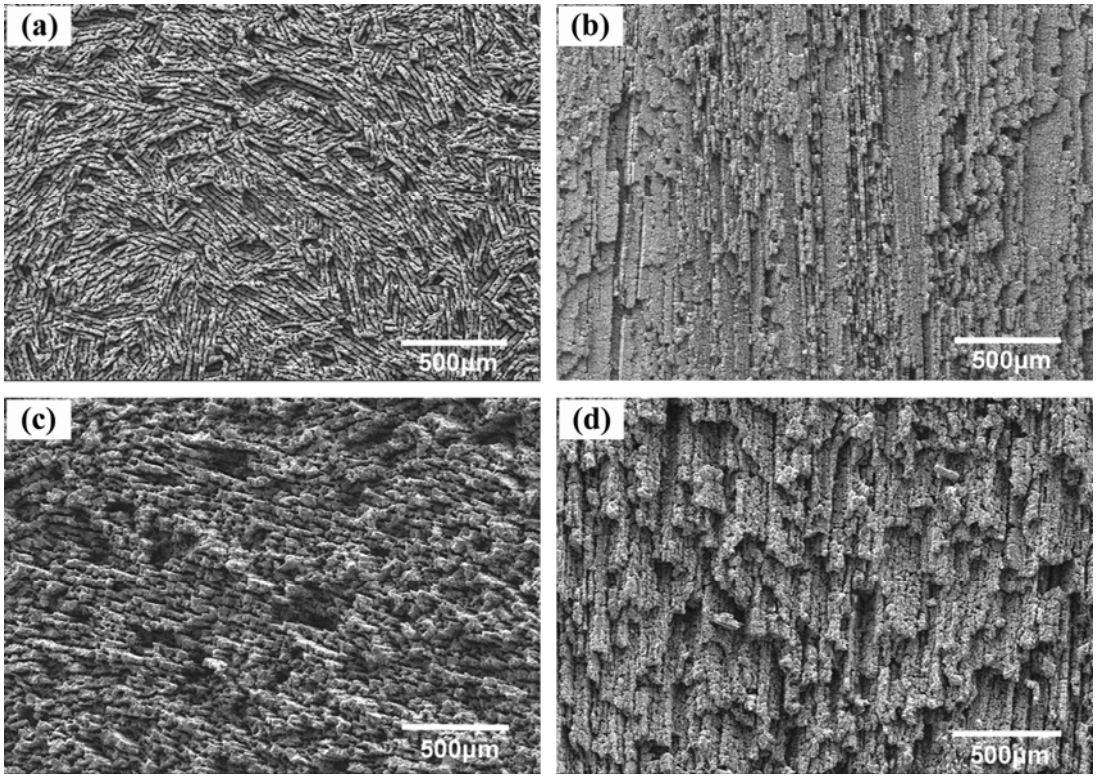

Figure 8. SEM images of the cross section perpendicular (a), (c), and parallel (b), (d), to the freezing direction, for sintered HA samples fabricated by freezing the suspension on substrates at (a), (b) –50°C; (c), (d) –196°C.

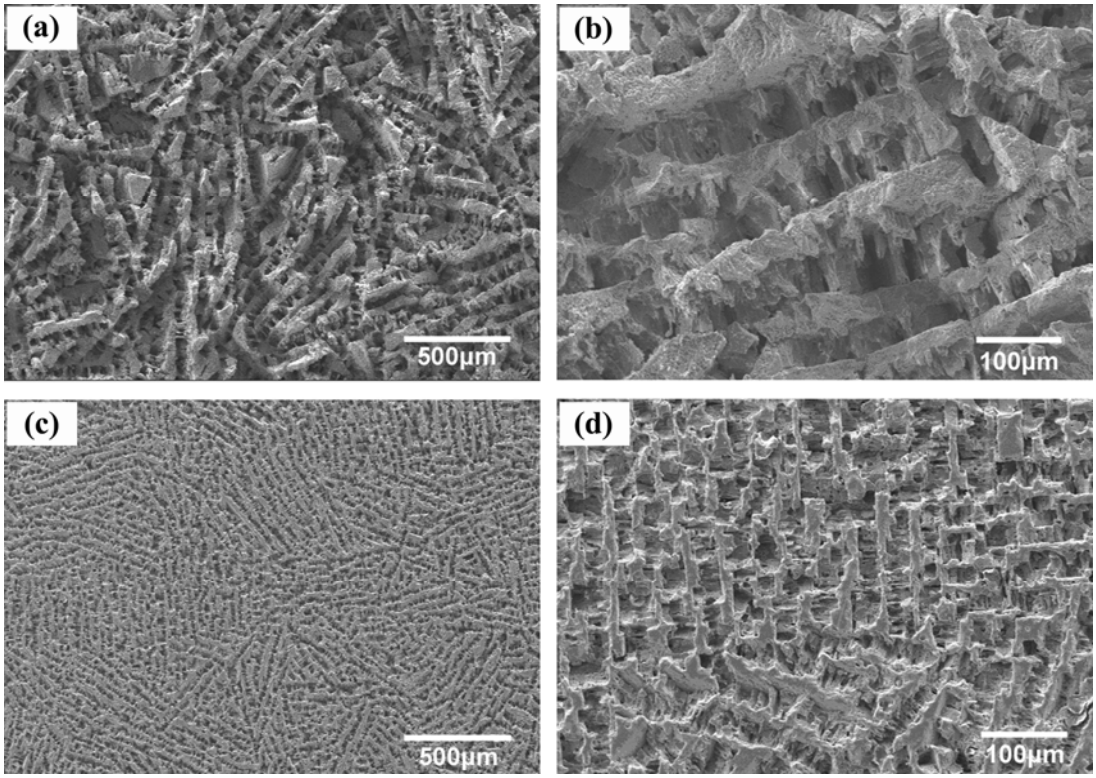

Figure 9. Effects of glycerol concentration on the microstructure of the sintered HA sample (a), (b) 5 wt%; (c), (d) 20 wt%. (The cross section is perpendicular to the freezing direction.)

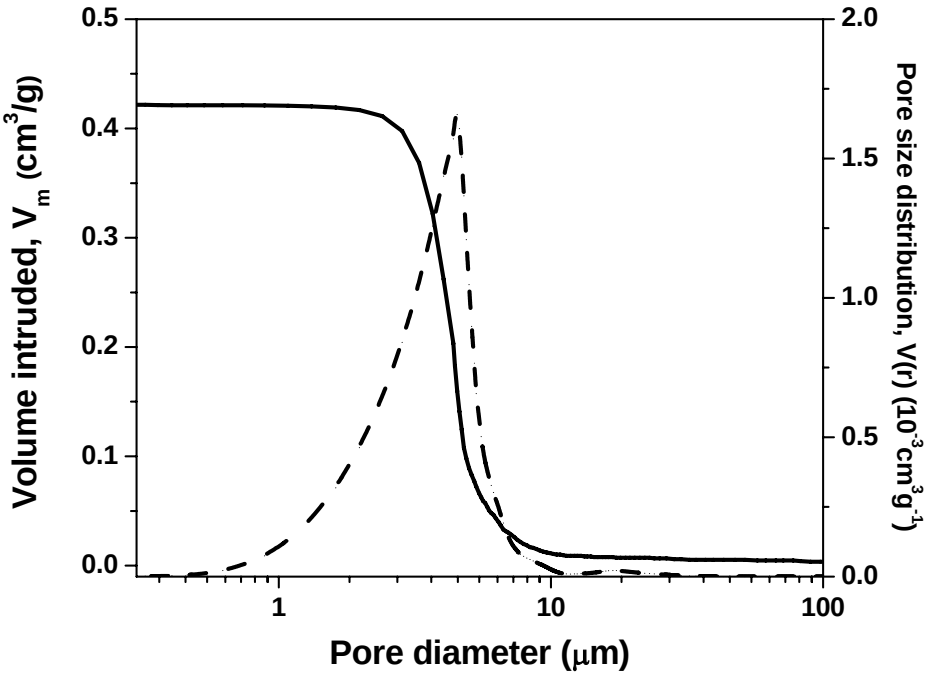

Figure 10. Mercury porosimetry data for the sintered HA sample prepared from suspensions with 20 wt% glycerol, showing the pore volume and the pore size distribution as functions of the pore diameter.

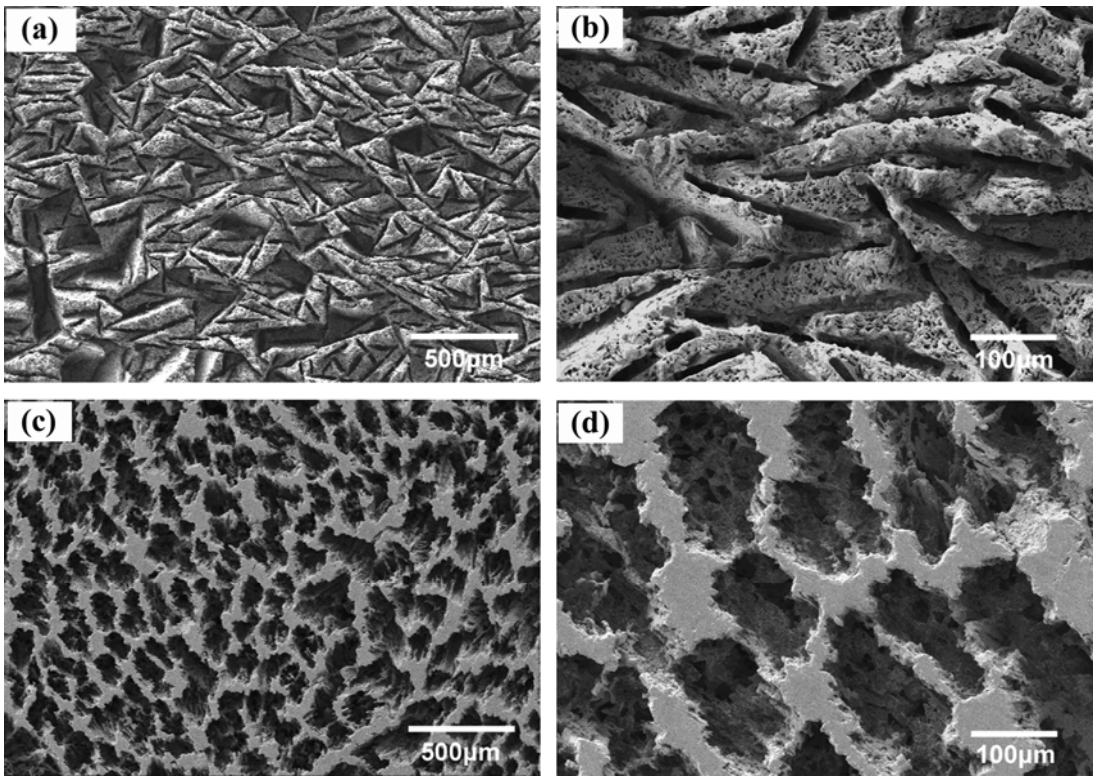

Figure 11. Effects of dioxane concentration on the microstructure of the sintered HA sample (a), (b) 30 wt%; (c), (d) 60 wt%. (The cross section is perpendicular to the freezing direction.)

2. FREEZE CASTING OF POROUS HYDROXYAPATITE SCAFFOLDS – II. SINTERING, MICROSTRUCTURE AND MECHANICAL BEHAVIOR

Qiang Fu[1], Mohamed N. Rahaman[1*], Fatih Dogan[1], and B. Sonny Bal[2]

[1]University of Missouri-Rolla, Department of Materials Science and Engineering, Rolla, Missouri 65409

[2]B. Sonny Bal, University of Missouri-Columbia, Department of Orthopaedic Surgery, Columbia, Missouri 65212

2.1. ABSTRACT

In Part I, the influence of processing parameters on the general microstructure of freeze-cast hydroxyapatite (HA) constructs was explored. This work is an extension of Part I, to investigate the effect of sintering conditions on the microstructure and mechanical behavior of freeze-cast HA. For constructs prepared from aqueous suspensions (5–20 vol% HA), sintering for 3 h at temperatures from 1250°C to 1375°C produced a decrease in porosity of <5% but an increase in strength of nearly 50%. Constructs with a porosity of 52%, had compressive strengths of 12 ± 1 MPa and 5 ± 1 MPa in the directions parallel and perpendicular to the freezing direction, respectively. The mechanical response showed high strain tolerance (5–10% at the maximum stress), high strain to failure (>20%), and high strain rate sensitivity. Manipulation of the freeze-cast microstructure, achieved by additions of glycerol and 1,4-dioxane to the aqueous

---

* Correspondence to: M.N. Rahaman (e-mail: rahaman@mst.edu)

suspensions, produced changes in the magnitude of the mechanical response, but little change in the general nature of the response. The favorable mechanical behavior of the porous constructs, coupled with the ability to modify their microstructure, indicates the potential of the present freeze casting route for the production of porous scaffolds for bone tissue engineering.

Keywords: biomaterials; scaffolds; hydroxyapatite; freeze casting; mechanical behavior

2.2. INTRODUCTION

In Part I, the influence of processing parameters on the general microstructure of porous hydroxyapatite (HA) constructs prepared by freeze casting of suspensions on a cold substrate was explored [1]. The effects of particle concentration of the suspension, temperature of the substrate, and modification of the solidification (freezing) behavior of the solvent by the addition of glycerol or 1,4-dioxane were investigated. Freeze casting of aqueous HA suspensions produced porous constructs with a uniform, lamellar-type microstructure in which plate-like HA lamellas were oriented in the direction of freezing. Changes in the particle concentration of the suspension and temperature of the cold substrate did not severely alter the lamellar-type microstructure but changed the porosity, the pore cross section, and thickness of the HA lamellas. With increasing particle concentration in the suspension (5–20 vol%), the porosity and pore cross-section of the constructs decreased, but the thickness of the HA lamellas increased. The addition of 5–20 wt% of glycerol to the aqueous suspension resulted in sintered constructs with finer pores and a larger number of dendritic structures connecting the HA lamellas. On the

other hand, the addition of 60 wt% of 1,4-dioxane to the aqueous suspension resulted in constructs with a cellular microstructure and larger pores. This work is an extension of Part I, to investigate the effect of sintering conditions on the final microstructure, and to characterize the mechanical behavior of the fabricated HA constructs.

In addition to being biocompatible, scaffold materials should have the ability to be formed into porous constructs with the relevant anatomical shape, as well as the ability to be formed economically and reproducibly. The fabricated scaffold should have the requisite microstructure to support tissue ingrowth. Interconnected or unidirectional pores with a mean diameter (or width) of 100 μm or greater, and open porosity of >50% are generally considered to be the minimum requirements to permit tissue ingrowth and function in porous scaffolds [2,3] Scaffolds for load-bearing applications such as bone repair and regeneration should also possess adequate mechanical properties to support physiological loads.

Bone is generally classified into two types: cortical bone, also referred to as compact bone, and trabecular bone, also referred to as cancellous or spongy bone. Cortical bone, found primarily in the shaft of long bones and as the outer shell around cancellous bone, is much denser, with a porosity of 5–10% [4]. Trabecular bone, found at the end of long bones, in vertebrae, and in flat bones such as the pelvis, is much more porous, with porosity in the range 50–90% [5]. The mechanical properties of bone vary between subjects, from one bone to another, and within different regions of the same bone. The mechanical properties are also highly anisotropic, as a result of the oriented microstructure. However, based on the testing of large specimens, the compressive strength and elastic modulus of cortical bone has been reported in the range 100–150

MPa and 10–20 GPa in the direction parallel to the orientation (long axis) axis [6-8]. The strength and modulus in the direction perpendicular to the long axis are typically 1.5 to 2 times lower. A wide range has been reported for the Young's modulus (0.1–5 GPa) and compressive strength (2–12 MPa) of cancellous bone [7,8].

A variety of methods have been used to produce porous scaffolds for bone repair and regeneration, including consolidation with a pore-producing phase such as NaCl, starch, or PVA, [9-11], the use of foaming agents [12-14], and solid freeform fabrication [15-17]. Table I provides a summary which is not meant to be exhaustive, but rather to indicate representative approaches. Freeze casting has been widely used for the production of synthetic polymer scaffolds, such as poly(lactic acid), PLA, poly(glycolic acid), PGA, and their coploymers, PLGA, as well as natural polymer scaffolds, such as collagen [21,23,35]. It has been applied more recently to the production of composites of HA and polymers (collagen or biodegradable polymers) [20, 24], and to bioceramic (HA) scaffolds [1,18,19]. The low strength (typically <1 MPa) of porous constructs of synthetic and natural polymers, and HA–polymer composites is a limitation for the repair of load-bearing bones. Recent investigations have shown that porous HA scaffolds, with a lamellar-type microstructure and unidirectional pores, can be obtained by freeze casting of aqueous suspensions [18,19]. The microstructure and strength of the scaffolds can be modified by altering the particle concentration of the suspension, freezing rate, and sintering conditions. Compressive strengths as high as 65 MPa (56% porosity) and 147 MPa (47% porosity) in the direction parallel to the freezing direction were obtained by testing small thin disks (4 mm × 5 mm × 5 mm) cut from the freeze-cast sample.

However, the pore width (or diameter) of these HA constructs (less than ~20 μm) is too low for tissue ingrowth.

The objective of the present work was to investigate the effect of sintering conditions on the microstructure of the freeze –cast HA constructs, and to characterize the mechanical behavior of the fabricated HA constructs. During sintering, it is expected that the HA lamellas, consisting of a packing of fine particles and fine pores, will undergo densification and grain growth, leading to an enhancement in strength. On the other hand, the unidirectional pores separating the HA plates are expected to undergo little change because the pore widths are much larger than the particle (or grain) size of the HA plates [36]. Because the properties of the sintered constructs are controlled by their microstructure, an understanding of the microstructural development during sintering, as well as the influence of the microstructure on properties, is important.

2.3. MATERIALS AND METHODS

Cylindrical HA constructs (~8 mm diameter × 16 mm) were prepared by freeze casting suspensions (20 vol% particles) on a cold steel substrate (–20°C), and subliming the frozen liquid. The solvent in the suspensions consisted of water, a mixture of water and 5–20 wt% glycerol, or a mixture of water and 40-60 wt% 1,4-dioxane (referred to henceforth as dioxane). The glycerol and dioxane additions were used to modify the freezing (or solidification) of water, which provided an additional method for manipulating the microstructure of the freeze cast constructs. The procedures were identical to those described in detail in Part I [1].

Sintering was carried out in air for 3 h at temperatures between 1250°C and 1375°C, with a heating and cooling rate of 3°C/min. The microstructures of the cross-section of the green and sintered constructs were observed using scanning electron microscopy, SEM (Hitachi S-4700, Hitachi Co., Tokyo, Japan). X-ray diffraction, XRD (D/mas 2550 v; Rigaku; The Woodlands, TX), was used to identify the phases present in the starting powder and sintered samples, using Cu K_α radiation (λ=0.15406 nm) at a scanning rate of 1.8°/min in the 2θ range of 10–80°. The volume of open porosity in the sintered samples was measured using the Archimedes method. The grain size of sintered constructs was measured using the linear-intercept method [24]. More than 200 grain boundary intercepts were measured for the polished samples sintered at different temperature to obtain a mean value and standard deviation.

The mechanical behavior of the sintered constructs (~8 mm in diameter × 16 mm) in compressive loading was measured according to ASTM-C773 using an Instron testing machine (Model 4204, Norwood, MA) at a crosshead speed of 0.5 mm/min. Eight samples were tested, and the average strength and standard deviation were determined. The samples were tested in the directions parallel and perpendicular to the freezing direction. The crosshead speed of 0.5 mm/min is typical for the testing dense specimens according to ASTM-C773. To investigate the strain-rate sensitivity of the compressive mechanical response, additional tests were performed at cross-head speeds of 0.05 mm/min and 5 mm/min. Cross-head speeds higher than 5 mm/min were impractical with the instrument and the size of specimens used.

The flexural strength of the sintered constructs was measured by loading unnotched cylindrical samples (~8 mm in diameter × 25 mm) at a crosshead speed of 0.5

mm/min in three-point bending (overall span = 20 mm) using an Instron testing machine (Model 4204). Eight specimens were tested. The flexural strength was determined from the equation

$$\sigma = \frac{8PL}{\pi d^3}$$

where P is the loading applied to the specimens, L is the overall span and d is the diameter of the specimens.

Strength and porosity values were determined as means ± standard deviations. Statistical analysis was carried our using one-way analysis of variance (ANOVA) and Turkey's post hoc test, with the level of significance set at $p < 0.05$.

2.4. RESULTS

Figure 1 shows the XRD patterns of the as-received HA powder, the powder calcined for 1 h at 900°C, and of the freeze-cast material sintered for 3 h at 1375°C, the highest sintering temperature used in the experiments. Each pattern corresponded to the reference pattern of HA (JCPSD 72-1243). The XRD peaks for the as-received powder were broader and had a lower intensity (peak height) than those for the sintered material, which is an indication that the as-received powder may have a size in the nanocrystalline range, incompletely crystallized, or a combination of both. Within the limits of detection by the XRD (< 0.5 wt%), no additional peaks corresponding to any second phases could be found in the patterns. It has been reported that HA decomposed into tricalcium phosphate and tetracalcium phosphate at temperatures above ~1300°C [37], and that this decomposition resulted in a sharp drop in strength and affected the osteocalstic resorption activity of HA [38,39]**.** However, for the HA powder used in the present work, the results

indicated that sintering temperatures as high as 1375°C can be used without detectable decomposition. *In vitro* cell culture experiments are currently being performed to evaluate the effect of the sintered HA constructs on cell viability, and the ability of the constructs to support cell infiltration into the unidirectional pores.

The effect of the sintering temperature on the open porosity and compressive strength of HA constructs sintered for 3 h at temperatures between 1250°C and 1375°C is shown in Figure 2. The constructs were prepared from aqueous suspensions containing 20 vol% HA. With increasing temperature, the porosity decreased slightly, from a value of 55% at 1250°C to a limiting value of ~52% at 1350°C. This is an indication that the HA plates in the lamellar-type microstructure had reached their highest density at 1350°C. Sintering for much longer time at 1350°C or at higher temperatures will lead primarily to grain growth in the HA lamellas, without any increase in density. Therefore, sintering for 3 h at 1350°C can be taken as approximately the optimum sintering conditions for the present system. The compressive strength in the direction of freezing increased with sintering temperature (Figure 2), reaching its highest value of 12 ± 1 MPa at 1350°C, and showed no further improvement as the sintering temperature was increased to 1375°C. This increase in the compressive strength is a reflection of the decrease in porosity, indicating that the strength improvement is controlled by the increase in density of the HA lamellas.

As observed in Part I [1], the addition of glycerol to the aqueous solvent produced a modification of the freeze-cast microstructure, giving smaller pore diameters and resulting in a larger number of dendrites connecting the HA plates. Figure 3 shows the effect of glycerol additions on the porosity and compressive strength of the constructs

sintered for 3 h at 1350°C. The constructs were prepared from suspensions with 20 vol% solids. The porosity decreased by ~6%, from ~52% to ~46%, as the glycerol concentration in the solvent increased from 0 to 20 wt%. On the other hand, the compressive strength (in the direction of freezing) increased by ~50%, from 12 ± 1 MPa to 18 ± 2 MPa . This increase in the strength can be attributed to the finer pores, the lower porosity, the larger number of dendrites connecting the HA lamellas or a combination of the three.

Figure 4 shows stress–strain curves in compression testing for freeze-cast HA constructs prepared from aqueous suspensions (20 vol% HA) without glycerol and sintered for 3 h at 1350°C. The curves show the behavior of the constructs in the direction parallel and perpendicular to the freezing direction. The data shown are engineering stresses and strains, based on the initial cross-sectional area and length of the test sample, and do not represent the true stresses and strains. An interesting feature of the stress-strain response is the high strain tolerance of the constructs. Unlike common ceramics which show brittle behavior with just an elastic response and failure at low strain (typically <0.1%), the constructs produced in the present work showed three distinct regions: an elastic regime in which the stress–strain response was linear, a stress plateau region representing a region of highest sustainable loading, and a failure region of decreasing load-beating ability. The elastic modulus, determined from the slope of the linear region, was 0.2 GPa. While the three regions can be observed in both curves, the stress-strain curve in the freezing direction had a different shape from that perpendicular to the freezing direction. In the freezing direction, the curve had a more smoothly varying, asymmetric bell shape, with a compressive strength (taken as the stress at the

peak) of ~10 MPa at a strain of ~7%. In contrast, the curve for the perpendicular testing direction had a large plateau region, in a strain range of 2–10%, with numerous bumps and valleys. The average compressive strength in this plateau region was ~4 MPa. The small peaks and valleys in the curve presumably resulted from progressive breakage of the HA lamellas and the dendrites between the lamellas.

Figure 5 shows the effect of strain rate on the compressive mechanical response (in the direction of freezing) for constructs prepared from aqueous suspension (20 vol% HA). The response was quite sensitive to the rate of loading (taken as proportional to the cross-head speed). With increasing strain rate, the peak compressive stress increased in magnitude and shifted to lower strain. For the same specimen length (16 mm), increasing the cross-head speed from 0.05 mm/min to 0.5 mm/min and 5mm/min, produced an increase in the peak compressive stress of ~25 and ~125% respectively. On the other hand, the strain at the peak compressive stress decreased from 8% to 5% and 2%, respectively.

Figure 6 shows the stress-strain curve in three-point bending for freeze-cast HA constructs prepared from aqueous suspensions (20 vol% HA) without glycerol and sintered for 3 h at 1350ºC. The constructs showed a high strain tolerance (~6%) in flexure, similar in nature to the response observed in compression testing, indicating that the high strain tolerance is not just restricted to compression. The small peaks and valleys in stress–strain curve presumably resulted to crack deflection during delamination of the HA lamellas. The flexural strength (taken as the stress at the peak of the stress–strain curve) was 2.5 ± 0.9 MPa at a strain of ~6%.

The stress–strain behavior in compression for constructs prepared from suspensions (20 vol% HA particles) with 20 wt% glycerol and sintered for 3 h at 1350°C is shown in Figure 7. In general, the curves showed features similar to those for constructs prepared without glycerol, but the load-bearing capacity was higher. The compressive strengths in the directions parallel and perpendicular to the freezing direction were 18 ± 2 MPa and 7 ± 1 MPa, respectively, compared to values of 12 ± 1 MPa and 5 ± 1 MPa for similar constructs prepared from suspensions without glycerol. The elastic modulus in the direction of freezing, determined from the linear region of the curve, was 0.6 GPa. The use of glycerol also improved the strain tolerance, with the constructs able to support a stress of ~6 MPa at a strain as high as 20%.

Figure 8 shows the stress-strain curves, in the direction of freezing, for constructs prepared from suspensions (10 vol% HA particles) in which the solvent was 40 wt% water and 60 wt% dioxane. The mechanical response of these constructs showed a higher strain tolerance (~60%) than constructs prepared from aqueous suspensions (Figure 4) or from suspensions with glycerol (Figure 6). As observed for the testing of constructs prepared from aqueous suspensions (Figure 5), the mechanical response is also sensitive to the rate of loading. The stress–strain curve consisted of three distinct regions: an approximately linear regime, a plateau region in which the stress was almost constant with increasing strain, and a region of sharply rising stress. For testing at a cross-head speed of 0.5 mm/min, the peak compressive stress was 7.5 MPa at a strain of 8%. The elastic modulus, determined from the approximately linear region, was 0.1 GPa.

SEM images of the top and middle portions of an HA construct after completion of the compressive strength testing are shown in Figure 9. The construct was prepared

from aqueous suspensions (without glycerol or dioxane) containing 20 vol% HA, A highly tortuous surface was observed at the top surface (Figure 9(a)), unlike the relatively smooth fracture surface commonly observed for brittle materials. The middle portion of the broken construct (Figure 9(b)), showed almost equally-spaced cracks, perpendicular to the length of the HA lamellas. Furthermore, the cracks did not propagate across the entire sample. Instead, they appeared to terminate after traversing each HA lamella.

The fractured surfaces, following compressive strength testing, for the sintered constructs prepared from suspensions (20 vol% HA) with 20 wt% glycerol are shown in Figure 10. The top part of the fractured surface (Figure 10(a)) appeared to show tortuous crack patterns, not unlike those in Figure 9(a). Dendrites between the HA plates were also observed. When compared to the HA constructs prepared from suspensions without glycerol (Figure 9(b)), no cracks perpendicular to the length of the HA lamellas were observed (Figure 10(b)).This is presumably due to the fine pores and the presence of a larger number of dendrites between the HA lamellas, which provided an alternative fracture mechanism.

2.5. DISCUSSION

The present freeze casting route relied on densifying the HA lamellas, with little modification of the macropores between the lamellas, for developing the optimum strength of the construct. The results indicated that the optimum strength was achieved without any detectable change in the XRD pattern of the material by sintering for 3 h at 1350°C. For constructs prepared from aqueous suspensions (20 vol% HA) without glycerol or dioxane, the compressive strength in the direction of freezing (12 ± 1 MPa)

was at the upper limit of the values for cancellous bone (2–12 MPa) [8], whereas the elastic modulus (0.2 GPa) was closer to the lower limit for cancellous bone (0.1–5 GPa) [8]. The porosity (55%) was at the lower end for cancellous bone (50–90%), but the pore size (15 ± 10 μm) was considered to be too low to support tissue ingrowth [40,41].

Because of differences in pore characteristics (such as porosity and pore size), a true comparison cannot be made between the strength values obtained in the present work and those summarized in Table I for constructs fabricated by a variety of methods. Nevertheless, the compressive strengths of the HA scaffolds fabricated in the present work were at least one order of magnitude higher than the values for polymer scaffolds or polymer–ceramic composites prepared by a unidirectional freeze casting method [20-24]. The strengths obtained in the present work were also one order of magnitude higher than those for porous bioceramic constructs with a more isotropic microstructure, such as those fabricated by infiltration of a polymer sponge or by a gas foaming technique [12,25-27,28-30]. Furthermore, the strengths were comparable to the values for porous bioceramic constructs fabricated by solid freeform fabrication routes and by more conventional methods [15-17,31-34].

When compared to the results of Deville et al. [18,19], who reported compressive strengths of 65 MPa (56% porosity) and 147 MPa (47% porosity) for HA constructs in the direction of freezing, the strengths obtained in this work were far lower. One factor which might contribute to the difference is the cooling rate of the suspension. The results of Deville et al. [18] showed a large increase in strength with increasing cooling rate, and the high strengths reported were for the highest cooling rate used. Faster cooling rates lead to the production of constructs with finer pores. While the strength was higher, the

finer pores were less favorable for supporting tissue ingrowth. In the present work, the suspensions were frozen on a substrate at a fixed temperature (–20°C), and the cooling rate corresponded approximately to the lowest cooling rates used by Deville et al. [18]. The compressive strengths obtained in the present work are comparable to the values reported by Deville et al. for the lowest cooling rates used in their work. There was also a difference between the sizes of the specimens used in the two studies. Deville et al. [18] used test samples (4 × 5 × 5 mm) cut from the sintered material in which the height to the cross-sectional width was only 0.8. In the present work, the as-fabricated specimens were tested according to ASTM-C773 in which the height to diameter ratio was >2.

An interesting property of the HA constructs prepared in this work was the high strain tolerance, leading to a high strain to failure (Figure 4). SEM images of the constructs after compressive strength testing (Figure 9(a)) showed a highly tortuous crack path. This type of tortuous fracture surface provided a large increase in the crack path, and has been proposed as an effective toughening mechanism in biological composites [42]. Furthermore, deflection, branching, and blunting of the cracks were also observed in the constructs after testing (Figure 9(b)). These toughening mechanisms, coupled with the fine, homogeneous microstructure presumably resulted in delocalized failure, which provided the high strain tolerance observed in the stress–strain curves.

Similar to the behavior of bone [43,44] and other natural materials, the mechanical response of the HA constructs fabricated in this work was quite sensitive to the rate of loading (Figure 5). The elastic modulus and the compressive strength were observed to increase with higher loading rate but the strain to failure decreased. Since HA

itself is brittle, the strain rate sensitivity resulted from the lamellar-type microstructure developed by the freeze-casting route.

The use of glycerol to modify the freezing behavior of the solvent resulted in the production of HA constructs with higher compressive strength and higher strain tolerance (Figure 7). The enhanced mechanical response presumably resulted from the lower porosity, smaller pores, and the larger number of dendrites between the HA lamellas [1]. More numerous peaks and valleys were also observed in the stress–strain curves (Figure 7), particularly in testing parallel the freezing direction, which presumably resulted from the progressive rupture of the larger number of dendrites between the HA lamellas. The additional work required to rupture these dendrites presumably provided a strong contribution to the increase in compressive strength and strain tolerance [45].

As described in Part I [1], addition of dioxane (60 wt%) to the aqueous suspension resulted in the production of HA constructs with a cellular microstructure and larger pores. Constructs prepared from suspensions with 10 vol% HA had a porosity of 65% and an average pore diameter of (100 ± 10 μm). These pore characteristics are considered to be more favorable for tissue ingrowth [2,3] when compared to the fine pores obtained in constructs prepared from aqueous suspensions with or without glycerol additions. The mechanical response of the HA constructs (Figure 8) was similar in nature to the response of bone and other natural materials such as wood and cork [46], as well as the response of synthetic scaffolds with an oriented microstructure prepared by solid freeform fabrication techniques [31]. Furthermore, for a cross-head speed of 0.5 mm/min, the compressive strength (7.5 MPa), taken as the value at the peak stress, and the strain (8%) at the peak compressive stress were in upper range of values for human cancellous

bone (compressive strength = 2–12 MPa and strain to failure = 5–7%) [8]. Based on their microstructure and mechanical response, these porous HA constructs prepared from aqueous suspensions with 60 wt% dioxane may provide favorable substrates for tissue engineering of bone. Experiments are currently being performed to evaluate the biocompatibility of the constructs, and to optimize their mechanical response.

2.6. CONCLUSIONS

The compressive strength of freeze-cast HA constructs was strongly dependent on the sintering temperature used to densify the HA. Optimum strength was obtained after sintering for 3 h at 1350°C, presumably due to the HA lamellas in the porous structure reaching nearly full density. XRD indicated that no new phase was formed in the HA constructs after sintering at 1350°C. Constructs prepared from aqueous suspensions had compressive strengths of 12 ± 1 MPa and 5 ± 1 MPa in the directions parallel and perpendicular to the freezing direction, respectively, a flexural strength of 2.5 ± 0.9 MPa, and strain to failure of >20%. However, the porosity (52%) and pore size (5–30 μm) were considered to be too low to support tissue ingrowth. Constructs prepared from aqueous suspensions with 20 wt% glycerol had higher strength, but lower porosity and finer pores. HA constructs prepared from aqueous suspensions (10 wt% particles) with 60 wt% dioxane had a compressive strength of 7.5 MPa, strain to failure of 60%, and favorable microstructure for tissue ingrowth (porosity ~ 65% and pore size = 100 ± 10 μm). The mechanical response of the HA constructs was similar in nature to that for bone and other natural materials (high strain to failure and strain rate sensitivity). The favorable mechanical response of the porous constructs, coupled with the ability to modify the

microstructure and mechanical properties indicates the potential of the present freeze casting route for the fabrication of porous scaffolds for bone tissue engineering.

2.7. REFERENCES

1. Fu Q, Rahaman MN, Dogan F, Bal BS. Freeze casting of porous hydroxyapatite scaffolds – I. Processing and general microstructure. J Biomed Mater Res Part B: Appl Biomater 2007. Forthcoming.
2. Hollinger JO, Leong K. Poly(α-hydroxy acids): carriers for bone morphogenetic proteins. Biomaterials 1996;17:187-194.
3. Hu YH, Grainger DW, Winn SR, Hollinger JO. Fabrication of poly(α-hydroxy acid) foam scaffolds using multiple solvent systems. J Biomed Mater Res 2002;59:563-572.
4. Martin RB, Burr DB, Sharkey NA. Skeletal Tissue Mechanics. New York, Springer-Verlag, 1998.
5. Goldstein SA. The mechanical properties of trabecular bone: dependence on anatomic location and function. J Biomech 1987;20:1055-1062.
6. Reilly DT, Burstein AH, Frankel VH. The elastic modulus of bone. J Biomech 1974;7:271-275.
7. Rho JY, Hobatho MC, Ashman RB. Relations of density and CT numbers to mechanical properties for human cortical and cancellous bone. Med Eng Phys 1995;17:347-355.
8. Fung YC. Biomechanics: Mechanical Properties of Living Tissues. New York: Springer; 1993:500.
9. Mikos AG, Sarakinos G, Leite SM, Vacanti JP, Langer R. Laminated three-dimensional biodegradable foams for use in tissue engineering. Biomaterials 1993;14:323-330.
10. Rodríguez-Lorenzo LM, Vallet-Regí M, Ferreira JMF. Fabrication of porous hydroxyapatite bodies by a new direct consolidation method: starch consolidation. J Biomed Mater Res 2002; 60(2): 232-240
11. Li SH, De Wijn JR, Layrolle P, De Groot K. Synthesis of macroporous hydroxyapatite scaffolds for bone tissue engineering. J Biomed Mater Res 2002; 61(1): 109-120
12. Sepulveda P, Binner JG, Rogero SO, Higa OZ, Bressiani JC. Production of porous hydroxyapatite by the gel-casting of foams and cytotoxic evaluation. J Biomed Mater Res 2000;50: 27–34.
13. Almirall A, Larrecq G, Delgado JA, Martinez S, Planell JA, Ginebra MP. Fabrication of low temperature macroporous hydroxyapatite scaffolds by foaming and hydrolysis of an α-TCP paste. Biomaterials 2004; 25(17): 3671-3680
14. Ebaretonbofa E, Evans JRG. High porosity hydroxyapatite foam scaffolds for bone substitute. J Porous Mater 2004; 9(4): 257-263

15. Hutmacher DW, Schantz T, Zein I, Ng KW, Teoh SH, Tan KC. Mechanical properties and cell cultural response of polycaprolactone scaffolds designed and fabricated via fused deposition modeling. J Biomed Mater Res 2001;55:203-216
16. Chu T-MG, Oron DG, Hollister SJ, Feinberg SE, Halloran JW. Mechanical and *in vivo* performance of hydroxyapatite implants with controlled architectures. Biomaterials 2002;23:1283-1293.
17. Woodard JR, Hilldore AJ, Lan SK, Park CJ, Morgan AW, Eurell JAC, Clark SG, Wheeler MB, Jamison RD, Johnson AJ. The mechanical properties and osteoconductivity of hydroxyapatite bone scaffolds with multi-scale porosity. Biomaterials 2007;28:45-54.
18. Deville S, Saiz E, Tomsia A. Freeze casting of hydroxyapatite scaffolds for bone tissue engineering. Biomaterials 2006;27:5480-5489.
19. Deville S, Saiz E, Nalla RK, Tomsia A. Freezing as a path to build complex composites. Science 2006;311:515–518.
20. Zhang R, Ma PX. Poly(α-hydroxyl acids)/hydroxyapatite porous composites for bone-tissue engineering. I. Preparation and morphology. J Biomed Mater Res 1999;44:446-455
21. Ma PX, Zhang R. Microtubular architecture of biodegradable polymer scaffolds. J Biomed Mater Res 2001;56:469-477.
22. Blaker JJ, Maquet V, Jérôme R, Boccaccini AR, Nazhat SN. Mechanical properties of highly porous PDLLA/Biolgass® composite foams as scaffolds for bone tissue engineering. Acta Biomater 2005;1:643-652
23. Yang F, Qu X, Cui W, Bei J, Yu F, Lu S, Wang S. Manufacturing and morphology structure of polylactide-type microtubular orientation-structure scaffolds. Biomaterials 2006;27:4923-4933
24. Yunoki S, Ikoma T, Tsuchiya A, Monkawa A, Ohta K, Sotome S, Shinomiya K, Tanaka J. Fabrication and mechanical and tissue ingrowth properties of unidirectionally porous hydroxyapatite/collagen composite. J Biomed Mater Res Part B: Appl Biomater 2007;80B:166-173.
25. Kim HW, Knowles JC, Kim HE. Hydroxyapatite porous scaffold engineered with biological polymer hybrid coating for antibiotic vancomycin release. J Mater Sci Mater Med 2005;16:189–195.
26. Callcut S, Knowles JC. Correlation between structure and compressive strength in a reticulate glass-reinforced hydroxyapatite foam. J Mater Sci: Mater Med 2002;13:485–489.
27. Ramay HRR, Zhang M. Preparation of porous hydroxyapatite scaffolds by combination of the gel-casting and polymer sponge methods. Biomaterials 2003;24:3293–3302.
28. Chen QZ, Thompson ID, Boccaccini AR. 45S5 Bioglass®-derived glass-ceramic scaffold for bone tissue engineering. Biomaterials 2006; 27(11): 2414-2425
29. Wu C, Chang J, Zhai W, Ni S, Wang J. Porous akermanite scaffolds for bone tissue engineering: preparation, characterization, and *in vitro* studies. J Biomed Mater Res Part B: Appl Biomater 2006;78B:47-55
30. Sepulveda P, Ortega FS, Innocentini MDM, Pandolfelli VC. Properties of highly porous hydroxyapatite obtained by the gelcasting of foams. J Am Ceram Soc 2000;83:3021-3024

31. Fu Q, Rahaman MN, Bal BS, Huang W, Day DE. Preparation and bioactive characterization of a porous 13-93 glass, and fabrication into the articulating surface of a proximal tibia. J Biomed Mater Res Part A 2007;82A:222-229
32. Cyster LA, Grang DM, Howdle SM, Rose FRAJ, Irvine DJ, Freeman D, Scotchfor CA, Shakesheff KM. The influence of dispersant concentration on the pore morphology of hydroxyapatite ceramics for bone tissue engineering. Biomaterials 2005;26:697-702
33. Harris LD, Kim BS, Mooney DJ. Open pore biodegradable matrices foamed with gas foaming. J Biomed Mater Res 1998;42(3)396-402
34. Chang BS, Lee CK, Hong KS, Youn HJ, Syu HS, Chung SS, Park KW. Osteoconduction at porous hydroxyapatite with various pore configurations. Biomaterials 2000;21:1291-1298.
35. Schoof H, Apel J, Heschel I, Rau G. Control of pore structure and size in freeze-dried collagen sponges. J Biomed Mater Res Appl Biomater 2001; 58: 352-357
36. Rahaman MN. Ceramic Processing and Sintering. 2nd ed. New York: Marcel Dekker; 2003:591-592.
37. Chaki TK, Wang PE. Densification and strengthening of silverreinforced hydroxyapatite-matrix composite prepared by sintering. J Mater Sci Mater Med 1994;5:533–542.
38. Ruys AJ, Wei M, Sorrell CC, Dickson MR, Brandwood A, Milthorpe BK. Sintering effects on the strength of hydroxyapatite. Biomaterials 1995;16: 409-415.
39. Yamada S, Heymann D, Bouler JM, Daculsi G. Osteoclastic resorption of calcium phosphate ceran&s with different Hydroxyapatite/tricalciumphosphate ratios. Biomaterials 1997;18:1037-1041.
40. Hulbert SF, Young FA, Mathews RS, Klawitter JJ, Talbert CD, Stelling FH. Potential of ceramic materials as permanently implantable skeletal prostheses. J Biomed Mater Res 1970;4:433–456
41. Hollinger JO, Brekke J, Gruskin E, Lee D. Role of bone substitutes. Clin Orthop Relat Res. 1996;324:55-65.
42. Sarikaya M. An introduction to biomimetics: a structural viewpoint. Microc Res Techn 1994;27:360-375.
43. Carter DR. Bone compressive strength: the influence of density and strain rate. Science. 1976;194:1174-1176
44. Linde F, Norgaard P, Hvid I, Odgaard A, Soballe K. M Mechanical properties of trabecular bone. Dependency on strain rate. J Biomech 1991;24:803-809
45. Wachtman JB. Mechanical Properties of Ceramics. New York: Wiley; 1996:159-163.
46. Gibson LJ, Ashby MF. Cellular Solids: Structure and Properties. New York: Cambridge University Press, 1997.

Table I. Summary of pore characteristics and compressive strength of porous scaffolds fabricated by a variety of methods.

Technique	Material	Open porosity (%)	Pore size or dimension (μm)	Compressive strength (MPa)	Reference
Freeze casting	HA	47-52	5-30	12-18	Present
	HA	50-65	80-110	7.5-20	work
	HA	40-65	20	40-145	[18, 19]
TIPS	PLLA/HA (50:50)	90	50-200	0.4	[20]
	PLGA	93-94	50-60	0.38-0.58	[21]
	PDLLA/Biolgass®	93.5-94		0.07-0.08	[22]
	PLGA	90-96	114-137	0.2-0.9	[23]
	HA/Collagen	95	200-500	0.03	[24]
Polymer sponge	HA	86	420-560	0.21	[25]
	Glass reinforced HA	85-97.5	420-560	0.01-0.175	[26]
	HA	70-77	200-400	0.55-5	[27]
	45S5 Bioglass®	89-92	510-720	0.27-0.42	[28]
	$Ca_2MgSi_2O_7$	63-90	300-500	0.53-1.13	[29]
Gel casting	HA	76-80	20-1000	4.4-7.4	[17]
	HA	72-90	17-122	1.6-5.8	[30]
Solid free-form fabrication	PCL	61	360×430×620	3.1	[15]
	HA	35	334×469	30	[16]
	HA	41	250-350	34	[17]
Slip casting	13-93 glass	40-45	100-300	21-23	[31]
	HA	85	200-500	1.09-1.76	[32]
Gas foaming	PLGA	85-96	193-439	0.16-0.29	[33]
Fiber compacting	HA	13-33	50-500	6-13	[34]

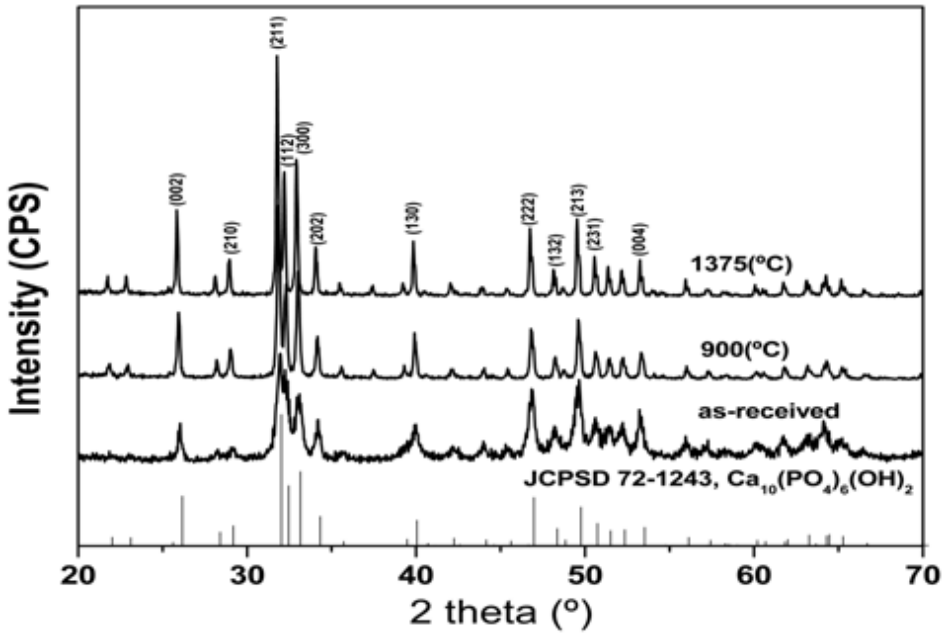

Figure 1. X-ray diffraction (XRD) patterns of the as-received HA powder, the powder heated for 1 h at 900°C, and the freeze-cast construct sintered for 3 h at 1375°C.

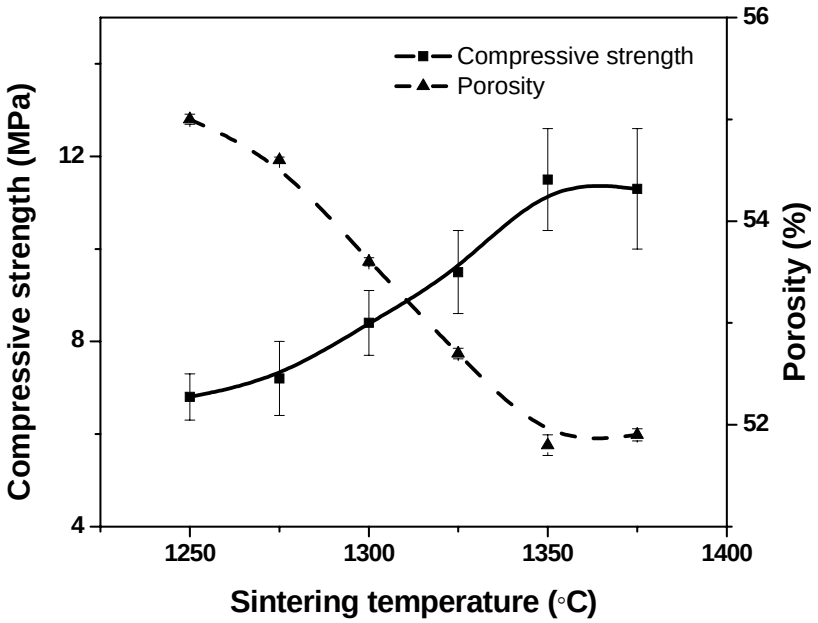

Figure 2. Influence of sintering temperature on the porosity and compressive strength (in the direction of freezing) for HA constructs prepared from aqueous suspensions with 20 vol% particles. All pairs of the porosity were significantly different except the pair between HA constructs sintered at 1350 and 1375 ºC (p = 0.99); all pairs of compressive strength were significantly different except the pairs between 1250 and 1275 ºC, 1300 and 1325, 1350 and 1375 ºC (p = 0.97, 0.22, 1.0 respectively).

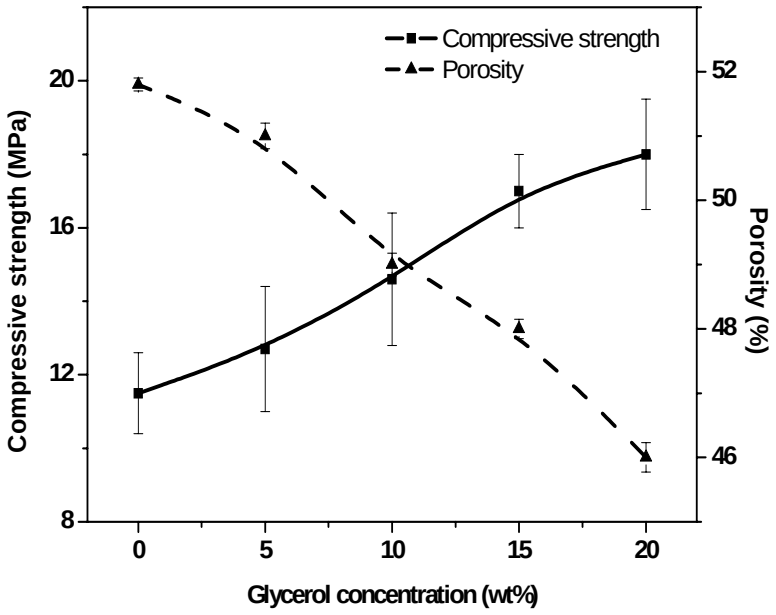

Figure 3. Effect of glycerol addition to the aqueous suspension (20 vol% particles) on the porosity and compressive strength of constructs sintered for 3 h at 1350°C. All pairs of the porosity of the HA constructs with different glycerol addition were significantly different; all pairs of the compressive strength of HA construct were significantly different except the pairs between HA constructs prepared from 0 and 5, 5 and 10, 15 and 20 wt% glycerol (p = 0.69, 0.28, 0.50 respectively).

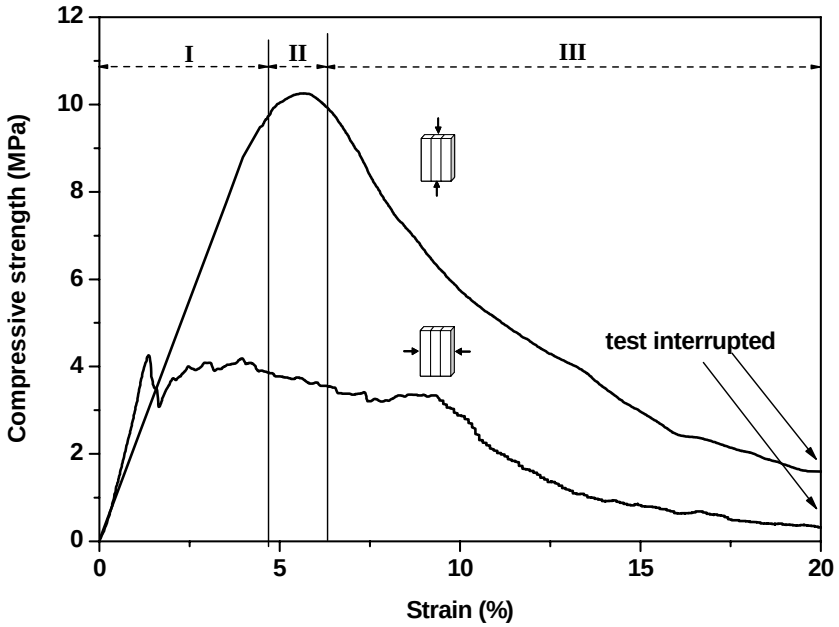

Figure 4. Stress-strain behavior in compression testing parallel and perpendicular to the freezing direction, for HA constructs prepared from aqueous suspensions (20 vol% particles) and sintered for 3 h at 1350°C. Three different regions are outlined for the curve corresponding to the parallel testing direction: I, elastic region; II, stress plateau region; III, failure region.

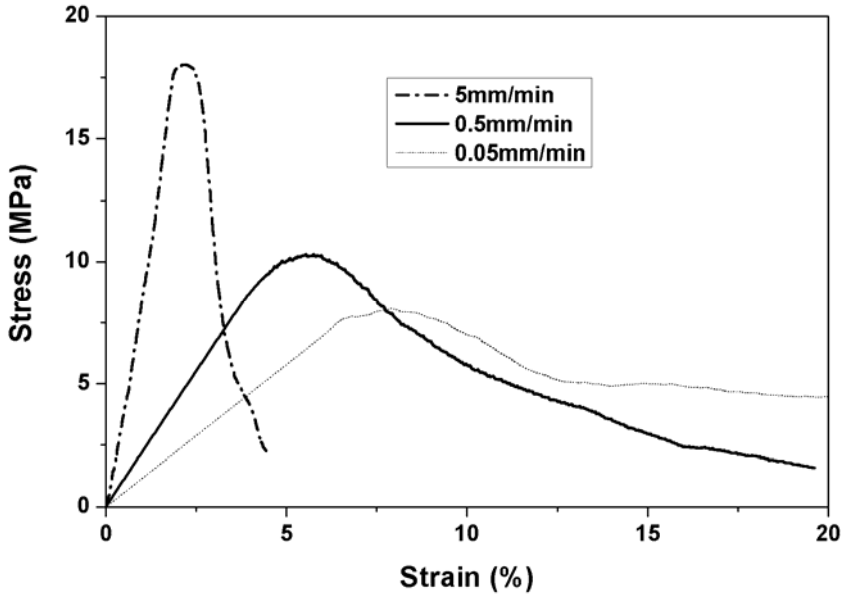

Figure 5. Effect of loading rate on the compressive mechanical response of HA constructs prepared from aqueous suspension with 20 vol% particles.

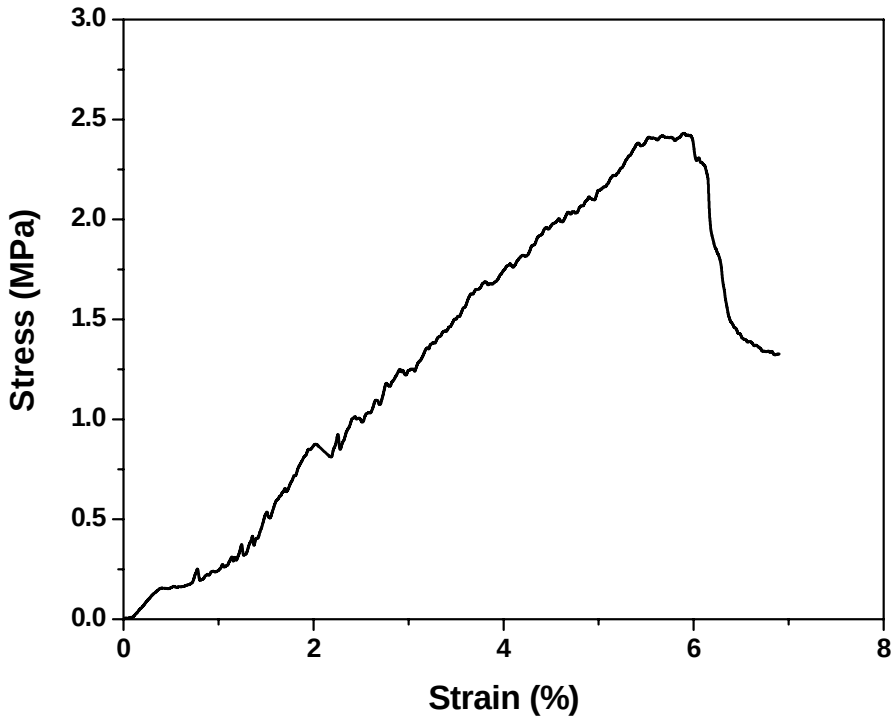

Figure 6. Stress-strain behavior in three-point bending for HA constructs prepared from aqueous suspensions (20 vol% particles) and sintered for 3 h at 1350°C.

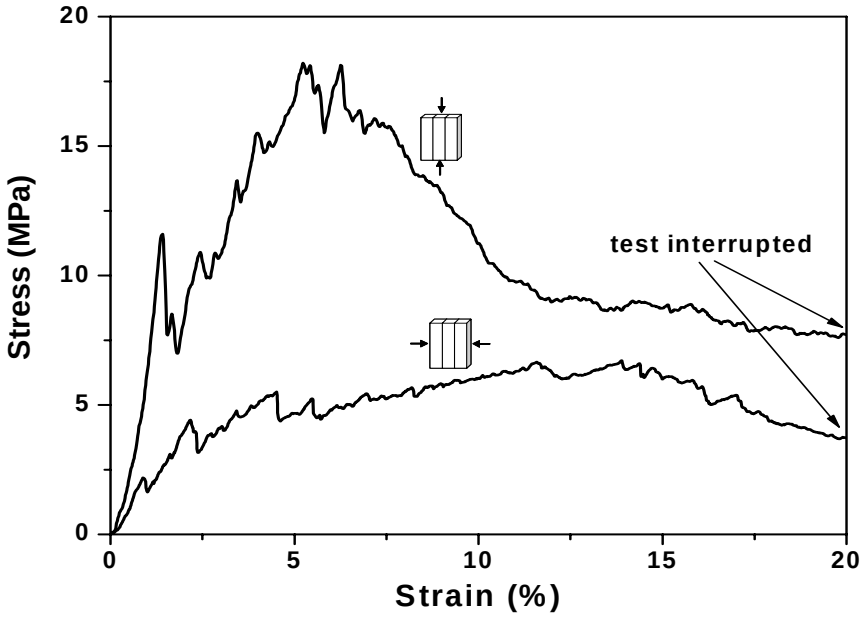

Figure 7. Stress-strain behavior of HA constructs prepared from suspensions with 20 wt% glycerol and sintered fro 3 h at 1350°C. The load was applied in compression, parallel and perpendicular to the freezing direction.

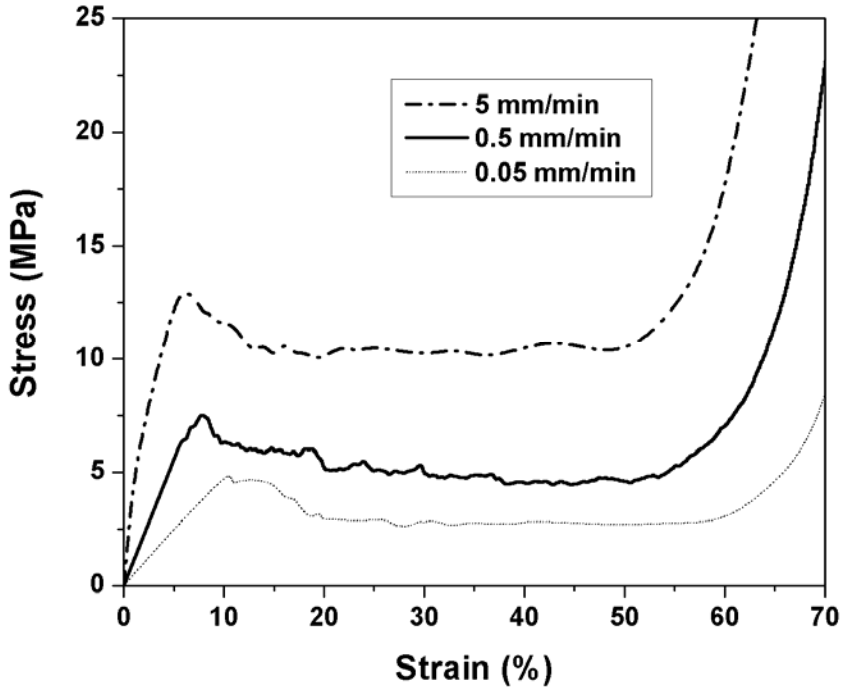

Figure 8. Effect of loading rate on the mechanical response of the HA constructs prepared from aqueous suspensions (10 vol% particles) containing 60 wt% dioxane.

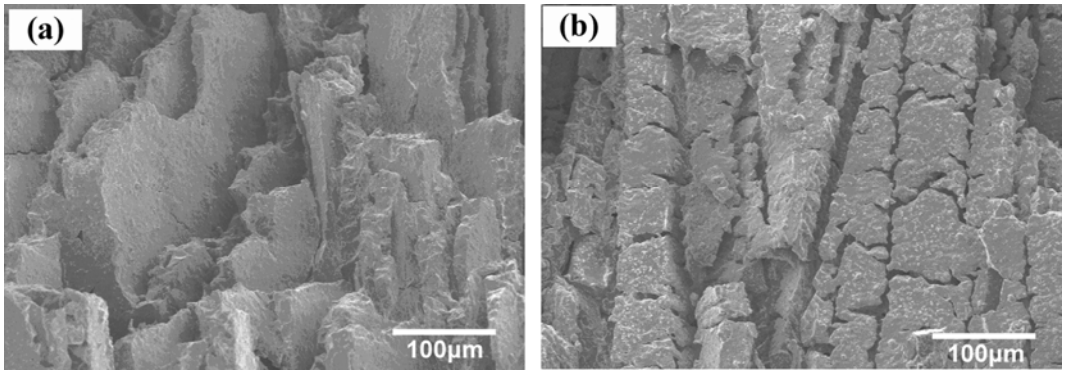

Figure 9. Fractured surfaces, after compression testing, of HA constructs prepared from suspensions without glycerol: (a) top surface, perpendicular to the freezing direction; (b) surface parallel to the freezing direction.

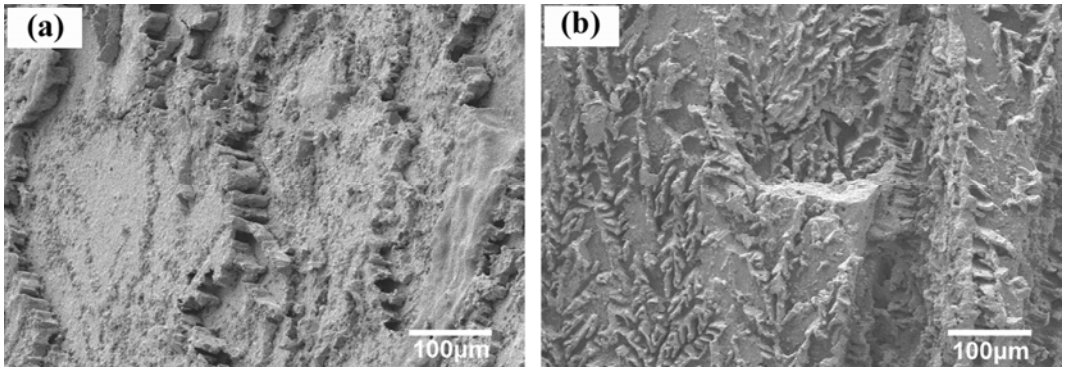

Figure 10. Fractured surfaces, after compression testing, of HA constructs prepared from suspensions with 20 wt% glycerol: (a) top surface, perpendicular to the freezing direction; (b) surface parallel to the freezing direction.

3. FREEZE-CAST HYDROXYAPATITE SCAFFOLDS FOR BONE TISSUE ENGINEERING APPLICATIONS

Qiang Fu[1*], Mohamed N. Rahaman[1], Fatih Dogan[1], and B. Sonny Bal[2]

[1]Missouri University of Science and Technology, Department of Materials Science and Engineering, 223 McNutt Hall, Rolla Missouri 65409

[2]University of Missouri-Columbia, Department of Orthopaedic Surgery, 1 Hospital Drive, Columbia, Missouri 65212

3.1. ABSTRACT

Freeze casting of aqueous suspensions was investigated as a method for preparing porous hydroxyapatite (HA) scaffolds for eventual application to bone tissue engineering. Suspensions of HA particles (10–20 volume percent) were frozen unidirectionally in a cylindrical mold placed on a cold steel substrate (–20°C). After sublimation of the ice, sintering for 3 h at 1350°C produced constructs with dense HA lamellae, porosity of ~50%, and inter-lamellar pore widths of 5–30 μm. These constructs had compressive strengths of 12 ± 1 MPa and 5 ± 1 MPa in the direction parallel to and perpendicular to the freezing direction, respectively. Manipulation of the microstructure was achieved by modifying the solvent composition of the suspension used for freeze casting. The use of water–glycerol mixtures (20 wt% glycerol) resulted in the production of constructs with finer pores (1–10 μm) and a larger number of dendritic growth connecting the HA lamellae, and higher strength. On the other hand, the use of water–dioxane mixtures (60

* Correspondence author: Q. Fu (qf7r9@mst.edu)

wt% dioxane) resulted in a cellular-type microstructure with larger pores (90-110 μm). The mechanical response showed high strain tolerance (5–10% at the maximum stress), high strain for failure (>20%), and sensitivity to the loading rate. The favorable mechanical behavior of the porous constructs, coupled with the ability to modify their microstructure, indicates the potential of the present freeze casting route for the production of porous scaffolds for bone tissue engineering.

Keywords: biomaterials; scaffolds; hydroxyapatite; freeze casting; porous ceramics

3.2. INTRODUCTION

Tissue engineering, involving the implantation of cells and tissues, or stimulating host cells to grow in an implanted scaffold, has emerged as a promising approach for the repair or regeneration of lost or damaged tissues [1-2]. The applicability of the tissue-engineered construct is critically dependent on the composition and structure of the porous three-dimensional scaffold which guides the growth of new tissue *in vitro* and *in vivo* [3-5]. For bone tissue engineering, the scaffold material should possess certain desirable properties, such as biocompatibility, the ability to be formed into porous, three-dimensional constructs with the relevant anatomical shape and with the appropriate mechanical properties to support physiologic loads, and the ability to be formed economically and reproducibly [6-8].

Bioactive ceramics have been widely investigated for repairing bone defects, because of their good biocompatibility and ability to bond to surrounding tissues [3, 9-10]. A variety of methods has been used to produce porous scaffolds for tissue

engineering, including consolidation with a pore-producing fugitive phase such as starch or PVA [11, 12], the use of foaming agents [4, 5, 13, 14], thermally induced phase separation, TIPS, [15-17], solid freeform fabrication [18-20], slip casting, foam replication and fiber packing methods, [21-23]. Freeze casting has been widely applied to the production of synthetic and natural polymer scaffolds for tissue engineering applications [15-17, 24], and its application to the production of porous bioceramic scaffolds is now receiving interest [25-29]. Recent investigations have shown the ability to prepare porous HA scaffolds with a lamellar-type microstructure and oriented pores by unidirectional freezing of aqueous suspensions [27-29]. The microstructure and strength of the scaffolds were modified by altering the particle concentration of the suspension, freezing rate, and sintering conditions. However, the average pore diameter or width was 10–40 μm, which is too small to support tissue ingrowth.

Another way to manipulate the microstructure of the freeze cast construct is to control the freezing (or solidification) behavior of the liquid in the suspension, but this has received little attention. Certain liquids, such as glycerol and 1,4-dioxane (referred to hereafter simply as dioxane), are miscible with water, and when added to water modify the local structure of the aqueous liquid. As a result, they modify the nucleation and growth of the ice crystals, thereby modifying the freezing behavior of the aqueous liquid. Glycerol has been shown to lead to a localized structure, resulting in a reduced size of the growing ice crystals and inhibiting solute rejection [25]. A study of the local solvent structure of dioxane–water mixtures indicated that structural changes of the mixture occurred at three specific compositions [30].

The objective of the present work was to explore how key processing factors influenced the microstructure of freeze cast HA constructs, and to characterize the effect of the microstructure on the mechanical properties of the fabricated constructs. HA was chosen as the material system because of its biocompatibility, being the main mineral constituent of bone. The processing parameters investigated were the solids content of the suspension, the freezing rate, and the composition of the solvent in the suspension. The effects of sintering conditions on the microstructure and mechanical behavior of the fabricated HA constructs were investigated. An understanding of the relationship between the processing parameters and the resulting microstructure and mechanical strength is useful for controlling the microstructure and properties of scaffolds for bone repair and replacement.

3.3. MATERIALS AND METHODS

3.3.1. Freeze Casting of Suspensions. Suspensions containing 5–20 vol% HA particles (average particle size <1 μm; Alfa Aesar, Haverhill, MA), 0.75 wt% of a dispersant, Dynol 604 (Air Products & Chemicals, Inc., Allentown, PA), and 1.5 weight percent (wt%) of an organic binder poly(vinyl alcohol), PVA, (DuPont Elvanol® 90-50, DuPont, DE), based on the dry weight of the HA powder, were prepared by ball-milling for 48 h in polypropylene containers using Al_2O_3 grinding media. The preparation and characterization of the HA suspension are described in detail elsewhere [29]. The suspensions were de-aired by ball-milling at a low speed prior to freeze casting. To explore the effects of solvent composition, aqueous suspensions containing 5–20 wt% of

glycerol (Fisher Scientific, Pittsburg, PA) or 40–70 wt% dioxane (Fisher Scientific), were also prepared using the same procedure.

Unidirectional freeze casting was performed by pouring the suspensions into polyvinyl chloride (PVC) tubes (~10 mm internal diameter × 20 mm long) placed on a cold steel substrate kept at –20°C using a freeze dryer (Genesis 25 SQ Freeze Dryer, VirTis Co., Gardiner, NY). Polyurethane foam was used to cover the PVC tubes to reduce heat transfer from the surrounding environment to the slurry, ensuring optimum directional freezing of the system. The frozen constructs were subjected to a vacuum of 4 Pa for 48 h in a freeze dryer (Genesis 25 SQ Freeze Dryer) to cause sublimation of the frozen solvent. The green bodies were sintered in air for 3 h at temperatures between 1250 and 1375°C, with a heating and cooling rate of 3°C min^{-1}.

The microstructure of the surfaces and cross-section of the green and sintered constructs was observed using scanning electron microscopy, SEM (S-4700; Hitachi, Tokyo, Japan). X-ray diffraction, XRD (D/mas 2550 v; Rigaku; The Woodlands, TX), was used to identify the phases present in the starting powder and sintered samples, using Cu K_α radiation (λ=0.15406 nm) at a scanning rate of 1.8°/min in the 2θ range of 10–80°. The volume of open porosity in the sintered samples was measured using the Archimedes method. The compressive strength of cylindrical samples (8 mm in diameter × 16 mm) in the directions parallel and perpendicular to freezing was measured according to ASTM-C773 using an Instron testing machine (Model 4204; Instron Inc., Norwood, MA) at a crosshead speed of 0.5 mm min^{-1}. Eight samples were tested, and the mean strength and standard deviation were determined. To investigate the effect of loading (strain) rate on

the compressive mechanical response, testing was also performed at cross-head speeds of 0.05 and 5 mm min^{-1}.

3.4. RESULTS AND DISCUSSION

3.4.1. Microstructure of Constructs Prepared from Aqueous Suspensions.

Figure 1 shows the XRD patterns of the as-received HA powder and freeze-cast material sintered for 3 h at 1350°C. Both patterns corresponded to the reference pattern of HA (JCPDS 72-1243). Within the limits of detection by XRD (< 0.5 wt%), no additional peaks corresponding to any second phases were found in the patterns.

After freeze casting and sintering, the constructs maintained a uniform cylindrical shape. The green constructs, after sublimation of the frozen liquid, were weak, so most of the microstructural characterization studies were performed on constructs after they were sintered. Figure 2 shows SEM images of constructs prepared from suspensions with 20 vol% HA particles. A uniform lamellar-type microstructure was observed throughout the construct, with the pores oriented in the direction of freezing. The lamellar-type microstructure shown in Figure 2 is quite similar to the microstructures of polymeric materials such as collagen prepared for tissue engineering applications [24]. For the present system, the HA lamellae and the macropores between them were oriented in the direction of freezing. The lamellae had a thickness of 20–30 μm and a length of 100–250 μm in cross section (Figure 2(a)) and extended from the bottom of the construct to the top (Figure 2(b)). A higher magnification image (Figure 2(c)) indicated that the average pore width was ~20 μm, and that the lamellae were almost fully dense, with some dendritic bridges between the lamellae. Determination of the porosity by the Archimedes method

and by mercury intrusion porosimetry, reported elsewhere [29], showed that the pores in the sintered constructs were interconnected with the porous surface (Figure 2(d)).

For aqueous suspensions, a reduction of the particle concentration produced a higher porosity, pores with a larger cross section, and thinner HA lamellae (Table 1), which was due to fewer nucleation sites for ice nuclei and fewer barriers for water molecules to diffuse to the surface of the formed crystals. On the other hand, lowering the substrate temperature during freezing resulted in pores with finer cross sections. From the thermodynamic point of view, a lower substrate temperature means a large driving force for nucleation of ice crystals, which results in the formations of a larger number of ice nuclei and the decreased growth of the formed ice crystals, and therefore to smaller inter-lamellar pores. By adjusting the particle concentration and substrate temperature, the microstructure of the construct can be controlled over a wide range.

3.4.2. Effects of Sintering Conditions. The effect of the sintering temperature on the open porosity and compressive strength (in the freezing direction) of HA constructs sintered for 3 h at temperatures between 1250°C and 1375°C is shown in Figure 3. With increasing temperature, the porosity decreased slightly, but the compressive strength increased significantly. Both the porosity and mechanical strength reached their limiting values at 1350°C, which is an indication that the HA lamellae in the microstructure had reached their highest density. Sintering for 3 h at 1350°C represented approximately the optimum sintering conditions for the present system. Sintering for much longer times at 1350°C or at higher temperatures will lead primarily to grain growth in the HA lamellae. The compressive strength of the HA constructs in the

direction of freezing reached its highest value of 12 ± 1 MPa at 1350°C. While this value is far lower than the compressive strength of cortical bone (100-150MPa) [31], it is equal to the highest values reported for trabecular (or cancellous) bone (2-12 MPa) [32].

3.4.3. Effect of Solvent Composition on Microstructure. Figure 4 shows the microstructure of sintered HA constructs formed from suspensions (10 vol% HA particles) in which the solvent consisted of water, water + 20 wt% glycerol, and water + 60 wt% dioxane. When compared to the microstructure of the construct formed from the aqueous suspension (Figure 4(a)), the addition of glycerol to the solvent had the effect of increasing the number of dendritic bridges between the HA lamellas (Figure 4(b)). This increased to such an extent that the cross-section of the pores changed from a plate-like morphology to a more dendritic shape. The microstructure was quite uniform, the pores became smaller, and the number of dendritic bridges between the HA lamellas increased. The pore widths were in the range 1–10 μm, compared to values 20–30 μm for similar constructs prepared without glycerol. Glycerol addition to the suspension was capable of reducing the size of ice crystals [25, 29]. The large lamellar ice crystals disappeared due to the formation of the localized ice crystals and smaller crystals produced in the frozen samples, which corresponded to fine dendritic pores in the sintered HA samples (Figure 4(b)). The addition of dioxane to the aqueous solvent resulted in the production of constructs with a cellular type microstructure (Figure 4(c)). The pore diameter, 100 ± 10 μm, was much larger than the pore width of the constructs prepared from the aqueous suspensions. The change in microstructure of the freeze-cast constructs may be attributed to the presence of stable dioxane–water complexes [33, 34].

3.4.4. Mechanical Response of HA Constructs. Figure 5 shows stress–strain curves in compression testing for freeze-cast HA constructs prepared from aqueous suspensions with 20 vol% particles. The curves show the behavior of the constructs in the direction parallel and perpendicular to the freezing direction. The data shown are engineering stresses and strains, based on the initial cross-sectional area and length of the test sample, and do not represent the true stresses and strains. An interesting feature of the stress-strain curves is the high strain tolerance (high strain for failure) of the constructs. Unlike common ceramics which show brittle behavior with just an elastic response and failure at low strain (typically < 0.1%), the constructs produced in the present work showed three distinctive regions: an 'elastic' regime in which the stress–strain response is linear, a 'stress plateau' region representing a region of highest sustainable loading, and a 'failure' region of decreasing load-bearing ability.

While the three regions can be observed in both curves, the stress-strain curve in the freezing direction had a different shape from that perpendicular to the freezing direction. The curve for the response in the freezing direction had a more smoothly varying, asymmetric bell-shaped curve, indicating a compressive strength (taken as the stress at the peak) of ~10 MPa at a strain of ~7%. In contrast, the curve for the perpendicular testing direction had a large plateau region, in a strain range of 2–10%, with numerous bumps and valleys. The average compressive strength in this plateau region was ~4 MPa.

The mechanical response of the fabricated constructs showed a high dependence on the loading (or strain) rate (Figure 6). Typically, a high stain rate led to a high compressive strength of the constructs. An increase in the strain rate from 0.05 mm min^{-1}

to 0.5 and 5 mm min^{-1}, resulted in an increase in the compressive strength of the constructs of 25 and 125% respectively. On the other hand, the failure strain decreased from 8% to 5 and 2%, respectively.

The mechanical response of the HA constructs prepared from suspensions with glycerol or dioxane addition was similar in nature to that shown in Figure 5 for constructs prepared from aqueous suspensions, but the magnitude of the response was different. The nature of the observed mechanical response was attributed to the anisotropic microstructure produced by the unidirectional freeze-casting process. This type of mechanical behavior with a high strain tolerance has been found in natural materials with anisotropic structure such as bone, and it is considered to be important for the remodeling of bone structure in response to the applied load [35, 36].

The mechanical response of porous materials, such as brittle foams, has been modeled by Gibson and Ashby [35]. According to the model, the compressive crushing strength σ_{cr} of brittle foams is given by:

$$\frac{\sigma_{cr}}{\sigma_{fs}} = C\left(\frac{\rho}{\rho_o}\right)^{3/2} \frac{1+(t_i/t)^2}{\sqrt{1-(t_i/t)^2}} = C(1-P)^{3/2} \frac{1+(t_i/t)^2}{\sqrt{1-(t_i/t)^2}} \quad (1)$$

where σ_{fs} is the modulus of rupture of the solid struts, C is a constant of proportionality, ρ and ρ_o are the densities of the porous cellular material and the fully dense solid phase, respectively, P is the porosity of the cellular material, and t_i/t is the ratio of width of the box-like void in the struts to the thickness of the solid strut. In the case of brittle foams [35], $C = 0.2$. For HA, the reported values for σ_{fs} are in the range 115–200 MPa [3]. In the present work, the struts were almost fully dense, so $t_i/t = 0$.

Using these values, the strength predicted by the model is in the range 5–8 MPa for a porosity $P = 0.65$. This value is not vastly different from the measured compressive strengths (7.5–18 MPa) for the constructs investigated in the present work with $P = 0.65$–0.70, and tested under a loading rate of 0.5 mm min^{-1} along the pore orientation direction.

Scaffolds intended for bone repair and regeneration should have not only adequate mechanical properties to support physiologic loads but also favorable pore characteristics for supporting tissue ingrowth into the scaffolds to allow strong bonding and facile integration with surrounding tissues. Interconnected pores with a mean pore diameter or width of 100 μm or greater, and open porosity of >50% are generally considered the minimum requirements to permit tissue ingrowth and function in porous scaffolds [37, 38]. Scaffolds prepared in this work from aqueous suspensions and from suspension with glycerol additions had pores (1–30 μm) that were too small to support tissue ingrowth. On the other hand, the pore diameter or width (100 ± 10 μm) of the scaffolds prepared from suspensions with dioxane additions was more favorable. Further work is in progress to (1) prepare freeze-cast scaffolds with larger pore size, while retaining strength and porosity, and (2) evaluate the cell proliferation and differentiation on the surface and within the porous scaffolds.

3.5. CONCLUSION

Freeze casting of aqueous suspension of HA particles on a cold substrate produced porous constructs with a uniform, lamellar-type microstructure in which plate-like HA lamellas were oriented in the direction of freezing. The sintering conditions had

a marked effect on the microstructure and mechanical behavior of the fabricated constructs. An increase in the sintering temperature from 1250°C to 1375°C produced a small (5%) decrease in porosity, but an increase in the compressive strength of nearly 50%. Constructs with a porosity of 52%, formed by sintering for 3 h at 1350°C had compressive strengths of 12 ± 1 MPa and 5 ± 1 MPa in the directions parallel and perpendicular to the freezing direction, respectively. Significant changes in microstructure and properties were achieved by modifying the solvent composition of the suspensions used in the freeze-casting process. The addition of glycerol (~20 wt%) to the aqueous solvent used in the suspensions produced finer pores and a larger number of dendritic structures connecting the HA lamellas. On the other hand, the addition of 60 wt% dioxane produced a cellular microstructure with much larger pores. The fabricated constructs showed gradual failure behavior in compression, high strain tolerance (~5% at the maximum stress), high strain for failure (>20%), and sensitivity to the loading rate.

3.6. REFERENCES

1. Nerem RM 1991 Cellular engineering *Ann. Biomed. Eng.* 19 529-45
2. Langer R and Vacanti JP 1993 Tissue engineering *Science.* 260 920-6
3. Hench LL 1998 Bioceramics *J. Am. Ceram. Soc.* 81 1705-28
4. Sepulveda P, Binner JG, Rogero SO, Higa OZ and Bressiani JC 2000 Production of porous hydroxyapatite by the gel-casting of foams and cytotoxic evaluation *J. Biomed. Mater. Res.* 50 27–34.
5. Tamai N, Myoui A, Tomita T, Nakase T, Tanaka J, Ochi T and Yoshikawa H 2002 Novel hydroxyapatite ceramics with an interconnective porous structure exhibit superior osteoconduction *in vivo J. Biomed. Mater. Res.* 59110 –7
6. Langer R and Vacanti JP 1999 Tissue engineering: the challenges ahead. *Sci. Am.* 280 86-9
7. Hutmacher DW 2000 Scaffolds in tissue engineering bone and cartilage *Biomaterials* 21 2529–43
8. Stock UA and Vacanti JP 2001 Tissue engineering: current state and prospects *Annu. Rev. Med.* 52 443-51.

9. Fu Q, Rahaman MN, Zhou N, Huang W, Wang D, Zhang L and Li H 2008 *In vitro* study on different cell response to spherical hydroxyapatite nanoparticles *J. Biomater. Appl.* DOI: 10.1177/0885328207081350
10. Fu Q, Zhou N, Huang W, Wang D, Zhang L and Li H 2005 Effects of nano HAP on biological and structural properties of glass bone cement *J. Biomed. Mater. Res. A* 74 156-63
11. Rodríguez-Lorenzo LM, Vallet-Regí M and Ferreira JMF 2002 Fabrication of porous hydroxyapatite bodies by a new direct consolidation method: starch consolidation. *J. Biomed. Mater. Res.* 60 232-40
12. Li SH, De Wijn JR, Layrolle P and De Groot K 2002 Synthesis of macroporous hydroxyapatite scaffolds for bone tissue engineering *J. Biomed. Mater. Res.* 61 109-20
13. Almirall A, Larrecq G, Delgado JA, Martinez S, Planell JA and Ginebra MP 2004 Fabrication of low temperature macroporous hydroxyapatite scaffolds by foaming and hydrolysis of an α-TCP paste *Biomaterials* 25 3671-80
14. Ebaretonbofa E and Evans JRG 2004 High porosity hydroxyapatite foam scaffolds for bone substitute *J. Poro. Mater.* 9 257-63
15. Zhang R, Ma PX. Poly(α-hydroxyl acids)/hydroxyapatite porous composites for bone-tissue engineering. I. Preparation and morphology. *J. Biomed. Mater. Res.* 1999;44:446-455
16. Ma PX and Zhang R 2001 Microtubular architecture of biodegradable polymer scaffolds *J. Biomed. Mater. Res.* 56 469-77
17. Yang F, Qu X, Cui W, Bei J, Yu F, Lu S and Wang S 2006 Manufacturing and morphology structure of polylactide-type microtubular orientation-structure scaffolds *Biomaterials* 27 4923-33
18. Roy TD, Simon JL, Ricci JL, Rekow ED, Thompson VP and Parsons JR 2003 Performance of hydroxyapatite bone repair scaffolds created via three-dimensional fabrication techniques. *J. Biomed. Mater. Res.* 67A 1228-37
19. Ramay HR and Zhang M 2003 Hydroxyapatite cement scaffolds with controlled macroporosity: fabrication protocol and mechanical properties *Biomaterials* 24 3293-302
20. Wilson CE, de Bruijn JD, van Blitterswijk CA, Verbout AJ and Dhert WJA 2004 Design and fabrication of standardized hydroxyapatite scaffolds with a defined macro-architecture by rapid prototyping for bone-tissue-engineering research *J. Biomed. Mater. Res.* 68A123-32
21. Fu Q, Rahaman MN, Huang W, Day DE and Bal BS 2007 Preparation and bioactive characteristics of a porous 13-93 glass, and its fabrication into the articulating surface of a proximal tibia *J. Biomed. Mater. Res. A* 82 222-9
22. Fu Q, Rahaman MN, Brown RF, Bal BS and Day DE 2008 Mechanical and *In vitro* Performance of 13-93 Bioactive Glass Scaffolds Prepared by a Polymer Foam Replication Technique *Acta Biomater.* at press
23. Brown RF, Day DE, Day TE, Jung S, Rahaman MN and Fu Q 2008 Growth and differentiation of osteoblastic cells on 13-93 bioactive glass fibers and scaffolds *Acta Biomater.* 4 387-96
24. Schoof H, Apel J, Heschel I and Rau G 2001 Control of pore structure and size in freeze-dried collagen sponges *J. Biomed. Mater. Res. Appl. Biomater.* 58 352-7

25. Sofie SW and Dogan F 2001 Freeze casting of aqueous alumina slurries with glycerol *J. Am. Ceram. Soc.* 84 1459-64
26. Halloran JW 2006 Making better ceramic composites with ice *Science* 311 479-80
27. Deville S, Saiz E and Tomsia A 2006 Freeze casting of hydroxyapatite scaffolds for bone tissue engineering *Biomaterials* 27 5480-9
28. Deville S, Saiz E, Nalla RK and Tomsia A 2006 Freezing as a path to build complex composites *Science* 311 515–8
29. Fu Q, Rahaman MN, Dogan F and Bal BS 2007 Freeze casting of porous hydroxyapatite scaffolds - I. processing and general microstructure solution *J. Biomed. Mater. Res. B* DOI: 10.1002/jbm.b.30997
30. Wu YG, Tabata M and Takamuku T 2001 A local solvent structure study on 1,4-dioxane-water binary mixtures by total isotropic Rayleigh light scattering method *J. Mol. Liq.* 94 273-82
31. Fung YC 1993 Biomechanics. Mechanical properties of living tissues (New York, Springer, p. 500)
32. Carter DR and Hayes WC 1976 Bone compressive strength: the influence of density and strain rate *Science* 1941174-6.
33. Zoidis E, Yarwood J, Tassing T, Danten Y and Besnard M 1995 Vibrational spectroscopic studies on the state of aggregation of water in carbon tetrachloride, in dioxane and in the mixed solvent *J. Mol. Liq.* 64 197-210
34. Buzko VY, Sukhno IV, Panytushkin VT and Ramazanova 2005 Theoretical investigation of 1,4-dioxane complexes with water in the chair conformation by semiempiric MNDO/PM3 method *J. Struct. Chem.* 46 596-602
35. Gibson LJ and Ashby MF 1997 Cellular solids: structure and properties (Cambridege: Cambridge University Press)
36. Hayes WC and Carter DR 1976 Postyield behavior of subchondral trabecular bone *J. Biomed. Mater. Res.* 7 537-44
37. Hollinger JO, Leong K 1996 Poly(-hydroxy acids): Carriers for bone morphogenetic proteins. *Biomaterials* 17 187-194
38. Hu YH, Grainger DW, Winn SR, Hollinger JO 2002 Fabrication of poly(-hydroxy acid) foam scaffolds using multiple solvent systems *J. Biomed. Mater. Res*. 59 563-572

Table 1: Comparison of porosity, pore width, microstructure and compressive mechanical properties of HA constructs prepared from aqueous suspensions, suspensions with glycerol, and suspensions with dioxane.

Solvent composition	HA concentration (vol%)	Pore width (μm)	Porosity (%)	Microstructure	Compressive strength (MPa)	Strain (%)
Aqueous	10	25±5	70±5	Lamellar	--	--
	20	15±10	55±2	Lamellar	12 ± 1	7
Water–Glycerol (20 wt%)	10	10±5	67±2	Rectangular	18 ± 2	5
Water–dioxane (60 wt%)	10	100±10	65±2	Cellular	7.5	8

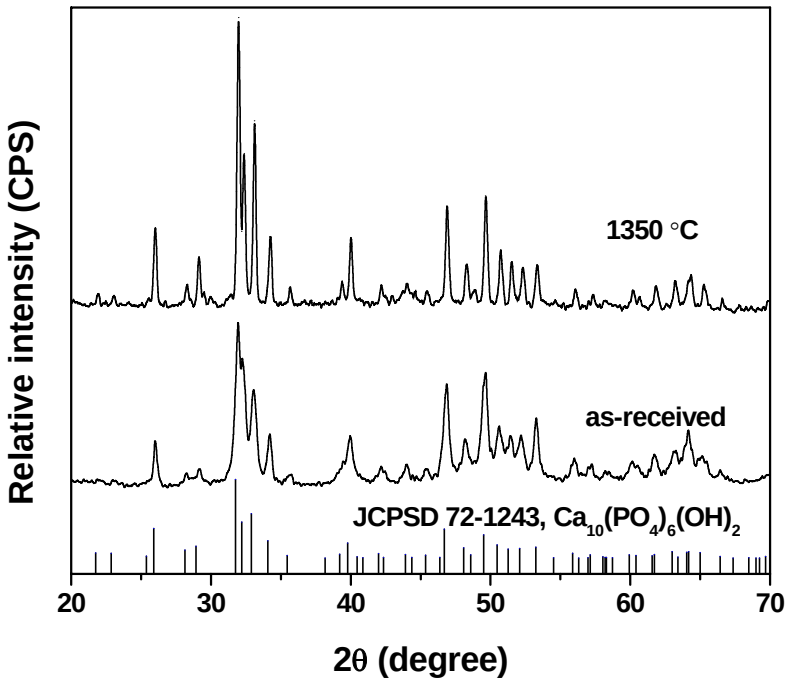

Figure 1. X-ray diffraction (XRD) patterns of as-received HA powder, the freeze-cast constructs sintered for 3 h at 1350ºC. The pattern for a reference HA (JCPDS 72-1243) is also shown.

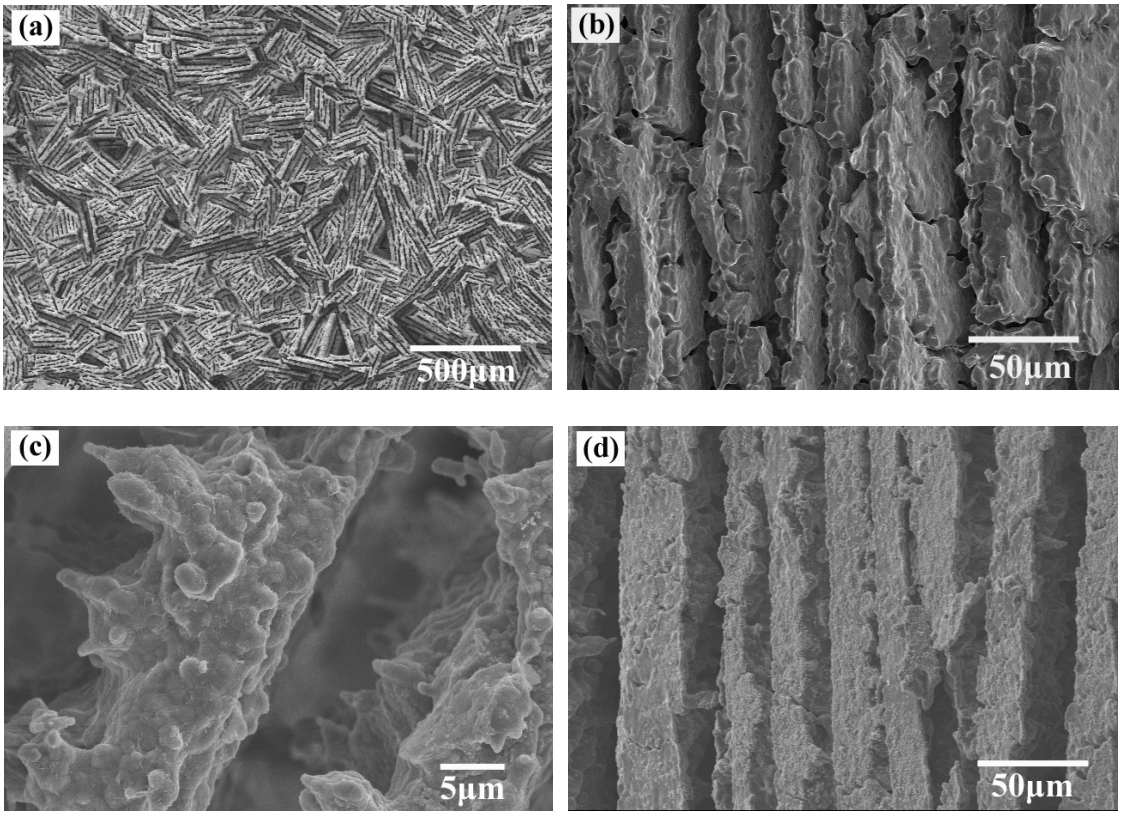

Figure 2. SEM images of the HA sample cross section (a) perpendicular, and (b) parallel to the freezing direction; (c) higher magnification image of the cross section in (b), showing the pore structure; (d) surface of the sample. The sample was sintered for 3 h at 1350°C.

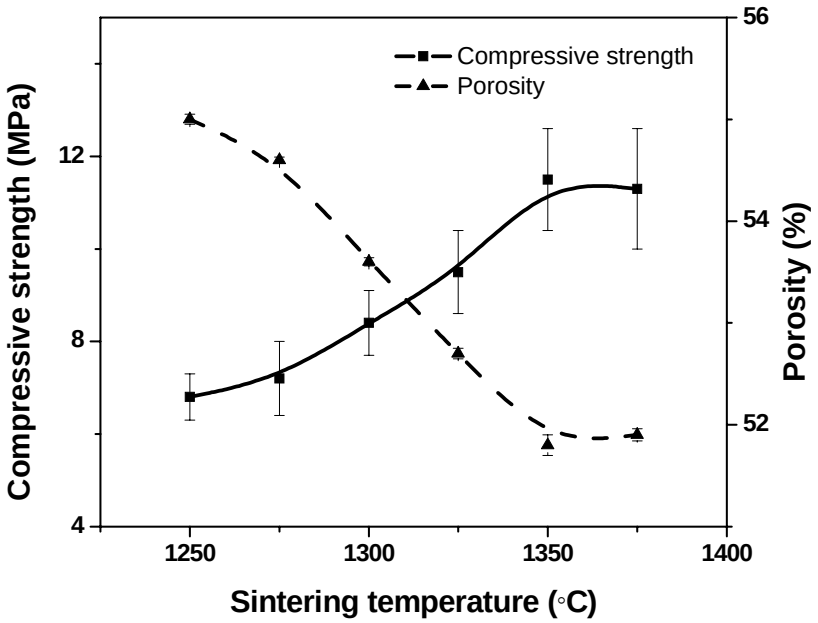

Figure 3. Influence of sintering temperature on porosity and compressive strength of HA samples.

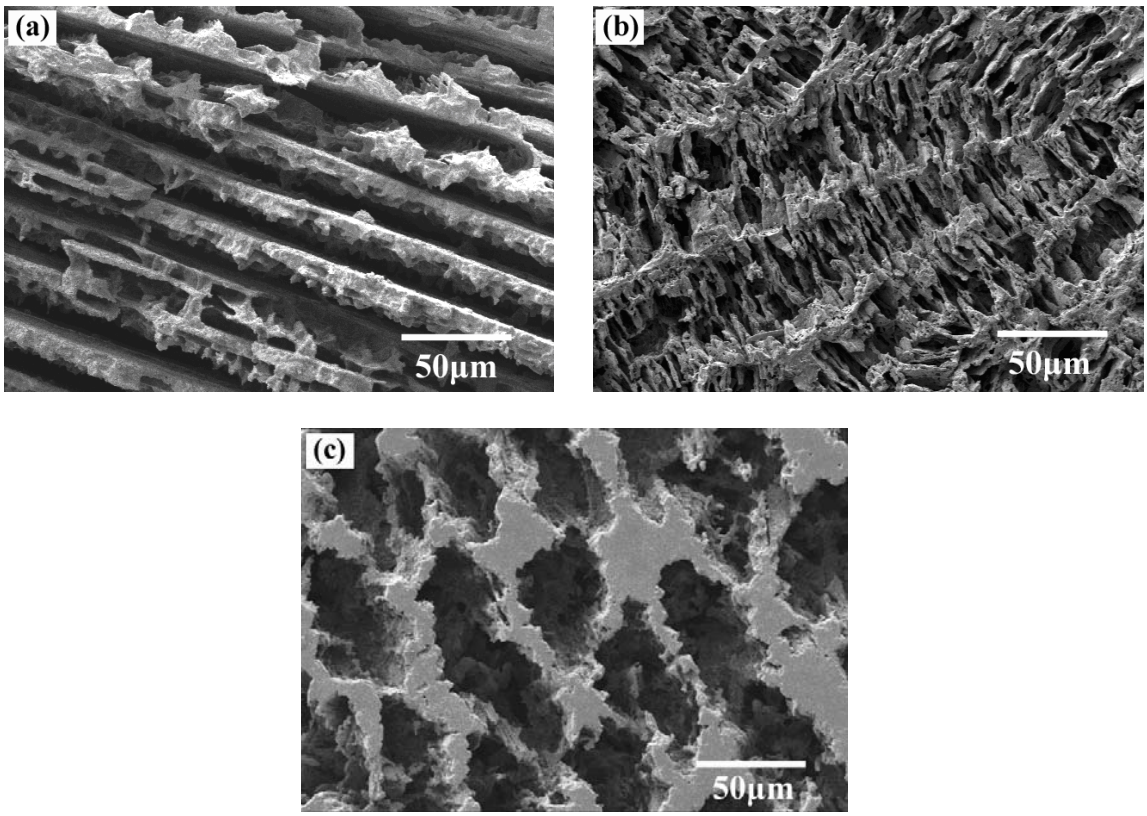

Figure 4. Effects of solvent composition on the microstructure of HA constructs prepared from 10 vol% suspension: (a) water; (b) water + 20 wt% glycerol; (c) water + 60 wt% dioxane.

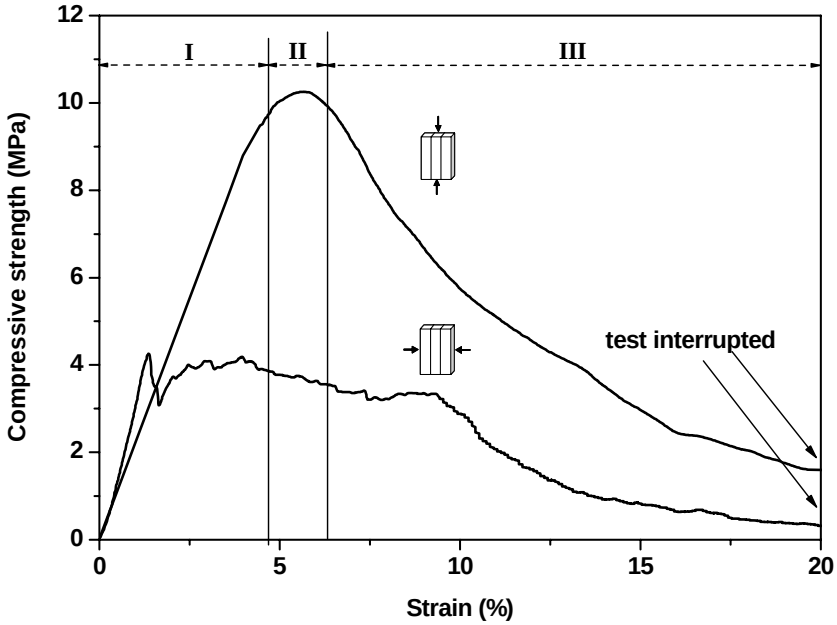

Figure 5. Stress-strain response in compression testing parallel and perpendicular to the freezing direction, for HA constructs prepared from aqueous suspensions (20 vol% particles) and sintered for 3 h at 1350°C. Three different regions are outlined for the curve corresponding to the parallel testing direction: I, elastic region; II, stress plateau region; III, failure region.

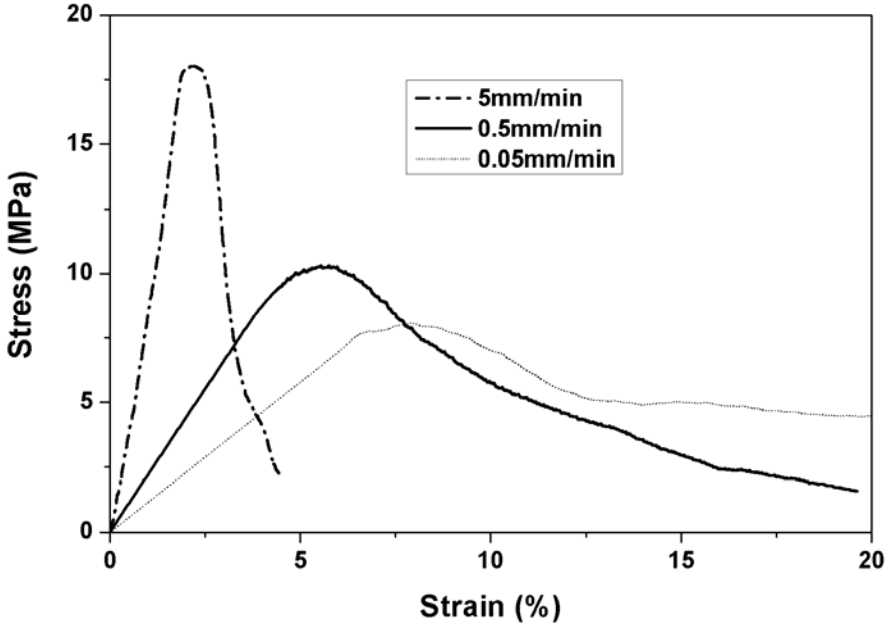

Figure 6. Effect of strain (or strain) rate on the mechanical response of the HA constructs prepared from aqueous suspension (20 vol% particles).

4. PROLIFERATION AND FUNCTION OF MC3T3-E1 CELLS ON FREEZE-CAST HYDROXYAPATITE SCAFFOLDS WITH ORIENTED PORE ARCHITECTURES

Qiang Fu[1], Mohamed N. Rahaman[1*], B. Sony Bal[2], Roger F. Brown[3]

[1]Department of Materials Science and Engineering, and Center for Bone and Tissue Repair and Regeneration, Missouri University of Science and Technology, Rolla, MO 65409, USA

[2] Department of Orthopaedic Surgery, University of Missouri-Columbia, Columbia, Missouri 65212, USA

[3]Department of Biological Sciences, and Center for Bone and Tissue Repair and Regeneration, Missouri University of Science and Technology, Rolla, MO 65409, USA

4.1. ABSTRACT

Previous work by the authors showed that hydroxyapatite (HA) scaffolds with different types of oriented microstructures and a unique 'elastic–plastic' mechanical response could be prepared by unidirectional freezing of suspensions. The objective of the present work was to evaluate the *in vitro* cellular response to these freeze-cast HA scaffolds. Unidirectional scaffolds with approximately the same porosity (65–70%) but different pore architectures, described as 'lamellar' (pore width = 25 ± 5 μm) and 'cellular' (pore diameter = 100 ± 10 μm), were evaluated. Whereas both groups of

* Email: rahaman@mst.edu

scaffolds showed excellent ability to support the proliferation of MC3T3-E1 pre-osteoblastic cells on their surfaces, scaffolds with the cellular-type microstructure showed far better ability to support cell proliferation into the pores and cell function. These results indicate that freeze-cast HA scaffolds with the cellular-type microstructure have better potential for bone repair applications.

Keywords: scaffolds; hydroxyapatite; cell culture; porous ceramics

4.2. INTRODUCTION

Bioactive glass, glass-ceramics, and ceramics, such as 45S5 bioactive glass and hydroxyapatite (HA), referred to collectively as 'bioactive ceramics', are an important category of biomaterials that have promising potential for use in bone repair and regeneration [1–3]. Several methods have been used to produce porous scaffolds of bioactive ceramics, such as incorporation of a pore-producing fugitive phase such as starch or PVA [4, 5], the use of foaming agents [6, 7], polymer foam replication techniques [8–10], slip casting [11], and solid freeform fabrication [12, 13]. A limitation of scaffolds prepared by current methods is that they often lack the combination of high strength and high porosity for skeletal substitution of load-bearing bones. They are limited to low-stress applications instead, such as filling of contained bone defects, where adjacent, intact bone provides mechanical rigidity and support. The repair of large defects in load-bearing bones requires scaffolds with far higher strengths. Situations in which long bone discontinuity is encountered include traumatic injuries suffered in war or in

automobile accidents, bone resection for tumors, and bone loss from complex, revision total hip or total knee surgery.

Recently, a method based on unidirectional freezing of aqueous suspensions has been shown to produce porous HA constructs with an oriented, lamellar-type microstructure and high compressive strength in the direction of orientation [14–18]. Compressive strengths as high as 65 MPa (56% porosity) in the direction parallel to the freezing direction were reported for testing of small HA disks [14, 15]. However, the pore width of these lamellar-type HA constructs was only 10–40 lm, a value that is considered too low for tissue ingrowth. A porosity of >50% with pore size (diameter or width) of 100 μm or larger are the minimum values reported for scaffolds capable of supporting cell proliferation and function [19, 20].

Our previous work [16–18] using a unidirectional freezing method showed that the addition of polar organic solvents such as 1,4-dioxane (referred to simply as dioxane) and glycerol to aqueous suspensions of HA resulted in drastic changes to the microstructure. Compared to the lamellar-type microstructure (pore width 10–40 μm) obtained from aqueous suspensions, scaffolds with approximately the same porosity (65–70%) prepared from suspensions with 60 wt% dioxane had a cellular-type microstructure with nearly cylindrical pores of diameter 90–110 μm. When compared to the common brittle failure of ceramics, the deformation of the freeze-cast scaffolds in compression showed a unique ‘elastic–plastic’ response. The freeze-cast constructs were deformed to large strains (>20–50%) without disintegrating in a brittle manner.

Based on the unique mechanical response and the favorable pore characteristics of the HA constructs with the cellular-type microstructure [17], this *in vitro* investigation

was undertaken to evaluate the ability of these oriented constructs to support cell proliferation and function. For comparison, the *in vitro* cellular response to the lamellar-type constructs was also studied. The mouse MC3T3-E1 cell line chosen for this study is a well-characterized preosteoblastic cell line that has been used extensively in previous *in vitro* investigations of biomaterials for bone repair and tissue engineering [21, 22].

4.3. MATERIALS AND METHODS

4.3.1. Preparation of HA Scaffolds. Methods for preparing HA scaffolds with an oriented microstructure by unidirectional freezing of HA suspensions are described in detail elsewhere [16]. Briefly, the suspensions contained 10 vol% HA particles (average particle size <1 μm; Alfa Aesar, Haverhill, MA), 0.75 wt% dispersant (Dynol 604; Air Products & Chemicals, Inc., Allentown, PA), and 1.5 wt% binder (DuPont Elvanol® 90-50; DuPont, Wilmington, DE). Aqueous suspensions, as well as suspensions containing 60 wt% dioxane (Fisher Scientific, St. Louis, MO), were prepared using the same method. A concentration of 60 wt% dioxane was used because it resulted in the preparation of HA scaffolds with larger pore width than the scaffolds prepared from aqueous suspensions. Unidirectional freezing was performed by pouring the suspensions into poly(vinyl chloride), PVC, tubes (~10 mm internal diameter × 20 mm long) placed on a cold steel substrate at -20ºC in a freeze dryer (Genesis 25 SQ Freeze Dryer, VirTis Co., Gardiner, NY). After sublimation of the frozen solvent in the freeze dryer, the constructs were sintered in air, for 3 h at 1350 ˚ C (heating and cooling rate = 3ºC/min). Scaffolds for cell culture experiments were prepared by sectioning the sintered

constructs using a diamond-coated blade, washing three times with de-ionized water and ethanol, and drying at 100ºC.

4.3.2. Cell Culture. HA scaffolds (8 mm in diameter × 2 mm thick) were dry heat sterilized for 24 h at 500ºC prior to cell culture. The established MC3T3-E1 line of mouse pre-osteoblastic cells was obtained from ATCC and cultured in α-MEM medium supplemented with 10% fetal bovine serum plus 100 U/ml penicillin and 100 μg/ml streptomycin sulfate. The scaffolds were seeded with 60,000 MC3T3-E1 cells suspended in 100 μl of complete medium, and incubated for 4 h to permit cell attachment. The cell-seeded constructs were then transferred to a 24-well plate containing 2 ml of complete medium per well. The control group consisted of the same number of cells seeded in wells containing 2 ml of complete medium. All cultures were maintained at 37ºC in a humidified atmosphere of 5% CO_2, with the medium changed every 2 days.

4.3.3. MTT Staining of Viable Cells. Cell-seeded scaffolds (four from each group) were placed in 400 μl serum-free medium containing 100 μg of the tetrazolium salt MTT for the last 4 h of incubation to permit visualization of metabolically active cells on and within the porous HA constructs. After the incubation, the constructs were briefly rinsed in PBS and blotted dry. Images of the constructs were obtained using a stereomicroscope fitted with a digital camera to qualitatively assess the distribution of insoluble purple formazan, a product of mitochondrial reduction of MTT by viable cells. The MTT-labeled constructs were then frozen at -70ºC, and fractured with a cooled microtome blade, and the fracture cross-section was visually examined to assess the presence of purple formazan within the interior of the constructs. Finally, the formazan

product was extracted from the HA constructs with 1.0 ml ethanol and measured spectrophotometrically at 550 nm in a BMG FLUORstar Optima plate reader.

4.3.4. Cell Morphology. At culture intervals of 2, 4 and 6 days, HA scaffolds with attached cells were removed, washed twice with warm PBS, and soaked overnight in 2.5% glutaraldehyde in PBS. The fixed samples were then washed with PBS three times, dehydrated with a graded ethyl alcohol series, and soaked for 10 min in hexamethyldisilazane (HMDS). After a second soak in HMDS, the samples were allowed to dry in air for 12 h at room temperature for the liquid to fully evaporate, sputter-coated for 60 s with Au/Pd, and observed in a scanning electron microscope, SEM (Hitachi S-4700), at 5 kV accelerating voltage.

4.3.5. Quantitative Protein Assay. Total protein in lysates recovered from the cell-seeded scaffolds was measured to assess cell proliferation on the scaffolds. The scaffolds were placed in 500 µl of 1% Triton X-100 and the cells lysed by two freeze-thaw cycles (-80/37ºC). Aliquots of the released lysate were mixed with a working reagent prepared from a micro-BCA Protein Assay Kit (Piece Biotechnology, Rockford, IL) and incubated at 50ºC for 20 min. Sample absorbance values were measured at 550 nm in a BMG FLUORstar Optima plate reader with bovine serum albumin used as a standard for comparison.

4.3.6. Alkaline Phosphatase Activity. MC3T3-E1 cells were seeded onto HA constructs and plastic control wells with a density of 60,000 cells/scaffold or well. Cell cultures were stopped at the intervals of 2, 4 and 6 days, and washed twice with PBS. Cells were lysed twice using freeze-thaw cycle at -80/37ºC with 500 µl of 1 % Triton X-100 in PBS. 120 µl of lysate were placed in a 96-well plate for quantitation of alkaline

phosphate (ALP) using 0.5 M 2-amino-2-methyl-l-propanol (AMP) buffer containing 50 mM *p*-nitrophenyl phosphate (*p*-NPP) according to a previously described method [23]. ALP activity is expressed as nanomoles of p-NP released per min.

4.3.7. Statistical Analysis. All biological experiments (4 samples in each group) were run either in duplicate or triplicate. The data are presented as the mean ± standard deviation. Statistical analysis was performed using Student's t-test. Values were considered to be significantly different when $P<0.05$.

4.4. RESULTS AND DISCUSSION

Table 1 summarizes the microstructural characteristics of the two groups of HA scaffolds used in the experiments. SEM images of the cross-sections perpendicular to the direction of freezing (Fig. 1a, b) showed no marked changes in the microstructure along the length of the sample, so each cross-section was, in general, representative of the whole construct. The two groups of scaffolds contained approximately the same total porosity (65–70%), but their microstructure and pore size (diameter or width) were different. Scaffolds prepared from aqueous suspensions had a lamellar-type microstructure (Fig. 1a), resulting from the hexagonal crystal structure of ice [24]. The inter-lamellar pores were 100–250 μm long and 25 ± 5 μm wide in cross section. Addition of dioxane to the aqueous suspension produced drastic changes in the microstructure, resulting from phase separation of the binary water–dioxane mixture during freezing and modification of the hydrogen bonding of water by the polar dioxane molecules [24]. Scaffolds prepared from suspensions with 60 wt% dioxane had a cellular-

type microstructure, approximately cylindrical pores, and pore diameters of size 100 ± 10 μm (Fig. 1b).

We were unable to prepare cellular- and lamellar-type scaffolds with comparable pore diameters (or widths). Freezing of aqueous suspensions of ceramic particles typically leads to the production of scaffolds with narrow lamellar-type pores (typically <40 μm wide) [14–18]. The primary objective of the present work was to evaluate the *in vitro* cell culture response to scaffolds with the cellular-type microstructure because these scaffolds had the requisite porosity and pore size reported for scaffolds capable of supporting cell proliferation and function [19, 20]. Scaffolds with the lamellar-type microstructure were evaluated for comparison because they were reported to have high strength and potential for bone repair applications despite their narrow pore widths [14, 15].

SEM images in Fig. 1a–f show the morphology of MC3T3-E1 cells after 2, 4, and 6 days of culture on the scaffolds with the lamellar- and cellular-type microstructures. Cells grown on the lamellar constructs were elongated and appeared to align along the walls of the construct at low cell density after culturing for 2 and 4 days (Fig. 1a, c). A high magnification image (Fig. 1a, inset) shows the formation of numerous cell projections along the walls of the lamellae, features that indicated firm cell attachment to the surface. After culturing for 6 days (Fig. 1e), the cell number increased, and the cells bridged the lamellae and covered the surface of the constructs. After 2 and 4 days, the morphology of cells grown on the cellular constructs was generally similar to that observed on lamellar constructs. The cells were attached to the constructs with cell projections at day 2 interval (Fig. 1b, and inset). The cell density increased with culture

time and, after 4 days, the cells colonized the surface of the constructs (Fig. 1d). After 6 days, the surface was almost completely covered with cells (Fig. 1f). However, instead of bridging the pores and concentrating on the surface as observed for the lamellar constructs (Fig. 1e), the cells apparently grew along the pore walls of the cellular constructs and were observed down into the pores. The cells were aggregated, and appeared to maintain physical contact with each other by multiple extensions with neighboring cells.

Results of the quantitative assay of total protein in cell lysates recovered from the HA constructs with the lamellar and cellular microstructures and from the control wells after incubations for 2, 4, and 6 days are shown in Fig. 2. The amounts of protein recovered from both types of scaffolds showed a nearly linear increase in cell proliferation during the 6-day incubation, a finding that complemented the progressive increase in cell density seen in the SEM images. The cell proliferation kinetics on the HA constructs were faster than on the control wells. Furthermore, cell proliferation on the cellular constructs was higher than on the lamellar constructs.

Photographic images of cell-seeded scaffolds treated with MTT during the last 4 h of incubation are shown in Fig. 3. The purple pigment visible on the scaffold was the result of mitochondrial reduction of MTT to an insoluble formazan product, an indication of viable cells. The increase in intensity of the purple color on the surface of both types of constructs with culture time indicated the proliferation of viable, metabolically active cells on the scaffolds (Fig. 3a, c). The relative amount of purple formazan visible on the freeze-fracture face of the scaffolds cultured for 6 days indicated that most of the metabolically active cells were predominantly near the surface of the lamellar construct

(Fig. 3b). On the other hand, purple formazan covered a larger area of the freeze-facture surface and extended almost halfway into the interior of the cellular construct, indicating far higher cell proliferation into the interior.

Figure 4 shows results of spectrophotometric measurement of the amount of the formazan extracted from the constructs described in Fig. 3. The optical density (OD) value of the extraction was an indication of the amount of formazan and hence the viable cells in the constructs. The higher OD value indicated a larger amount of viable cells. The data showed that HA constructs with the cellular microstructure had larger OD values than the lamellar constructs at day 4 and 6, indicating that the cellular constructs had a better ability to support cell growth, a finding complemented by the higher amount of protein measured in the cellular constructs than the lamellar ones.

Results of spectrophotometric measurement of alkaline phosphatase activity of MC3T3-E1 cells cultured on the HA constructs for 2, 4 and 6 days are presented in Fig. 5. The alkaline phosphatase activity increased with the duration of incubation. This finding is an indication that the seeded cells were able to function as osteoblasts on the HA constructs. The higher alkaline phosphatase activity of the HA constructs with the cellular microstructure indicated that these constructs were better able to support cell function than the lamellar constructs.

In addition to being bioactive and providing adequate mechanical strength, scaffolds intended for the repair of large defects in load-bearing bones should also support the ingrowth of cells and new tissues. Oriented bioceramic microstructures prepared by unidirectional freezing of aqueous suspensions have shown the ability to develop higher strength in the orientation direction, when compared to more random

microstructures prepared by conventional freezing and other methods [14–18]. However, scaffolds prepared by unidirectional freezing of aqueous suspensions typically have a lamellar-type microstructure with narrow slot-like pores (width = 10–40 μm). The results of the present work showed that these lamellar-type scaffolds have limited ability to support cell infiltration and, therefore, the ingrowth of new tissues.

Scaffolds with the cellular-type microstructure (pore width = 100 ± 10 μm), prepared from HA suspensions with dioxane (60 wt%), not only had better ability to support the proliferation and function of MC3T3-E1 cells but also supported the proliferation of the cells down the porosity into the interior of the scaffolds. This coupled with the ability of the scaffolds to develop high compressive strength and large strain for failure shown in our previous work [16–18] indicates that these freeze-cast scaffolds may have potential applications in bone repair. Additional work is presently underway to evaluate the performance of these scaffolds for use in the repair of large defects in load-bearing bones *in vivo*.

4.5. CONCLUSIONS

The ability of two groups of hydroxyapatite (HA) scaffolds with different oriented pore architectures to support the proliferation and function of MC3T3-E1 pre-osteoblastic cells *in vitro* was evaluated. While both groups of scaffolds supported greater cell proliferation and differentiation when compared to control wells, scaffolds with the cellular-type microstructure (pore diameter = 100 ± 10 μm) showed better ability to support cell proliferation and function than lamellar-type scaffolds with slot-like pores of width 25 ± 5 μm. Cells proliferated predominantly on the surface of the lamellar scaffolds

with little growth into the pores. On the other hand, cells proliferated both on the surfaces as well as deeper into the interior of the pores for the cellular microstructure. HA scaffolds with the oriented, cellular microstructure should have potential applications as biological scaffolds for bone repair and regeneration.

4.6. REFERENCES

1. L.L. Hench, Bioceramics. J. Am. Ceram. Soc. 81, 1705–1728 (1998)
2. A. El-Ghannam, Bone reconstruction: from bioceramics to tissue engineering. Expert Rev. Med. Devices 2, 87–101 (2005). doi:10.1586/17434440.2.1.87
3. M.N. Rahaman, R.F. Brown, B.S. Bal, D.E. Day, Bioactive glasses for non-bearing applications in total joint replacement. Semin. Arthroplasty 17, 102–112 (2006). doi:10.1053/j.sart.2006.09.003
4. L.M. Rodríguez-Lorenzo, M. Vallet-Regí, J.M.F. Ferreira, Fabrication of porous hydroxyapatite bodies by a new direct consolidation method: starch consolidation. J. Biomed. Mater. Res. 60, 232–240 (2002). doi:10.1002/jbm.10036
5. S.H. Li, J.R. De Wijn, P. Layrolle, K. De Groot, Synthesis of macroporous hydroxyapatite scaffolds for bone tissue engineering. J. Biomed. Mater. Res. 61, 109–120 (2002). doi:10.1002/jbm.10163
6. P. Sepulveda, J.G. Binner, S.O. Rogero, O.Z. Higa, J.C. Bressiani, Production of porous hydroxyapatite by the gel-casting of foams and cytotoxic evaluation. J. Biomed. Mater. Res. 50, 27–34 (2000). doi:10.1002/(SICI)1097-4636(200004)50:1<27::AID-JBM5>3.0.CO;2-6
7. N. Tamai, A. Myoui, T. Tomita, T. Nakase, J. Tanaka, T. Ochi, H. Yoshikawa, Novel hydroxyapatite ceramics with an interconnective porous structure exhibit superior osteoconduction *in vivo*. J. Biomed. Mater. Res. 59, 110–117 (2002). doi:10.1002/jbm.1222
8. Q.Z. Chen, I.D. Thompson, A.R. Boccaccini, 45S5 Bioglass®-derived glass-ceramic scaffold for bone tissue engineering. Biomaterials 27, 2414–2425 (2006). doi:10.1016/j.biomaterials.2005.11.025
9. C. Wu, J. Chang, W. Zhai, S. Ni, J. Wang, Porous akermanite scaffolds for bone tissue engineering: preparation, characterization, and *in vitro* studies. J. Biomed. Mater. Res. B Appl. Biomater. 78B, 47–55 (2006). doi:10.1002/jbm.b.30456
10. Q. Fu, M.N. Rahaman, B.S. Bal, R.F. Brown, D.E. Day, Mechanical and *in vitro* performance of 13-93 bioactive glass scaffolds prepared by a polymer foam replication technique. Acta Biomater. 4, 1854–1864 (2008). doi:10.1016/j.actbio.2008.04.019
11. Q. Fu, M.N. Rahaman, W. Huang, D.E. Day, B.S. Bal, Preparation and bioactive characteristics of a porous 13-93 glass, and its fabrication into the articulating surface of a proximal tibia. J. Biomed. Mater. Res. A 82A, 222–229 (2007). doi:10.1002/jbm.a.31156

12. J.G. Dellinger, J. Cesarano III, R.D. Jamison, Robotic deposition of model hydroxyapatite scaffolds with multiple architectures and multiscale porosity for bone tissue engineering. J. Biomed. Mater. Res. A 82A, 383–394 (2007). doi:10.1002/jbm.a.31072
13. C.Y. Lin, T. Wirtz, F. LaMarca, S.J. Hollister, Structural and mechanical evaluations of a topology optimized titanium interbody fusion cage fabricated by selective laser melting process. J. Biomed. Mater. Res. A 83A, 272–279 (2007). doi:10.1002/jbm.a.31231
14. S. Deville, E. Saiz, A. Tomsia, Freeze casting of hydroxyapatite scaffolds for bone tissue engineering. Biomaterials 27, 5480–5489 (2006). doi:10.1016/j.biomaterials.2006.06.028
15. S. Deville, E. Saiz, R.K. Nalla, A. Tomsia, Freezing as a path to build complex composites. Science 311, 515–518 (2006). doi:10.1126/science.1120937
16. Q. Fu, M.N. Rahaman, F. Dogan, B.S. Bal, Freeze casting of porous hydroxyapatite scaffolds—I. Processing and general microstructure. J. Biomed. Mater. Res. B Appl. Biomater. 86B,125–135 (2008). doi:10.1002/jbm.b.30997
17. Q. Fu, M.N. Rahaman, F. Dogan, B.S. Bal, Freeze casting of porous hydroxyapatite scaffolds—II. Sintering, microstructure, and mechanical properties. J. Biomed. Mater. Res. B Appl. Biomater. 86B, 514–522 (2008). doi:10.1002/jbm.b.31051
18. Q. Fu, M.N. Rahaman, F. Dogan, B.S. Bal, Freeze-cast hydroxyapatite scaffolds for bone tissue engineering applications. Biomed Mater 3, 025005 (2008). doi:10.1088/1748-6041/3/2/025005
19. J.O. Hollinger, K. Leong, Poly(a-hydroxy acids): carriers for bone morphogenetic proteins. Biomaterials 17, 187–194 (1996).doi:10.1016/0142-9612(96)85763-2
20. Y.H. Hu, D.W. Grainger, S.R. Winn, J.O. Hollinger, Fabrication of poly(a-hydroxy acid) foam scaffolds using multiple solvent systems. J. Biomed. Mater. Res. 59, 563–572 (2002). doi:10.1002/jbm.1269
21. S. Foppiano, S.J. Marshall, G.W. Marshall, E. Saiz, A.P. Tomsia, The influence of novel bioactive glasses on *in vitro* osteoblast behavior. J. Biomed. Mater. Res. A 71A, 242–249 (2004). doi:10.1002/jbm.a.30159
22. R.F. Brown, D.E. Day, T.E. Day, S. Jung, M.N. Rahaman, Q. Fu, Growth and differentiation of osteoblastic cells on 13-93 bioactive glass fibers and scaffolds. Acta Biomater. 4, 387–396 (2008). doi:10.1016/j.actbio.2007.07.006
23. A. Sabokar, P.J. Millett, B. Myer, N. Rushton, A rapid, quantitative assay for measuring alkaline phosphatase in osteoblastic cells *in vitro*. Bone Miner. 27, 57–67 (1994). doi:10.1016/S0169-6009(08)80187-0
24. M.N. Rahaman, Q. Fu, Manipulation of porous bioceramic microstructures by freezing of aqueous suspensions with binary mixtures of solvents. J. Am. Ceram. Soc. 91(12), 4137–4140 (2008). doi:10.1111/j.1551-2916.2008.02795.x

Table 1. Microstructural characteristics of HA scaffolds prepared by a unidirectional freezing of suspensions (10 vol% particles).

Solvent composition	Microstructure	Pore width (μm)	Porosity (%)
Water	Lamellar	25 ± 5	70 ± 5
Water + dioxane (60 wt %)	Cellular	100 ± 10	65 ± 2

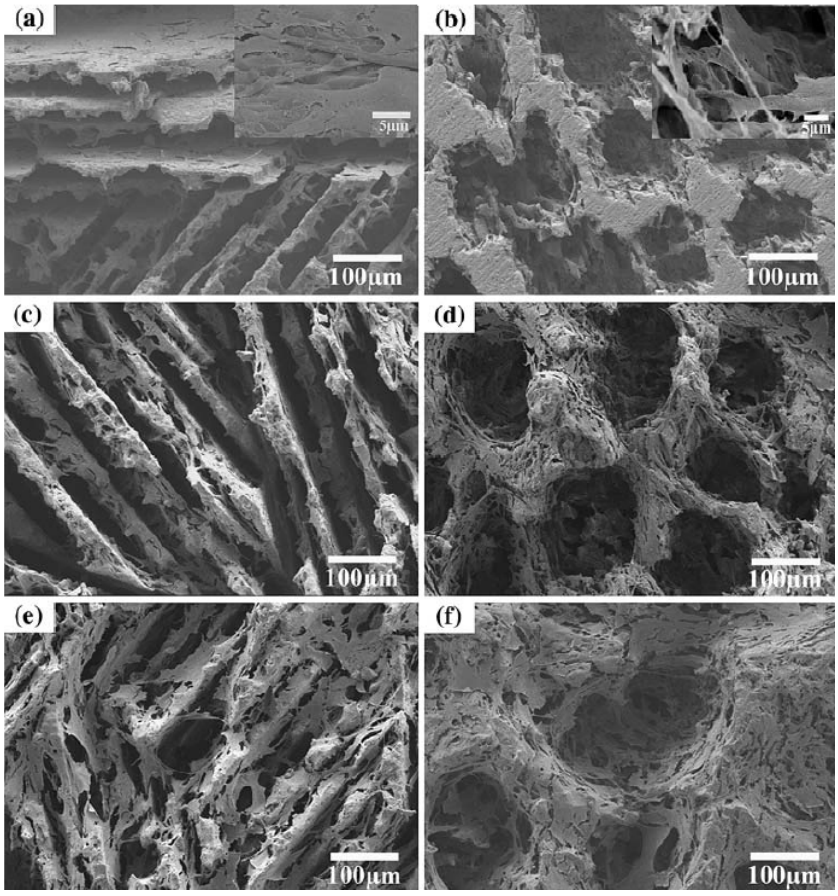

Figure 1. SEM images of MC3T3-E1 cell morphology on freeze-cast constructs with a, c, e lamellar-type and b, d, f cellular-type microstructures after culturing for a, b 2 days; c, d 4 days; e, f 6 days

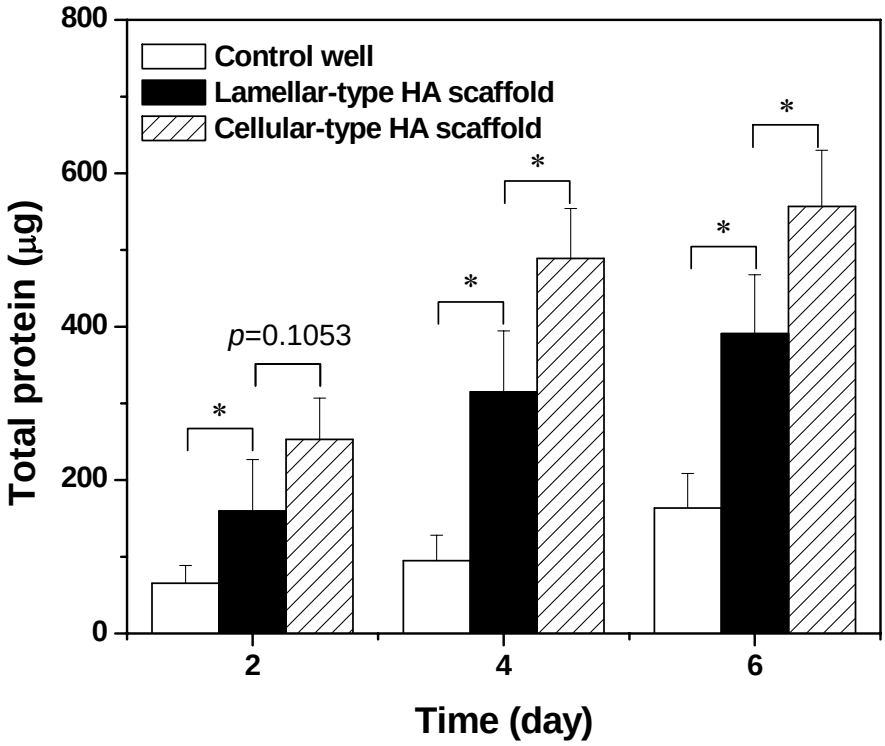

Figure 2. Quantitative measurement of total protein content of cell-seeded scaffolds or control incubated for 2, 4, and 6 days. Mean ± sd; n = 4. *Significant increase in total amount of protein on the porous HA constructs with increasing culture duration (p<0.05).

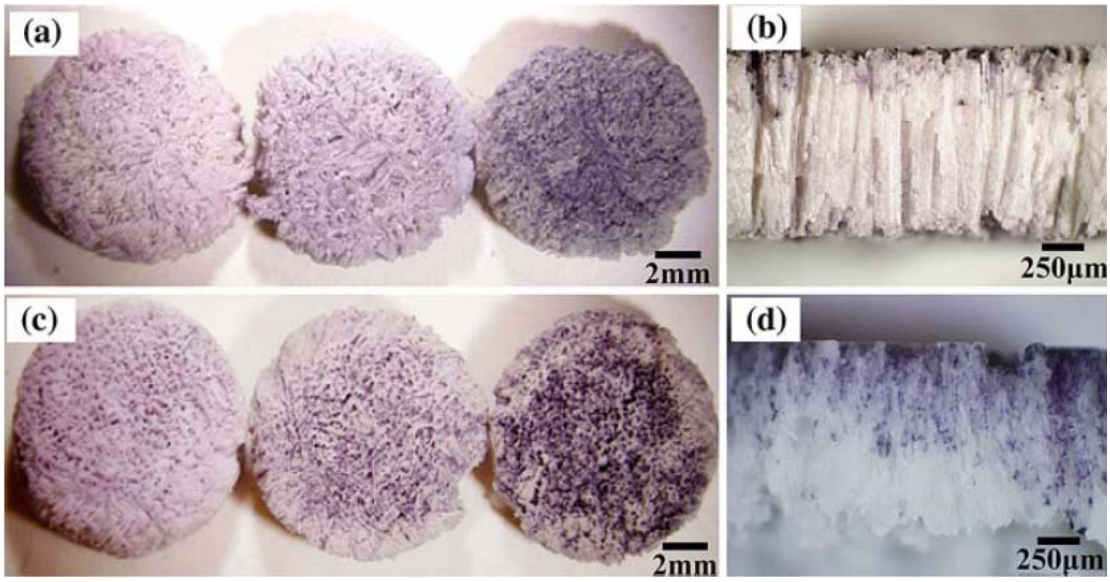

Figure 3. Cell-seeded HA constructs treated with MTT: (left) surface of constructs with a lamellar-type and c cellular-type microstructure after culture intervals of 2, 4, and 6 days (left to right, respectively); (right) freeze-fracture section of scaffold cultured for 6 days, showing considerably greater infiltration of MTT-labeled cells into the interior of the cellular microstructure d than in the lamellar microstructure b.

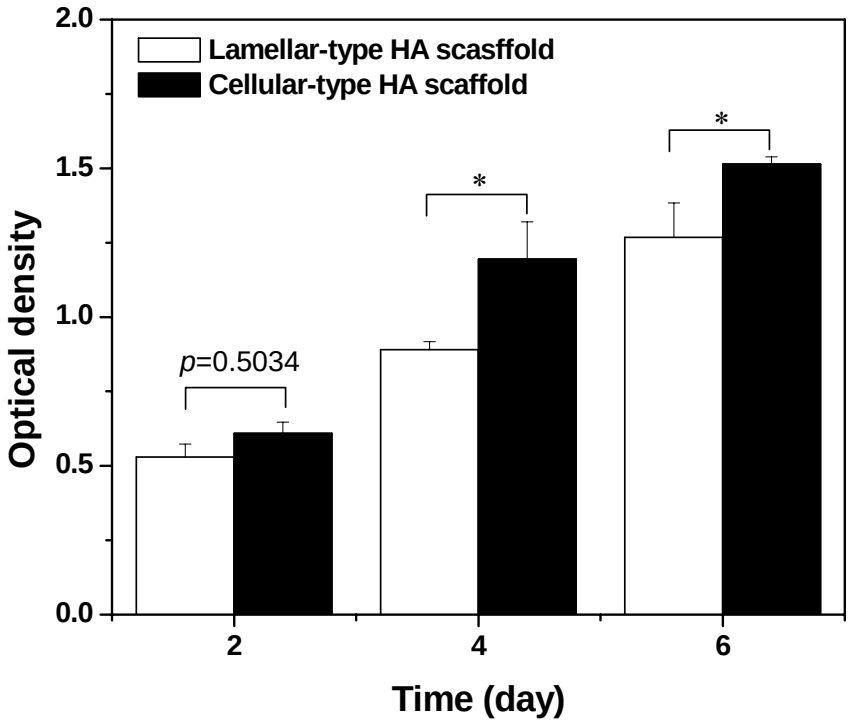

Figure 4. Quantitative analysis of the purple formazan on the HA constructs with lamellar- and cellular-type microstructures. Mean ± sd; n = 4. *Significant increase in formazan extracted from the porous HA constructs with increasing culture duration ($p<0.05$).

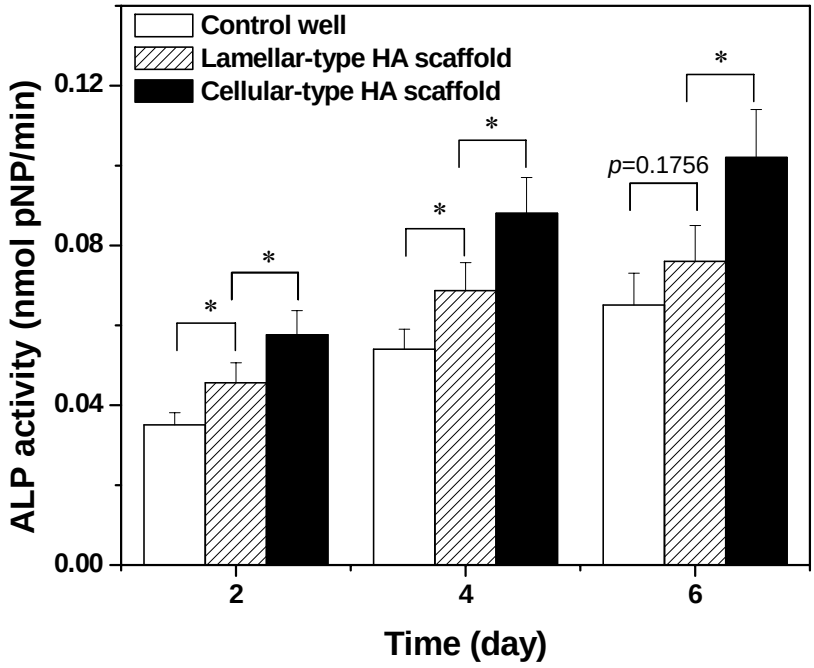

Figure 5. Alkaline phosphatase activity in MC3T3-E1 cells cultured on two types (lamellar- and cellular-type) of freeze-cast HA scaffolds and control wells. Enzyme activity is expressed as nmol of p-NP formed per min. Mean ± sd; n = 4. *Significant increase in enzyme activity on the porous HA constructs with increasing culture duration (p<0.05).

5. *IN VITRO* CELL RESPONSE TO HYDROXYAPATITE SCAFFOLDS WITH ORIENTED PORE ARCHITECTURES

Qiang Fu[a,b], Mohamed N. Rahaman[a,b,*], B. Sonny Bal[c], and Roger F. Brown[b,d]

[a]Department of Materials Science and Engineering, Missouri University of Science and Technology, Rolla, MO 65409, USA

[b]Center for Bone and Tissue Repair and Regeneration, Missouri University of Science and Technology, Rolla, MO 65409, USA

[c]Department of Orthopaedic Surgery, University of Missouri-Columbia, Columbia, Missouri 65212, USA

[d]Department of Biological Sciences, Missouri University of Science and Technology, Rolla, MO *65409, USA*

5.1. ABSTRACT

The objective of the present work was to evaluate the *in vitro* cellular response to hydroxyapatite (HA) scaffolds with oriented pore architectures. Hydroxyapatite scaffolds with approximately the same porosity (60–70%) but two different microstructures, described as 'columnar' (pore diameter = 90–110 μm) and 'lamellar' (pore width = 20–30 μm), were prepared by unidirectional freezing of suspensions. The response of murine MLO-A5 cells, an osteogenic cell line, to these oriented scaffolds was evaluated using

* Corresponding author: M. N. Rahaman (rahaman@mst.edu)

assays of MTT hydrolysis, alkaline phosphatase (ALP) activity, and alizarin red staining. While the cellular response to both groups of scaffolds was better than control wells, the columnar scaffolds with the larger pore width provided the most favorable substrate for cell proliferation and function. These results indicate that HA scaffolds with the columnar microstructure could be used for bone repair applications *in vivo*.

Keywords: Scaffold; Hydroxyapatite; Cell culture; Oriented microstructure

5.2. INTRODUCTION

Unidirectional freezing of suspensions provides a method for preparing porous bioceramic scaffolds with an oriented microstructure [1–9]. The method involves rapid unidirectional freezing of an aqueous suspension of fine particles in a nonporous mold, and sublimation of the frozen solvent under cold temperatures in a vacuum. After drying, the porous construct is sintered to densify the solid phase, thereby improving the mechanical strength without significantly altering the porosity between the solid phase which resulted from sublimation of the frozen liquid. The microstructure and, hence, the properties of the final sintered construct are determined essentially by the concentration of particles in the aqueous suspension and the freezing rate.

Because of the hexagonal crystal structure of the growing ice columns, unidirectional freezing of aqueous suspensions typically result in a lamellar-type microstructure, in which the lamellae and inter-lamellar pores are oriented in the direction of freezing [3,6]. Hydroxyapatite (HA) constructs with inter-lamellar pore widths in the range 10–40 μm have been prepared from aqueous suspensions. Our recent

work showed that by manipulating the solvent composition of the HA suspensions, porous constructs with drastically different oriented microstructures could be obtained by the unidirectional freezing method [6]. The addition of 5–20 weight percent (wt%) glycerol to the suspension resulted in the formation of a rectangular-type microstructure with finer pores (pore width = 5–20 μm). On the other hand, the addition of 60 wt% 1–4 dioxane resulted in a columnar-type microstructure with much larger pores, approximately circular in cross section (diameter = 90–110 μm). The formation of these different oriented microstructures is discussed in detail elsewhere [8].

These oriented HA microstructures obtained by unidirectional freezing of suspensions mimicked those of natural materials, such as trabecular bone, cork, and wood [10]. When tested in the direction of pore orientation, the HA constructs (porosity = 65–70%) showed compressive strengths of up to 15–20 MPa, far higher than the compressive strengths reported for trabecular bone (2–12 MPa). The constructs also showed a unique 'elastic–plastic' response in compression, with a large deformation for failure (>20%), and strain rate sensitivity [7,8]. This type of mechanical response, which is unlike the brittle response of ceramics, is more characteristic of natural materials [11–16].

Based on the unique mechanical response and the favorable pore characteristics of the HA constructs with the columnar microstructure, this *in vitro* investigation was undertaken to evaluate the ability of these oriented constructs to support cell proliferation and function. For comparison, the cellular response to the lamellar constructs was also evaluated. MLO-A5 cells, an established osteogenic cell line, was chosen for these experiments because of its highly elevated expression of osteogenic phenotype traits such as alkaline phosphatase activity and mineralization [17,18]. The ability of the constructs

to support the attachment, infiltration, proliferation, and differentiation of MLO-A5 cells was evaluated to assess the potential application of these constructs as scaffolds for bone repair and replacement.

5.3. MATERIALS AND METHODS

5.3.1. Preparation of HA Scaffolds. Hydroxyapatite scaffolds with an oriented microstructure were prepared by unidirectional freezing of suspensions as described in detail elsewhere [6]. Briefly, the suspensions contained 10 vol% HA particles (average particle size <1 μm; Alfa Aesar, Haverhill, MA), 0.75 wt% dispersant (Dynol 604; Air Products & Chemicals, Inc., Allentown, PA), and 1.5 wt% binder (DuPont Elvanol® 90-50; DuPont, Wilmington, DE). Aqueous suspensions, as well as aqueous suspensions containing 60 wt% dioxane (Fisher Scientific, St. Louis, MO) were used to prepare HA scaffolds with approximately the same porosity (65–70%) but with widely different pore characteristics. Unidirectional freezing was performed by pouring the suspensions into poly(vinyl chloride), PVC, tubes (~10 mm internal diameter × 20 mm long) placed on a cold steel substrate at –20°C in a freeze dryer (Genesis 25 SQ Freeze Dryer, VirTis Co., Gardiner, NY). After sublimation of the frozen solvent in the freeze dryer, the constructs were sintered in air for 3 h at 1350°C (heating and cooling rate = 3°C/min). Scaffolds (~8 mm in diameter × 2 mm thick) for cell culture experiments were prepared by sectioning the sintered constructs using a diamond-coated blade, washing 3 times with deionized water and ethanol, and dry heat sterilized for 24 hours at 500°C.

5.3.2. Cell Culture. The established MLO-A5 post-osteoblast/pre-osteocyte murine cell line, kindly provided by Professor Lynda F. Bonewald, University of Missouri-Kansas City, was used in this study. The stock cells were maintained in

collagen-coated plates (rat tail collagen type I, 0.15 mg/ml) containing α-MEM medium supplemented with 5% fetal bovine serum (FCS) and 5% newborn calf serum (NCS) plus 100 U/ml penicillin. The dry-heat sterilized constructs (8 mm in diameter × 2 mm thick) were seeded with 60,000 MLO-A5 cells suspended in 100 µl of complete medium and incubated for 4 h to permit cell attachment. The cell-seeded constructs were then transferred to a 24-well plate containing 2 ml of complete medium per well. The control group consisted of the same number of cells seeded in wells containing 2 ml of media. All cell cultures were maintained at 37 ºC in a humidified atmosphere of 5% CO_2, with the medium changed every 2 days. For induction of mineralization, some scaffolds and control wells were incubated in mineralizing media, α-MEM with 10% FCS, 5 mM β-glycerol phosphate (βGP), 100 µg/ml ascorbic acid, following the method described elsewhere [18].

5.3.3. Cell Morphology. After selected intervals, HA scaffolds with attached cells were removed, washed twice with warm PBS, and placed in 2.5% glutaraldehyde in PBS. After an overnight soak in glutaraldehyde, the fixed samples were washed extensively with PBS and dehydrated through a graded series of ethyl alcohol, followed by two soaks in hexamethyldisilazane (HMDS) for 10 min each. The samples were allowed to fully evaporate, sputter-coated with Au/Pd, and then observed in a scanning electron microscope, SEM (Hitachi S-4700), at 5 kV accelerating voltage.

5.3.4. MTT Detection of Viable Cells. To visualize the metabolically active cells on and within the porous HA constructs, the cell-seeded constructs were placed in 400 µl serum-free medium containing 100 µg of the tetrazolium salt MTT for the last 4 h of incubation. After incubation, the constructs were briefly rinsed in PBS, blotted, and

allowed to dry. Images of the constructs were obtained using a stereomicroscope fitted with a digital camera to qualitatively assess the distribution of insoluble purple formazan, a product of mitochondrial reduction of MTT by viable cells. The MTT-labeled constructs were then frozen at –80ºC and fractured with a cooled microtome blade. The fracture cross-section was visually examined to assess the presence of purple formazan within the interior of the constructs. Finally, the formazan product was extracted from the HA constructs with 1.0 ml ethanol and measured spectrophotometrically at 550 nm in a BMG FLUORstar Optima plate reader.

5.3.5. Quantitative Protein Assay. The amount of protein in lysates recovered from the cell-seeded scaffolds was measured to assess the cell proliferation on the scaffold. The scaffolds were placed in 500 μl of 1% Triton X-100 and the cells lysed by two freeze-thaw cycles (–80/37ºC). Aliquots of the released lysate were mixed with working reagent prepared from a micro-BCA Protein Assay Kit (Piece Biotechnology, Rockford, IL). Resultant absorbance values were measured at 550 nm in a BMG FLUORstar Optima plate reader with bovine serum albumin used as standard for comparison.

5.3.6. Alkaline Phosphatase (ALP) Activity. The cell-seeded constructs were removed at the intervals of 2, 4, 6 and 8 days and washed twice with PBS. The samples were placed in 500 μl of 1 % Triton X-100 and cells were lysed using two –80/37ºC cycles. Aliquots of lysate were placed in a 96-well plate for spectrophotometric measurement of alkaline phosphatase (ALP) activity with *p*-nitrophenyl phosphate (*p*-NPP) substrate as described elsewhere [18].

5.3.7. Alizarin Red S staining for Mineralization and Quantitation. After incubating for 3, 6, 9 and 12 days, the cell-seeded constructs and control wells were washed twice with PBS. The cells with adherent mineralized nodules were removed from the constructs and control wells with trypsin-EDTA, washed with isotonic NaCl, and stained with 4 nM alizarin red S (pH = 4.2) for 2 minutes. The stained cells were then rinsed with nanopure water and centrifuged 5 times to remove the nonspecific stain. The pellets of stained cells were placed into a 96-well plate and observed using a stereomicroscope fitted with a digital camera. The bound alizarin red S stain was extracted by sonicating for 10 min with 10 mM HCl in 70% ethanol. The extracts were then diluted with 5 volumes of PBS and the absorbance measured at 550 nm in a BMG FLUORstar Optima plate reader for the determination of mineralization.

5.3.8. Statistical Analysis. All biological experiments (4 samples in each group) were run either in duplicate or triplicate. The data are presented as the mean ± standard deviation. Statistical analysis was performed with one-way analysis of variance (ANOVA) followed by a Tukey's *post hoc* test, with the level of significance set at $p<0.05$.

5.4. RESULTS

5.4.1. Microstructure of HA Scaffolds. The microstructure and pore characteristics of the HA scaffolds used in the present work are summarized in Table 1. SEM images in Fig. 1 show microstructures of scaffolds sectioned perpendicular to the freezing direction. There were no marked changes in the microstructure along the length of the sample, so each cross-section was, in general, representative of the whole

construct. Unidirectional freezing of suspensions containing dioxane (60 wt%) resulted in a columnar microstructure (Fig. 1a) with pores approximately circular in cross section (diameter = 90–110 μm) aligned in the direction of freezing. In contrast, a lamellar microstructure was obtained by freezing aqueous suspensions, with the lamellae and the inter-lamellar pores oriented in the direction of freezing (Fig. 1b). The lamellar pores had a length of 100–300 μm and a width of 20–30 μm.

5.4.2. SEM Examination of Cultures. SEM images in Fig. 2 show the morphology of MLO-A5 cells grown on the surface of the columnar and lamellar scaffolds for 2, 4 and 6 days. The cells seeded on the columnar scaffolds appeared to be attached to the scaffolds by slender cell projections at day 2 (Fig. 2a), and show a large increase in density with the duration of culture. It is apparent that the cells had grown along the walls of the columnar-type pores and down into the interior of these scaffolds. After 4 days, cell colonization of the walls of the scaffolds was evident (Fig. 2b) and after 6 days, the walls were completely covered with cells (Fig. 2c). The cells showed evidence of physical contact and aggregation with neighboring cells via multiple extensions. The cells visible in the micrographs of the lamellar scaffolds were elongated and appeared to align along the walls of the scaffolds at low cell density after culturing for 2 and 4 days (Figs. 2d and 2e). After culturing for 6 days (Fig. 2f), there was greater cell density on the surface of the scaffolds, with more cells bridging the lamellar pores.

5.4.3. MTT Assay. Photographic images of cell-seeded scaffolds treated with MTT during the last 4 h of incubation are shown in Fig. 3. The purple pigment visible on the scaffold was the result of mitochondrial reduction of MTT to an insoluble formazan product and an indication of viable cells. The increase in intensity of the purple

color on the surface of the scaffolds with culture time indicated the proliferation of viable, metabolically active cells on the surface of the scaffolds (Figs. 3a and c). The purple staining visible on the freeze-fracture surface of the scaffolds cultured for 6 days (Figs. 3b and d) indicated the relative density of metabolically active MLO-A5 cells within the interior of the construct. The larger and more uniform purple area on the fracture surface of the columnar scaffolds, relative to that seen on the lamellar scaffolds, indicated the proliferation of more metabolically active cells into the columnar scaffolds.

Results of the quantitative measurement of the amounts of the purple formazan extracted from the scaffolds are presented in Fig. 4. The results show a linear increase in the absorbance values with the incubation time, indicative of a larger number of cells present in the scaffolds. The results of the absorbance measurements also show that a higher amount of the formazan extract was recovered from cells cultured on columnar HA scaffolds at all time intervals. This is additional evidence of greater cell growth in the columnar scaffolds, and is consistent with the photographic images of the MTT labeled scaffolds.

The proliferation MTT-labeled of MLO-A5 cells into the pores of the columnar-type scaffolds is shown in Fig. 5. A linear growth rate of ~150 μm/day was determined. The pores of the scaffold were completely covered by MTT-labeled cells after culturing for 12 days (Fig. 5; inset image). The ability of the columnar-type scaffolds to support live cell ingrowth was further investigated by dipping one end of an as-fabricated scaffold (to a depth of < 1mm) in a cell suspension (150,000 cells/ml) and monitoring the cell migration into the scaffold. As a result of the capillary pressure of the pores, the cell suspension was pulled up to completely fill the pores within <5 s. After incubation for 4

h, the scaffolds were treated with MTT for another 4 h. Photographic images of the MTT-labeled construct are shown in Fig. 6. The coverage of the purple color on the surface of the constructs (Figs. 6a and 6b) indicates that viable cells are able to migrate along the pores at the surface. The color within the cross section of the constructs is evidence that the columnar pores are large enough for cell to migrate through the constructs and to provide enough nutrients for the cells.

5.4.4. Quantitation of Protein. Results of the quantitative assay of total protein in cell lysates recovered from the HA scaffolds and the control wells after incubation for 2, 4, 6, and 8 days are shown in Fig. 7. The amounts of protein recovered the HA scaffolds showed a nearly linear increase in cell proliferation during the 6-day incubation, a finding that complements the progressive increase in cell density seen in the SEM images. The amount of protein recovered from the lamellar HA scaffolds and the control wells reached a plateau at 6 days. In comparison, the amount of protein recovered from the cultures on the columnar HA scaffolds continued to increase. This is evidence that the columnar scaffolds are capable of supporting continuous ingrowth of the cells, a finding that complemented the SEM observation of the cell morphology (Fig. 2). The higher amounts of protein on the columnar scaffolds, compared with that recovered from the lamellar scaffolds, indicated that the cells were better able to grow in scaffolds with pores of size ~100 μm rather than in those with smaller lamellar-type pores. These data also indicate that the MLO-A5 cells were able to grow at a higher rate on the HA scaffolds than they did on the surface of plastic culture vessels.

5.4.5. Alkaline Phosphatase Activity. Results of spectrophotometric measurement of alkaline phosphatase activity of MLO-A5 cells cultured on the HA scaffolds for 2, 4, 6 and 8 d are presented in Fig. 8. As shown, alkaline phosphatase activity increased with the duration of incubation. This finding is an indication that these cells were able to carry out osteogenic function on the HA scaffolds. The higher alkaline phosphatase activity of the columnar scaffolds than that of the lamellar scaffolds indicates the better ability of the columnar scaffolds to support cell differentiation.

5.4.6. Mineralization. To assess the ability of the scaffolds to support mineralization by MLO-A5 cells, the cells and extracellular materials were removed from the HA constructs by trypsinization after various culture intervals and stained with alizarin red S to test for the presence of calcium deposits. The stained nodules recovered from the columnar-type scaffolds are shown in Fig. 9. At day 3, almost no nodules were observed. An increasing amount of stained nodules was seen as the culture time increased from 6 to 12 days. A higher magnification image of the red stained bone nodules is shown in Fig. 10. Quantification of the mineralization from the HA scaffolds was done by spectrophotometric measurement of the amount of dye extracted from the stained nodules. Fig. 11 shows the absorbance of alizarin red S extracted from cells and nodules on the HA scaffolds and control wells. Higher absorbance values measured for cell lysates recovered from the columnar HA scaffolds demonstrate a greater capacity of these scaffolds for supporting mineralization.

5.5. DISCUSSION

Our previous work showed that HA scaffolds with oriented microstructures and unique mechanical properties could be prepared by unidirectional freezing of suspensions [6-8]. The method is applicable not just to HA, but also to other inorganic materials. In the present work, the potential applicability of oriented HA scaffolds for repairing bone defects was evaluated using MLO-A5 cells as an *in vitro* model of newly forming bone tissue.

The results showed that while both groups of scaffolds supported the cell attachment and cell proliferation on their surfaces, the columnar scaffolds with larger pore widths (diameter = 100 ± 10 μm were favored by the MLO-A5 cells. The ability to support cell proliferation into the pores in the interior of the scaffold is a major requirement for a scaffold [19]. The considerably greater amount of purple color seen on the freeze-fracture surface of the columnar scaffolds (Fig. 3) indicated much more viable cells within the interior of these scaffolds. This is an indication that the pore size of the columnar scaffolds is sufficient to allow enough nutrient to permeate the scaffolds to keep the cells metabolically viable. The cell infiltration experiment (Fig. 6) provides additional evidence that the columnar scaffolds have the capacity to allow cells to migrate through it.

Alkaline phosphatase is one of the most widely recognized biochemical markers for bone progenitor cell activity and is believed to play a role in bone mineralization [20]. Scaffolds for bone tissue engineering applications must support the differentiation of bone progenitor cells to functional bone tissue. The results of the study shows that MLO-A5 cell cultured on both groups of HA scaffolds expressed higher levels of this enzyme

than those on control wells, and the activity level continued to increase with incubation time up to 8 days. The columnar scaffolds expressed the highest level of alkaline phosphatase activity, evidence of a more optimal structure for support of bone progenitor cell function.

In addition to the initial evaluation of the alkaline phosphatase activity as indicative of differential function of the MLO-A5 cells, the identification of alizarin red-positive nodules is evidence of mineralization, a late event in bone differentiation [18,21]. The production of mineralized matrix and nodules by bone progenitor cells is an important evaluation criteria for the development of scaffolds for bone tissue engineering. Columnar HA scaffolds showed enhanced ability to support MLO-A5 cells to mineralize when compared with the lamellar- and celllar-type pores and the control wells (Fig. 11). This is an indication of the improved cell response of the HA constructs with columnar-type pores.

The *in vitro* cell culture response observed in the present work, coupled with the favorable pore characteristics, microstructure, and mechanical response described in our previous work [6-8], indicates the potential usefulness of the columnar HA constructs for eventual application in bone repair and regeneration. The *in vivo* evaluation of these scaffolds in an animal model is currently underway.

5.6. CONCLUSION

Hydroxyapatite (HA) scaffolds with two different oriented microstructures (columnar and lamellar) were prepared by unidirectional freezing of suspensions. The ability of the constructs to support cell proliferation and function was evaluated *in vitro*

using murine MLO-A5 cells, an osteogenic cell line. Whereas both groups of scaffolds showed the ability to support cell proliferation, differentiated function, and mineralization, the columnar scaffolds were most favored by these progenitor cells. The columnar scaffolds also supported ingrowth of cells throughout the unidirectional pores during culture, and were rapidly infiltrated with a cell suspension by capillary action of the pores. These *in vitro* cell culture results suggest that freeze-cast constructs with the columnar microstructure could be potentially used as scaffolds for bone repair and regeneration.

5.7. REFERENCES

1. Araki K, Halloran JW. J. Am. Ceram. Soc. 87 (2004) 2014.
2. Araki K, Halloran JW. J. Am. Ceram. Soc. 88 (2005) 1108.
3. Deville S, Saiz E, Tomsia AP. Biomaterials 27 (2006) 5480.
4. Deville S, Saiz E, Nalla RK, Tomsia AP. Science 311 (2006) 515.
5. Song JH, Koh YH, Kim HE, Li LH, Bahn HJ. J. Am. Ceram. Soc. 89 (2006) 2649.
6. Fu Q, Rahaman MN, Dogan F, Bal BS. J. Biomed. Mater. Res. B Appl. Biomater. 86B (2008) 125.
7. Fu Q, Rahaman MN, Dogan F, Bal BS. J. Biomed. Mater. Res. B Appl. Biomater. 86B (2008) 514.
8. Rahaman MN, Fu Q. J. Am. Ceram. Soc. 91 (2008) 4137.
9. Landi E, Valentini F, Tampieri A. Acta Biomater. 4 (2008) 1620.
10. Fu Q, Rahaman MN, Dogan F, Bal BS. Ceramic Trans 2008 (in press).
11. Ashby MF, Gibson LJ, Wegst U, Olive R. Proc. Roy. Soc. Lond A 450 (1995) 141.
12. Gibson LJ, AShby MF. Cellular solids: structure and properties, 2nded, Cambridge University Press, New York 1997.
13. Weiner S, Wagner HD. Ann. Rev. Mater. Sci. 28 (1998) 271.
14. Peterlik H, Roschger P, Klaushofer K, Fratzl P. Nature Mater. 5 (2006) 52.
15. Fratzl P, Weinkamer R. Prog. Mater. Sci. 52 (2007) 1263.
16. Meyers MA, Chen P, Lin AY, Seki Y. Prog. Mater. Sci. 53 (2008) 1.
17. Kato Y, Boskey A, Spevak L, Dallas M, Hori M, Bonewald LF. J. Bone Miner. Res. 16 (2001) 1622.
18. Barragan-Adjemian C, Nicolella D, Dusevich V, Dallas MR, Eick JD, Bonewald LF. Calcif. Tissue Int. 79 (2006) 340.
19. Hutmacher D W. Biomaterials 21 (2000) 2529.
20. Sabokbar A, Millett PJ, Myer B, Rushton N. Bone Miner 27 (1994) 57.
21. Chang YL, Stanford CM, Keller JC. J. Biomed. Mater. Res. 52 (2000) 270.

Table 1. Microstructural characteristics of HA scaffolds prepared by unidirectional freezing of suspensions (10 vol% particles) and used in this work.

Solvent composition	Microstructure	Pore width (μm)	Porosity (%)
Water	Lamellar	25 ± 5	70 ± 5
Water + dioxane (60 wt%)	Columnar	100 ± 10	65 ± 2

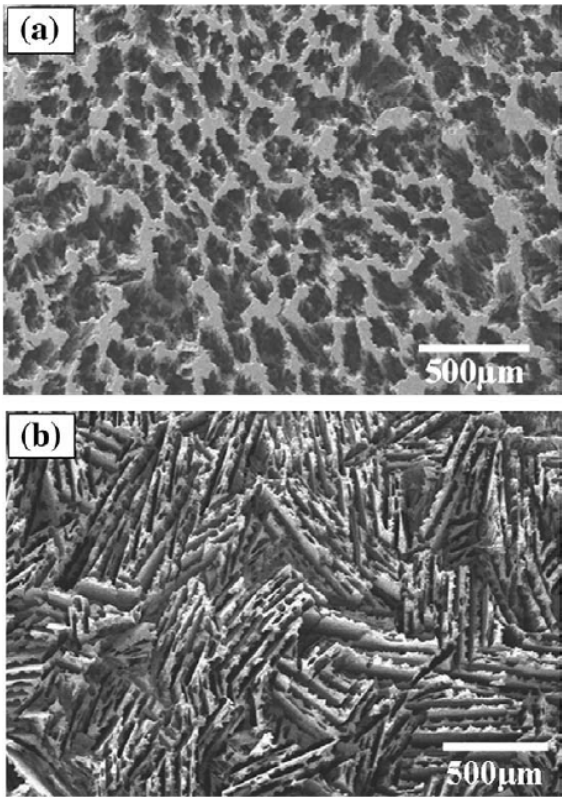

Figure 1. SEM images of HA constructs prepared by unidirectional freezing of suspensions (10 vol% particles) with three different microstructures: (a) columnar; (b) lamellar.

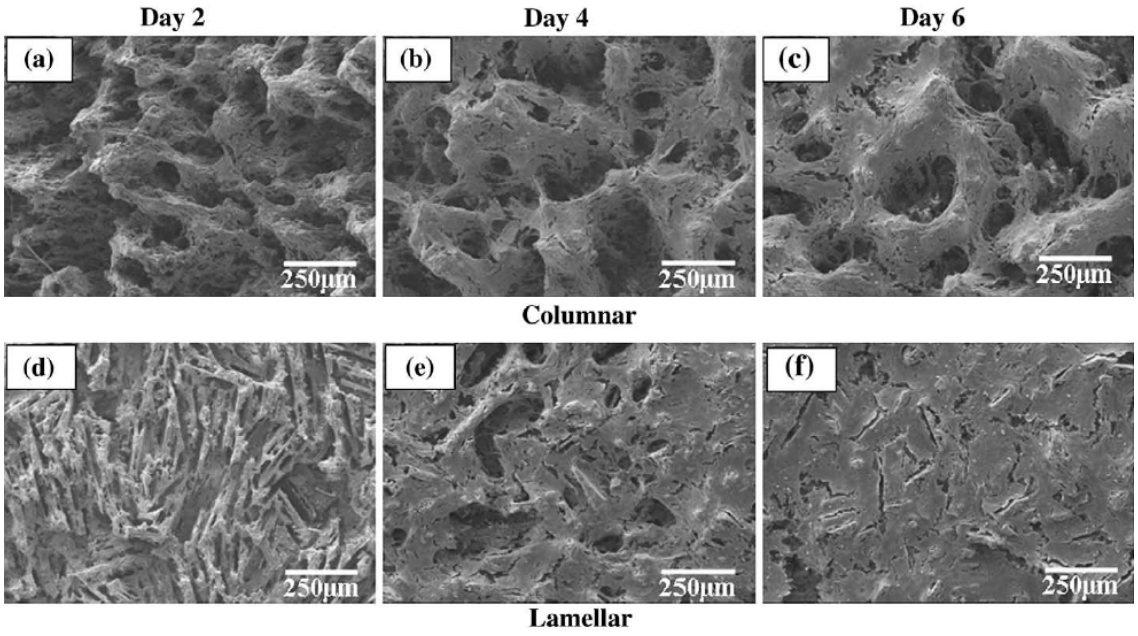

Figure 2. SEM images of MLO-A5 cell morphology on freeze-cast HA constructs with (a-c) columnar-type, (d-f) lamellar-type, after culturing for (a, d) 2 days; (b, e) 4 days; (c, f) 6 days.

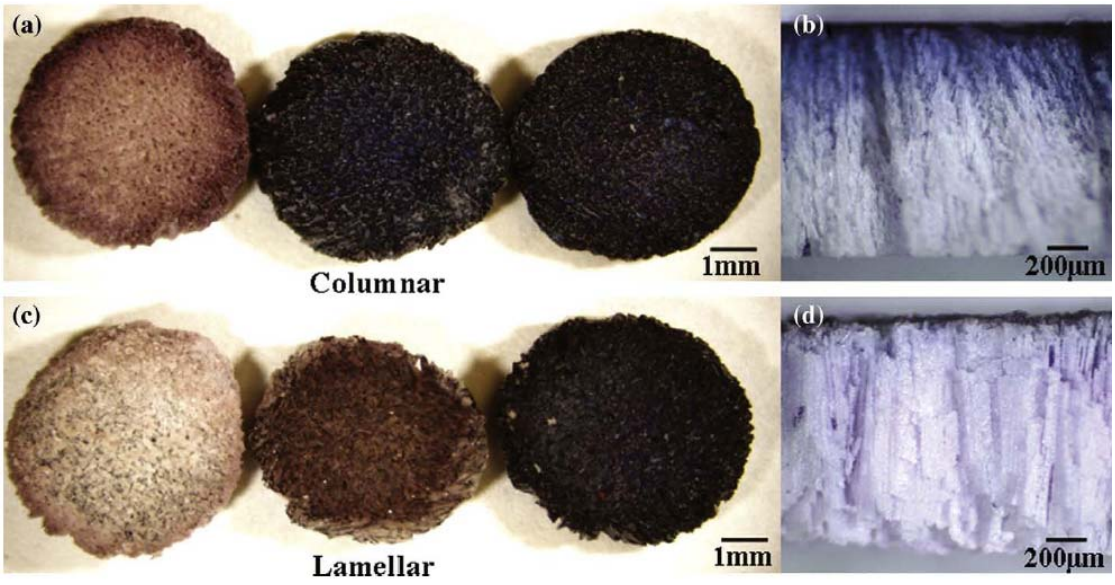

Figure 3. Cell-seeded HA constructs treated with MTT: surface of constructs with (a) columnar-type, (c) lamellar-type microstructure after culture intervals of 2, 4, and 6 days (left to right, respectively); (b, d) freeze-fracture face of scaffolds cultured for 6 days, showing clusters of MTT-labeled cells within the interior.

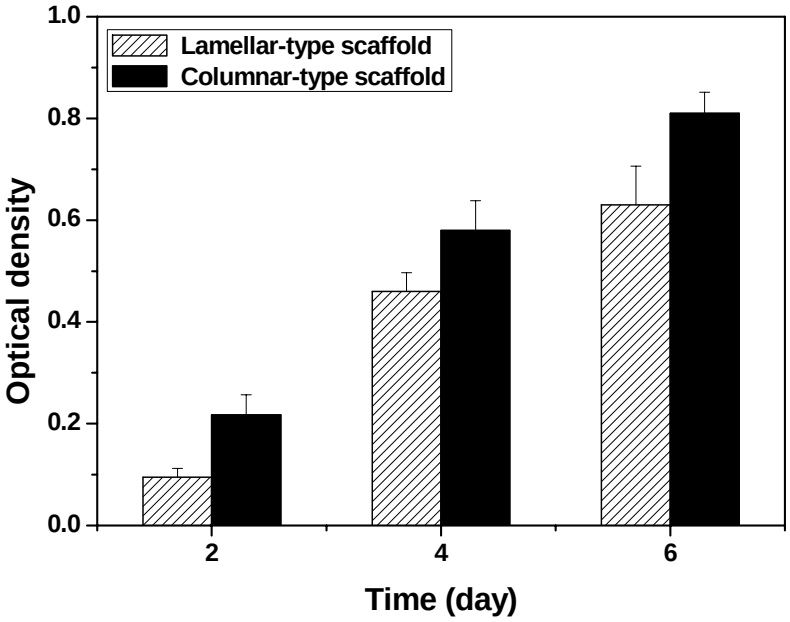

Figure 4. Quantitative measurement of the amount of the formazan present in the cell-seeded constructs after MTT labeling. Except where indicated, all pairs are significantly different (p<0.05).

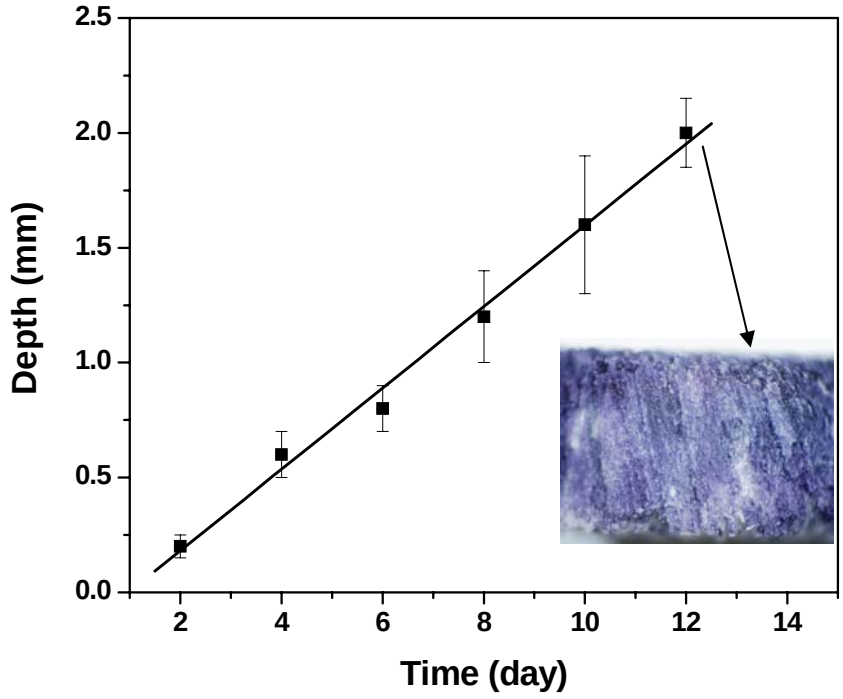

Figure 5. Proliferation of MLO-A5 cells into the unidirectional pores of the columnar-type scaffolds as a function of culture time. The ingrowth of cells was determined by measuring the depth of the purple color visible on the fracture face. The inset image indicates the ingrowth of cells throughout the porous construct after 12 days of culture.

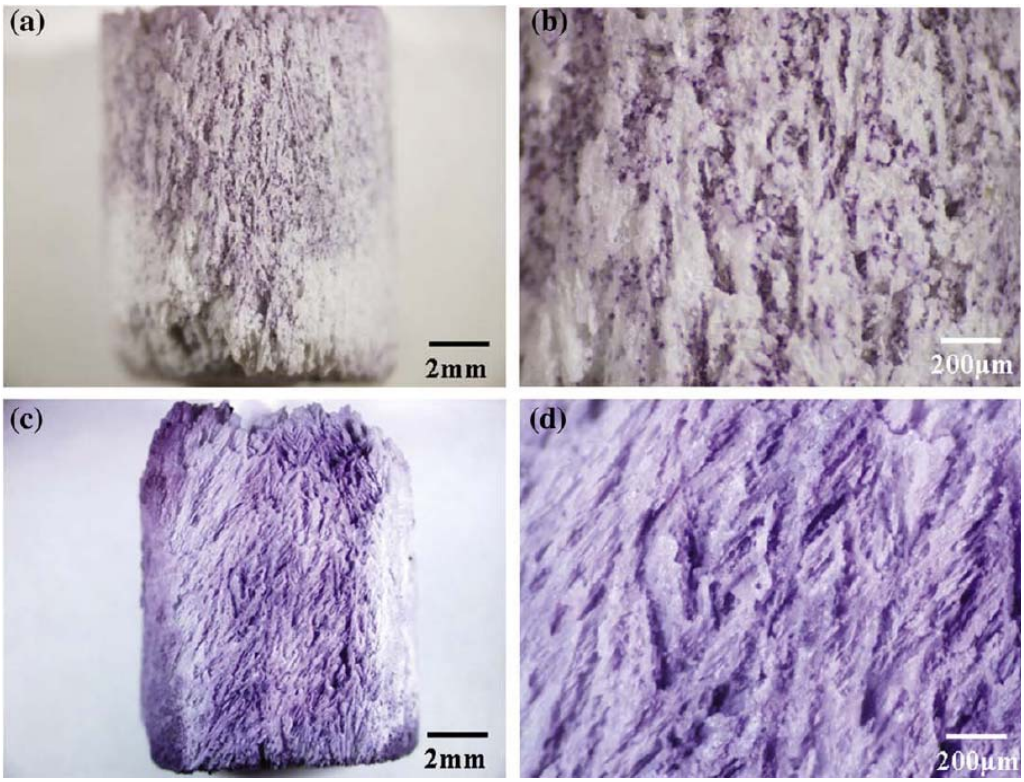

Figure 6. HA constructs with a columnar-type microstructure after they were dipped slightly (< 1 mm) in a cell suspension, and then treated with MTT: (a, b) surface and (c, d) cross section of construct, showing the MTT-labeled cell clusters on and within the scaffolds.

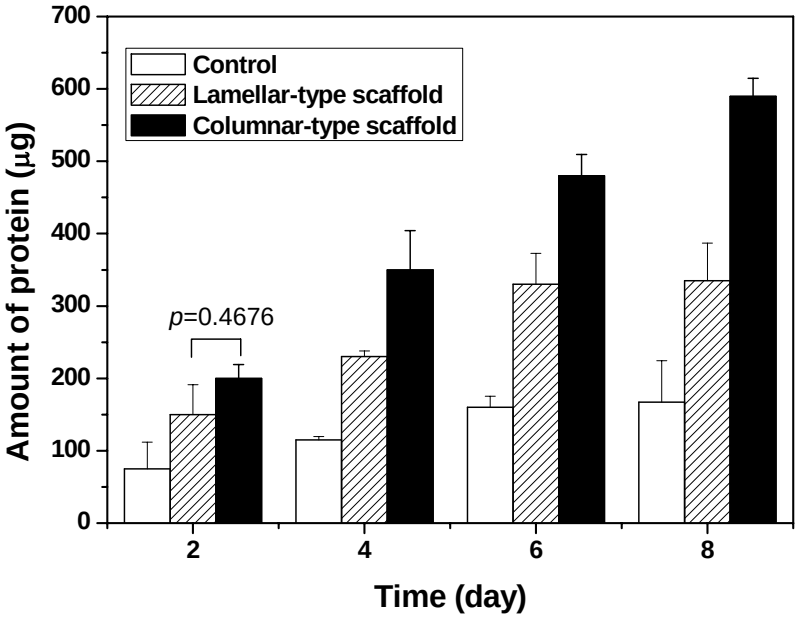

Figure 7. Quantitative measurement of total protein content per scaffold or well in MLO-A5 cell cultures incubated for 2, 4, 6 and 8 days on HA constructs with different pore morphology, and in control wells. Mean ± sd; n = 4. Except where indicated, all pairs are significantly different ($p<0.05$).

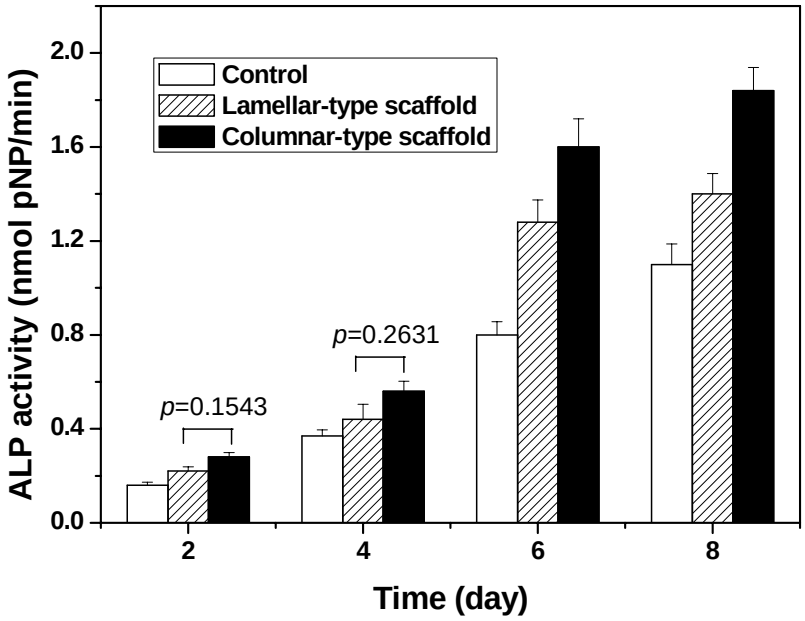

Figure 8. Alkaline phosphatase activity in MLO-A5 cells cultured on HA scaffolds with different pore morphology and control well for 2, 4, 6 and 8 days. Mean ± sd; n = 4. Except where indicated, all pairs are significantly different ($p<0.05$).

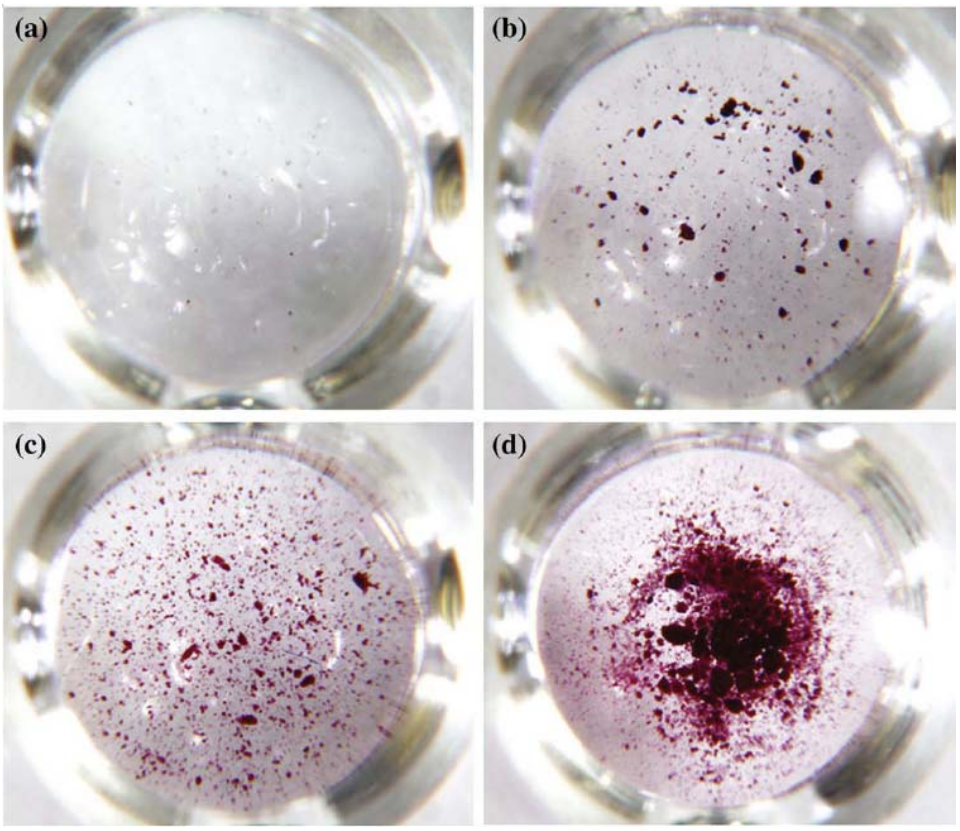

Figure 9. Optical images of bone nodules recovered from HA constructs with the columnar-type microstructure cultured for (a) 3, (b) 6, (c) 9 and (d) 12 days, and stained with alizarin red S.

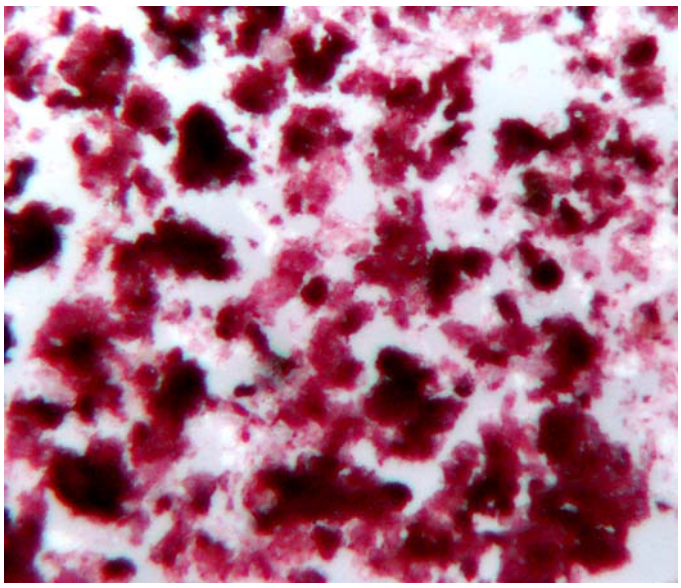

Figure 10. Optical image of bone nodules recovered by trypsinization from HA constructs with a columnar-type microstructure stained with alizarin red S. The construct was cultured for12 days.

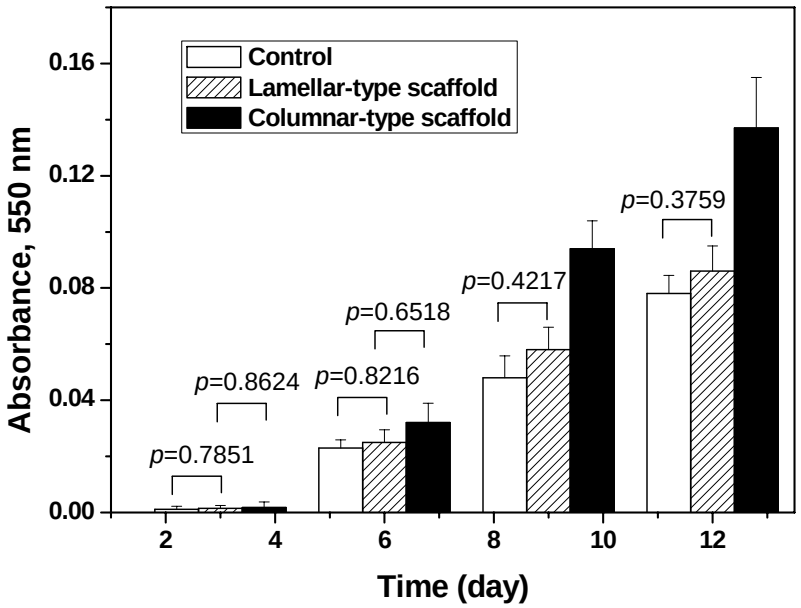

Figure 11. Quantitative analysis of the mineralization by measuring the absorbance of the extracted alizarin red dye. Except where indicated, all pairs are significantly different ($p<0.05$).

6. PREPARATION AND *IN VITRO* EVALUATION OF BIOACTIVE GLASS (13-93) SCAFFOLDS WITH ORIENTED MICROSTRUCTURES FOR REPAIR AND REGENERATION OF LOAD-BEARING BONES

Qiang Fu[1,2], Mohamed N. Rahaman[1,2*], Roger F. Brown[2,3], B. Sonny Bal[4]

[1]Department of Materials Science and Engineering, Missouri University of Science and Technology, Rolla, MO 65409, USA

[2]Center for Bone and Tissue Repair and Regeneration, Missouri University of Science and Technology, Rolla, MO 65409, USA

[3]Department of Biological Sciences, Missouri University of Science and Technology, Rolla, MO 65409, USA

[4] Department of Orthopaedic Surgery, University of Missouri-Columbia, Columbia, Missouri 65212, USA

6.1. ABSTRACT

Bioactive glass (13-93) scaffolds with oriented microstructures, referred to as 'columnar' and 'lamellar', were prepared by unidirectional freezing of suspensions, and evaluated *in vitro* for potential use in the repair and regeneration of load-bearing bones *in vivo*. Both groups of scaffolds showed an 'elastic–plastic' mechanical response in compression, large strain for failure (>20%), and strain rate sensitivity, but the columnar scaffolds had the additional advantages of higher strength and larger pore width. At the

* Corresponding author: M. N. Rahaman (rahaman@mst.edu)

equivalent porosity (55–60%) and deformation rate (0.5 mm/min), the columnar scaffolds had a compressive strength of 25 ± 3 MPa and pore width of 90–110 μm, compared to values of 10 ± 2 MPa and 20–30 μm, respectively, for the lamellar scaffolds. Cellular response to the scaffolds was evaluated using murine MLO-A5 cells, an osteogenic cell line. While the cellular response to both groups of scaffolds was better than control wells, the columnar scaffolds with the larger pore width provided the most favorable substrate for cell proliferation and function. These results indicate that 13-93 bioactive glass scaffolds with the columnar microstructure could be used for the repair and regeneration of load-bearing bones *in vivo*.

Keywords: bioactive glass; scaffold; freeze casting; cell culture; mineralization

6.2. INTRODUCTION

The demand for synthetic scaffolds to repair damaged or diseased bone in humans and animals is increasing because of concerns associated with current treatments using bone autograft, bone allograft, or metal implants (e.g., limited supply, donor site morbidity, immune rejection, potential transmission of pathogens, unpredictable long-term durability, uncertain healing to host bone, and high costs). However, synthetic scaffolds prepared by current methods from biodegradable polymers, bioactive ceramics, and bioactive glasses often lack the combination of high strength and high porosity for skeletal substitution at load-bearing sites. They are limited to low-stress applications instead, such as filling of contained bone defects, where adjacent intact bone provides mechanical rigidity and support.

The repair and regeneration of large defects in load-bearing bones of the limbs, remains an unsolved clinical problem. Situations in which long bone discontinuities are encountered include traumatic injuries suffered in war or in automobile accidents, bone resection for tumors, and bone loss from complex, revision total hip or total knee surgery. When compared to bone allografts and custom metal augments currently used to address segmental skeletal deficiency, porous scaffolds that mimic bone would be ideal bone substitutes. However, such porous scaffolds should have mechanical strengths far higher than those obtained with currently-used fabrication methods. The scaffolds should also support tissue growth into the porous scaffolds, to allow strong bonding and facile integration with apposing host bone and surrounding soft tissues.

Bioactive glass, glass-ceramics, and ceramics, referred to collectively as 'bioactive ceramics', are attractive scaffold materials for repairing diseased or damaged bone because of their ability to bond to surrounding tissue and to. enhance bone formation [1] As the main mineral constituent of bone, hydroxyapatite (HA) has been widely investigated for bone repair applications.[1] There is a growing interest in the use of bioactive glass as scaffolds for bone repair.[1,2] Bioactive glasses have a widely recognized ability to support the growth of bone cells[3,4] and to bond strongly with hard and soft tissue.[1,5] Upon implantation, bioactive glasses convert to HA, which is responsible for their strong bonding with surrounding tissue.[1] Bioactive glasses are also reported to release ions that activate expression of osteogenic genes,[6,7] and to stimulate angiogenesis.[8,9] The bioactivity of glass, as measured by its conversion rate to HA, can be varied over a wide range, from hours to months, depending on the glass composition.[10,11]

Because of the compositional and fabrication flexibility of glass, scaffolds with a wide range of chemical and physical properties as well as porous architectures can be prepared.

Unidirectional freezing of suspensions has been used to produce porous constructs with oriented microstructures,[13–15] and the method has been applied recently to the production of porous bioceramics, such as HA.[16–19] Unidirectional freezing of aqueous suspensions resulted in the production of HA constructs with a lamellar-type microstructure and high compressive strength (e.g., 65 MPa; 56% porosity) in the direction parallel to the freezing direction, but the inter-lamellar pores were only 10–40 μm wide.[16,17] These pore widths are considered too small to support cell ingrowth into the interstices of the scaffold. A porosity of >50% with pore size (diameter or width) of 100 μm or larger are the minimum values reported for scaffolds capable of supporting cell proliferation and function.[20,21]

Our previous work[18,19,22] showed that the addition of polar organic solvents such as 1,4–dioxane (referred to simply as dioxane) and glycerol to aqueous suspensions of HA resulted in drastic changes to the oriented microstructure obtained by unidirectional freezing. In particular, the addition of 60 wt% dioxane to the aqueous suspensions resulted in the formation of a columnar microstructure, with pores approximately circular in cross section, and with pore widths (diameters) of 100 ± 10 μm. When tested in the direction of pore orientation, the HA scaffolds (porosity = 65–70%) had compressive strengths of up to 15–20 MPa, higher than the compressive strength of trabecular bone (2–12 MPa). The HA scaffolds also showed a unique ‘elastic–plastic’ response in compression, with a large deformation for failure (>20%), and strain rate sensitivity.[19]

This type of mechanical response, which is unlike the brittle response of ceramics, is more characteristic of natural materials.[24,25]

Based on the promising microstructure and mechanical behavior observed for freeze-cast HA scaffolds,[18,19] this investigation was undertaken to assess the performance of bioactive glass scaffolds prepared by the unidirectional freezing method for potential bone repair applications. The assessment included the evaluation of the mechanical properties of the scaffolds plus performance with cell cultures *in vitro*. We hypothesized that bioactive glass scaffolds with a columnar microstructure would have compressive strengths superior to that of trabecular bone plus the ability to support cell proliferation into the pores in the interior of the scaffold as well as cell function.

Bioactive glass with the 13-93 composition was used because of its proven bioactivity,[26] capability of supporting cell proliferation,[27] and ability to be formed into porous constructs with relevant anatomical shapes by viscous flow sintering.[28,29] The 13-93 glass is also approved for *in vivo* use in the United States and elsewhere. Mouse MLO-A5 cells, an established osteogenic cell line, were chosen for these experiments because of their highly elevated expression of osteogenic phenotype traits such as alkaline phosphatase activity and mineralization.[30,31]

6.3. MATERIALS AND METHODS

6.3.1. Preparation of Porous 13-93 Glass Scaffolds. Glass with the 13-93 composition (wt%): 53 SiO_2, 6 Na_2O, 12 K_2O, 5 MgO, 20 CaO, 4 P_2O_5, was prepared by melting a mixture of the appropriate quantities of analytical grade Na_2CO_3, K_2CO_3, $MgCO_3$, $CaCO_3$, SiO_2 and $NaH_2PO_4.2H_2O$ (Fisher Scientific, St. Louis, MO) in a

platinum crucible for 2 h at 1300°C, and quenching the molten glass between stainless steel plates. Particles of size <5 μm were obtained by crushing, grinding, and sieving the glass to a size <106 μm, followed by wet attrition milling (Model 01-HD, Union Process, Akron, OH).

Except for the sintering conditions, the procedure for preparing 13-93 bioactive glass scaffolds was similar to that used in our previous work for HA.[18] Briefly, the suspensions contained 5–20 vol% glass particles, 0.5 wt% Easysperse as dispersant (ISP, Wayne, NJ), and 1 wt% poly(vinyl alcohol), PVA, (DuPont Elvanol® 90-50) as binder. The solvent consisted of either water, or a mixture of water and 60 wt% dioxane (Fisher Scientific, St. Louis, MO). The suspensions were balled-milled for 48 h in polypropylene containers using Al_2O_3 grinding media, and de-aired by milling at a low speed prior to the freezing step.

Unidirectional freezing was performed by pouring the suspensions into poly(vinyl chloride), PVC, tubes (~10 mm internal diameter × 20 mm long) placed on a cold steel substrate at –20°C in a freeze dryer (Genesis 25 SQ Freeze Dryer, VirTis Co., Gardiner, NY). After sublimation of the frozen solvent in the freeze dryer (Genesis 25 SQ), the sample was heated at 1°C/min to 500°C in flowing O_2 gas to decompose the organic binder and dispersant, then at 5°C/min to 690°C, and kept at this temperature for 1 h to densify the glass network and form a porous, cylindrical glass construct without crystallizing the glass.

6.3.2. Characterization of Porous 13-93 Glass Constructs. The microstructure of the cross-sections of the sintered constructs, in the planes parallel to and perpendicular to the direction of freezing, was observed using scanning electron microscopy, SEM

(Hitachi S-4700, Hitachi Co., Tokyo, Japan). The volume of open porosity in the sintered samples was measured using the Archimedes method. The pore size was determined from SEM micrographs of the cross sections. For each construct, at least 5 samples were used for pore size evaluation, and at least 10 measurements were done on each sample to get a mean pore size and standard deviation.

The mechanical behavior of cylindrical samples (8 mm in diameter × 16 mm) in compressive loading was measured according to ASTM-C773 using an Instron testing machine (Model 4881; Instron Corp., Norwood, MA) at a crosshead speed of 0.5 mm/min. Eight samples were tested, and the average strength and standard deviation were determined. A crosshead speed of 0.5 mm/min is typical for the testing of dense specimens according to ASTM-C773. To investigate the strain rate sensitivity of the compressive mechanical response, additional tests were performed at crosshead speeds of 0f 0.05 and 5.0 mm/min. Crosshead speeds higher than 5 mm/min were impractical with the instrument and size of specimens used.

6.3.3. Cell Culture. The established MLO-A5 post-osteoblast/pre-osteocyte murine cell line, was kindly provided by Professor Lynda F. Bonewald, University of Missouri-Kansas City. The stock cells were maintained in collagen-coated plates (rat tail collagen type I, 0.15 mg/ml) containing α-MEM medium supplemented with 5% fetal bovine serum (FCS) and 5% newborn calf serum (NCS) plus 100 μg/ml penicillin. Dry-heat sterilized scaffolds (8 mm in diameter × 2 mm thick) were seeded with 60,000 MLO-A5 cells suspended in 100 μl of complete medium and incubated for 4 h to permit cell attachment. The cell-seeded scaffolds were then transferred to a 24-well plate containing 2 ml of complete medium per well. The control group consisted of the same

number of cells seeded in wells containing 2 ml of media. All cell cultures were maintained at 37 ºC in a humidified atmosphere of 5% CO_2, with the medium changed every 2 days.

6.3.4. Cell Morphology. After selected intervals, 13-93 bioactive glass scaffolds with attached cells were removed, washed twice with PBS, and placed in 2.5% glutaraldehyde in PBS. After an overnight soak in glutaraldehyde, the fixed samples were washed with PBS and dehydrated through a graded series of ethyl alcohol, followed by two soaks in hexamethyldisilazane (HMDS) for 10 min each. The samples were allowed to fully evaporate, sputter-coated with Au/Pd, and observed in a SEM (Hitachi S-4700) at 5 kV accelerating voltage.

6.3.5. Cell Viability and Growth. To visualize the metabolically active cells on and within the porous scaffolds, the cell-seeded scaffolds were placed in 400 µl serum-free medium containing 100 µg of the tetrazolium salt MTT for the last 4 h of incubation. After incubation, the constructs were rinsed in PBS, blotted, and allowed to dry. Images of the constructs were obtained using a stereomicroscope fitted with a digital camera to qualitatively assess the distribution of insoluble purple formazan, a product of mitochondrial reduction of MTT by viable cells. The MTT-labeled constructs were then frozen at –80ºC and fractured with a cooled microtome blade. The fracture cross-section was visually examined to assess the presence of purple formazan within the interior of the constructs. Finally, the formazan product was extracted from the HA constructs with 1.0 ml ethanol and measured spectrophotometrically at 550 nm in a BMG FLUORstar Optima plate reader.

The ability of the scaffold to support cell infiltration was assessed by dipping one end of a scaffold (~8 mm in diameter × 10 mm) to a depth of ~1 mm into a cell suspension (150,000 cells/ml), and allowing the suspension to be drawn up into the pores by capillary pressure. After incubation for 4 h to permit cell attachment, the scaffolds were treated with MTT for another 4 h.

6.3.6. Quantitative Protein Assay. The amount of protein in lysates recovered from the cell-seeded scaffolds was measured to assess the extent of cell proliferation on the scaffold. The scaffolds were placed in 500 μl of 1% Triton X-100 and the cells lysed by two freeze-thaw cycles (–80/37ºC). Aliquots of the released lysate were mixed with working reagent prepared from a micro-BCA Protein Assay Kit (Piece Biotechnology, Rockford, IL). Resultant absorbance values were measured at 550 nm in a BMG FLUORstar Optima plate reader with bovine serum albumin used as standard for comparison.

6.3.7. Alkaline Phosphatase (ALP) Activity. The cell-seeded constructs were removed at intervals of 2, 4, 6 and 8 days of incubation and washed twice with PBS. The samples were placed in 500 μl of 1% Triton X-100 and cells were lysed using two –80/37ºC cycles. Aliquots of the lysate were placed in a 96-well plate for spectro-photometric measurement of alkaline phosphatase (ALP) activity with *p*-nitrophenyl phosphate (*p*-NPP) substrate as described elsewhere.[32]

6.3.8. Alizarin Red S Staining for Mineralization and Quantitation. MLO-A5 cells were seeded as described above onto the glass scaffolds and into control wells, and were cultured for 3 days in standard α-MEM medium supplemented with 5% FCS and 5% NCS. After 3 days, the standard media was removed, and the scaffolds and control

wells were incubated in mineralization media, α-MEM with 10% FCS, 5 mM β-glycerol phosphate (βGP) and 100 μg/ml ascorbic acid, following the method described elsewhere.[31]

After incubation for 3, 6, 9 and 12 days in mineralization media, the cell-seeded constructs and control wells were washed twice with PBS. The cells with adherent mineralized nodules were removed from the constructs and control wells with trypsin-EDTA, washed with isotonic NaCl, and stained with 4 nM alizarin red S (pH = 4.2) for 2 minutes. The stained cells were then rinsed with nanopure water and centrifuged 5 times to remove the nonbound dye. The pellets of stained cells were placed into a 96-well plate and observed using a stereomicroscope fitted with a digital camera. The bound alizarin red S stain was extracted by sonicating for 10 min with 10 mM HCl in 70% ethanol. The extracts were then diluted with 5 volumes of PBS and the absorbance measured at 550 nm in a BMG FLUORstar Optima plate reader for the determination of mineralization.

6.3.9. Statistical Analysis. All biological experiments (4 samples in each group) were run either in duplicate or triplicate. The values are presented as means ± standard deviations. Statistical analysis was performed with one-way analysis of variance (ANOVA) followed by a Tukey's *post hoc* test, with the level of significance set at $p<0.05$.

6.4. RESULTS

6.4.1. Microstructure of the Freeze-cast 13-93 Glass Scaffold. SEM images (Fig. 1) show microstructures of bioactive glass scaffolds that were sectioned perpendicular to the freezing direction. The scaffolds shown were prepared from

suspensions containing 15 vol% particles. There were no marked changes in the microstructure along the length of the sample, so each cross-section was, in general, representative of the whole construct. Unidirectional freezing of suspensions containing dioxane (60 wt%) resulted in a columnar microstructure (Figs. 1a and 1b) with the pores approximately circular in cross section with diameters of 90–110 μm aligned in the direction of freezing. In contrast, freezing aqueous suspensions yielded a lamellar microstructure with the lamellae and the inter-lamellar pores oriented in the direction of freezing (Fig. 1c and 1d). The lamellar pores have a length of 100–300 μm and a width of 20–30 μm. Varying the particle concentration of the suspension (5–20 vol%) caused no change in the type of microstructure, but did change the porosity and pore size. Lower porosity and smaller pore size were obtained with higher particle concentration.

6.4.2. Mechanical Behavior of the Freeze-cast 13-93 Glass Scaffold. The effect of the particle concentration of the suspensions on the porosity and compressive strength (in the direction parallel to the freezing direction) of the columnar and lamellar scaffolds is shown in Fig. 2. For both groups of scaffolds, the strength increased and the porosity decreased with increasing particle concentration. The compressive strength (taken as the peak stress on the stress vs. deformation curve) increased from ~10 MPa to ~50 MPa as the porosity of the columnar scaffolds decreased from 70% to 35% (Fig. 2a). In comparison, the compressive strength of the lamellar scaffolds increased from ~5 MPa to ~20 MPa for the same decrease in porosity.

Figure 3 shows data for the compressive stress vs. deformation for the columnar and the lamellar scaffolds tested in the direction parallel to the freezing direction at three different deformation rates (0.05–5 mm/min). The scaffolds were prepared from

suspensions containing 15 vol% particles. The data shown are the engineering stress and deformation, based on the initial cross-sectional area and length of the test samples, and do not represent the true stress and strain. Both groups of scaffolds showed an 'elastic–plastic' response, with a deformation for failure of >20% (deformation rate = 0.5 mm/min), as well as a gradual failure mode. The response of the scaffolds also showed a strong strain-rate dependence. With increasing deformation rate, the peak stress increased and shifted to lower strain.

6.4.3. SEM Examination of Cultures. Scaffolds used in the cell culture experiments were prepared from suspensions containing 15 vol% particles (Fig. 1 and Table 1). SEM images (Fig. 4) show the morphology of MLO-A5 cells grown on the surface of the columnar and lamellar scaffolds for 2, 4 and 6 days. The cells visible in the micrographs of the columnar scaffolds appeared to be attached by slender cell projections at day 2 (Fig. 4a), and show a large increase in density with the duration of culture. It is apparent that the cells had grown along the walls of the columnar pores and down into the interior of these scaffolds. After 4 days, cell colonization of the walls of the scaffolds was evident (Fig. 4b), and after 6 days, the walls were completely covered with cells (Fig. 4c). The cells on the columnar scaffolds showed evidence of aggregation and physical contact with neighboring cells via multiple cytoplasmic extensions. The cells seeded on the lamellar scaffolds also show a large increase in density (Figs. 4d–4f), although this increase appears mostly on the surface of the scaffolds with cells completely bridging the lamellar pores after 6 days (Fig. 4f).

6.4.4. Cell Proliferation and Cell Infiltration. Figure 5 shows the photographic images of cell-seeded scaffolds treated with MTT after culture intervals of 2, 4 and 6 days . The purple pigment visible on the scaffold, the result of mitochondrial reduction of MTT to an insoluble formazan product by metabolically viable cells. The increase in intensity of the purple color with culture time is evidence of increased number of metabolically active cells on the surface of both groups of scaffolds (Figs. 5a and 5c). The purple staining visible on the freeze-fracture surface of the scaffolds cultured for 6 days (Figs. 5b and 5d) indicated the relative density of metabolically active MLO-A5 cells within the interior of the scaffold. The larger purple area on the fracture surface of the columnar scaffolds indicated the presence of greater number of metabolically active cells within these scaffolds. Furthermore, the larger depth of the purple staining into the columnar scaffolds indicated that these scaffolds had better capacity to support the proliferation of viable cells into the pores.

Quantitative measurement of the amount of the formazan present in the scaffolds (Fig. 6) showed a linear increase in the absorbance value with the incubation time, indicating an increasing number of cells present in both groups of scaffolds. The larger amount of formazan extract recovered from the cells cultured on columnar scaffolds provides additional evidence of better cell growth into the columnar scaffolds, and is consistent with the photographic images of the MTT labeled scaffolds.

Figure 7 shows the growth rate of MLO-A5 cells into the pores of the columnar scaffolds, determined by the measuring of the depth of purple formazan present on the fractured surface. A linear growth rate of ~ 130 μm/day was determined. The full coverage of the cross section was obtained after culturing for 15 days (Fig. 7 inset). The

ability of the columnar scaffolds to support live cell ingrowth was further investigated by dipping one end of an as-fabricated scaffold (to a depth of < 1mm) in a cell suspension and monitoring the cell migration into the scaffold. The pores of the scaffold were completely infiltrated with the cell suspension by capillary action in less than 5 s. Figure 8 shows the photographic images of the MTT-labeled constructs after infiltration. Both the surface and cross section of the scaffold were covered with the purple color, indicating that the columnar pores were large enough to permit cell migration and to provide enough nutrients for the cells.

Figure 9 shows the results of the quantitative assay of total protein in cell lysates recovered from the columnar and lamellar scaffolds and the control wells after 2, 4 and 6 days. An increase in the amount of protein recovered from both groups of scaffolds was observed during the 6-day incubation, a finding that complements the progressive increase in cell density observed in the SEM images (Fig. 4). The higher amount of protein recovered from the columnar scaffolds after 4 and 6 days indicates the better ability of the these scaffolds to support cell proliferation than the lamellar scaffold. The data also show a higher growth rate of MLO-A5 cells on the bioactive glass constructs than on the surface of plastic culture vessels.

6.4.5. Cell Function. The results of alkaline phosphatase (ALP) activity of MLO-A5 cells cultured on the bioactive glass scaffolds (Fig. 10) indicated a linear increase of ALP activity during the 6-day incubation. This result demonstrates the ability of the bioactive glass scaffolds to support ostogenic cell function. The higher ALP activity of the cells on columnar scaffolds after 4 and 6 days is evidence that the columnar scaffolds are better able to support cell differentiation.

The MLO-A5 cells and extracellular materials were removed from the glass scaffolds by trypsinization, and stained with alizarin red S to test for the presence of calcium deposits, an indication of mineralization.[31,34] Figure 11 shows the morphology of the stained bone nodules. The dark red areas were an indication of a higher amount of calcium deposits, a sign of the formation of the mineralized bone nodules. Figure 12 shows the absorbance of alizarin red S dye extracted from cells on the glass scaffolds and control wells. The increase in absorbance values for the scaffolds and control wells is evidence of the increasing number of mineralized nodules. The higher absorbance values measured for the cell lysates recovered from the columnar scaffolds after 9 days in the mineralization media indicates a greater capacity of these scaffolds to support mineralization.

6.5. DISCUSSION

The 13-93 bioactive glass microstructures obtained in this work (Fig. 1) were generally similar to those obtained in our earlier work for HA prepared by a similar process.[18] In the unidirectional freezing process, the particles in the suspensions are pushed aside by the growing ice crystals. The particles play a passive role, and are mainly along for the ride, so for a stable suspension of fine particles, the resulting freeze-cast microstructure should be independent of the particle composition, as observed. The formation of different freeze-cast microstructures by manipulating the solvent composition of the suspension is discussed in our previous work.[22]

While differences in the shapes of the stress vs. deformation curves existed, the mechanical response in compression for the 13-93 bioactive glass scaffolds showed

trends similar to those observed in our earlier work for freeze-cast HA scaffolds.[19] The stress vs. deformation curves showed an elastic–plastic response, consisting of three regions: an approximately linear region at low deformation, a region of peak stress, and a plateau region (or a region of slowly decreasing stress) at higher deformation. Both groups of scaffolds showed a large strain for failure (>20% at a deformation rate = 0.5 mm/min), and strain rate sensitivity.

The results presented in Figs. 3 and 4 show that at equivalent porosities columnar scaffolds of 13-93 bioactive glass have higher strength than the lamellar scaffolds. In particular, at a deformation rate of 0.5 mm/min, columnar scaffolds with a porosity of 55–60% have a compressive strength of 25 ± 3 MPa, compared to a value of 10 ± 2 for the lamellar scaffolds. The strength of these columnar bioactive glass scaffolds is more than 2 times the highest strength reported for trabecular bone (2-12 MPa), and is also approximately 2 times the strength of columnar HA scaffolds prepared in our earlier work.[19] The higher strength of the bioactive 13-93 glass scaffolds, when compared to the strength of HA scaffolds, resulted presumably from thicker walls of the columnar microstructure plus the ability of glass to sinter more easily than HA, thereby providing a nearly fully-dense glass network that was better able to withstand the applied load.

While the rates of growth and function of MLO-A5 cells on both groups of scaffolds were greater than the control wells, the columnar scaffolds with the larger pore width provided the most favorable substrate for cell proliferation and function. Scaffolds intended for bone tissue engineering applications should support cell growth into the interstices of the scaffolds and differentiation of progenitor cells to functional bone tissues.[33] The columnar scaffolds with the larger pore width supported far greater cell

ingrowth into the pores in the interior of the scaffolds (Figs. 4 and 5), and allowed rapid cell migration and the flow of nutrients into the interior of the scaffolds (Fig. 7). The highest level of ALP activity and mineralization expressed by the columnar scaffolds indicates the optimal structure of these scaffolds to support bone progenitor cell function (Fig. 10). The columnar scaffolds also showed enhanced ability to support MLO-A5 cells to mineralize (Fig. 12).

Results of the present investigation provide support for the potential use of 13-93 bioactive glass scaffolds with the columnar microstructure in the repair and regeneration of large defects in load-bearing bones *in vivo*. In addition to the bioactivity of the glass, the columnar scaffolds have high strength (25 ± 3 MPa; porosity = 55–60%). The scaffolds did not fail in a brittle manner characteristic of ceramics and glass. Instead, they showed a unique elastic–plastic response, with a high strain for failure (>20% at a deformation rate of 0,5 mm/min). In addition to providing a favorable substrate for the proliferation and differentiated function by MLO-A5 osteoblastic cells, the columnar scaffolds with pore diameters of 100 ± 10 μm supported cell ingrowth into the pores in the interior of the scaffolds, and the rapid migration of a cell suspension by capillary action of the pores to completely fill the porosity. Follow-up *in vivo* evaluation of these scaffolds is currently underway in an animal model.

6.6. CONCLUSIONS

Results of the mechanical testing of 13-93 bioactive glass scaffolds with a columnar microstructure, prepared by a unidirectional freezing method, provided encouraging data to support potential use of these scaffolds in the repair of load-bearing

bones *in vivo*. When tested in compression (deformation rate = 0.5 mm/min), columnar scaffolds (porosity = 55–60%; pore diameter = 90–110 μm) had a strength of 25 ± 3 MPa in the direction of pore orientation, and showed an 'elastic–plastic' response with a large strain for failure (>20%). These columnar scaffolds also showed better ability to support the proliferation and differentiated function by MLO-A5 cells as compared to plastic control wells or scaffolds with a lamellar microstructure of narrow, slot-like pores. Bioactive glass scaffolds with the columnar microstructure also supported proliferation of MLO-A5 cells down into the interior pores of the scaffolds, as well as rapid migration of a MLO-A5 cell suspension by capillary to completely fill the interior pores.

6.7. REFERENCES

1. Hench LL. Bioceramics. J Am Ceram Soc 1998; 81:1705-28.
2. Rahaman MN, Brown RF, Bal BS, Day DE. Bioactive glasses for nonbearing applications in total joint replacement. Semin Arthroplasty 2007;17;102–12.
3. Wheeler DL, Stokes KE, Park HE, Hollinger JO. Evaluation of particulate bioglass in a rabbit radius ostectomy model. J Biomed Mater Res 1997; 35:249–54.
4. Wheeler DL, Stokes KE, Hoellrich RG, Chamberland DL, McLoughlin SW. Effect of bioactive glass particle size on osseous regeneration of cancellous defects. J Biomed Mater Res 1998; 41:527–33.
5. Hench LL, Splinter RJ, Allen WC, Greenlee TK Jr. Bonding mechanisms at the interface of ceramic prosthetic materials. J Biomed Mater Res 1971; 2:117–41.
6. Xynos ID, Edgar AJ, Buttery LD, Hench LL, Polak JM. Ionic products of bioactive glass dissolution increase proliferation of human osteoblasts and induce insulin-like growth factor II mRNA expression and protein synthesis. Biochem Biophys Res Commun 2000;276:461–65.
7. Xynos ID, Edgar AJ, Buttery LD, Hench LL, Polak JM. Gene-expression profiling of human osteoblasts following treatment with ionic products of bioglass 45S5 dissolution. J Biomed Mater Res 2001;55:151–57.
8. Leach JK, Kaigler D, Wang Z, Krebsbach PH, Mooney DJ. Coating of VEGF-releasing scaffolds with bioactive glass for angiogenesis and bone regeneration. Biomaterials 2006;27: 3249–55.
9. Leu A, Leach JK. Proangiogenic Potential of a collagen/bioactive glass substrate," Pharmaceut Res 2008;25,1222–29.

10. Huang W, Day DE, Kittiratanapiboon K, Rahaman MN. Kinetics and mechanisms of the conversion of silicate (45S5), borate, and borosilicate glasses to hydroxyapatite in dilute phosphate solutions. J Mater Sci: Mater Med 2006;17:583–96.
11. Yao A, Wang D, Huang W, Fu Q, Rahaman MN, Day DE. *In vitro* bioactive characteristics of borate-based glasses with controllable degradation behavior. J Am Ceram Soc 2007;90:303–6.
12. Wang HW, Tabata Y, Ikada Y. Fabrication of porous gelatin scaffolds for tissue engineering. Biomaterials 1999: 20:1339–44.
13. Schoof H, Bruns L, Fischer A, Heschel I, Rau G. Dendritic ice morphology in unidirectionally solidified collagen suspensions. J Cryst Growth 2000; 209;122–29.
14. Schoof H, Apel J, Heschel I, Rau G. Control of pore structure and size in freeze-dried collagen sponges. J Biomed Mater Res Appl Biomater 2002;58:352–57.
15. Zhang H, Hussain I, Brust M, Butler MF, Rannard SP, Cooper AI. Aligned two- and three-dimensional structures by directional freezing of polymers and nanoparticles. Nature Mater 2005;4:787–93.
16. Deville S, Saiz E, Tomsia AP. Freeze casting of hydroxyapatite scaffolds for bone tissue engineering. Biomaterials 2006;27:5480–9.
17. Deville S, Saiz E, Nalla RK, Tomsia AP. Freezing as a path to build complex composites. Science 2006;311,515–8.
18. Fu Q, Rahaman MN, Dogan F, Bal BS. Freeze casting of porous hydroxyapatite scaffolds - I. Processing and general microstructure. J Biomed Mater Res Part B: Appl Biomater 2008;86B: 125–35.
19. Fu Q, Rahaman MN, Dogan F, Bal BS. Freeze casting of porous hydroxyapatite scaffolds - II. Sintering, microstructure, and mechanical properties. J Biomed Mater Res Part B: Appl Biomater 2008;86B:514–22.
20. Hollinger JO, Leong K. Poly(-hydroxy acids): carriers for bone morphogenetic proteins. Biomaterials 1996;17:187–94.
21. Hu YH, Grainger DW, Winn SR, Hollinger JO. Fabrication of Poly(a-hydroxy acid) foam scaffolds using multiple solvent systems. J Biomed Mater Res 2002;59:563–72.
22. Rahaman MN, Fu Q. Manipulation of porous bioceramic microstructures by freezing of aqueous suspensions with binary mixtures of solvents. J Am Ceram Soc 2008;91:4137–40.
23. Fu Q, Rahaman MN, Dogan F, Bal BS. Bioinspired ceramic microstructures prepared by freezing of suspensions. Ceramic Trans 2008; in press.
24. Gibson LJ, Ashby MF. Cellular Solids: Structure and Properties, 2nd ed., Cambridge University Press, New York, 1997.
25. Meyers MA, Chen P, Lin AY, Seki Y. Biological materials: structure and mechanical properties. Prog Mater Sci 2008;53:1–206.
26. Brink M, Turunen T, Happonen R, Yli-Urppo A. Compositional dependence of bioactivity of glasses in the system Na2O-K2O-MgO-CaO-B2O3-P2O5-SiO2. J Biomed Mater Res 1997;37: 114–21.
27. Brown RF, Day DE, Day TE, Jung S, Rahaman MN, Fu Q. Growth and differentiation of osteoblastic cells on 13–93 bioactive glass fibers and scaffolds. Acta Biomater 2008;4:387–96.

28. Fu Q, Rahaman MN, Bal BS, Huang W, Day DE. Preparation and bioactive characteristics of a porous 13–93 glass, and fabrication into the articulating surface of a proximal tibia. J Biomed Mater Res 2007; 82A:222–9.
29. Fu Q, Rahaman MN, Bal BS, Brown RF, Day DE. Mechanical and *in vitro* performance of 13-93 bioactive glass scaffolds prepared by a polymer foam replication technique. Acta Biomater 2008;4:1854-64.
30. Kato Y, Boskey A, Spevak L, Dallas M, Hori M, Bonewald LF. Establishment of an osteoid preosteocyte-like cell MLO-A5 that spontaneously mineralize in culture. J Bone Miner Res 2001; 16:1622–33.
31. Barragan-Adjemian C, Nicolella D, Dusevich V, Dallas MR, Eick JD, Bonewald LF. Mechanism by which MLO-A5 late osteoblast/early osteocytes mineralize in culture: similarities with mineralization of lamellar bone. Calcif Tissue Int 2006;79:340–53.
32. Sabokar A, Millett PJ, Myer B, Rushton N. A rapid, quantitative assay for measuring alkaline phosphatase in osteoblastic cells *in vitro*. Bone Miner 1994;27:57–67.
33. Hutmacher DW. Scaffolds in tissue engineering bone and cartilage. Biomaterials 2000;21: 2529–43.
34. Chang YL, Stanford CM, Keller JC. Calcium and phosphate supplementation promotes bone cell mineralization: implications for hydroxyapatite (HA)-enhanced bone formation. J Biomed Mater Res 2000;52:270–78.

Table 1. Microstructural characteristics of 13-93 bioactive glass scaffolds prepared by unidirectional freezing of suspensions (15 vol% particles) which were used in cell culture experiments.

Solvent composition	Microstructure	Pore size (μm)	Porosity (%)
Water + 60 wt% dioxane	Columnar	100 ± 10	55 ± 2
Water	Lamellar	100 – 300 (length) 25 ± 5 (width)	62 ± 3

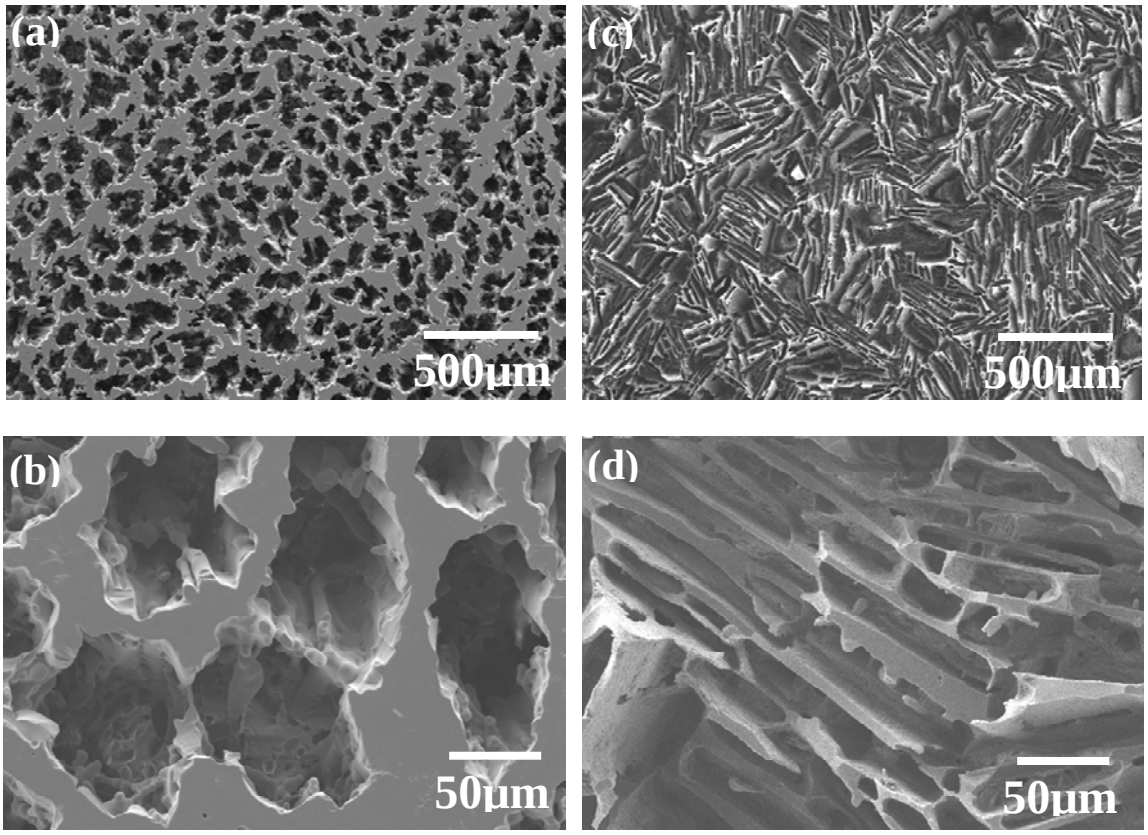

Figure 1. SEM images of the cross sections of 13-93 bioactive glass scaffolds prepared with different microstructures from suspensions containing 15 vol% particles: (a, b) columnar microstructure (solvent: water + 60 wt% dioxane); (c, d) lamellar microstructure (aqueous solvent). The cross sections are perpendicular to the freezing direction.

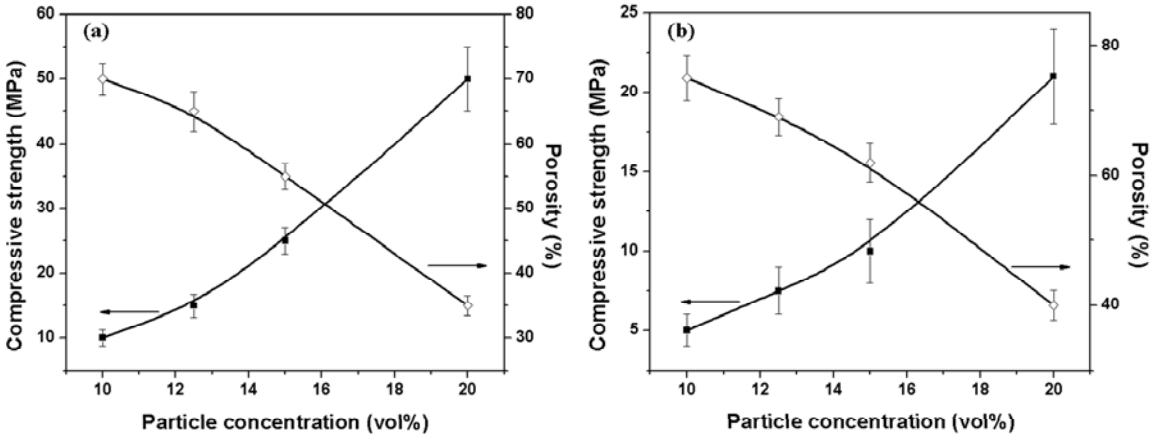

Figure 2. Compressive strength (in the direction of pore orientation) and porosity of 13-93 bioactive glass scaffolds with (a) columnar microstructure and (b) lamellar microstructure, prepared from suspensions containing different concentrations of particles.

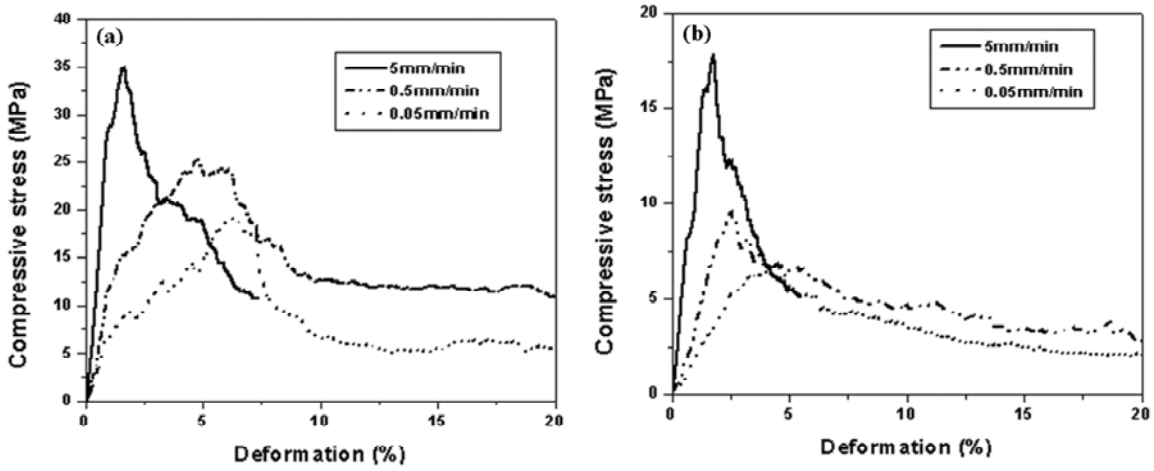

Figure 3. Compressive stress vs. deformation for 13-93 bioactive glass scaffolds tested at the deformation rates shown: (a) columnar scaffolds; (b) lamellar scaffolds.

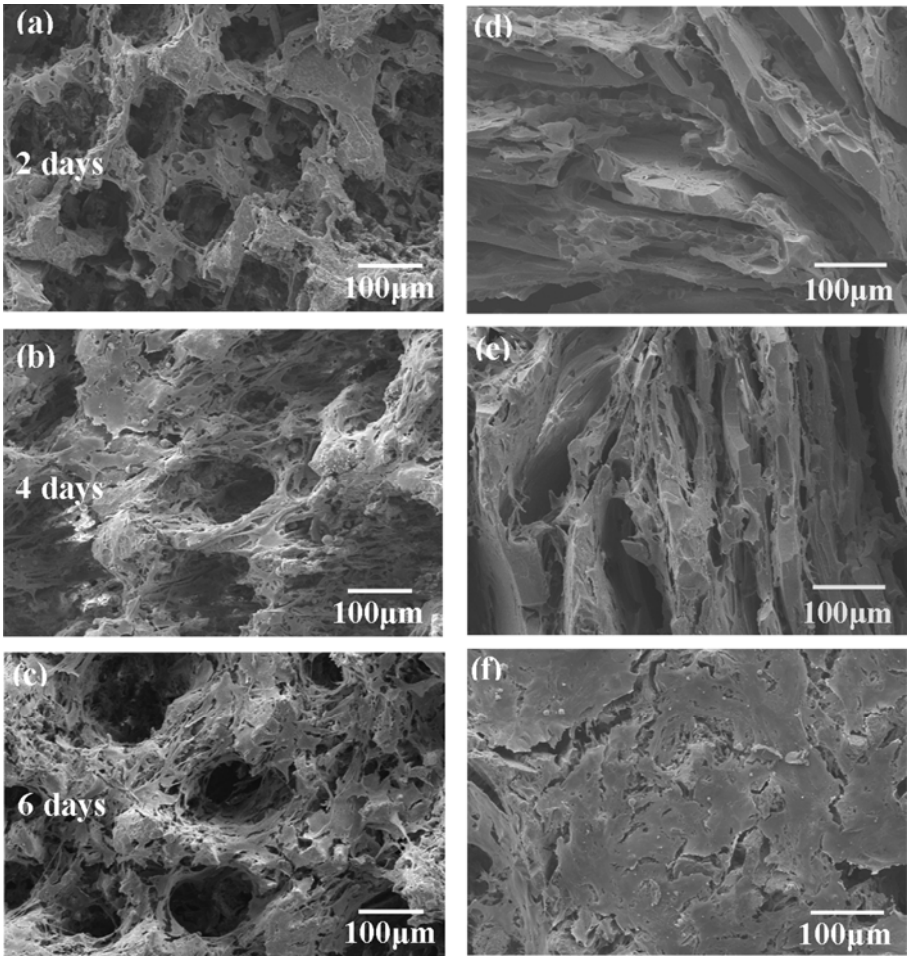

Figure 4. SEM images showing the cell growth on (*left*) columnar scaffolds, and (right) lamellar scaffolds after (a, b) 2 days, (c, d) 4 days, and (e, f) 6 days of culture.

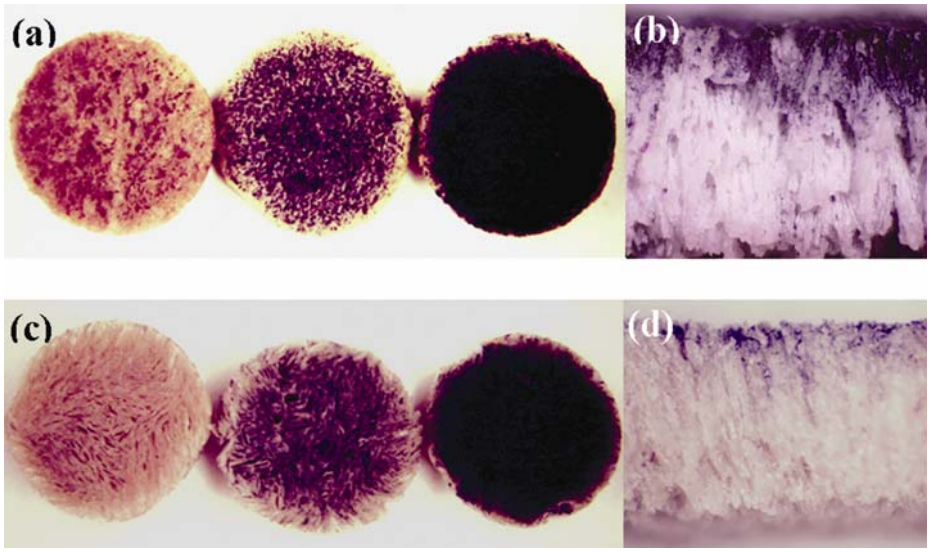

Figure 5. Cell-seeded glass scaffolds treated with MTT: surface of (a) columnar scaffolds, and (c) lamellar scaffolds after culture intervals of 2, 4, and 6 days (left to right, respectively); (b, d) freeze-fracture cross section of the corresponding scaffolds cultured for 6 days, showing MTT-labeled cells within the interior.

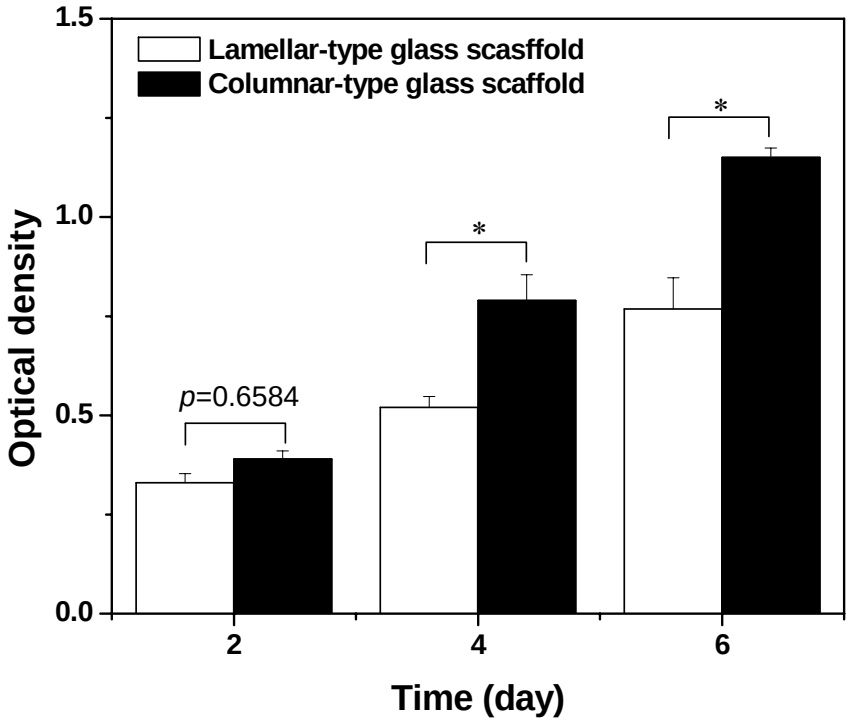

Figure 6. Quantitative analysis of the purple formazan extracted from cell-seeded columnar and lamellar scaffolds. Mean ± sd; n = 4. *Significant increase in formazan extracted from the porous glass constructs with increasing culture duration (p<0.05).

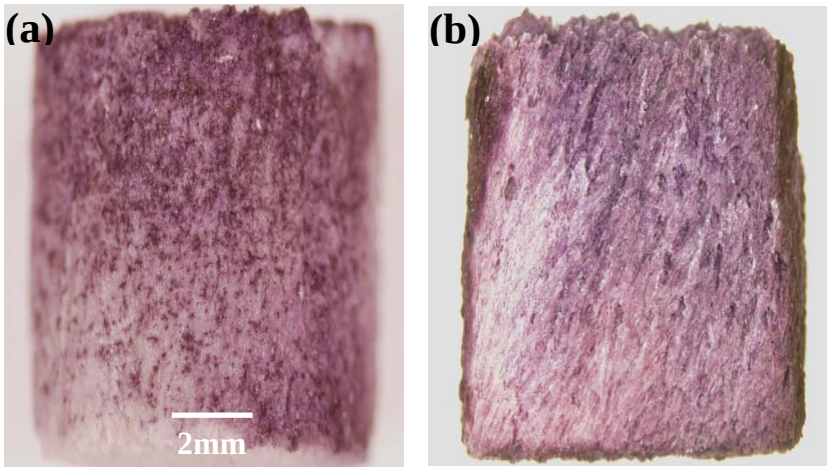

Figure 7. Bioactive glass scaffold with the columnar microstructure after one end was dipped slightly (< 1 mm) in a suspension of MLO-A5 cells, and treated with MTT: (a) surface and (b) cross section, showing the MTT-labeled cells on and within the scaffolds.

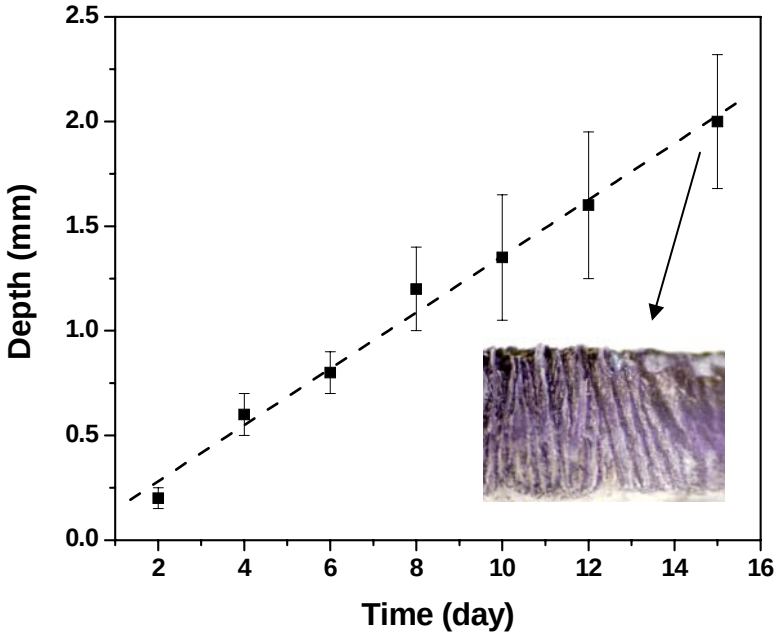

Figure 8. Proliferation of MLO-A5 cells into the pores in the interior of the columnar scaffolds, determined by measuring the depth of the purple color across a fracture cross section. The inset image shows complete cell proliferation into scaffold after 15 days of culture.

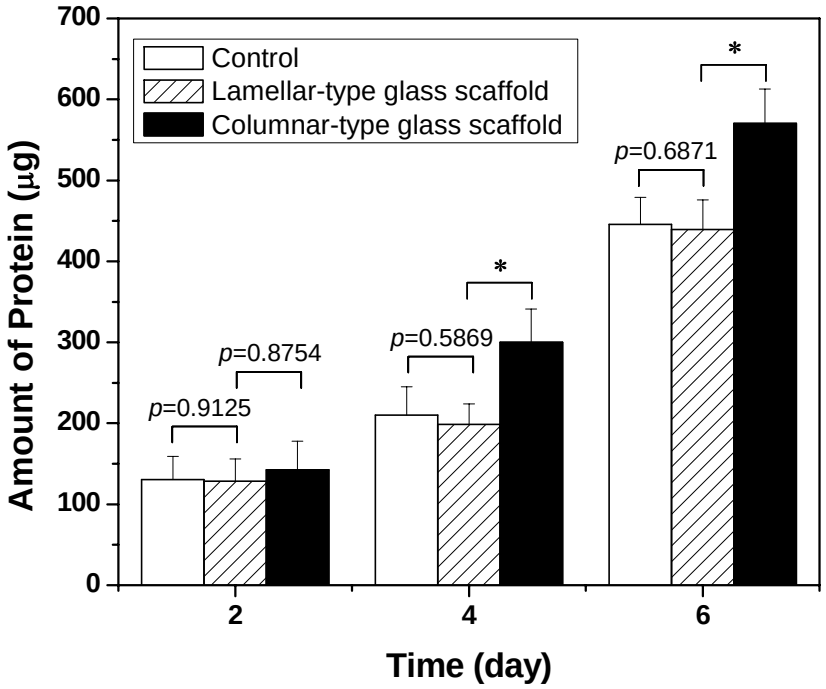

Figure 9. Total protein content in MLO-A5 cells cultured on columnar and lamellar scaffolds and in control wells. Mean ± sd; n = 4. *Significant increase in total amount of protein on the porous 13-93 glass constructs with increasing culture incubation ($p < 0.05$).

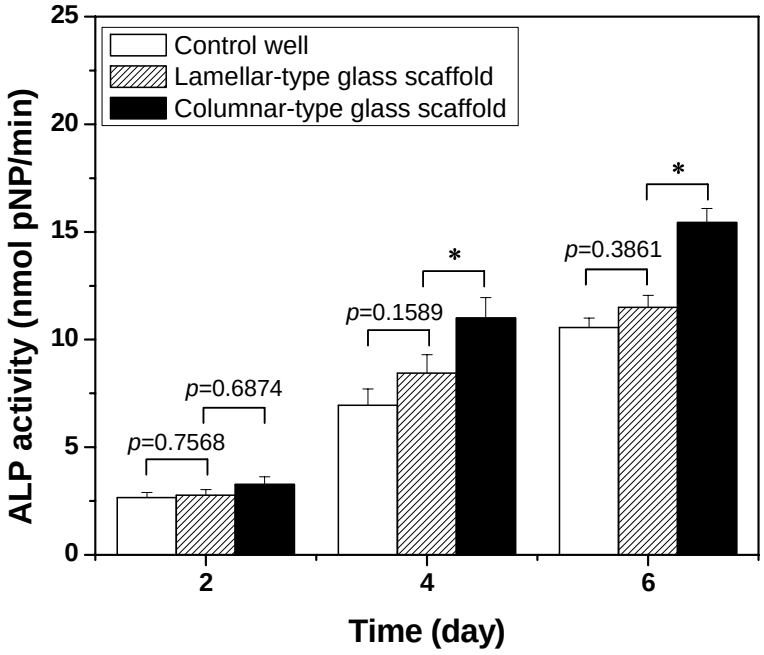

Figure 10. Alkaline phosphatase activity in MLO-A5 cells cultured on columnar and lamellar scaffolds and in control wells for 2, 4 and 6 days. Mean ± sd; n = 4. *Significant increase in alkaline phosphatase activity on the porous 13-93 glass constructs with increasing culture incubation ($p < 0.05$).

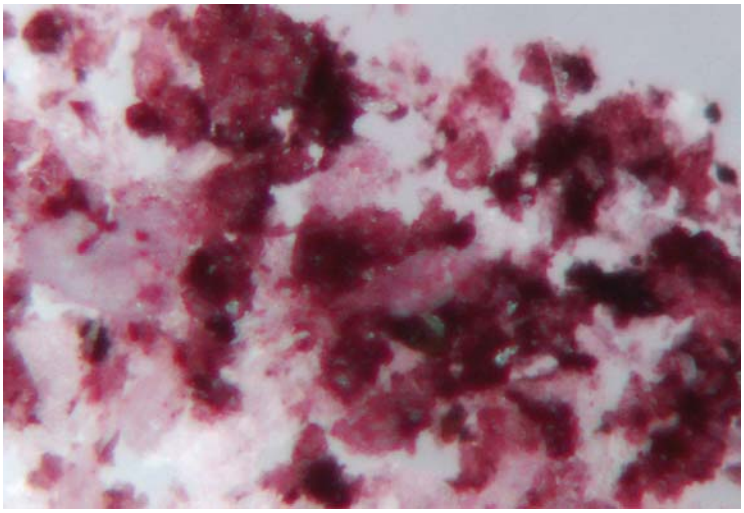

Figure 11. Bone nodule formation by MLO-A5 cells cultured on columnar scaffold for 9 days.

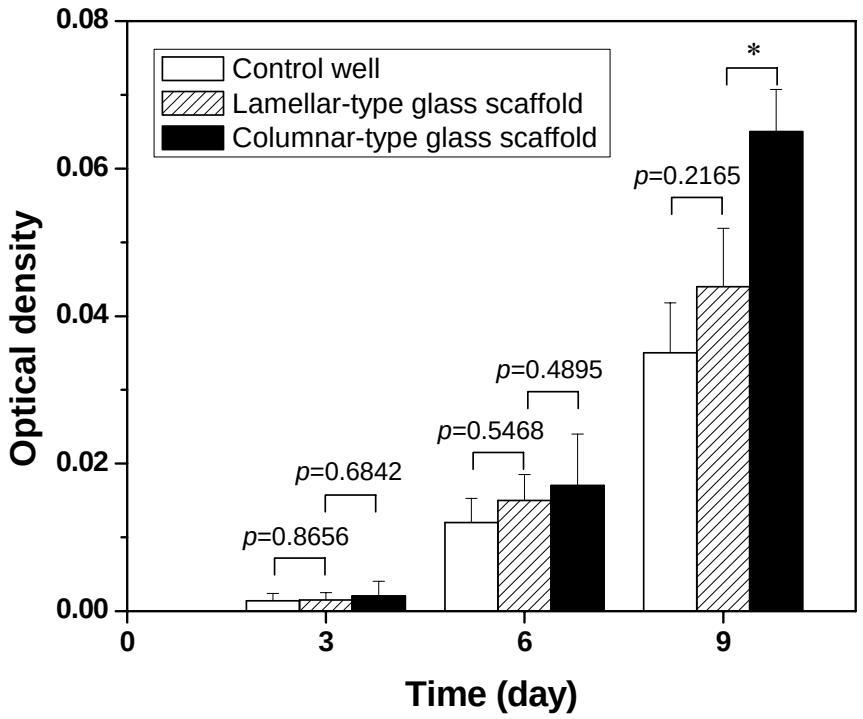

Figure 12. Quantitative analysis of mineralization in columnar and lamellar scaffolds and in control wells, by measuring the absorbance (optical density) of the extracted alizarin red staining dye using an Optima plate reader at 520 nm. *Significant increase in the extracted red staining dye on the porous 13-93 glass constructs with increasing culture incubation ($p < 0.05$).

7. *IN VIVO* EVALUATION OF 13-93 BIOACTIVE GLASS SCAFFOLDS WITH TRABECULAR AND ORIENTED MICROSTRUCTURES IN A SUBCUTANEOUS RAT IMPLANTATION MODEL

Qiang Fu[a,b], Mohamed N. Rahaman[a,b,*], B. Sonny Bal[c], Keiichi Kuroki[d], Roger F. Brown[b,e]

[a]Department of Materials Science and Engineering, Missouri University of Science and Technology, Rolla, Missouri 65409, USA

[b]Center for Bone and Tissue Repair and Regeneration, Missouri University of Science and Technology, Rolla, Missouri 65409, USA

[c]Department of Orthopaedic Surgery, University of Missouri-Columbia, Columbia, Missouri 65211, USA

[d]Comparative Orthopaedic Laboratory, University of Missouri-Columbia, Columbia, Missouri 65211, USA

[e]Department of Biological Sciences, Missouri University of Science and Technology, Rolla, Missouri 65409, USA

7.1. ABSTRACT

The ability of two groups of 13-93 bioactive glass scaffolds to support tissue ingrowth was evaluated after implantation for 4 weeks into subcutaneous pockets in the dorsum of Fisher 344 rats. One group of scaffolds (porosity = 85%; pore size = 100–500

* Corresponding author: M. N. Rahaman (rahaman@mst.edu)

μm) had a ‘trabecular’ microstructure similar to that of dry human trabecular bone, whereas the other group had a ‘columnar’ microstructure of oriented pores (porosity = 65%; pore width = 90–110 μm). Despite the lower porosity and pore width, the columnar scaffolds supported abundant soft tissue ingrowth (glycosaminoglycan and collagen), whereas the trabecular scaffolds showed only limited tissue ingrowth. When seeded with mesenchymal stem cells (MSCs), both groups of scaffolds supported abundant tissue infiltration. Bone-like tissue was formed in both groups of scaffolds seeded with MSCs, but not in the scaffolds without MSCs. The new tissues integrated with the hydroxyapatite-like surface layer of the scaffolds which resulted from the conversion of the bioactive glass in the body fluids. The results indicate that the trabecular bioactive glass scaffolds seeded with MSCs, as well as the columnar bioactive glass scaffolds, seeded with MSCs or unseeded, could serve as substrates for bone repair and regeneration.

Keywords: Scaffold; Bioactive glass; Subcutaneous implantation; Histology; Bone repair

7.2. INTRODUCTION

There is a growing need for the creation of synthetic scaffolds with the requisite properties for bone repair and regeneration because of an aging population and shortcomings of current treatments based on the use of bone autografts (limited supply and donor site morbidity) and bone allografts (immune rejection and possible transmission of pathogens. In addition to being biocompatible, scaffolds for bone repair and regeneration should have mechanical properties comparable to the tissue they are

intended to replace. Scaffolds should also have a porous three-dimensional structure with an interconnected pore network and surface characteristics suitable for supporting tissue ingrowth and integration of the scaffolds with surrounding tissues [1-5].

Although brittle, bioactive glass is of interest as a scaffold material for bone repair because of its proven ability to bond strongly with surrounding bone and tissues, and to promote new bone formation. Bioactive glass reacts in the body fluids to form a hydroxyapatite-like phase, similar in composition to the main mineral constituent in living bone, which is responsible for the strong chemical bond between bioactive glass and bone [6]. Bioactive glass has a widely recognized ability to support the growth of bone cells [7,8], and the glass is reported to release ions that activate expression of osteogenic genes [9,10]. More recent work indicates that bioactive glass has the ability to stimulate angiogenesis [11,12].

In our previous work, we created bioactive glass (13-93) scaffolds with anatomically relevant microstructures, unique mechanical properties, and promising *in vitro* response to cells. [13, 14]. One group of scaffolds, prepared by a polymer foam infiltration technique, had a microstructure similar to that of dry human trabecular bone. Another group of scaffolds, prepared by unidirectional freezing of suspensions, had an oriented microstructure of columnar pores. Mechanical testing of these 'trabecular' and 'columnar' bioactive glass scaffolds showed promising as well as unique properties for bone repair. Trabecular bioactive glass scaffolds (porosity = 85%; pore size = 100–500 μm) had a compressive strength of 10–12 MPa, and an elastic modulus of 2.5–3.5 GPa, approximately equal to the highest values reported for trabecular bone [15]. The columnar bioactive glass scaffolds had a unique 'elastic–plastic' mechanical response

with large strain for failure (>20%), and strain rate sensitivity. At the same deformation rate used for the trabecular scaffolds, the columnar scaffolds (porosity = 65%; pore width = 90–110 μm) had an elastic modulus of 1–1.5 GPa and a compressive strength of 22–28 MPa, more than twice the highest compressive strength reported for trabecular bone. *In vitro* cell culture showed that both the trabecular scaffolds and the columnar scaffolds had the ability to support the attachment, proliferation, and function of MLO-A5 cells, an osteogenic cell line. Furthermore, both groups of scaffolds supported the proliferation of cells into the interior pores of the scaffolds.

In view of the promising *in vitro* performance of these trabecular and columnar bioactive glass (13-93) scaffolds, this study was undertaken to evaluate the ability of these two groups of scaffolds to support tissue ingrowth *in vivo*. A rat subcutaneous implantation model was used because of the widely accepted validity of the model. Scaffolds seeded with rat bone marrow-derived stem cells or unseeded were implanted into subcutaneous pockets in the dorsum of rats. After implantation, tissue ingrowth into the scaffolds was evaluated using histology and scanning electron microscopy (SEM). We hypothesized that because of their larger porosity and pore size, the trabecular scaffolds would be better able to support new tissue ingrowth than the columnar scaffolds, and that seeding the scaffolds with MSCs would enhance new tissue ingrowth.

7.3. MATERIALS AND METHODS

7.3.1. Preparation of Trabecular and Columnar Scaffolds. Scaffolds of 13-93 bioactive glass bioactive glass (composition in wt%: 53 SiO_2, 6 Na_2O, 12 K_2O, 5 MgO, 20 CaO, 4 P_2O_5) with the trabecular and columnar microstructures were prepared using

procedures described in detail elsewhere [13, 14]. Trabecular scaffolds (6 mm in diameter × 2 mm) were prepared using a polymer foam infiltration technique, whereas columnar scaffolds (9 mm in diameter × 2 mm) were prepared unidirectional freezing of suspensions (Table 1). The scaffolds were washed twice with water and ethanol, and sterilized by heating for 24 h at 500ºC, prior to seeding with cells and implantation.

7.3.2. Seeding of Scaffolds with Mesenchymal Stem Cells. Scaffolds, either seeded with rat bone marrow-derived stem cells (MSCs) or unseeded (no MSCs), were used in the animal implantation experiments. The MSCs were harvested from the femurs and tibias of Fisher 344 rats. Briefly, two 6-week-old Fisher rats were sacrificed by CO_2 inhalation. Both ends of the femurs and tibias of each rat were removed at the level of the epiphysis, and marrow plugs were flushed out from the epiphysis using 10 ml of a culture medium expelled from a syringe through a 23-gauge needle. The culture medium consisted of α-minimum essential medium (α-MEM) containing 10% fetal bovine serum, 100 U/ml penicillin, 50 μg/ml ascorbic acid, 10 mM β-glycerolphosphate, 10^{-8} M dexamethasone, 0.25 μg/ml amphotericin. Marrow samples were collected and mechanically disrupted by passing through successively smaller-gauge needles attached to the 10-ml syringe, starting with 16-gauge and ending with 20-gauge. The resulting cells were collected in two culture plates, each containing 10 ml medium. The medium was changed after the first 24 h to remove non-adherent cells and,subsequently, every 2 days. Cultures were maintained in a humidified atmosphere of 95% air with 5% CO_2 at 37ºC. Typically, cells were maintained for 7–14 days as primary culture or upon formation of large colonies.

Sterilized trabecular and columnar scaffolds were each seeded with 60,000 MSCs, and incubated for 4 h to permit cell attachment. The cell-seeded scaffolds were then transferred to a 24-well plate containing 2 ml of complete medium per well, and cultured for 24 h prior to implantation. The control group consisted of the same types of scaffolds but without seeding with MSCs.

7.3.3. Animal Implantation. Fisher 344 rats (4–6 weeks old) were used for the implantation. All procedures were approved by the institutional animal care and use committee. The rats were anesthetized by isofluorance inhalation. Trabecular and columnar bioactive glass scaffolds, seeded with MSCs or unseeded, were implanted into subcutaneous pockets in the dorsum of syngenic rats under sterile conditions. For each animal, two unseeded and two MSC-seeded scaffolds were implanted into four sites in the dorsum.

7.3.4. Histology. Scaffolds were harvested 4 weeks after implantation, photographed, and fixed in 10% buffered formalin. After dehydration through a serial of graded ethyl alcohol, the specimens were embedded in poly(methyl methacrylate), PMMA, and stained at the Department of Surgical Sciences, School of Veterinary Medicine, University of Wisconsin, Madison, WI. Specimens were sectioned along the axial direction, and polished to give 50 μm sections. The sections were stained with toluidine blue and Goldner's trichrome to detect the formation of glycosaminoglycan (GAG) and collagen, respectively, and examined using transmitted light microscopy. The quantity of tissue infiltrated into the implant, as well as the amount of toluidine blue stained matrix (GAG), and the amount of trichrome stained matrix (collagen) within the implant were subjectively evaluated by a 'blinded' observer with no previous knowledge

of the implants, using the following scale: 0 – none; 1 – small amount; 2 – moderate amount; 3 – abundant.

The sections were also stained at Missouri University of Science and Technology with Sanderson™ Bone Stain (Surgipath Medical Industries, Richmond, IL), and then counterstained for ~40 s with a solution consisting of 1 g acid fuchsin, 99 ml distilled water, and 1 ml acetic acid. This technique provides sufficient contrast to differentiate between soft tissue (blue), bone tissue (red), and osteoid production (purple) [16].

7.3.5. SEM Observation. Scanning electron microscopy, SEM (S-4700, Hitachi Co., Tokyo, Japan) Co., Tokyo, Japan) in the backscattered electron (BSE) and secondary electron (SE) modes, as well as X-ray mapping in the SEM, was used to identify the compositional change of the glass scaffolds and the morphologies of the tissues formed inside the scaffolds after implantation. Cross sections of the implants were ground with SiC paper, polished with diamond paste, and examined at an accelerating voltage of 5 kV and a working distance of 12 mm.

7.3.6. Statistical Analysis. Four samples in each group were used for the implantation. The data are presented as the mean ± standard deviation. Statistical analysis was carried out using one-way analysis of variance (ANOVA) and Tukey's post hoc test, with the level of significance set at $p < 0.05$.

7.4. RESULTS

7.4.1. Microstructure of As-prepared Scaffolds. Figure 1 shows typical Microstructures of the as-prepared trabecular and columnar scaffolds. The trabecular scaffold (Fig. 1a) consisted of an interconnected porous network, with pores of size 100–

500 μm, and porosity = 85 ± 2%, and had a microstructure similar to that of dry human trabecular bone. In comparison, the columnar scaffolds (Fig. 1b) consisted of an oriented microstructure of columnar pores, with a pore diameter of 90–110 μm and porosity = 65 ± 2%. The two groups of scaffolds were prepared using different techniques, which did not allow a closer match of the pore characteristics. Table 1 summarizes the characteristics of the scaffolds used in this work.

7.4.2. Morphological and Compositional Changes of Scaffolds *In vivo*.

Examination of the scaffolds after subcutaneous implantation for 4 weeks (Fig. 2) indicated that both groups of scaffolds maintained their original shapes. The implants were surrounded by a band of fibrovascular tissue, with blood vessels apparently more frequently present in the scaffolds seeded with MSCs (Figs. 2c, 2d) than in the unseeded scaffolds (Figs. 2a, 2b). Backscattered electron (BSE) images of cross sections of the implants (Fig. 3) revealed morphological changes in the bioactive glass resulting from the implantation. The light-gray areas (labeled G) in the images represented the glass scaffold, whereas the medium-gray areas (labeled T) showed the tissue infiltrated into the implants, and the dark-gray areas (P) show the PMMA. Qualitatively, it is clear that there is little tissue infiltrated into the unseeded trabecular scaffolds (without MSCs) (Fig. 3a), but more abundant tissue in the MSC-seeded trabecular scaffold and the columnar scaffolds (MSC-seeded or unseeded).

A high magnification BSE image of the cross section of an unseeded trabecular scaffold after implantation (Fig. 4a) showed differences in contrast across the glass phase which resulted from *in vivo* degradation of the bioactive glass. The glass cross section consisted of three regions: a light-gray core (C), a darker-gray transition layer (S), and a

light-gray surface layer (H). Several microcracks are present in the glass cross section, which presumably resulted from the method used to prepare the section. Compositional information (Figs. 4b–4d), obtained from X-ray maps for Ca(K), P(K), and Si(K) of the area in Fig. 4a, showed that the surface layer H was rich in Ca and P. Energy dispersive X-ray (EDS) analysis in the SEM showed that the Ca:P atomic ratio of this surface layer was ~1.6, which is close to the value of 1.67 for hydroxyapatite (HA). Presumably, the surface layer (~20 μm thick) was a HA-type product formed by conversion of the bioactive glass *in vivo*. The core (C), rich in Ca and Si, is presumably the unconverted core, whereas the Si-rich transition layer (~5 μm thick) is a SiO_2-layer commonly observed in the conversion of silicate bioactive glass to HA.

7.4.3. Histological Evaluation of Tissue Infiltration of Implants. Figures 5 and 6 show transmitted light images of the toluidine-blue stained matrix and the trichrome stained matrix (stained red) in the bioactive glass implants with the trabecular and columnar microstructures. There is only a small amount of toluidine stained matrix (glycosaminoglycan, GAG) and trichrome stained matrix (collagen) in the unseeded trabecular scaffold (Figs. 5a1, 5a2, 6a1, 6a2), whereas abundant toluidine stained matrix and trichrome stained matrix have infiltrated the MSC-seeded trabecular scaffolds (Figs. 5b1, 5b2, 6b1, 6b2). In comparison, abundant toluidinestained matrix and trichrome stained matrix have infiltrated both the unseeded and MSC-seeded columnar scaffolds (Figs. 5c1–5d2, 6c1–6c2).

A semi-quantitative analysis of the amount of tissue infiltrated into the implants, as well as the amount of toluidine stained matrix (GAG) and trichrome stained matrix (collagen) is given in Table 2. Statistical analysis showed significantly higher amount of

tissue, GAG, and collagen infiltrated into the trabecular scaffolds with MSCs when compared to the trabecular scaffolds without MSCs. For the columnar scaffolds, a higher amount tissue was formed within the scaffolds seeded with MSCs, when compared to the unseeded columnar scaffolds. However, for these columnar scaffolds, seeding with MSCs did not produce a significant enhancement of the amount of GAG and collagen infiltrated. A comparison of the histological data for the two groups of scaffolds without MSCs (Table 2) showed a significantly higher amount of tissue, GAG, and collagen infiltrated into the columnar scaffolds than in the trabecular scaffolds. However, for the scaffolds seeded with MSCs, there was no significant difference in the amount of tissue, GAG, and collagen between the two groups of scaffolds.

Figure 7 shows images of sections stained with Sanderson^{TM} Bone Stain and counter stained with acid fuchsin for the bioactive glass implants with the trabecular and columnar microstructures. In both groups of scaffolds, seeded with MSCs or unseeded, tissue was found to be in close contact with the bioactive glass surface. A small amount of soft tissue (stained blue) was formed adjacent to the surface of the bioactive glass (G) in the unseeded trabecular scaffolds (Fig. 7a), whereas abundant osteoid deposition (stained purple), along with a number of osteoids (stained blue within the purple-stained deposition) was found within the MSC-seeded trabecular scaffold (Fig. 7b). Whereas soft tissue ingrowth was observed in the pores of the unseeded columnar scaffolds (Fig, 7c), abundant osteoid deposition (stained purple) was observed in the pores of the MSC-seeded scaffolds (Fig. 7d), and osteoids were also found within the purple-stained depositions.

7.5. DISCUSSION

The results showed that in addition to tissue infiltration into the scaffolds, degradation of the bioactive glass scaffolds occurred during the 4-week subcutaneous implantation. The degradation of silicate-based bioactive glass, such as 45S5 and 13-93, in an aqueous phosphate solution has been widely investigated [17, 18]. Upon immersion of the glass into the phosphate solution, an amorphous SiO_2-rich layer (typically 1 to a few microns thick) first forms on the surface of the glass, after which a growing HA-type layer forms on the surface of SiO_2-rich layer as the SiO_2-rich layer migrates into the glass. At a nearly constant temperature, such as the body temperature (37°C), the rate at which a bioactive glass converts to HA depends on several factors, such as the glass composition, the curvature of the glass surface, the concentration of the aqueous phosphate solution, and the presence of polyanions in the phosphate solution [19, 20].

In the present work, the thickness of the HA layer formed on the trabecular bioactive glass scaffolds *in vivo*, after subcutaneous implantation for 4 weeks, was ~20 μm (Fig. 4). Our previous *in vitro* work on the conversion of similar 13-93 bioactive glass scaffolds in a simulated body fluid (SBF) showed the formation of a HA layer of thickness ~7 μm after 2 weeks, and ~ 10 μm after 4 weeks [21]. This comparison indicates that the conversion of the 13-93 bioactive glass scaffold in the present *in vivo* experiments was approximately twice as fast as the *in vitro* conversion in a SBF. The faster conversion could be attributed to the more 'dynamic' *in vivo* conditions, when compared to more 'static' conditions present in the *in vitro* experiments involving only intermittent stirring of the SBF. Another factor that could contribute to the enhanced *in vivo* conversion of the 13-93 bioactive glass scaffolds is the presence of proteins,

polysaccharides, and other polymeric species in the extracellular matrix which contain electron-donating moieties such as carboxyl and hydroxyl groups. Some polyanion species added to a SBF *in vitro* have been shown to markedly enhance the conversion of 13-93 bioactive glass to HA [20].

For the unseeded 13-93 bioactive glass scaffolds (no MSCs), abundant amount of soft tissue, GAG, and collagen infiltrated the columnar scaffolds, whereas only limited amount of tissue was formed in the trabecular scaffolds. The total porosity and range of pore sizes of the trabecular scaffolds were far larger than those for the columnar scaffolds (Table 1), so these two pore parameters cannot account for the limited amount of tissue infiltrated into the trabecular scaffolds. Instead, the orientation or topography of the pores, random for the trabecular scaffolds vs. oriented for the columnar scaffolds, appeared to have a marked influence.

The oriented pores in the columnar scaffolds could serve as guiding pattern for the directional migration of cell and tissues, allowing faster vascularization of the implants. On the other hand, the tortuous path of the randomly arranged pores in the trabecular scaffolds could provide an increased path for cell and tissue migration, leading to a reduce rate of tissue infiltration. Oriented poly(L-lactic acid) (PLLA) scaffolds have shown better ability to support *in vitro* osteoblastic cell growth and formation into neo-tissue than scaffolds with the same porosity but with a random three-dimensional pore architecture [22]. The enhanced neo-tissue formation in the oriented scaffolds was attributed to the improved mass transport or/and cell–cell interaction. The importance of pore orientation on their *in vitro* and *in vivo* performance of scaffold is widely recognized in axonal and nerve regeneration [23-29]. The extent of neurite outgrowth and Schwann

cell migration *in vitro*, and the number of regenerated axons per cross section *in vivo* are both found to be significantly higher in oriented fiber scaffolds than in random scaffolds [28]. The topographical cue (i.e. orientation) has been suggested to have a vastly influencing on endogenous repair mechanisms for promoting nerve regeneration across challenging gaps.

Although soft tissue infiltration (GAG and collagen) into the trabecular glass scaffolds was limited, the results of the present work showed that the ability this group of scaffolds to support tissue ingrowth was markedly enhanced by seeding the trabecular scaffolds with MSCs prior to subcutaneous implantation. Previous investigations have also shown that the incorporation of MSCs into scaffolds can play an important role in promoting the formation of tissues and extracellular matrix *in vitro* [30-33]. The higher amount of tissue, GAG, and collagen formation was believed to be the triggered by the seeded MSCs which were initially on the surface, but then grew within the scaffolds.

For the columnar scaffolds, seeding with MSCs did not produce as marked an enhancement of tissue infiltration as that observed for the trabecular scaffolds (Table 2). A possible reason for this difference is that the unseeded columnar scaffolds were by themselves able to support moderate tissue infiltration, so the potential of seeding with MSCs to further enhance new tissue formation was limited.

The seeding of both groups of scaffolds with MSCs induced the formation of osteoid deposition (stained purple in Fig. 7). The MSCs have intrinsically different responses to osteoinductive agents and can be differentiated into osteoblastic lineage [33,34]. Seeding porous calcium carbonate, HA and β-tricalcium phosphate with MSCs has been reported to result in the bone formation upon subcutaneous implantation

[36,37]. In the present work, a HA-type layer was observed to form on the surface of the implanted glass scaffolds (Figure 4). The formation of the HA layer has been shown to be osteoinductive [6], which may be responsible for the differentiation of MSCs into the bone-like tissue. Furthermore, the ions released from bioactive glass have been shown to induce the expressions of genes relevant to osteoblast metabolism and bone homeostasis [9, 10]. The release of ions such as Si, Ca, P and Na at critical concentrations due to the surface reaction of bioactive glasses has been reported to induce specific intracellular and extracellular responses at the interface of glass with its cellular environment [38]. The ions release from the 13-93 bioactive glass scaffolds may contribute to the formation of osteoid deposition from the MSCs.

As outlined earlier, the trabecular and columnar bioactive glass scaffolds used in the present work were shown to be biocompatible *in vitro* and to have promising mechanical properties. The present results showed the *in vivo* biocompatibility of both groups of scaffolds, and their ability to support abundant soft tissue infiltration and osteoid deposition when seeded with MSCs. Current work is investigating the ability of these scaffolds to repair contained and segmental defects in bone in an animal model.

7.6. CONCLUSION

After subcutaneous implantation for 4 weeks in the dorsum of rats, trabecular scaffolds (porosity = 85%; pore size = 100–500 μm), with a microstructure similar to that of dry human trabecular bone, showed limited ability to support ingrowth of soft tissue (glycosaminoglycan; collagen). On the other hand, columnar scaffolds with oriented pores (porosity = 65%; pore width = 90–110 μm) supported moderate to abundant soft

tissue infiltration. Seeding with mesenchymal stem cells (MSCs) prior to implantation vastly improved the amount of soft tissue infiltrated into the trabecular scaffolds, and the amount of bone-like tissue formed in both groups of scaffolds. The implants were surrounded by a band of fibrovascular tissue (100–300 μm thick), indicating good integration with surrounding tissue. These *in vivo* results, coupled with previous *in vitro* mechanical and cell culture results, indicate considerable potential for the use of these MSC-seeded trabecular and columnar scaffolds in bone repair and regeneration.

7.7. REFERENCE

1. Stock UA, Vacanti JP. Tissue engineering: Current state and prospects. Annu Rev Med 2001;52:443–451.
2. Hutmacher D W. Scaffolds in tissue engineering bone and cartilage. Biomaterials 2000;21:2529-2543
3. Vats A, Tolley NS, Polak JM, Gough JE. Scaffolds and biomaterials for tissue engineering: A review of clinical applications. Clin Otolaryngol 2003;28:165–172.
4. Langer R, Vacanti JP. Tissue engineering: The challenges ahead. Sci Am 1999;280:86–89.
5. Rezwan K, Chen QZ, Blaker JJ, Boccaccinic AR. Biodegradable and bioactive porous polymer/inorganic composite scaffolds for bone tissue engineering. Biomaterials 2006;27:3413-3431
6. Hench LL. Bioceramics. J Am Ceram Soc 1998; 81:1705–28.
7. Wheeler DL, Stokes KE, Park HE, Hollinger JO. Evaluation of particulate bioglass in a rabbit radius ostectomy model. J Biomed Mater Res 1997; 35:249–54.
8. Wheeler DL, Stokes KE, Hoellrich RG, Chamberland DL, McLoughlin SW. Effect of bioactive glass particle size on osseous regeneration of cancellous defects. J Biomed Mater Res 1998; 41:527–33.
9. Xynos ID, Edgar AJ, Buttery LD, Hench LL, Polak JM. Ionic products of bioactive glass dissolution increase proliferation of human osteoblasts and induce insulin-like growth factor II mRNA expression and protein synthesis. Biochem Biophys Res Commun 2000;276:461–65.
10. Xynos ID, Edgar AJ, Buttery LD, Hench LL, Polak JM. Gene-expression profiling of human osteoblasts following treatment with ionic products of bioglass 45S5 dissolution. J Biomed Mater Res 2001;55:151–57.
11. Leach JK, Kaigler D, Wang Z, Krebsbach PH, Mooney DJ. Coating of VEGF-releasing scaffolds with bioactive glass for angiogenesis and bone regeneration. Biomaterials 2006;27: 3249–55.

12. Leu A, Leach JK. Proangiogenic Potential of a collagen/bioactive glass substrate. Pharmaceut Res 2008;25,1222–29.
13. Fu Q, Rahaman MN, Bal BS, Brown RF, Day DE. Mechanical and *in vitro* performance of 13-93 bioactive glass scaffolds prepared by a polymer foam replication technique. Acta Biomater 2008;4:1854-64.
14. Fu Q, Rahaman MN, Brown RF, Bal BS. Preparation and *in vitro* evaluation of bioactive glass (13-93) scaffolds with oriented microstructures for repair and regeneration of load-bearing bones. J Biomed Mater Res Part A 2009 (In press)
15. Fung YC. Biomechanics: mechanical properties of living tissues. New York: Springer; 1993.
16. Wang ML, Massie J, Allen RT, Lee YP, Kim CW. Altered bioreactivity and limited osteoconductivity of calcium sulfate-based bone cements in the osteoporotic rat spine. Spine J 2008;8:340-50
17. Huang W, Day DE, Kittiratanapiboon K, Rahaman MN. Kinetics and mechanisms of the conversion of silicate (45S5), and borosilicate glasses to hydroxyapatite in dilute phosphate solutions. J Mater Sci Mater Med 2006;17:583-96
18. Yao A, Wang DP, Huang W, Fu Q, Rahaman MN, Day DE. *In vitro* bioactive characteristics of borate-based glasses with controllable degradation behavior. J Am Ceram Soc 2007;90:303-6
19. Kamitakahara M, Kawashita M, Kokubo T, Nakamura T. Effect of polyacrylic acid on the apatite formation of a bioactive ceramic in a simulated body fluid: fundamental examination of the possibility of obtaining bioactive glass-ionomer cements for orthopaedic use. Biomaterials 2001;22:3191-6
20. Fu Q, Rahaman MN, Day DE. Accelerated Conversion of Silicate Bioactive Glass (13-93) to Hydroxyapatite in Aqueous Phosphate Solution Containing Polyanions. J Am Ceram Soc (2009). In press.
21. Fu Q, Rahaman MN, Bal BS, Huang W, Day DE. Preparation and bioactive characteristics of a porous 13-93 glass, and fabrication into the articulating surface of a proximal tibia. J Biomed Mater Res 2007;82A:222–9.
22. Ma PX, Zhang R. Microtubular architecture of biodegradable polymer scaffolds. J Biomed Mater Res 2001;56:469-77.
22. Stokols S, Tuszynski MH. The fabrication and characterization of linearly oriented nerve guidance scaffolds for spinal cord injury. Biomaterials 2004;25:5839-46
24. Mahoney MJ, Chen RR, Tan J, Saltzman WM. The influence of microchannels on neurite growth and architecture. Biomaterials 2005;26:771-8
25. Yu TT, Shoichet MS. Guided cell adhesion and outgrowth in peptide-modified channels for neural tissue engineering. Biomaterials 2005;26:1507-14.
26. Stokols S, Tuszynski MH. Freeze-dried agarose scaffolds with uniaxial channels stimulate and guide linear axonal growth following spinal cord injury. Biomaterials 2006;27:443-51
27. Prang P, Müller R, Eljaouhari A, Heckmann K, Kunz W, Weber T, Faber C, Vroemen M, Bogdahn U, Weidner N. The promotion of oriented axonal regrowth in the injured spinal cord by alginate-based anisotropic capillary hydrogels. Biomaterials 2006;27:3560-9

28. Kim Y, Haftel VK, Kumar S, Bellamkonda RV. The role of aligned polymer fiber-based constructs in the bridging of long peripheral nerve gaps. Biomaterials 2008;29:3117-3127
29. Li J, Rickett TA, Shi R. Biomimetic nerve scaffolds with aligned intraluminal microchannels: a "sweet" approach to tissue engineering. Langmuir 2009;25:1813-17
30. Livingston T, Ducheyne P, Garino J. *In vivo* evaluation of a bioactive scaffold for bone tissue engineering. J Biomed Mater Res 2002;62:1-13
31. Fan HB, Hu YY, Zhang CL, Li XS, LV R, Qin L, et al. Cartilage regeneration using mesenchymal stem cells and a PLGA-gelatin/chondroitin/hyaluronate hybrid scaffold. Biomaterials 2006;27:4573-80
32. Quyang HW, Goh JCH, Thambyah A, Teoh SH, Lee EH. Knitted poly-lactide-co-glycolide scaffold loaded with bone marrow stromal cells in repair and regeneration of rabbit Achilles tendon. Tissue Eng 2003;9:431-9
33. Liu H, Fan H, Toh SL, Goh JCH. A comparison of rabbit mesenchymal stem cells and anterior cruciate ligament fibroblasts responses on combined silk scaffolds. Biomaterials 2008;29:1443-53
34. Solchaga LA, Cassiede P, Caplan AI. Different response to osteo-inductive agents in bone marrow and periosteum-derived cell preparations. Acta Orthop Scand 1998;69:426-32
35. Haynesworth SE, Goshima J Goldberg VM, Caplan AI. Characterization of cells with osteogenic potential from human marrow. Bone 1992;13:81-88
36. Ohgushi H, Okumura M, Yoshikawa T, Inoue K, Senpuku N, Tamai S. Bone formation process in porous calcium carbonate and hydroxyapatite. J Biomed Mater Res 1992;26:885-895
37. Yamada Y, Boo JS, Ozawa R, Nagasaka T, Okazaki Y, Hata K, Ueda M. Bone regeneration following injection of mesenchymal stem cells and fibrin glue with a biodegradable scaffold. J Cranio Maxill Surg 2003;31:27-33.
38. Hench LL, Polak JM. Third-generation biomedical materials. Science 2002;295:1014-1017.

Table 1. Characteristics of the 13-93 bioactive glass scaffolds with trabecular and columnar microstructure

Scaffold group	Porosity	Pore size (μm)	Strength (MPa)	Fabrication method
Trabecular	85 ± 2	100–500	11 ± 1	Polymer foam replication
Columnar	65 ± 2	90–110	25 ± 3	Unidirectional freezing of suspensions

Table 2. Tissue ingrowth scores[#] for total amount of tissue, glycosaminoglycan (GAG), and collagen infiltrated into the trabecular and columnar implants seeded with mesenchymal stem cells (MSCs) or unseeded (without MSCs).

Implants	**Tissue**	**GAG**	**Collagen**
Trabecular scaffold without MSCs	1.0	1.0	0.5 ± 0.5
Trabecular scaffold with MSCs	3.0*	1.8 ± 1.0*	1.8 ± 1.2*
Columnar scaffold without MSCs	2.3 ± 0.5[†]	2.5 ± 0.6[†]	1.5 ± 1.0[†]
Columnar glass with MSCs	2.8 ± 0.5*	1.8 ± 0.5	2.3 ± 0.5

[#]Note: Scores based on the following scale: 0: none, 1: small amount, 2: moderate amount, and 3: abundant.

* $p < 0.05$ when compared with the score for the same group of implants without MSCs.

[†] $p < 0.05$ when compared with the score for the trabecular group of implants without MSCs.

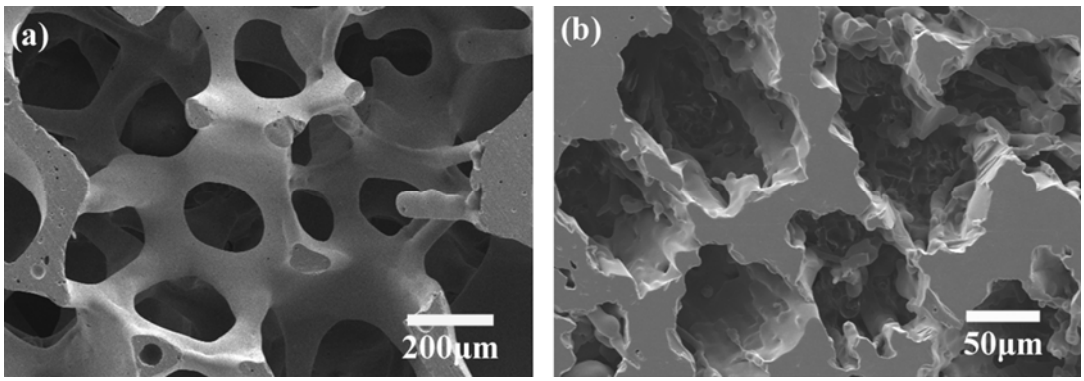

Figure 1. SEM images of 13-93 bioactive glass scaffolds with (a) trabecular microstructure, similar to the microstructure of dry human trabecular bone, and (b) columnar microstructure of oriented pores (cross section perpendicular to the pore orientation direction).

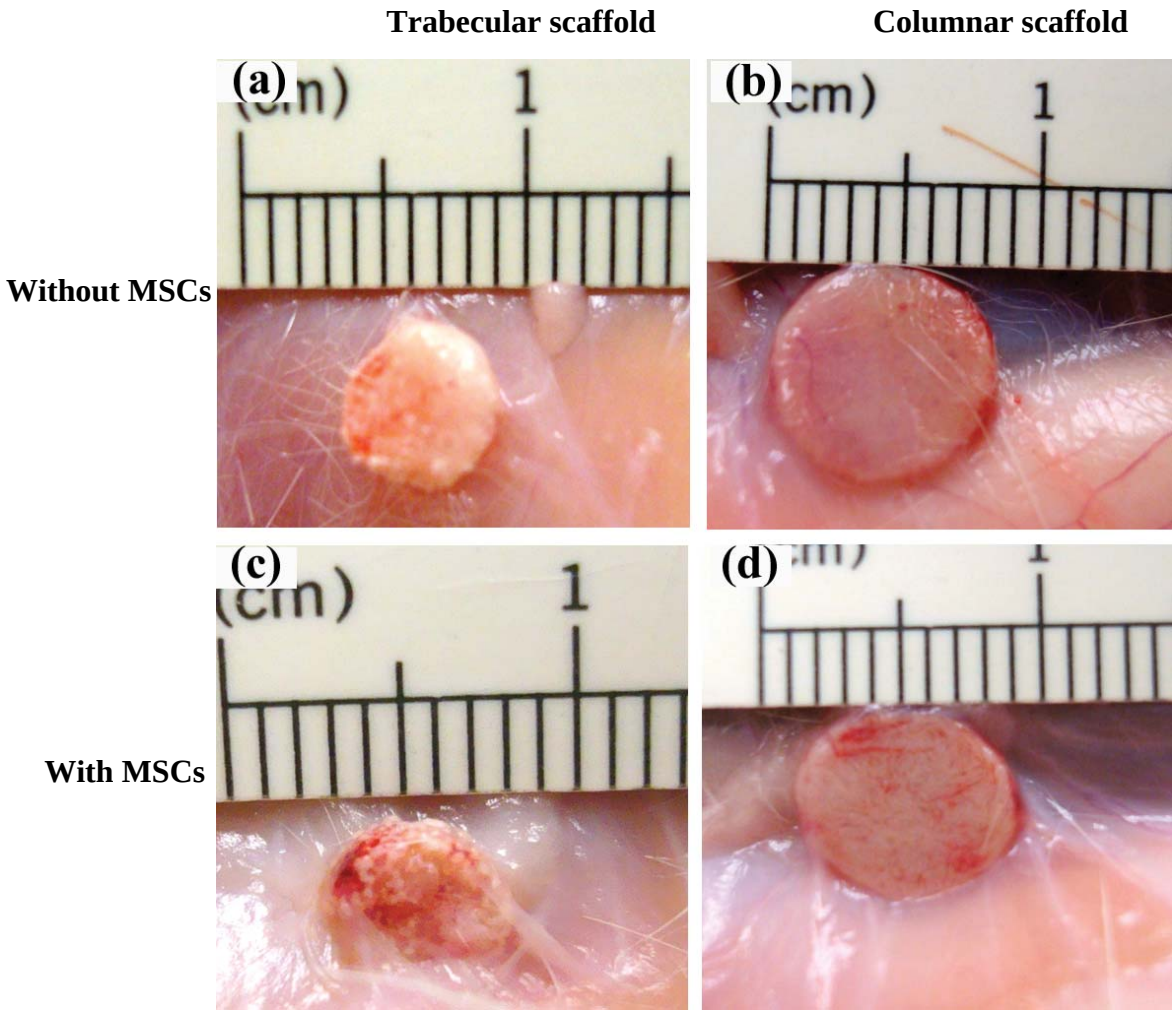

Figure 2. Gross appearance of bioactive glass scaffolds 4 weeks after subcutaneous implantation in the dorsum of rats.

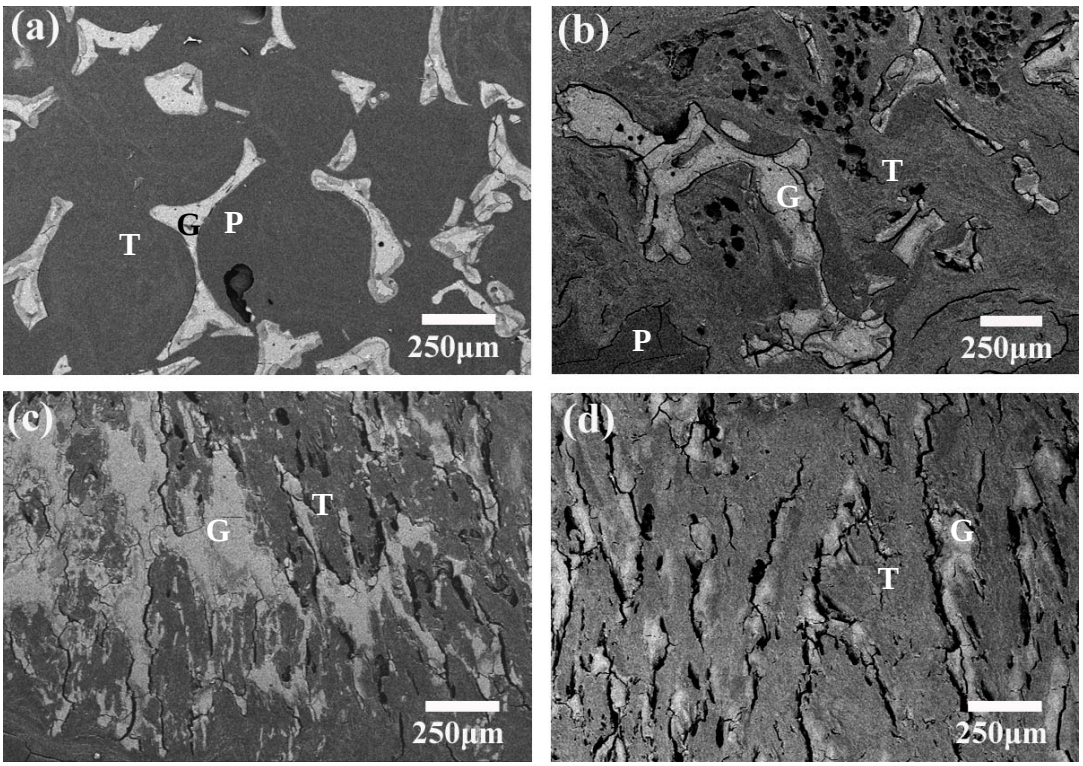

Figure 3. SEM backscattered electron images of trabecular implants (a) without MSCs and (b) seeded with MSCs; and columnar implants (c) without MSCs and (d) seeded with MSCs, after subcutaneous implantation for 4 weeks. G denotes glass; T denotes tissue; P denotes PMMA.

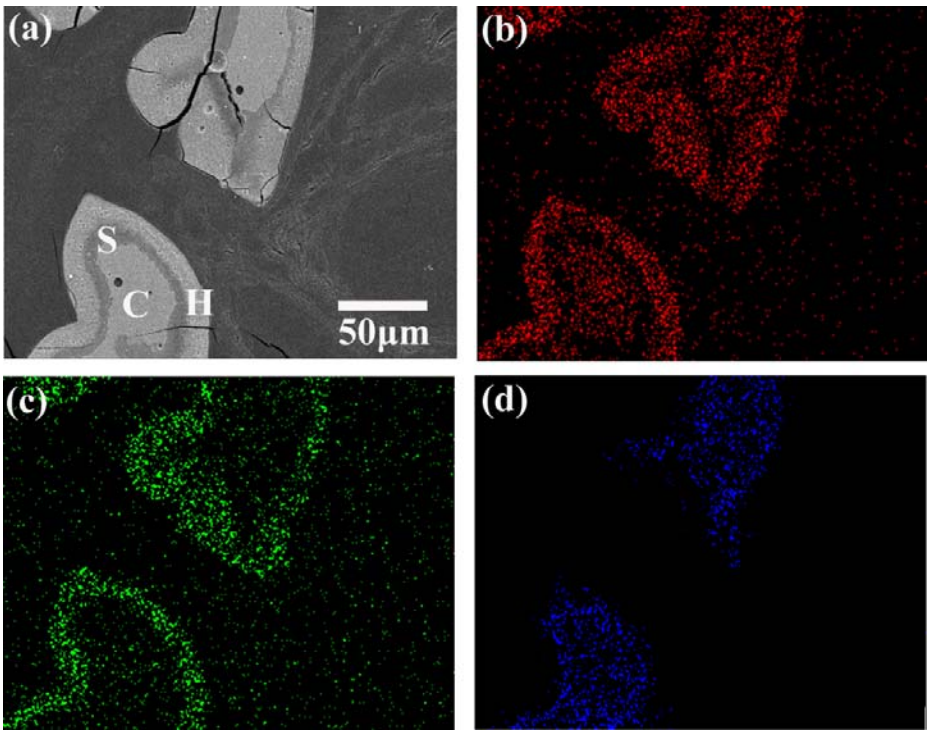

Figure 4. SEM backscattered electron image of bioactive glass in trabecular scaffold (without MSCs) after subcutaneous implantation for 4 weeks (a), and corresponding X-ray maps for Ca(K) (b), P(K) (c), and Si(K) (d). C denotes unconverted glass core; S denotes SiO_2-rich layer; H denotes hydroxyapatite layer.

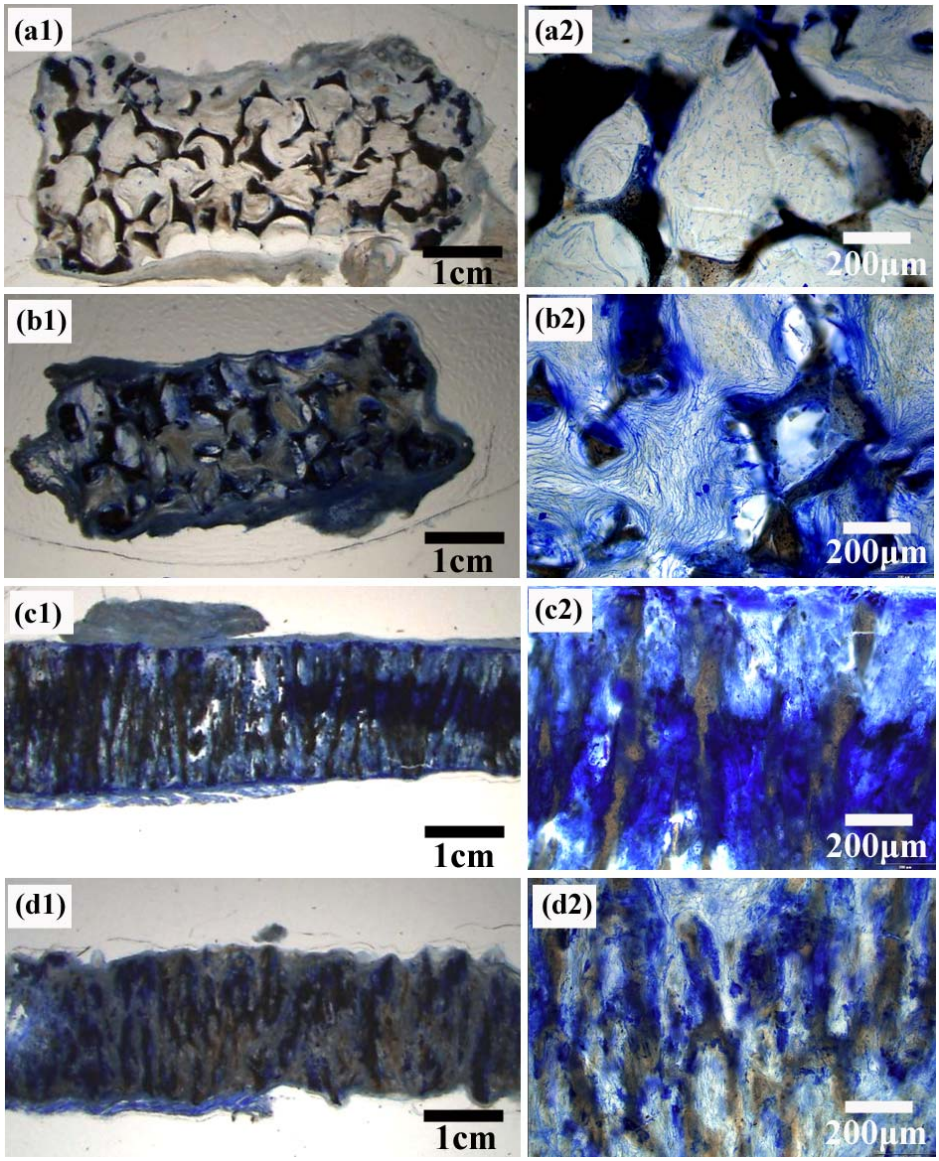

Figure 5. Transmitted light images of toluidine blue stained sections for trabecular implants (a) without MSCs, (b) seeded with MSCs, and for columnar implants (c) without MSCs, and (d) seeded with MSCs, after implantation for 4 weeks.

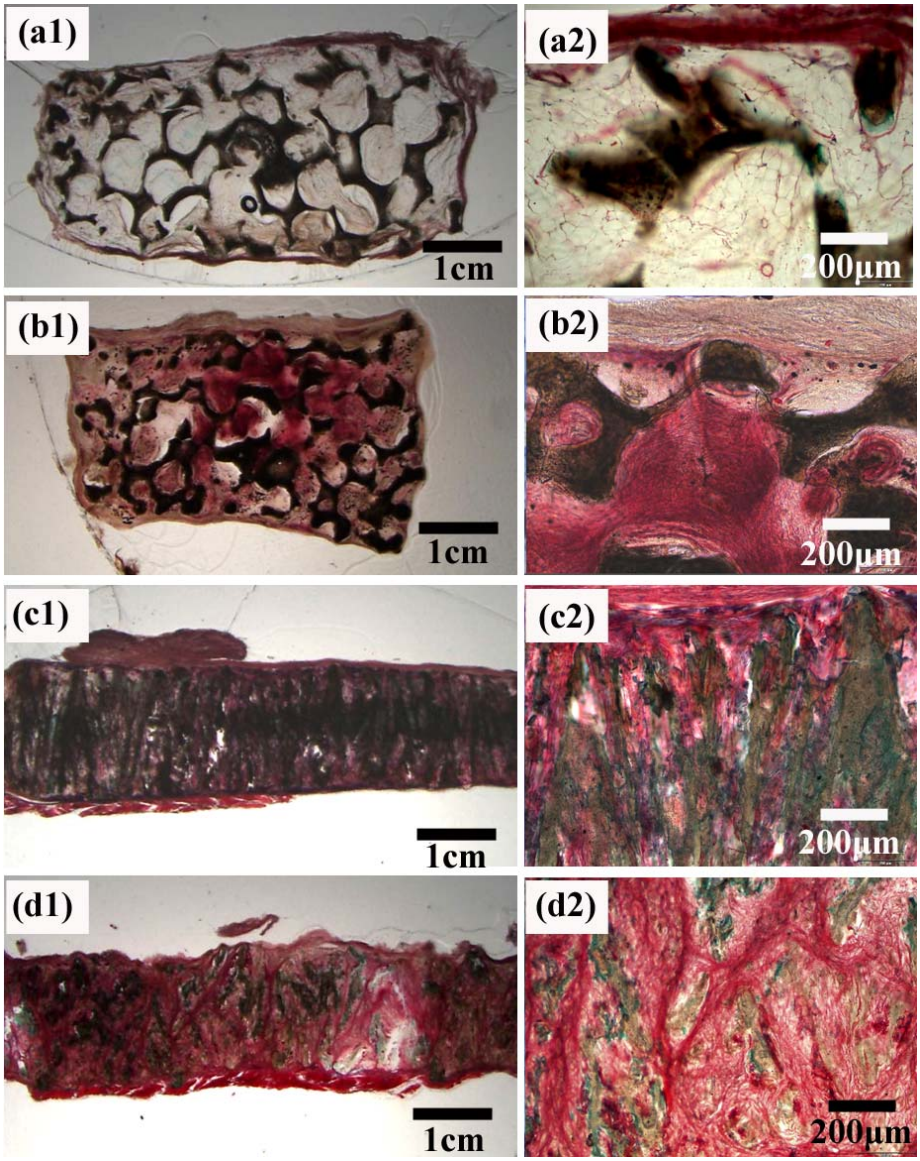

Figure 6. Transmitted light images of Goldner's trichrome stained sections for trabecular implants (a) without MSCs, (b) seeded with MSCs, and for columnar implants (c) without MSCs, and (d) seeded with MSCs, after implantation for 4 weeks.

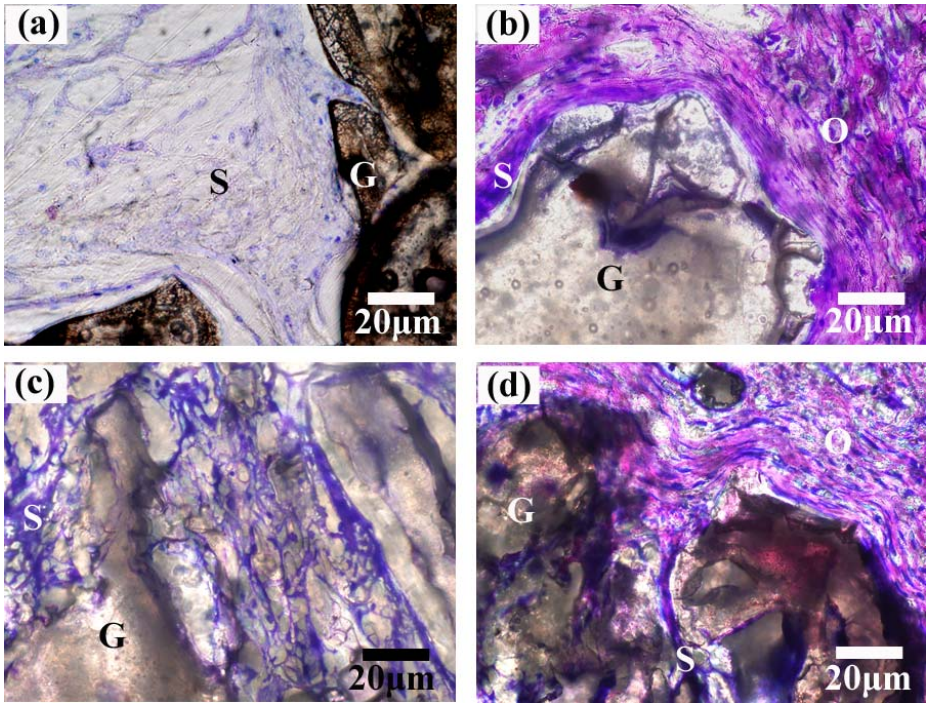

Figure 7. Transmitted light images of thin sections stained with Sanderson™ Bone Stain for trabecular implants (a) without MSCs, and (b) seeded with MSCs, and columnar implants (c) without MSCs, and (d) seeded with MSCs, after subcutaneous implantation for 4 weeks. G denotes bioactive glass; S denotes soft tissue; O denotes osteoid production.

3. CONCLUSIONS

This section summarizes the overall conclusions drawn from the research reported in the seven manuscripts that make up the body of the dissertation.

1. Freeze casting of aqueous hydroxyapatite (HA) suspension on a cold substrate produced porous constructs with a lamellar-type microstructure (pore width 5-30 μm) in which plate-like HA lamellas were oriented in the direction of freezing. Varying the processing parameters, such as that the particle concentration in the suspension, the temperature of the cold substrate (the freezing rate), and the addition of glycerol to the aqueous solvent changed the porosity and pore size to a limited extent with no significant change in pore morphology. On the other hand, the addition of 60 wt% 1,4-dioxane to the aqueous solvent drastically changed the pore width and pore morphology, giving scaffolds with columnar-type pores of width 90-110 μm.
2. The compressive strength of the freeze-cast HA constructs was strongly dependent on the sintering temperature, and optimum strength was obtained by sintering for 3 hr at 1350ºC without the formation of secondary crystal phases. The mechanical response of the porous HA constructs showed a unique 'elastic-plastic' response, similar in nature to that of bone and other natural materials, with high strain tolerance ~5% at the maximum stress, high strain for failure >20%, and strain rate sensitivity.
3. HA scaffolds with approximately the same porosity (65-70%) but different pore architecture (lamellar, pore width = 20-30 μm; columnar, pore diameter = 90-110 μm) were able to support the proliferation of MC3T3-E1 pre-osteoblastic cells on

their surfaces. HA scaffolds with the columnar-type microstructure showed far better ability to support cell growth into the interior pores and cell function than those with lamellar-type microstructure.

4. HA scaffolds with columnar microstructure showed better ability than the lamellar scaffolds to support the proliferation, differentiation and mineralization of MLO-A5 cells, an osteogenic cell line. The scaffolds also supported the ingrowth of cells throughout the unidirectional pores during culture, and were rapidly infiltrated with a cell suspension by capillary action of the pores. These results indicated that freeze-cast HA constructs with the columnar microstructure could serve as scaffolds for bone repair and regeneration.
5. Bioactive 13-93 glass scaffolds with unidirectional microstructures were prepared using the same freeze casting technique as for HA scaffolds. Columnar glass scaffolds (porosity=55-60%; pore diameter=90-110 μm) showed encouraging mechanical properties, including a compressive strength of 22-28 MPa in the direction of pore orientation and an "elastic-plastic" response with a large strain for failure (>20%).
6. 13-93 glass scaffolds with columnar microstructure showed better ability in supporting the proliferation and differentiated function by MLO-A5 cells as compared to scaffolds with a lamellar microstructure. The columnar glass could also support the proliferation of MLO-A5 cells down into the interior pores as well as rapid migration of cell suspension by capillary. These results indicate that 13-93 bioactive glass scaffolds with the columnar microstructure could be used for the repair and regeneration of load-bearing bones *in vivo*.

7. 13-93 glass scaffolds with columnar microstructure integrated well with the surrounding tissues upon subcutaneous implantation in the dorsum of rats. The scaffolds supported the ingrowth of significant amount of extracellular matrix (glycosaminoglycan and collagen) formation. The preseeding of mesenchymal stem cells (MSCs) on the columnar glass scaffolds increased the amount of tissue infiltration and resulted in the deposition of osteoid production. These results indicate that the porous 13-93 glass columnar scaffolds may be a desirable substrate for the bone tissue engineering applications.

4. FUTURE WORK

Based on the research discussed in the present work, there are many interesting possibilities for future work.

1. Toughening mechanism: The present study investigated the relationship between the microstructure and mechanical behavior of the freeze-cast HA and bioactive glass scaffolds with unidirectional porosity. The scaffolds showed an interesting "elastic-plastic" mechanical responses in compression parallel to the freezing direction. Along with the knowledge gained from the present work and the literature report on the toughening mechanism for natural materials such as bone and nacre, a proper toughening mechanism should be proposed to explain the mechanical behavior of such ceramic materials.
2. Modeling of crystal size control: Processing parameters including the particle concentration in the suspension, temperature of the substrate and solvent composition have been found to influence the size of the formed crystals. These factors have been discussed in terms of the thermodynamic and kinetic analysis. The estimation of the crystal size based on the theoretical modeling may provide guidance for future work.
3. Mechanical property improvement: The compressive strength (22-28 MPa) of the freeze-cast 13-93 glass scaffolds was almost twice the value for human trabecular bone (2-12 MPa). This makes the glass scaffolds promising for the repairing of load-bearing sites such as segmental bone defects. Furthermore improvement in the compressive strength to a level comparable to human cortical bone (120-180 MPa) at the expense of limited reduction of the porosity will make the scaffolds

more attractive. The refinement of the directionality and control of the sintering temperature of the glass are options to improve the mechanical strength.

4. Control of scaffold degradation: The present work investigated the fabrication, and *in vitro* and *in vivo* evaluation of bioactive 13-93 glass scaffolds. Little work was done on the *in vitro* and *in vivo* degradation behavior of the scaffolds. With regards to the application of scaffolds in bone repairing and regeneration, a match between the new bone growth and scaffold degradation rate should be achieved. The evaluation and control of the glass scaffold degradation rate will provide useful information for future *in vivo* application in bone repair.
5. Repair of segmental bone defects: The *in vivo* performance of the bioactive 13-93 glass was assessed by subcutaneous implantation in the dorsum of rats. This preliminary work showed evidence that 13-93 glass scaffolds could support tissue ingrowth and extracellular matrix formation. An investigation into the ability of the scaffold to support new bone formation in large bone defect sites will provide further guidance for the property and microstructure control of the scaffolds.

APPENDIX A

POSSIBLE TOUGHENING MECHANISMS IN UNIDIRECTIONAL HYDROXYAPATITE SCAFFOLDS PREPARED BY FREEZE CASTING

A. POSSIBLE TOUGHENING MECHANISMS IN UNIDIRECTIONAL HYDROXYAPATITE SCAFFOLDS PREPARED BY FREEZE CASTING

Qiang Fu, Mohamed N. Rahaman*

Department of Materials Science and Engineering, Missouri University of Science and Technology, Rolla, MO 65409, USA

ABSTRACT

In our previous work, oriented scaffolds prepared by unidirectional freezing of suspensions showed a unique elastic-plastic mechanical response during compression parallel to the freezing direction. The objective of the present work was to characterize changes in the microstructure resulting from the deformation of the scaffolds in compression to different strains. Scanning electron microscopy indicated that several mechanisms, including microcracking, crack deflection, tortuous crack path, lamellar sliding and ceramic bridges between the lamellas, might contribute to the elastic-plastic mechanical response. These results may provide a guide for the design of scaffold materials for the repair of load-bearing bones.

1. INTRODUCTION

Biological systems produce composites that are composed of both inorganic and organic components in complex anisotropic arrangement. They create hierarchically

* Corresponding author: M. N. Rahaman (rahaman@mst.edu)

organized composites that can achieve orders of magnitude increase in strength and toughness compared to their constituent phases [1-3]. Nacre consists of sub-micrometer (~ 500 nm) layered aragonite ($CaCO_3$) platelets in which adjacent platelets are bonded by a thin (20-30 nm) layer of organic protein, which are organized into a layered brick-like structure. The fracture toughness of nacre is roughly an order of magnitude higher than that of either the aragonite or the protein layer [1]. The toughening mechanisms of nacre occur through its multi-dimensional architectural design and the viscoelastic energy dissipation within the biopolymer layer. Microcrack formation, crack bridging and sliding of the aragonite layers also act as effective toughening mechanisms [1, 2].

Bone is another hierarchical composite of a fibrous polymer (collagen) and hard mineral nanoparticles (hydroxyapatite, HA) [1]. The enduring strength and toughness of bone is attributed to the simultaneous operation of the toughening mechanisms at the microscale level. Crack deflection, crack bridging, constrained microcracking, and viscoplastic flow have been reported as the main toughening mechanisms for cortical bone [4-7]. Wood is a cellular composite, consisting of cellulose, a high molecular weight polysaccharide. The specific stiffness (stiffness per unit weight) and specific strength of wood is comparable to steel [8]. Wood exhibits highly anisotropic fracture toughness, and its highest toughness is ten times larger than that of a fibrous composite with the same fraction of fibers and matrix. Fiber pull-out is the main toughening mechanism responsible for the high toughness of wood [9]. Inspired by these strong and tough biological materials, attempts are being made to fabricate synthetic materials with bone-like and nacre-like microstructures.

In our previous work, porous bioactive 13-93 glass and ceramic (HA) scaffolds with highly oriented microstructures were fabricated by a unidirectional freeze casting technique. Both lamellar- and columnar-type pores oriented along the freezing direction were observed within these scaffolds [10-12]. Upon compression in the pore orientation direction, the scaffolds exhibited a unique "elastic-plastic" response with a high deformation for failure (>20%) and strain rate sensitivity [11, 12]. This type of mechanical response is similar in nature to that of biological materials such as nacre, bone and wood [1, 13, 14], and is of importance for the potential application of these bioactive glass and HA scaffolds in the repair of load-bearing bones.

The objectives of the present work were to investigate the microstructure changes that occur during the compressive loading of HA scaffolds fabricated by the unidirectional freeze casting technique, and to provide a rationalization of the unique elastic-plastic response in terms of the observed microstrutural changes. An understanding of the relationship between the microstructure and mechanical behavior could provide useful information for the manipulation of the structure of these scaffolds for different applications. HA scaffolds with a lamellar-type microstructure prepared from aqueous suspension were investigated, since this system forms the basis for the development of other freeze casting structures.

2. MATERIALS AND METHODS

The procedures for preparing HA scaffolds with an oriented microstructure by unidirectional freezing of HA suspensions are described in detail elsewhere [10]. Briefly, the suspensions contained 20 vol% HA particles (average particle size <1 μm; Alfa

Aesar, Haverhill, MA), 0.75 wt% dispersant (Dynol 604; Air Products & Chemicals, Inc., Allentown, PA), and 1.5 wt% binder (DuPont Elvanol® 90-50; DuPont, Wilmington, DE). Unidirectional freezing was initiated by pouring the suspensions into poly(vinyl chloride), PVC, tubes (~10 mm internal diameter × 20 mm long) placed on a cold steel substrate at –20°C in a freeze dryer (Genesis 25 SQ Freeze Dryer, VirTis Co., Gardiner, NY). After sublimation of the frozen solvent in the freeze dryer (Genesis 25 SQ), the constructs were sintered in air for 3 h at 1350°C (heating and cooling rate = 3°C/min). The mechanical response of the sintered constructs (~8 mm in diameter × 16 mm) in compressive loading was measured according to ASTM-C773 using an Instron testing machine (Model 4204, Norwood, MA) at a crosshead speed of 0.5 mm/min. The samples were tested in the directions parallel to the freezing direction. The test was stopped at different stages of deformation, and the deformed samples were carefully removed. Scanning electron microscopy, SEM (Hitachi S-4700, Hitachi Co., Tokyo, Japan) was used to observe the microstructure of the deformed samples.

3. RESULTS AND DISCUSSION

Figure 1 shows the microstructure of HA scaffolds prepared from aqueous suspensions with 20 vol% particles. The scaffolds consisted of a uniform lamellar-type microstructure with the pores oriented in the direction of freezing. Ceramic bridges were observed between the adjacent lamellae. It has ben suggested that these ceramic bridges arose from the local ice crystal tip splitting and the engulfment of particle agglomerates due to particle repulsion from the solidification front and subsequent tip healing [15].

Figure 2 shows the mechanical response of the lamellar HA constructs prepared from aqueous suspension (20 vol% particles) upon compression parallel to the freezing direction. The data shown are engineering stress and deformation, based on the initial cross-sectional area and length of the test sample, and do not represent the true stress and deformation. The curve had a smoothly varying, asymmetric bell shape, and could be divided into three regions: an elastic regime in which the stress–deformation response was linear (Region I), a stress plateau region representing a region of highest sustainable loading (Region II), and a failure region of decreasing load-beating ability (Region III). Catastrophic failure of the samples was not observed during the compression test (up to 5% deformation). This type of stress–deformation curve, with an asymmetric bell shape, has been observed in nacre when the compression loading is applied parallel to the layered structure [16]. Crack deflection, delocalization of damage, plastic microbuckling, and viscoplastic deformation of the organic layers were considered to be the main mechanisms contributing to the mechanical properties of nacre [1, 2, 16].

In an attempt to understand the toughening mechanisms in the HA scaffolds prepared in this work, the microstructural changes in the HA constructs which resulted from mechanical testing in compression were observed using SEM. Figure 3 (a1-d1) shows SEM images (a1-d1) of the fractured surface of HA constructs after they were compressed to different strains and removed from the mechanical testing machine. The 4 images show representative microstructures of samples that were deformed to different regions of the stress vs. deformation curve shown in Figure 2. Figure 3a1 indicated that in the initial elastic region (Region I), microcracking in the lamellae occurred (deformation = 1%). These microcracks initiated in the lamellae, and did not grow to become

macrocracks. Instead they formed a process zone which decreased the stress concentration ahead of the crack tips. The presence of the microcracks is believed to dissipate the crack energy in flaws below the critical size for failure, thereby enhancing the toughness [17]. This toughening mechanism has the added benefit that strength need not be reduced substantially, and has been reported to be of importance in toughening bone and nacre [1, 2].

With an increase in the load (Region I; deformation = 4%), major cracks in the scaffolds were tilted and twisted out of the crack plane, leading to crack deflection (Figure 3 b1 and b2). Crack deflection enhanced the toughness by providing the initial barriers to crack propagation, and by changing the crack angle from the optimum 90º condition. This mechanism is reported to contribute over 50% to the overall toughness of bone [19].

The propagation of large cracks through the HA lamellae (Figure 3 c1 and c2) were observed as the load increased to around the maximum value (Region II; deformation = 6%). The SEM image showed a highly tortuous path, which provided a large increase in the crack path. This type of tortuous fracture mode has been proposed as an effective toughening mechanism in biological materials [1].

Figure 4 d1 shows the microstructure of the HA constructs after the testing into Region III (deformation = 15%). In addition to the propagation of large cracks through the lamellae, sliding of the lamellae was also observed. As bridges were observed between the adjacent lamellae (Figure 1 b, d), the breaking of these bridges also provided an effective toughening mechanism. This type of ceramic bridging between the mineral

layers has been observed in nacre and was reported to play a key role in the mechanical performance of nacre [2].

4. CONCLUSIONS

Hydroxyapatite scaffolds with an oriented microstructure of lamellar-type pores, fabricated by a unidirectional freeze casting technique, showed an “elastic-plastic” mechanical response with a high strain for failure (>20%) in compression parallel to the freezing direction. Scanning electron microscopy observation of the scaffolds deformed to different strains indicated that several mechanisms, including microcracking, crack deflection, tortuous crack path, lamellar sliding, and ceramic bridges between the lamellae, might contribute to the enhanced toughness of the scaffolds. The results may provide a guide to the design of scaffold materials for applications in the repair of load-bearing bones.

REFERENCES

1. Meyers MA, Chen PY, Lin AYM, Seki Y. Biological materials: structure and mechanical properties. Prog Mater Sci 2008;53:1-206
2. Song F, Soh AK, Bai YL. Structural and mechanical properties of the organic matrix layers of nacre. Biomaterials 2003;24:3623-31
3. Launey ME, Ritchie RO. On the fracture toughness of advanced materials. Adv Mater 2009;21:2103-10
4. Fantner GE, Hassenkam T, Kindt JH, Weaver JC, Birkedal H, Pechenik L, Cutroni JA, Hansma PK. Sacrificial bonds and hidden length dissipate energy as mineralized fibrils separate during bone fracture. Nat Mater 2005;4:612-6
5. Vashishth D, Tanner TE, Bonfield W. Experimental validation of a microcracking-based toughening mechanism for cortical bone. J Biomech 2003;36:121-4
6. Peterlik H, Roschger P, Klaushofer K, Fratzl P. From brittle to ductile fracture of bone. Nat Mater 2006;5:52-55.
7. Nalla RK, Kruzic JJ, Kinney JH, Ritchie RO. Mechanistic aspects of fracture and R-curve behavior in human cortical bone. Biomaterials 2005;26:217-31
8. Wegst UGK, Ashby MF. The mechanical efficiency of natural materials. Phil Mag 2004;84:2167-81
9. Jeronimidis G. The fracture behaviour of wood and the relations between toughness and morphology. Proc Roy Soc London Biolog Sci 1980;208:447-60
10. Fu Q, Rahaman MN, Dogan F, Bal BS. Freeze casting of porous hydroxyapatite scaffolds - I. Processing and general microstructure. J Biomed Mater Res Part B: Appl Biomater 2008;86B: 125–35.
11. Fu Q, Rahaman MN, Dogan F, Bal BS. Freeze casting of porous hydroxyapatite scaffolds - II. Sintering, microstructure, and mechanical properties. J Biomed Mater Res Part B: Appl Biomater 2008;86B:514–22.
12. Fu Q, Rahaman MN, R. F. Brown, and B. S. Bal. Preparation and *In vitro* Evaluation of Bioactive Glass (13-93) Scaffolds with Oriented Microstructures for Repair and Regeneration of Load-Bearing Bones. J. Biomed. Mater. Res. Part A (2009). In press.
13. Carter DR. Bone compressive strength: the influence of density and strain rate. Science 1976;194:1174-6
14. Linde F, Norgaard P, Hvid I, Odgaard A, Soballe, KM. Mechanical properties of trabecular bone. Dependency on strain rate. J Biomech 1991;24:803-9
15. Deville S. Freeze-casting of porous ceramics: a review of current achievements and issues. Adv Eng Mater 2008;10:155-69
16. Menig R, Meyers MH, Meyers MA, Vecchio S. Quasi-static and dynamic mechanical response of haliotis rufescens (abalone) shells. Acta Mater 2000;48:2382-98
17. Faber KT, Evans AG. Crack deflection process I-theory. Acta Metall 1983;31:565-76
18. Wiederhorn SM. Brittle fracture and toughening mechanisms in ceramics. Annu Rev Mater Sci 1984;14:374-403
19. Nalla RK, Kinney JH, Ritchie RO. Mechanistic fracture criteria for the failure of human cortical bone. Nat Mater 2003;2:164-8

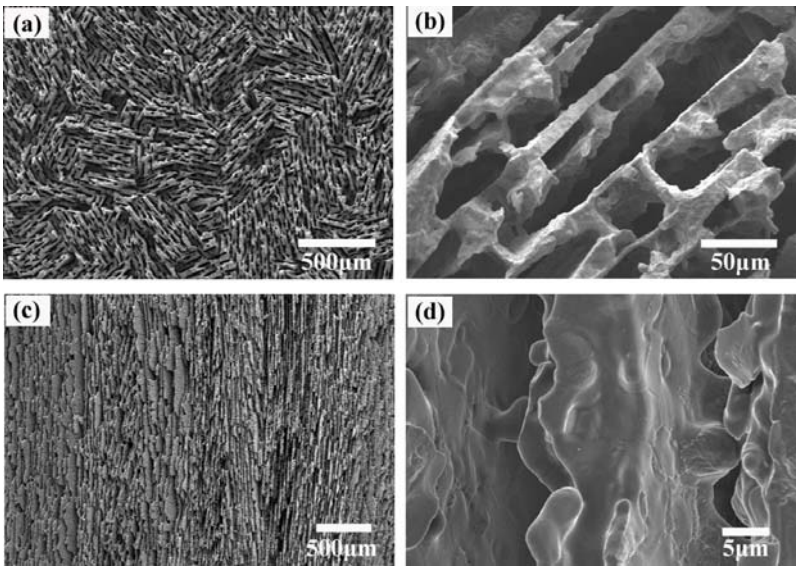

Figure 1. SEM images of the cross sections of HA scaffolds with a lamellar microstructure prepared by unidirectional freezing of suspensions: (a, b) perpendicular, and (c, d) parallel to the freezing direction.

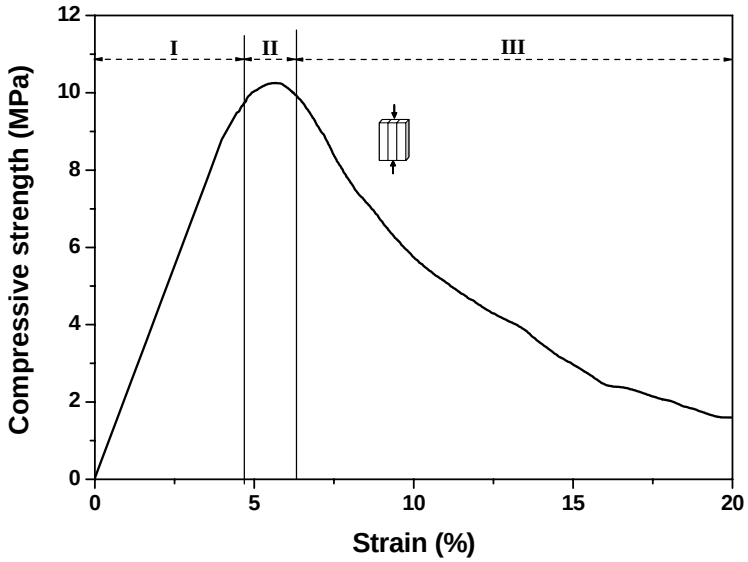

Figure 2. Stress-deformation curve in compression testing parallel to the freezing direction for HA constructs prepared from aqueous suspension (20 vol% particles). Three different regions are outline for the curve: I, elastic region; II, stress plateau region; III, failure region.

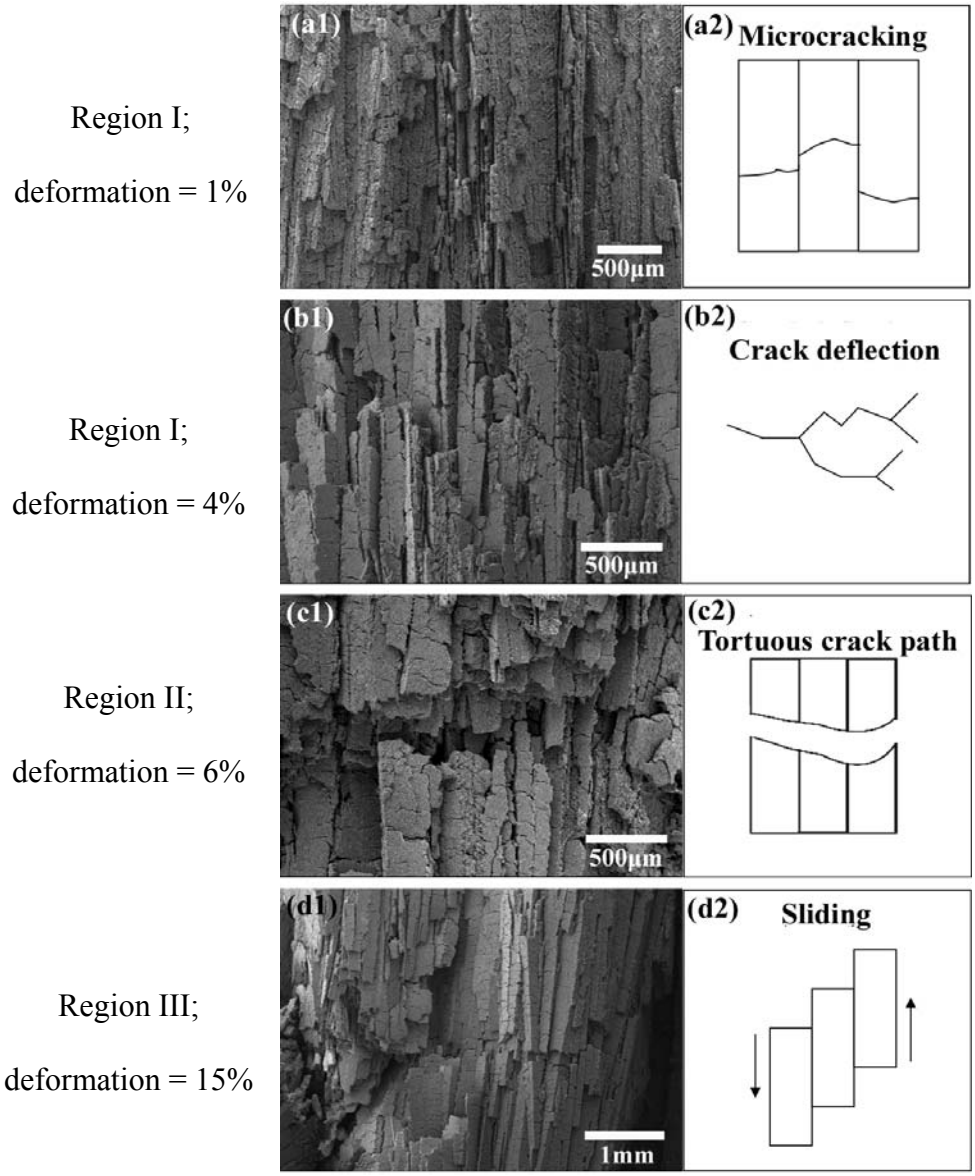

Figure 3. Microstructures (a1–d1) of lamellar-type HA scaffolds after testing in compression (in the direction of freezing) to increasing strains (deformation) shown. (Regions I, II, and III refer to the different regions of the strss vs. deformation curve in Fig, 2). The diagrams on the right illustrate the dominant toughening mechanisms: (a2) microcracking, (b2) crack deflection, (c2) tortuous crack path, and (d2) sliding.

APPENDIX B

PREPARATION AND BIOACTIVE CHARACTERIZATION OF A POROUS 13-93 GLASS, AND FABRICATION INTO THE ARTICULATING SURFACE OF A PROXIMAL TIBIA

B. PREPARATION AND BIOACTIVE CHARACTERIZATION OF A POROUS 13-93 GLASS, AND FABRICATION INTO THE ARTICULATING SURFACE OF A PROXIMAL TIBIA

Qiang Fu[1], Mohamed N. Rahaman[1*], B. Sonny Bal[2], Wenhai Huang[3,4], and Delbert E. Day[1,3]

[1]Department of Materials Science and Engineering, University of Missouri, Rolla, MO 65409

[2]Department of Orthopaedic Surgery, University of Missouri, Columbia, MO 65212

[3]Graduate Center for Materials Research, University of Missouri, Rolla, MO 65409

[4]School of Materials Science and Engineering, Tongji University, Shanghai, 200092, China

ABSTRACT

The silicate-based 45S5 bioactive glass, typically in particulate form, has been widely investigated for bone repair. However, its application as a scaffold for bone tissue engineering is limited due to the difficulty of forming porous three-dimensional constructs with complex shapes. In this study, the use of another silicate-based bioactive glass, referred to as 13-93, was investigated for the preparation of porous constructs. Particles of 13-93 glass (255–325 μm) were consolidated and sintered to form cylindrical constructs. Characterization of these constructs was performed using mercury

* Corresponding author: M. N. Rahaman (rahaman@mst.edu)

porosimetry, scanning electron microscopy (SEM), and mechanical testing. Constructs with porosities of 40–45% and pore sizes in the range 100–300 μm were found to have a compressive strength of 22 ± 1 MPa. The bioactivity of the 13-93 glass was studied by immersing disks in a simulated body fluid at 37°C and characterizing the reaction products. X-ray diffraction, Fourier transform infrared (FTIR) spectroscopy, and SEM showed the formation of a crystalline hydroxyapatite layer on the glass surface after ~7days. The ability to fabricate the complex geometrical shape of the articulating surface of a human tibia from 13-93 glass particles was demonstrated.

Keywords: bioactive glass; biomaterials, scaffold; tissue engineering

1. INTRODUCTION

Tissue engineering, involving the implantation of cells/tissues or stimulating host cells to grow in an implanted scaffold, has emerged as a promising approach for the regeneration of lost or damaged tissues [1,2]. The key components of this approach are a suitable supply of cells, environmental factors such as growth and differentiation supplements, and three-dimensional biomaterial scaffolds that can guide the growth of new tissue *in vitro* and *in vivo* [3-7]. Biomaterial constructs for bone tissue engineering must have a combination of desirable characteristics, such as biocompatibility, sufficient mechanical strength to support physiologic loads, and the ability to be fabricated into anatomically-correct shapes.

Both ceramics and polymers have been used as scaffold materials for bone tissue engineering [8,9]. Polymers such as polylactic acid (PLA), polyglycolic acid (PGA), and

their copolymers (PLGA) are degradable *in vivo*, so the scaffold can be gradually replaced by new bone matrix synthesized by tissue-forming cells [10-13]. The use of degradable polymers such as PLGA in replacing load-bearing bones is limited by their relatively low mechanical strength [8,9]. Attempts have been made to reinforce the degradable polymers to improve their load-bearing properties, but the usefulness of this approach is unclear [14,15].

Bioactive glasses, glass-ceramics, and ceramics have been widely investigated for healing bone defects, because of their ability to enhance bone formation and bond to surrounding tissue [16-19]. Cell seeded bioactive ceramics are also of interest as potential scaffolds for bone tissue engineering. Hydroxyapatite (HA) and tricalcium phosphate (TCP) ceramics, composed of the same ions as bone, are biocompatible and produce no systemic toxicity or immunological reactions. However, stoichiometric HA resorbs slowly or undergoes little conversion to a bone-like material after implantation [20,21]. Many bone regeneration applications require gradual resorption of the implanted biomaterials and their concurrent replacement by the host bone.

The silicate-based 45S5 bioactive glass, referred to as Bioglass® (composition: 45 wt% SiO_2; 24.5 wt% Na_2O; 24.5 wt% CaO; 6 wt% P_2O_5), has been of primary interest for biological applications [16,18,19]. *In vivo* studies have shown that 45S5 glass can stimulate bone regeneration [22-24], whereas *in vitro* studies have shown that the glass itself and the soluble ionic species released by dissolution have osteoinductive properties [25-28]. Porous 45S5 glass scaffolds with simple shapes have been developed [25,29] and cell culture experiments indicate that porous glass can function as a template for generating mineralization *in vitro* [29]. However, the formation of 45S5 glass into porous

constructs with complex, anatomically relevant shapes is limited by the difficulty of sintering the glass particles to form a strong interconnected network.

In the present work, the use of 13-93 bioactive glass for the preparation of porous constructs for bone tissue engineering applications was investigated. The 13-93 glass (composition: 53 wt% SiO_2, 6 wt% Na_2O, 12 wt% K_2O; 5 wt% MgO, 20wt% CaO and 4 wt% P_2O_5) has a silicate-based composition. Previous work has shown that 13-93 glass can be melted and pulled into fibers more easily than 45S5 glass, indicating enhanced viscous flow [30]. The glass has also been shown to support cell growth [31]. The better flow characteristics and the ability to support cell growth warrant further investigation of 13-93 glass as a scaffold material for bone tissue engineering. The objectives of the present work were to investigate the processing conditions for preparing porous constructs of 13-93 glass and to characterize the structure and mechanical properties of the fabricated constructs.

2. MATERIALS AND METHODS

2.1 Preparation of Porous 13-93 Glass Constructs

Glass with the 13-93 composition was prepared by melting a mixture of the appropriate quantities of analytical grade Na_2CO_3, K_2CO_3, $MgCO_3$, $CaCO_3$, SiO_2 and $NaH_2PO_4.2H_2O$ in a platinum crucible at 1300°C and quenching between cold stainless steel plates. The glass was crushed in a hardened steel mortar and pestle and classified using stainless steel sieves to provide particles with sizes in the range of 255–325μm. A slip casting method was used to form the particles into three-dimensional shapes because the process has the capability for producing complex shapes by casting in a

shaped mold [32]. Initially, only simple shapes such as cylinders and disks were required to determine the process variables and to characterize the fabricated material. The suspension for slip casting was prepared by dispersing 85 wt% glass particles in an aqueous solution containing 7.5 wt% poly(vinyl alcohol), PVA. Constructs were formed by casting the suspension into cylindrical cavities in a gypsum mold, followed by drying for ~24 h in air at 60°C.

The construct was heated to burn off the PVA binder, and sintered to join the glass particles together into a three-dimensional network with adequate strength. Since the glass can undergo undesirable crystallization if sintered under unsuitable conditions, experiments were carried out to determine the optimum conditions to bond the particles into a network without causing any measurable crystallization. Differential thermal analysis, DTA (Perkin Elmer DTA7, Perkin Elmer Corp., Norwalk, CT) was used to determine the glass transition temperature (T_g) and the crystallization temperature by heating 40 mg of 13-93 glass particles (<45 μm) at a rate of 10°C/min from 50°C to 1200°C. From a series of experiments, it was found that heating the slip-cast samples at 3°C/min to 550°C (holding time = 30 min), followed by 5°C/min to 700°C (holding time = 15 min), allowed the PVA binder to be burned out completely and sintering to take place without crystallization of the glass.

The ability to use the slip casting process to form porous constructs with anatomically-correct shapes was investigated. A plastic model of the proximal articulating end of a human tibia was used to prepare the shaped cavity in a gypsum mold, into which the suspension of glass particles was cast. The procedure for fabricating the tibial construct was similar to that described above for the cylindrical samples.

2.2 Characterization of Porous 13-93 Glass Constructs

The pore morphologies of the cylindrical constructs were observed using scanning electron microscopy, SEM (Hitachi S-4700), of the surfaces and cross-sections of the constructs. Cross-sections were prepared by infiltrating the construct with an epoxy resin under vacuum, followed by grinding with silicon carbide (SiC) paper and polishing with diamond paste. The porosity and pore size distribution of accessible (open) pores were measured using mercury intrusion porosimetry (Poremaster; Quantachrome, FL) [32]. The compressive strength of cylindrical samples (8 mm in diameter × 16 mm) was measured using an Instron testing machine (Model 4204) at a crosshead speed of 0.5 mm/min. Eight samples were tested, and the average strength and standard deviation were determined.

2.3 Conversion of 13-93 Glass to Hydroxyapatite in SBF

The formation of hydroxyapatite (HA) on the surface of 13-93 glass disks when immersed in a simulated body fluid (SBF) at 37°C was investigated using SEM (Hitachi S-4700), X-ray diffraction, XRD (Rigaku; Model D/mas 2550 v), and Fourier transform infrared reflectance spectroscopy, FT-IRRS (Model 1760-X, Perkin Elmer Corp., Norwalk, CT). Table 1 gives the composition of the SBF [33]. Glass samples with a regular geometry, such as disks, were required to facilitate the characterization of the HA formation, particularly for short reaction times. The disks were formed by casting the molten glass into graphite molds (1 cm in diameter and 2 mm in thickness), followed by annealing for 6 h at 500ºC to relieve thermal stresses. Prior to immersion in the SBF, the

surfaces of the glass disks were prepared by wet grinding with 320-grit SiC paper, followed by dry grinding with 600-grit SiC paper. The samples were then cleaned in ethanol in an ultrasonic bath, and dried in air.

To study the conversion to HA, the glass disks were suspended in sealed polyethylene bottles containing 20 cm^3 of SBF, to give a sample surface area to SBF volume ratio of 0.1 cm^{-1}. After immersion in SBF for various times, the disks were dried in air at room temperature for at least 24 h. Crystalline phases formed on the surface of the glass were detected using thin-film XRD (Cu K_α radiation; $\lambda = 0.15406$ nm) at a scanning rate of 1.8º/min in the 2θ range of 10–80°. The functional groups in the reacted surface layer were analyzed using FT-IRRS in the range of 400 to 2000 cm^{-1}. Following the thin film XRD and FT-IRRS characterization, cross-sections of disks soaked in SBF were prepared and observed in the SEM to characterize the thickness of the HA layer. Prior to observation in the SEM, the disks were mounted in epoxy resin, ground with SiC paper, and polished with diamond paste, using the procedure described earlier.

3. RESULTS AND DISCUSSION

The DTA pattern of the 13-93 glass is shown in Figure 1. Whereas the peaks and troughs are not as clearly identified as in other glasses with simpler compositions, the onset of the glass transition can be assumed to occur at 606°C. There appeared to be two crystallization events, with onset temperatures of 714°C and 851°C, respectively. Since one objective of the fabrication process was to bond the glass particles by viscous flow sintering into a porous construct without any measurable crystallization, the DTA pattern

indicated that the sintering temperature should be chosen between 606°C and 714°C. From preliminary experiments, it was found that sintering for 15 min at 700°C provided adequate strength for subsequent handing without any measurable crystallization of the glass. These sintering conditions were used in subsequent experiments.

Figure 2(a) shows an SEM micrograph of the surface of the porous glass construct after sintering. Joining of the particles at the contact points resulted in the formation of necks (Figure 2(b)), that produced an interconnected network with enhanced strength. A cross-section (Figure 2(c)) shows the network of bonded glass particles and porosity. Mercury porosimetry data (Figure3) showed that the porosity of the sintered constructs, determined from the volume of mercury intruded divided by the total volume of the sample, was 40 ± 2%. By taking the volume intruded for pore radius values between 50 and 150 μm and dividing by the total volume intruded, it was found that ~75% of the interconnected pores had channel diameters between 100 and 300 μm. Similarly, it was found that ~90% of the pores had channel diameters larger than 100 μm. Generally, it has been found that pores larger than ~100 μm are capable of supporting cell ingrowth [34,35]. Thus, the pores in the present constructs appear to have dimensions that are suitable for biomedical scaffolds.

The compressive strength of porous cylindrical samples was 22 ± 1 MPa. This value is significantly higher than the value for cancellous bone (2–12 MPa), but it is also significantly lower than that for cortical bone (100–200 MPa). While the design criteria for scaffolds for bone tissue engineering are unclear, it should be noted that the strength of the present constructs can be enhanced by a greater degree of sintering, at the expense of some reduction in the porosity and average pore size. It is possible that sintering at a

higher temperature or for a longer time could lead to crystallization of the glass. However, the preliminary studies in the present work indicated that sintering for 15 min at 710°C, which is 10°C higher than the temperature used in the experiments reported here, produced more rapid sintering without detectable crystallization. Based on data for 45S5 bioactive glass [36], a limited extent of crystallization would not affect the ability to bond to bone, although the rate of formation of HA would be reduced.

Thin-film XRD patterns for the as-prepared glass and for the glass after soaking in SBF for 1, 7, and 14 days are shown in Figure 4. The as-prepared glass showed the commonly observed band centered ~30° 2θ, which is typical of an amorphous glass. After 1 day in the SBF, the pattern became almost flat. A possible reason for the disappearance of the broad band, previously observed for the as-prepared glass, is the formation of an amorphous product on the surface of the glass. The thin-film technique analyzed the amorphous reaction layer, and not the underlying glass. After 7 days, peaks corresponding to those in a standard hydroxyapatite (HA) were observed. These peaks increased in intensity after 14 days of immersion, but the peak intensities were still well below those for a standard crystalline HA, indicating that the as-formed HA was incompletely crystallized or only weakly crystalline.

The FT-IRRS spectra (Fig. 5) demonstrated that the major resonances associated with crystalline HA, at wavenumbers of 560 and 605 cm^{-1} [37,38], were observed for the glass soaked in SBF for 7 days but not for the as-prepared glass, providing further indication for the formation of an HA layer on the surface of the glass soaked in SBF. The spectrum for the as-prepared glass showed resonances at 1050 and 940 cm^{-1} attributed to the stretching vibration modes of Si bonded to nonbridging O in the glass

network, as well as a resonance at 440 cm^{-1} corresponding to the bending vibration of the Si-O-Si bond. The spectrum for the glass soaked in SBF for 7 days also showed resonances at 1030 and 1243 cm^{-1} corresponding to the phosphate group. There was a resonance at 866 cm^{-1} as well, corresponding to the stretching vibration of CO_3^{2-} function group, which indicated that the as-formed HA had carbonate groups substituted into the structure [39]. The FT-IRRS spectra therefore indicated that the surface of the glass soaked in SBF was coated with a carbonate-substituted hydroxyapatite layer.

Figure 6(a, b) shows SEM micrographs of the cross-sections of the 13-93 glass prior to immersion in SBF and after immersion for 14 days. Micrographs were also obtained for immersion times of 1 day and 7 days but they are omitted for the sake of brevity. The as-formed HA layer in Figure 6(b) suffered from a greater degree of degradation during the sample preparation step (grinding and polishing of the cross-section), which accounted for the rough nature of the layer seen in the micrograph. The thickness of the HA formed after each immersion in SBF was determined from at least 5 SEM micrographs of the cross-section. Figure 7 shows data for the HA thickness versus the immersion time in SBF. Within the limits of experimental error, the growth of the HA layer was linear, increasing at a rate of ~0.4 μm per day. Since the HA product was porous, it might be expected that the diffusion of ions through the liquid in the pores of the HA would be fast, so the reaction at the planar interface between the HA and the glass would be rate-controlling. For an interface reaction-controlled mechanism, a linear increase in the reaction layer thickness would be expected, as indeed observed in Figure **7**.

The mechanism of formation of silicate-based bioactive glasses, such as 45S5 glass, in a dilute phosphate solution, such as an SBF, has been discussed by Hench [17-19]. It is expected that a similar mechanism would operate for the silicate-based 13-93 glass used in the present work because it is based on the 45S5 composition. The present work provided information on the structure and characteristics of the HA formed on the 13-93 glass surface, as well as the rate at which the HA layer formed. Recent data for the conversion of particles of 45S5 glass and 13-93 glass at 37°C in 0.02 M K_2HPO_4 solution with a pH of 7.0 indicated that the formation of HA was slower for the 13-93 glass than for the 45S5 glass [40,41].

Figure 8 shows SEM micrographs of the surface of the glass prior to, and after immersion in the SBF. Except for scratches and grooves resulting from the grinding process, the surface of the glass was flat and featureless (Fig. 8(a)). After 1 day (Fig. 8(b)), the surface of the glass was covered with a reaction layer, shown earlier by thin-film XRD to be amorphous. The reaction layer (but not the underlying glass) contained cracks, typical of capillary-induced drying cracks. After 7 days (Figure 8(c)), the glass surface was covered with a reaction layer on which another layer of precipitates were forming. The reaction layer, shown earlier to consist of a carbonate-substituted HA, also contained typical drying cracks. High-resolution SEM (Figure 8(d)) showed that the precipitates consisted of a porous network of nanoscale crystals, not unlike the rod-like HA crystals in human bone.

The ability to fabricate 13-93 glass particles into a complex shape was demonstrated by using the articulating surface of a proximal human tibia as a model. Figure 9 shows a [1/4] scale model of the tibial surface, measuring ~1.5 in × 1 in, with a

thickness of 0.5 inch. Since the tibial construct was prepared using the same conditions described previously, the structure, mechanical properties, and chemical properties should be almost identical to those described earlier for the cylindrical samples.

The present work demonstrated that 13-93 glass particles can be formed into constructs with the porous structure and complex shape suitable for applications in bone tissue engineering. Future work will examine the *in vitro* interaction with cells and the *in vivo* behavior of the glass constructs.

4. SUMMARY AND CONCLUSIONS

Porous cylindrical constructs of a silicate-based 13-93 glass were prepared using a process involving slip-casting and sintering of particles (255-325 μm). The cylinders had a porosity of 40–45%, with the majority of the pores having sizes in the range of 100–300 μm. The compressive strength of the porous cylinders was 22 ± 1 MPa. Upon immersion in a simulated body fluid at 37°C, a carbonate-substituted hydroxyapatite was detected on the glass surface in less than 7 days, indicating the bioactivity of the glass and the potential for bonding to bone. The rate of formation of the hydroxyapatite layer on the glass was ~0.5 μm per day. The ability to form a porous construct with the shape of a human tibia was demonstrated. The bioactivity of 13-93 glass, coupled with the ability to make porous constructs with anatomically correct dimensions, indicates the suitability of this material for applications in bone tissue engineering.

REFERENCES

1. Nerem RM. Cellular engineering. Ann Biomed Eng 1991; 19:529-545.
2. Langer R, Vacanti JP. Tissue engineering. Science 1993; 260:920-926.
3. Vacanti JP, Langer R. Tissue engineering: the design and fabrication of living replacement devices for surgical reconstruction and transplantation. The Lancet 1999; 354 (Suppl. 1): 32-34.
4. Langer R, Vacanti JP. Tissue engineering: the challenges ahead. Sci Am 1999; 280:86-89.
5. Mooney DJ, Mikos AG. Growing new organs. Sci Am 1999; 280:60-65.
6. Stock UA, Vacanti JP. Tissue engineering: current state and prospects. Annu Rev Med 2001; 52:443-451.
7. Vats A, Tolley NS, Polak JM, Gough JE. Scaffolds and biomaterials for tissue engineering: a review of clinical applications. Clin Otolaryngol 2003; 28:165-172.
8. Goldstein SA, Patil PV, Moalli MR. Perspectives on tissue engineering of bone. Clin Orthop 1999; 357S:S419-S423.
9. Kneser U, Schaefer DJ, Munder B, Klemt C, Andree C, Stark GB. Tissue engineering of bone. Min Invas Ther & Alllied Technol 2002; 11:107-116.
10. Griffith LG. Polymeric biomaterials. Acta Mater 2000; 48:263-277.
11. Agrawal CM, Ray RB. Biodegradable polymer scaffolds for musculoskeletal tissue engineering. J Biomed Mater Res 2001; 55:141-150.
12. Holy CE, Shoichet MS, Davi JE. Engineering three-dimensional bone tissue *in vitro* using biodegradable scaffolds: investigating initial cell-seeding density and culture period. J Biomed Mater Res 2000; 51:376-382.
13. Borden M, El-Almin SF, Attawia M, Laurencin CT. Structural and human cellular assessment of a novel microsphere-based tissue engineered scaffold for bone repair. Biomaterials 2003; 24:597-609.
14. Zhang R, Ma PX. Poly(α-hydroxyl acids)/hydroxyapatite porous composites for bone-tissue engineering. I. Preparation and morphology. J Biomed Mater Res 1999; 44:446-455.
15. Thomson RC, Yaszemski MJ, Powers JM, Mikos AG. Hydroxyapatite fiber-reinforced poly(α-hydroxy ester) foams for bone regeneration. Biomaterials 1998; 19:1935-1943.
16. Hench LL, Wilson J. Surface active biomaterials. Science 1984; 226:630-636.
17. Yamamuro T, Hench LL, Wilson J, eds. Handbook of Bioactive Ceramics. Vols. 1 & 2. Boca Raton (FL), CRC Press, 1990.
18. Hench LL. Bioceramics: from concept to clinic. J Am Ceram Soc 1991; 74:1487-1510.
19. Hench LL. Bioceramics. J Am Ceram Soc 1998; 81:1705-1728.
20. Klein C, Patka P, den Hollander W. Macroporous calcium phosphate bioceramics in dog femora: a histological study of interface and biodegradation. Biomaterials 1989; 10:59-62.
21. Martin RB, Chapman MW, Sharkey NA, Zissimos SL, Bay B, Shors EC. Bone ingrowth and mechanical properties of coralline hydroxyapatite 1 yr after implantation. Biomaterials 1993; 14:341-348.
22. Wheeler DL, Stokes KE, Park HM, Hollinger JO. Evaluation of particulate Bioglass® in a rabbit radius ostectomy model. J Biomed Mater Res 1997; 35:249-254.

23. Wheeler DL, Stokes KE, Hoellrich RG, Chamberland DL, McLoughlin SW. Effect of bioactive glass particle size on osseous regeneration of cancellous defects. J Biomed Mater Res 1998; 41:527-533.
24. Oonishi H, Hench LL, Wilson J, Sugihara F, Tsuji E, Kushitani S, Iwaki H. Comparative bone growth behavior in granules of bioceramic materials of various sizes. J Biomed Mater Res 1999; 44:31-43.
25. Effah Kaufmann EAB, Ducheyne P, Shapiro IM. Evaluation of osteoblast response to porous bioactive glass (45S5) by RT-PCR analysis. Tissue Eng 2000; 6:19-28.
26. Silver IA, Deas J, Erecińska M. Interactions of bioactive glasses with osteoblasts *in vitro*: effects of 45S5 Bioglass®, and 58S and 77S bioactive glasses on metabolism, intracellular ion concentrations and cell viability. Biomaterials 2001; 22:175-185.
27. Xynos ID, Hukkanen MVJ, Batten JJ, Buttery LD, Hench LL, Polak JM. Bioglass® 45S5 stimulates osteoblast turnover and enhances bone formation *in vitro*: implications and applications for bone tissue engineering. Calcif Tissue Int 2000; 67:321-329.
28. Xynos ID, Edgar AJ, Buttery LDK, Hench LL, Polak JM. Gene-expression profiling of human osteoblasts following treatment with the ionic products of Bioglass® 45S5 dissolution. J Biomed Mater Res 2001; 55:151-157.
29. El-Ghannam A, Ducheyne P, Shapiro IM. A bioactive glass template for *in vivo* synthesis of bone. J. Biomed Mater Res 1995; 29:359-370.
30. Paatola T, Pirhonen E, Törmälä P. Coating of bioactive glass (13-93) fibers with bioabsorbable polymer. Key Engineering Materials 2001;192-195:717-720.
31. Brink M, Turunen T, Happonen RP, Yli-Urpo A. Compositional dependence of bioactivity of glasses in the system Na_2O-K_2O-MgO-CaO-B_2O_3-P_2O5-SiO_2. J Biomed Mater Res 1997; 37:114-121
32. Rahaman, MN. Ceramic Processing and Sintering. 2nd ed. Marcel Dekker, New York, 2003.
33. Kokubo T, Kushitani H, Sakka S, Kitsugi T, Yamamuro T. Solutions able to reproduce *in vivo* surface-structure changes in bioactive glass ceramic A-W. J Biomed Mater Res 1990; 24:721-734
34. Freyman TM, Yannas IV, Gibson LJ. Cellular materials as porous scaffolds for tissue engineering. Prog Mater Sci 2001; 46:273-282.
35. Murphy W, Dennis RG, Kileny JL, Mooney DJ. Salt fusion: An approach to improve pore interconnectivity within tissue engineering scaffolds. Tissue Eng 2002; 8:43-52.
36. Hench LL, Paschall HA. Direct chemical bonding between bioactive glass-ceramic materials and bone. J Biomed Mater Res 1973; 4:25-42.
37. Clark AE, Hench LL. Early stages of calcium-phosphate layer formation in bioglass. J Non-Cryst Solids 1989; 113:195-202.
38. Filgueiras MR, LaTorre G, Hench LL. Solution effects on the surface reaction of a bioactive glass. J Biomed Mater Res 1993; 27:445-453.
39. Morgan H, Wilson RM, Elliott JC, Dowker SEP, Anderson P. Preparation and characterization of monoclinic hydroxyapatite and its precipitated carbonate apatite intermediate – a combined IR and XRD Rietveld analysis. Biomaterials 2000; 21:617-627.
40. Huang W, Day DE, Kittiratanapiboon K, Rahaman MN. Kinetics and mechanism of the conversion of silicate (45S5), borate, and boarsilicate glasses to hydroxyapatite in dilute phosphate solutions. J Mater Sci: Mater Med 2006; 17:583-596.

41. Yao A, Wang D, Fu Q, Huang W, Rahaman MN, Day DE. In vitro bioactive characteristics of borate-based glasses with controllable degradation behavior. J Am Ceram Soc 2007. In press.

Table 1. Ion concentration (mM) in SBF and in human blood plasma [31]

Ion	Na^+	K^+	Mg^{2+}	Ca^{2+}	Cl^-	HCO_3^-	HPO_4^{2-}	SO_4^{2-}
SBF	142.0	5.0	1.5	2.5	147.8	4.2	1.0	0.5
Human plasma	142.0	5.0	1.5	2.5	103.0	27.0	1.0	0.5

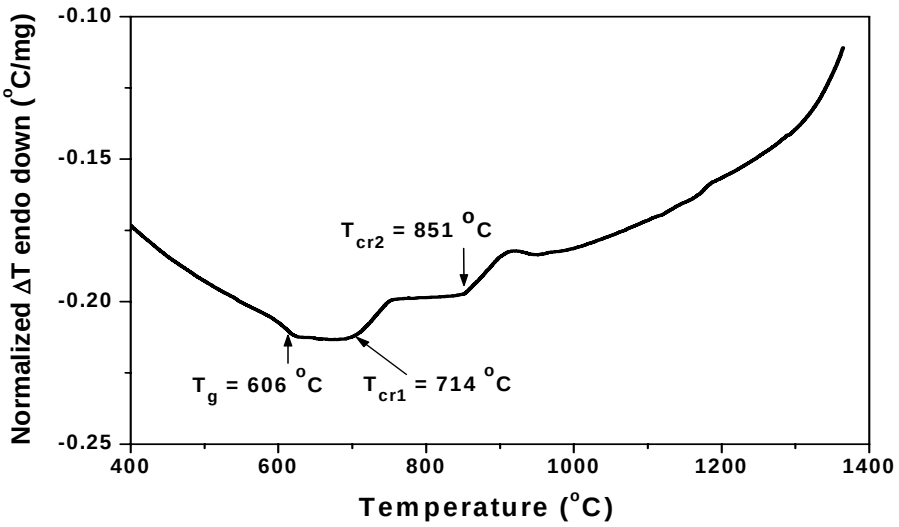

Figure 1. Differential thermal analysis of 13-93 glass, showing the glass transition and crystallization regions.

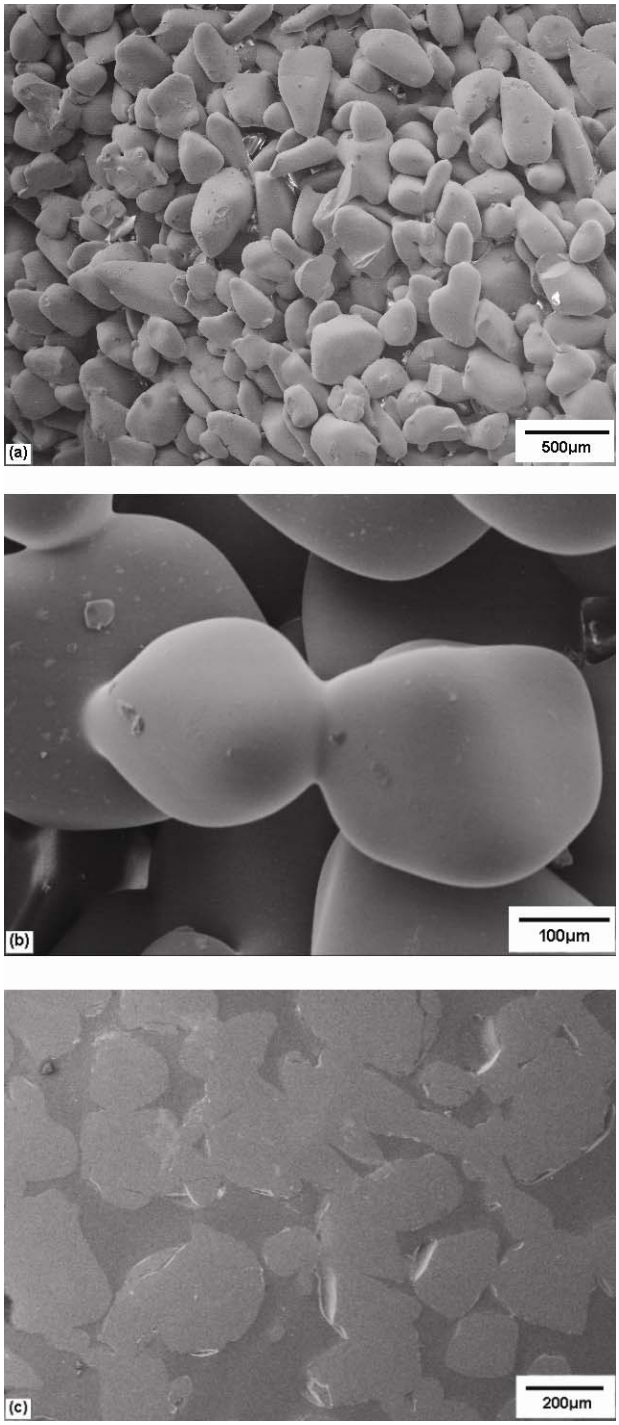

Figure 2. SEM of (a) the surface of a porous glass construct prepared by sintering, (b) the neck region between two particles, showing bonding between the particles, and (c) a cross-section of the construct showing the bonded particles and pores.

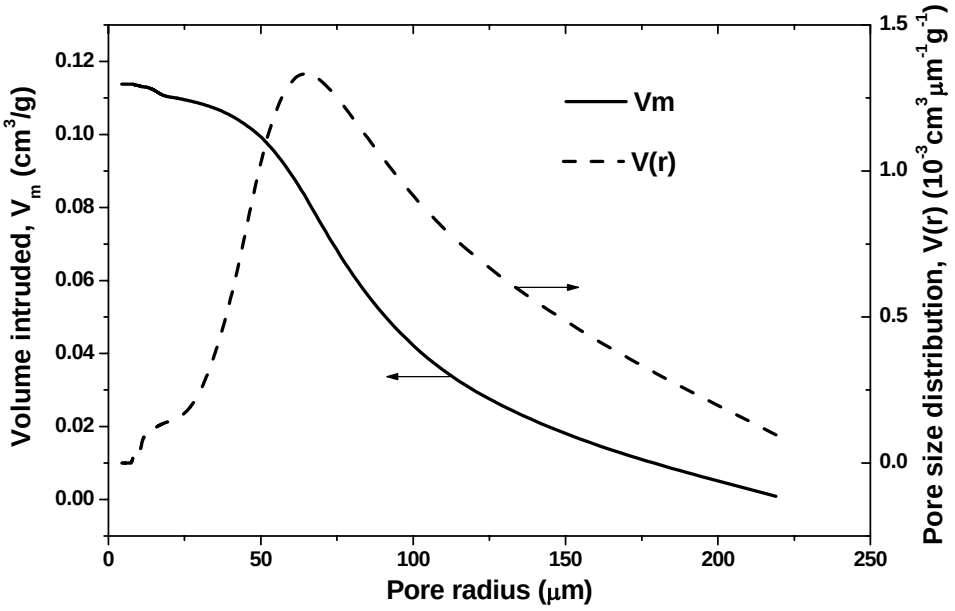

Figure 3. Mercury porosimetry of the fabricated constructs, showing the pore volume and the pore size distribution as functions of the pore radius.

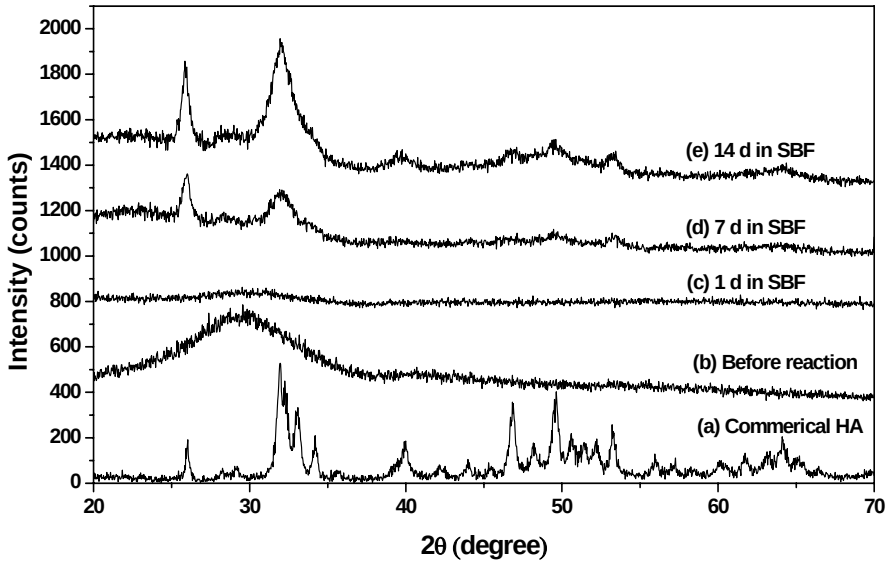

Figure 4. Thin-film XRD of the 13-93 glass, and the glass after immersion in a simulated body fluid at 37°C for various times.

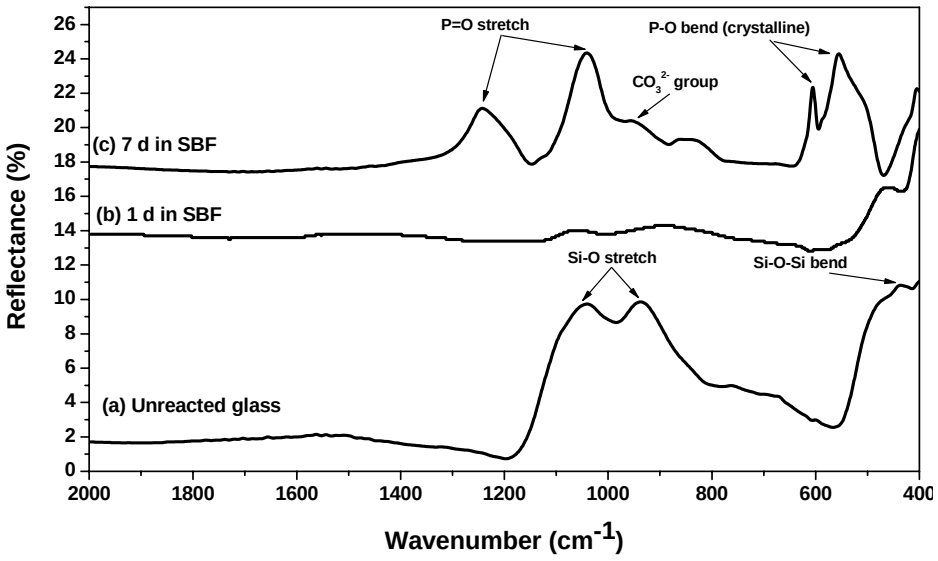

Figure 5. FTIR of the 13-93 glass and the glass after immersion in a simulated body fluid at 37°C for various times.

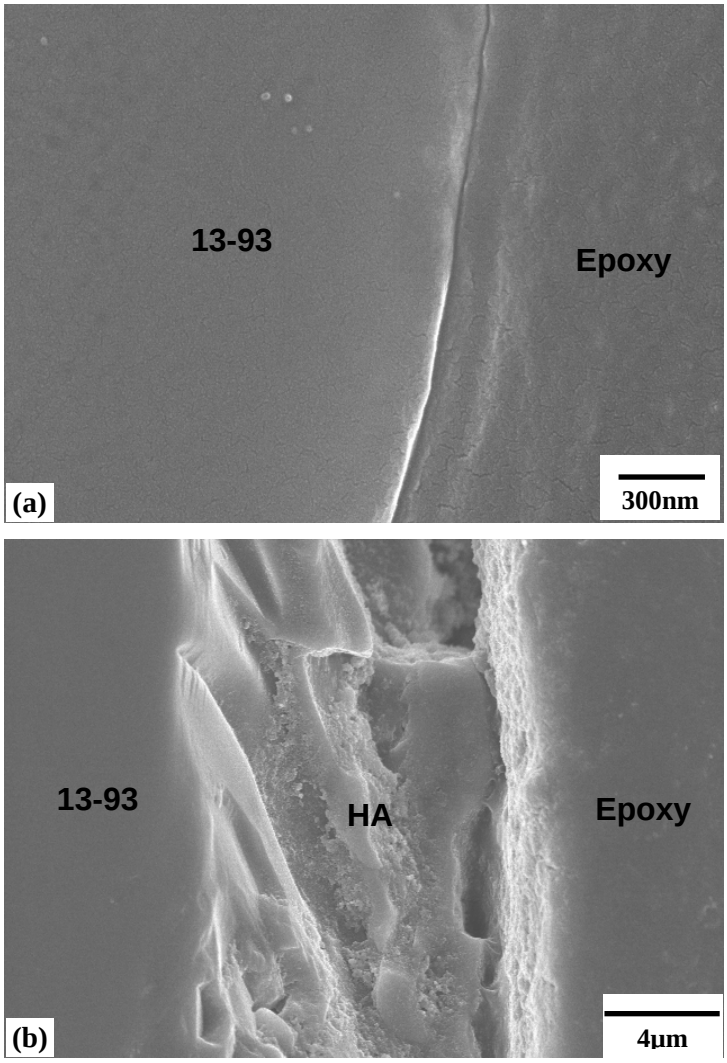

Figure 6. SEM micrographs of the cross-sections of the 13-93 glass (a) prior to immersion, and (b)after immersion for 14 d in a simulated body fluid at 37°C, showing the hydroxyapatite layer.

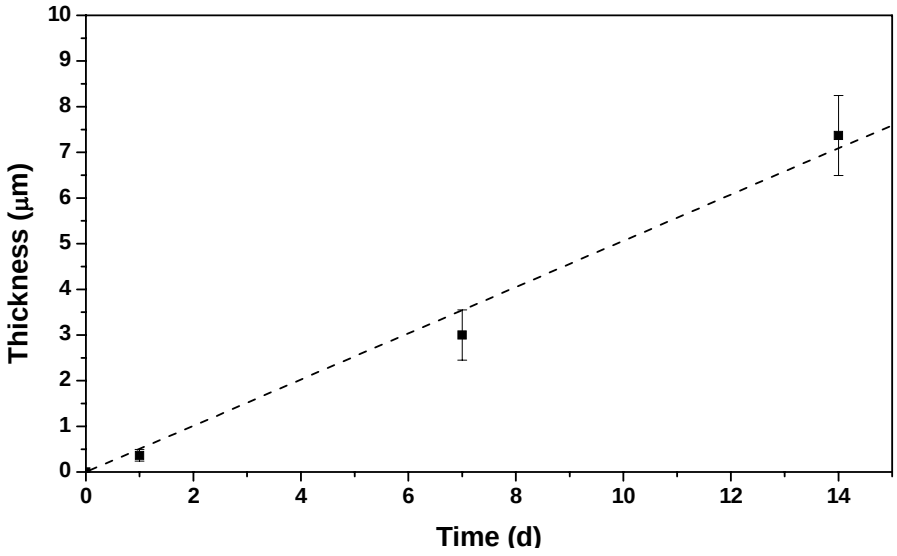

Figure 7. Thickness of the hydroxyapatite layer formed on the 13-93 glass as a function of the immersion time in a simulated body fluid at 37°C. (Linear regression, thickness vs. time: $Y=0.363X$, $r=0.9954$, $p<0.0001$).

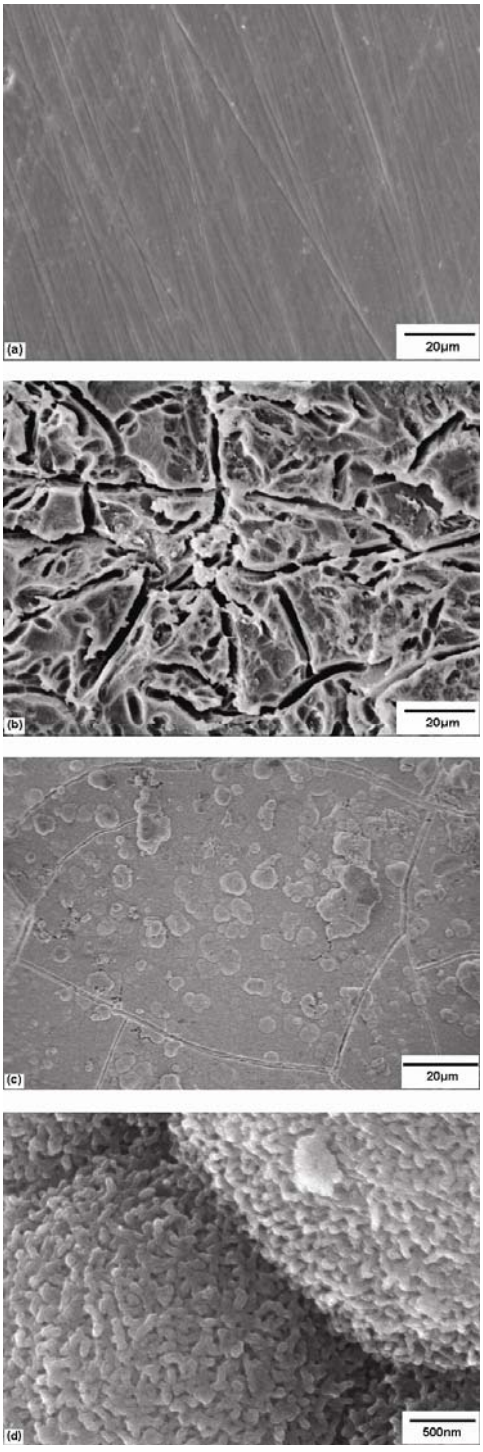

Figure 8. SEM of (a) the surface of 13-93 glass, and the surface after immersing the glass in a simulated body fluid for 1 day (b), and 7 days (c). A high magnification micrograph of the surface (7 days immersion) is shown in (d).

Figure 9. Optical micrograph of a porous construct with the shape of the articulating surface of a human proximal tibia prepared by slip casting and sintering 13-93 glass particles.

APPENDIX C

MECHANICAL AND *IN VITRO* PERFORMANCE OF 13-93 BIOACTIVE GLASS SCAFFOLDS PREPARED BY A POLYMER FOAM REPLICATION TECHNIQUE

C. MECHANICAL AND *IN VITRO* PERFORMANCE OF 13-93 BIOACTIVE GLASS SCAFFOLDS PREPARED BY A POLYMER FOAM REPLICATION TECHNIQUE

Qiang Fu[a], Mohamed N. Rahaman[a*], B. Sony Bal[b], Roger F. Brown[c], Delbert E. Day[a,d]

[a]Department of Materials Science and Engineering, University of Missouri-Rolla, Rolla, MO 65409, USA

[b] Department of Orthopaedic Surgery, University of Missouri-Columbia, Columbia, Missouri 65212, USA

[c]Department of Biological Sciences, University of Missouri-Rolla, Rolla, MO 65409, USA

[d]Graduate Center for Materials Research, University of Missouri-Rolla, Rolla, MO 65409, USA

ABSTRACT

A polymer foam replication technique was used to prepare porous constructs of bioactive 13-93 glass with a microstructure similar to that of human trabecular bone. The constructs, with a porosity of 85 ± 2% and pore size of 100–500 μm, had a compressive strength of 11 ± 1 MPa, approximately equal to the highest value reported for human trabecular bone. The strength was also considerably higher than the values reported for polymeric, bioactive glass-ceramic, and hydroxyapatite constructs prepared by the same

---

* Corresponding author. Tel.: +1 573 341 4406; fax: +1 573 341 6934. E-mail address: rahaman@mst.edu (M.N. Rahaman).

technique and with the equivalent level of porosity. The *in vitro* bioactivity of the fabricated constructs was observed by the conversion of the glass surface to a nanostructured hydroxyapatite layer within 7 days in a simulated body fluid at 37°C. Scanning electron microscopy indicated a continuous increase in cell density on the scaffolds during 6 days of culture. Protein and MTT assays of *in vitro* cell cultures showed excellent ability of the scaffolds to support the attachment and proliferation of MC3T3-E1 pre-osteoblastic cells, both on the surface and in the interior of the porous constructs. Scanning electron microscopy showed cells with a closely adhering, well spread morphology and a continuous increase in cell density on the scaffolds during 6 days of culture. The results indicate that the 13–93 bioactive glass scaffolds could be applied to bone repair and regeneration.

Keywords: scaffold; bioactive glass; cell culture

1. INTRODUCTION

The development of synthetic scaffolds and their processing into structures that have properties tailored for applications in bone repair and regeneration are becoming increasingly important, because of several shortcomings of autografts (limited supply and donor site morbidity) and allografts (immune rejection and possible transmission of pathogens). In addition to being biocompatible, scaffold materials for bone repair and regeneration should have adequate mechanical properties to support physiological loads. Tissue infiltration and facile integration of the scaffold with surrounding tissue are required for ultimate clinical application.

Some synthetic and natural polymers, such as poly(lactic acid) (PLA), poly(glycolic acid) (PGA), copolymers of PLA and PGA, and collagen are biodegradable, so the scaffold can be gradually replaced by new bone matrix synthesized by tissue-forming cells [1–4]. However, the use of degradable polymers for replacing load-bearing bones is often challenging, because of their low mechanical strength [1]. Reinforcement with particles or short fibers of hydroxyapatite (HA) or bioactive glass improves the load-bearing properties of these polymers, and provides scaffolds that are biodegradable as well as bioactive [5–7]. Bioactive glasses, glass–ceramics and ceramics are attractive scaffold materials for bone repair, because of their abilities to enhance bone formation and to bond to surrounding tissue [8,9]. Upon implantation, bioactive glasses gradually convert to HA, the main mineral constituent of bone [9–12], and are osteoconductive as well as osteoinductive [9]. Although brittle, bioactive glass scaffolds can provide higher mechanical strength than the aforementioned polymers [13]. The silicate-based bioactive glass designated 45S5, approved for *in vivo* use in the USA and elsewhere, has been widely investigated for biomedical applications [9]. The 45S5 glass cannot be easily pulled into fibers because of its tendency to devitrify (crystallize). Thermal bonding (sintering) of 45S5 particles into anatomically relevant shapes requires temperatures of ~ 1000 ºC and higher, which leads to devitrification to form a predominantly combeite crystalline phase ($Na_2O \cdot 2CaO \cdot 3SiO_2$). While devitrification does not inhibit the ability to form an HA surface layer, the rate of conversion to HA (the bioactive potential) is reduced [14,15].

Another silicate-based bioactive glass, designated 13–93, with a modified 45S5 composition [16,17], has more facile viscous flow behavior and less tendency to

crystallize than 45S5. The 13–93 glass is approved for *in vivo* use in Europe. The glass can be pulled into fibers, and particles or short fibers have been sintered, without devitrification, to form porous scaffolds with anatomically relevant shapes, such as the human proximal tibia [13]. Porous scaffolds consisting of 13–93 fiber rafts supported the *in vitro* growth and differentiation of MC3T3-E1 preosteoblastic cells [18]. Quantitative measurement of DNA showed no significant difference in cell proliferation between dense disks of 45S5 and 13–93 glass [18]. Several techniques have been employed to produce porous three-dimensional scaffolds of polymers and bioactive ceramics. These methods include thermally induced phase separation (TIPS) [19,20], solid freeform fabrication [21,22], solvent casting and particle leaching [23,24], freezecasting [25–28] and polymer foam replication [15,29–32]. Interconnected pores with a mean diameter (or width) of 100 μm or greater and open porosity of >50% are generally considered to be the minimum requirements to permit tissue ingrowth and function in porous scaffolds [33,34].

Using a foam with the appropriate architecture, scaffolds with a microstructure approximating trabecular bone can be prepared by the polymer foam infiltration technique [35]. In this technique, a polymer foam is infiltrated with a stable suspension of colloidal particles. After drying, the system is heated to decompose the polymer foam, and sintered at a higher temperature to densify the network of particles. The method has been used to prepare porous scaffolds of 45S5 glass–ceramic [15], HA [29,30], biphasic calcium phosphate [31] and akermanite [32]. The strength of the construct is critically dependent on the ability to achieve a solid network with high density. This is dependent on the particle packing of the infiltrated foam, which, in turn, is dependent on the colloid

stability of the suspension used to infiltrate the foam. Generally, a stable suspension leads to a more homogeneous and higher particle packing density in the infiltrated foam, which leads to more facile densification of the particulate network.

Based on the aforementioned forming characteristics and bioactivity of 13–93 glass, coupled with the ability of the polymer foam infiltration technique to produce a bone-like microstructure, an investigation of the mechanical and *in vitro* performance of 13–93 glass scaffolds prepared by this technique was undertaken. The microstructure and compressive mechanical properties of the fabricated scaffolds were characterized, and the ability of the constructs to support the attachment and growth of osteoblastic cells was evaluated. The mouse MC3T3-E1 cell line chosen for these experiments has been used extensively in previous *in vitro* investigations of biomaterials for bone repair and tissue engineering [36,37].

2. MATERIALS AND METHODS

2.1 Preparation of 13-93 Glass Scaffolds

Glass with the 13–93 composition (wt.%) (53SiO_2, 6Na_2O, 12K_2O, 5MgO, CaO, 4P_2O_5) was prepared by melting a mixture of analytical grade Na_2CO_3, K_2CO_3, $MgCO_3$, $CaCO_3$, SiO_2 and $NaH_2PO_4 \cdot 2H_2O$ (Fisher Scientific, St. Louis, MO) in a platinum crucible at 1300 ºC and quenching between stainless steel plates. The glass was crushed in a hardened steel mortar and pestle and classified using stainless steel sieves to provide particles of size <150 μm. These particles were further ground for 2 h in an attrition mill (Model 01-HD, Union Process, Akron, OH), using high-purity Y_2O_3-stabilized ZrO_2 milling media and ethanol as the solvent, to provide particles in the colloidal size range

(<5–10 μm). The average size and size distribution of the particles were measured using a laser diffraction particle size analyzer (Model LS 13 320; Beckman Coulter Inc., Fullerton, CA).

The colloidal properties of the 13–93 glass particles and the ability of different dispersants to stabilize the particles in water were investigated in order to prepare stable suspensions for use in the polymer foam replication technique. Preliminary experiments were performed to test the sedimentation behavior of suspensions (5 vol.% particles) stabilized with 0.25–2 wt.% of five different dispersants (based on the dry mass of the particles). The dispersants were ammonium polymethacrylate (Darvan C; mol. wt. = 10,000–16,000; R.T. Vanderbilt Co., Norwalk, CT), sodium polyacrylate (Darvan 811, mol. wt. = 5000; R.T. Vanderbilt Co.), poly(methylvinyl ether) (EasySperse; ISP, Wayne, NJ), Dynol 604 (Air Products & Chemicals Inc., Allentown, PA) and Targon 1128 (BK Ladenburg GmbH, Ladenburg, Germany). The suspensions were poured to a height of ~ 5 cm into test tubes (~ 3 cm in diameter × 6.5 cm) and, after vigorous shaking, allowed to settle for 24 h. The suspensions stabilized with Dynol 604 or Targon 1128 settled almost completely to give loose flocculated sediments, indicating that these two dispersants were ineffective for stabilizing the particles. On the other hand, the suspensions stabilized with EasySperse showed the least sedimentation, whereas Darvan C or Darvan 811 produced sedimentation results that were intermediate between those for EasySperse and Dynol 604 (or Targon 1128). Because of their ineffectiveness, Dynol 604 and Targon 1128 were not used in subsequent experiments.

The zeta-potential of the particles in an aqueous medium, with or without the presence of Darvan C, Darvan 811 or EasySperse, was measured as a function of the pH

of the aqueous medium using electrophoresis (Zeta-meter 3.0, Zeta-Meter Inc., NY). At each pH value, the zeta-potential was measured at least 10 times, and the results were determined as a mean ± standard deviation. To determine the concentration of dispersant for optimum stability, the viscosity of the suspension (35 vol.% particles) was measured as a function of the dispersant concentration using a rotating cylinder viscometer (VT500; Haake Inc., Paramus, NJ).

Aqueous suspensions containing 20–50 vol.% glass particles, 0.5 wt.% Easysperse as dispersant and 1 wt.% poly (vinyl alcohol) (PVA; DuPont Elvanol® 90–50) as binder were prepared by ball milling for 24 h in polypropylene bottles using Al_2O_3 as the milling media. (The concentrations of the dispersant and binder were based on the dry mass of glass powder used.) The viscosity of the suspensions vs. particle concentration was measured using a rotating cylinder viscometer (Haake VT500).

Based on the zeta-potential and viscosity data, an aqueous slurry containing 35 vol% glass particles, 0.5 wt% Easysperse as dispersant, and 1 wt% poly(vinyl alcohol), PVA, (DuPont Elvanol® 90-50) as binder, was prepared and used in subsequent experiments for preparation of the constructs. (The concentrations of the dispersant and binder were based on the dry mass of glass powder used.) The suspension, in polypropylene bottles and with Al_2O_3 as the milling media, was milled for 24 h in a ball mill to provide a homogeneous slurry.

Four commercial polymer foams were examined in a scanning electron microscope (Hitachi S-4700) and the structure of each foam was compared with that of human trabecular (or cancellous) bone. On the basis of these observations, a polyurethane foam with a structure close to that of trabecular bone was selected for the present

experiments. Scaffold was prepared by infiltrating the particulate slurry (35 vol.% particles) into a polyurethane foam (9mm in diameter × 20mm thick), so that the walls of the foam were coated with the slurry. Excess slurry was squeezed out of the foam. In the infiltration step, the immersed foam was compressed and released several times to let the slurry adhere to the walls of the polymer network. The as-coated foam was dried at room temperature for 24 h, and then subjected to a controlled heating schedule to first decompose the polymer phase, and then densify the network of glass particles. The sample was heated at 1°C/min to 500°C in flowing O_2 gas to decompose the foam, then at 5°C/min to 700°C, and kept at this temperature for 1 h to densify the glass network and form a porous, cylindrical glass construct without crystallizing the glass. A diamond-coated wafering blade was used to section the porous glass cylinder to disk-shaped scaffolds (6mm in diameter ×2mm thick) for use in the cell culture experiments.

2.2 Characterization of 13-93 Glass Scaffolds

To assess the crystallinity of the 13–93 glass after sintering, scaffolds were ground into a powder (particle size <45 μm) and analyzed using X-ray diffraction (XRD; Rigaku, Model D/mas 2550 v) in a step-scan mode (0.05º 2θ and 2 s per step; Cu Kα radiation; λ = 0.15406 nm). For comparison, the powder of a sample of dry human trabecular bone was also analyzed using XRD. Samples of the 13–93 glass constructs and a section of dry human bone were sputter-coated with Au/Pd and examined in a scanning electron microscope (SEM; Hitachi S-4700) to compare the pore morphology of the scaffolds with that of human trabecular bone. The open porosity of the samples was measured using the Archimedes method. Pore size distribution of the accessible (open)

pores was measured using mercury intrusion porosimetry (Poremaster; Quantachrome, FL) [38]. The compressive strength of cylindrical samples (6 mm in diameter × 12 mm long) was measured using an Instron testing machine (Model 4881; Instron Co., Norwood, MA) at a crosshead speed of 0.5 mm min^{-1}. Eight samples were tested, and the mean strength and standard deviation were determined.

2.3 Assessment of Scaffold Bioactivity

Porous scaffolds and dense disks of 13–93 glass were immersed in simulated body fluid (SBF) at 37ºC and then analyzed for the formation of a calcium phosphate layer on the glass surfaces as one indication of bioactivity. The composition of the SBF was identical to that described by Kokubo et al. [39]. Cylindrical scaffolds (6 mm in diameter × 2 mm thick) and disks (10 mm in diameter × 2 mm thick) were cleaned with ethanol in an ultrasonic bath, dried in air and placed in sealed polyethylene bottles containing 50 ml of SBF at 37 ± 2 ºC. The SBF was replaced every 24 h. After a given immersion time, the scaffolds and disks were dried for at least 24 h in air at room temperature and observed in the SEM. Crystalline phases formed on the surface of the glass disks were detected using thin-film XRD at a scanning rate of 1.8º/min in the 2h range 10–80º.

2.4 Cell Culture

The established MC3T3-E1 line of mouse pre-osteoblastic cells was obtained from ATCC and cultured in ascorbic acid-free α-MEM medium supplemented with 10% fetal bovine serum plus 100 U/ml penicillin and 100 μg/ml streptomycin sulfate. Prior to

seeding with cells, dry-heat sterilized scaffolds (6 mm in diameter × 2 mm thick) were soaked for 1 h in a 0.01% solution of polylysine (mol. wt. >150,000) to enhance cell adhesion. The pre-treated constructs were blotted dry, rinsed twice with phosphate buffered saline (PBS), placed on a 6 cm diameter Teflon disk, and seeded with 50,000 MC3T3-E1 cells suspended in 35 μl of complete medium. After incubation for 4 h to permit cell attachment, the cell-seeded constructs were transferred to a 24-well plate containing 2 ml of complete medium per well. The control group consisted of the same amount of cell suspension cultured in the wells with 2 ml of complete medium. All cell cultures were performed at 37 ºC in a humidified atmosphere of 5% CO_2, with the medium changed every 2 days.

2.5 MTT Detection of Viable Cells

Some of the cell-seeded scaffolds were laced in 400 μl serum-free medium containing 100 μg of the tetrazoliumTetrazolium salt MTT for the last 4 h to permit visualization of metabolically active cells on and within the porous 13-93 glass constructs. After the incubation, the constructs were briefly rinsed in PBS and blotted dry. Images of the constructs were obtained using a stereomicroscope fitted with a digital camera to qualitatively assess the distribution of purple formazan, a product of mitochondrial reduction of MTT by viable cells. The MTT-labeled scaffolds were frozen at -70 ºC and fractured with a cooled microtome blade, and the fracture cross section visually examined to assess the presence of purple formazan within the interior of the scaffold.

2.6 Cell Morphology

At selected culture intervals glass scaffolds with attached cells were removed, washed twice with warm PBS, and placed in 2.5% glutaraldehyde in PBS. After an overnight soak in glutaraldehyde, fixed samples were washed extensively with PBS, dehydrated with a graded ethyl alcohol series, and then soaked for 10 min in hexamethyldisilazane (HMDS). After a second wash in HMDS, the samples were were allowed to fully evaporate before being sputter-coated with Au/Pd. The samples were observed in an SEM at 5 kV accelerating voltage.

2.7 Quantitative Protein Assay

Total protein in lysates recovered from the cell-seeded scaffolds was measured with a micro-BCA Protein Assay Kit (Piece Biotechnology, Rockford, IL) to assess cell proliferation on the scaffolds. Cells were detached from the glass constructs and the control wells by lysis in 400 µl of 1% Triton solution for 1 h. Aliquots of the released lysate were mixed with 100 µl of micro-BCA working reagent and the resultant mixture incubated at 50ºC for 20 min. Sample absorbance values were measured at 550 nm in a BMG FLUORstar Optima plate reader with bovine serum albumin used as a standard for comparison.

2.8 Statistic Analysis

All biological experiments (4 samples in each group) were run either in duplicate or triplicate. The data are presented as the mean ± standard deviation. Statistical analysis

was performed using Student's t-test. Values were considered to be significantly different when $p<0.05$.

3. RESULTS

3.1 Particle and Suspension Properties

The median particle size (d_{50}) was 2.0 μm, with a standard deviation of the mean = 1.0 μm. Fig. 1 shows data for the zeta-potential of the 13-93 glass particles as a function of the pH of the aqueous suspension, for suspensions containing no dispersant, and for suspensions containing Darvan 811, Darvan C, or EasySperse (1.0 wt% based on the dry mass of the glass particles). The isoelectric point (the pH at which the zeta-potential is zero) was found to be pH ≈ 3.0. When a bioactive glass is immersed in an aqueous solution, ions (such as Na+) dissolve from the glass into the solution at different pH values [9,10], which might be expected to influence the zeta-potential of the glass particles. For silicate 45S5 bioactive glass, Hench [9] showed that the early stages of the dissolution process resulted in the formation of a silica-rich surface layer. Since the 13–93 composition is based on that of 45S5, a similar dissolution mechanism might be expected. Furthermore, the time frame for each zeta-potential measurement was <30 min, so the surface layer might correspond to that of a silicate glass. If additional changes occur, such as the formation of a calcium phosphate material on the surface of the glass particles, then changes in the zeta-potential might be expected at later times.

Both Darvan 811 and Darvan C caused no change in the zeta-potential of the particles, which may be an indication that these two anionic dispersants were not adsorbed (or only weakly adsorbed) on to the particle surfaces. These two anionic

dispersants are highly charged at pH values >4–5, due to a high degree of dissociation [38]. Significant adsorption should result in a marked change in the zeta-potential of the particles, which was not observed. On the other hand, a considerable increase in the magnitude of the zeta-potential occurred with the dispersant EasySperse, indicating that this anionic dispersant was adsorbed onto the particle surfaces. Since the higher zeta-potential was expected to provide enhanced colloidal stability of the suspension by the mechanism of electrosteric stabilization, the data indicated that EasySperse was more effective for dispersing 13–93 glass particles than Darvan C or Darvan 811.

The optimum concentration of EasySperse required to stabilize the glass particles was determined from the data for the viscosity of an aqueous suspension (35 vol% particles) as a function of the dispersant concentration at a constant shear rate (100 s^{-1}). Fig. 2 indicated that 0.5 wt% EasySperse gave the lowest viscosity of the suspension (~220 mPa.s). Henceforth, the aqueous suspensions used in the experiments were stabilized with 0.5 wt% EasySperse.

Fig. 3 shows the relative viscosity (shear rate =100 s^{-1}) of the suspension as a function of glass particle concentration. The data can be fitted by a modified Krieger-Dougherty equation [40, 41]:

$$\eta_r = \left(1 - \frac{\phi}{\phi_m}\right)^{-n} \qquad (1)$$

where η_r, the relative viscosity, is defined as the viscosity of the suspension, η, divided by the viscosity of the solvent (water) η_L, ϕ is the volume fraction of the particles, ϕ_m is the volume fraction of particles at which the viscosity becomes practically infinite, and *n* is a fitting parameter. The maximum solids loading predicted by this model was $\phi_m = 55$

vol%, with $n = 3.4$. The colloid stability and viscosity of the suspension are important parameters for the preparation of scaffolds by the polymer foam replication method. Highly concentrated suspensions (>40 vol.% particles) were difficult to infiltrate homogeneously into the foam, whereas suspensions containing less than ~20 vol.%) resulted in scaffolds that were too weak for handling. A suspension containing 35 vol.% particles was selected to provide a compromise between ease of infiltration and scaffold strength.

3.2 Microstructure of Fabricated 13-93 Glass Scaffolds

Fig. 4a shows that the microstructure of the polyurethane foam used in these experiments was generally similar to that of a sample of dry human trabecular bone (Fig. 4b). The microstructure of a fractured cross-section of the 13–93 glass scaffold (Fig. 4c and d) consisted of a dense network of glass and interconnected cellular pores. In general, the microstructural and morphological features of the scaffold were similar to those of human trabecular bone (Fig. 4b). The solid network (50–100 μm in diameter) of the scaffold appeared to be fully dense, with a smooth surface, and the diameter of the pores was in the range 100–500 lm. At the sintering temperature used, no visible deformation of the overall shape of the scaffold occurred. The porosity of the scaffolds was 85 ± 2%. Mercury intrusion porosimetry (Fig. 5) confirmed the SEM observations that the fabricated glass constructs contained interconnected pores of size ~100–500 μm.

3.3 Mechanical Properties of Fabricated 13-93 Glass Scaffolds

The stress–strain behavior of a fabricated 13-93 glass scaffold in compression is shown in Figure 6. The stresses and strains are the engineering values calculated from the initial cross-sectional area and length. The peaks and valleys in the curve may be related to progressive breaking of the solid particulate network. The response showed linear elastic behavior during the initial compression, followed by a decrease in stress, possibly because of the fracture of some struts in the solid network. As the strain increased, the additional struts were fractured. Finally, the macro-cracks propagated in the scaffold, leading to a decrease in stress to almost zero. The determination of the elastic modulus from compression tests is subject to several sources of error, which can lead to considerable variation. In the present experiments, the modulus determined from the initial linear region of the stress–stain curve was 3.0 ± 0.5 GPa. Taking the compressive strength as the highest stress on the stress–strain curve, the average compressive strength was 11 ± 1 MPa for eight samples tested (porosity = 85 ± 2%)..

3.4 *In vitro* Bioactivity

Fig. 7 shows SEM images of the surface of a 13–93 glass scaffold after immersion in an SBF for 7 days. Compared to the smooth glass surface of the as-fabricated construct (Fig. 4a and b), the treatment in the SBF produced a fine particulate surface layer. High-resolution SEM images (Fig. 7c) showed that the surface consisted of a porous network of nanometer-sized, needle-like crystals.

XRD analysis showed that the as-formed porous glass scaffolds were amorphous (Fig. 8b). The band centered at ~30º 2θ was indicative of an amorphous material. After immersion for 7 days in the SBF, the thin-film XRD pattern of the dense disks (Fig. 7c)

contained peaks corresponding to those of a reference HA(JCPDS 72-1243), indicating the formation of HA on the glass surface. The width of the major peaks may be caused by X-ray line broadening due to nanometer-sized crystals, confirming the presence of the fine, needle-like crystals observed by SEM. The major peaks in thepattern also occurred at approximately the same 2θ values as those for human trabecular bone (Fig. 8d).

3.5 Cell Culture

SEM images in Figure 9 show the morphology of MC3T3-E1 cell growth on the surface of the 13–93 glass scaffolds for 2, 4 and 6 days. The pre-osteoblastic cells visible in these micrographs were elongated and appeared to align along the long axis of the dense struts of the scaffold. The cells were well-spread at all three culture intervals with numerous cytoplastic projections, and they appeared to be well attached to the surface of the constructs (Figure 9(a). The number of cells on the scaffold increased as a function of culture time (Figure 9(b)). A highmagnification image (Figure 9(c)) showed cell growth into pores of size <100 μm, as well as the formation of numerous cell projections, features that indicated firm cell attachment to the surface. After culturing for 6 days, almost the whole surface of the scaffold was covered with cells (Figures 9(d) and 9(e)), and cell spreading on the struts was visible. The cells began to aggregate, and neighboring cells appeared to maintain physical contact with each other by multiple extensions (Figure 9(e)).

Results of the quantitative assay of total protein in cell lysates recovered from the 13–93 glass scaffolds and the control wells after incubations of 2, 4, and 6 days are shown in Figure 10. The amounts of protein recovered from the scaffolds showed a

nearly linear increase in cell proliferation during the 6-day incubation, a finding that complements the progressive increase in cell density seen in the SEM images. Furthermore, the results indicated that the cell proliferation kinetics on the scaffolds were the same as those in the control wells. These data indicated that the MC3T3-E1 cells were able to grow on the 13–93 glass scaffolds at essentially the same rate as they did on the surface of plastic culture vessels.

Photographic images of cell-seeded scaffolds treated with MTT during the last 4 h of incubation are shown in Figure 11. The purple pigment visible on the scaffold was an indication of viable cells, and was the result of mitochondrial reduction of MTT to an insoluble formazan product. The increase in intensity of the purple color with culture time indicated the proliferation of viable, metabolically active cells on the scaffold (Figure 11(a)). The purple formazan visible on the freeze-fracture face of a scaffold cultured for 6 days (Figure 11(b)) indicated the presence of metabolically active cells within the interior of the construct. Furthermore, the uniformly distributed purple formazan on the surface and within the interior of the constructs indicated that the pore network had good interconnectivity.

4. DISCUSSION

The colloid stability of the suspension is critical for achieving homogeneous particle packing in the construct formed by the polymer foam infiltration technique, and therefore for achieving a fully dense solid network during sintering. By optimizing the suspension characteristics and heating schedule, 13–93 glass scaffolds with a porosity of 85 ± 2% and pores of size 100–500 μm were produced. The use of a selected polymer

foam resulted in the production of constructs with a microstructure approximating that of trabecular bone (Figure 4). The compressive strength of the fabricated 13-93 glass constructs (11 ± 1 MPa) was approximately equal to the highest compressive strength reported for trabecular bone (2–12 MPa) [42,43]. The mechanical behavior of cellular solids with open cells has been described by the Gibson and Ashby model [35]. According to the model, the compressive strength scr of brittle cellular foams (ceramic or glass) is given by:

$$\frac{\sigma_{cr}}{\sigma_{fs}} = C_1(\frac{\rho}{\rho_0})^{3/2}\frac{1+(t_i/t)^2}{\sqrt{1-(t_i/t)^2}} = C_1(1-P)^{3/2}\frac{1+(t_i/t)^2}{\sqrt{1-(t_i/t)^2}} \qquad (2)$$

where σ_{cr} is the compressive crushing strength of the brittle foam, σ_{fs} is the modulus of rupture of the struts, C_1 is the constant of proportionality, ρ and ρ_o are the density of the porous cellular material and the fully dense solid, respectively, P is the porosity of the cellular material, t_i/t is the ratio of the box-like central voids and the struts size. The modulus of rupture in bending is the maximum stress at failure. For 13–93 glass fibers with a diameter of 50–100 μm, the tensile strength has been reported as 650 ± 390 MPa [44]. The diameter of the struts in the sintered 13-93 glass scaffolds was in the range 50–100 μm, so the modulus of rupture of the struts was estimated as the tensile strength of the 13–93 glass fibers. For brittle cellular foams, $C_1 = 0.2$ [35]. The struts in the present work were almost fully dense, so $t_i/t = 0$. Based on these values, the compressive strength of the 13–93 glass scaffolds ($P = 0.83$–0.87) was predicted to be 2–15 MPa, which is the same order of magnitude as the measured compressive strength (11 ± 1 MPa).

The measured compressive strength of the 13-93 glass constructs was at least one order of magnitude higher than the values reported for biodegradable polymer scaffolds or

polymer– ceramic composites prepared by the TIPS method or by the gas foaming method [5,20,45,46]. The strength was also considerably higher than the values reported for bioactive glass-ceramic and HA constructs with similar porosity, which were produced by a polymer foam replication technique. Glass-ceramic constructs formed from bioactive 45S5 glass had a compressive strength of 0.3–0.4 MPa (porosity = 89–92%) [15], and constructs formed from a calcium phosphate glass had a compressive strength of 0.8–1.4 MPa [47]. HA constructs had compressive strengths of 0.01–0.2 MPa (porosity = 86%) [29], 0.2 MPa (porosity = 86%) [48], and 0.6–5.0 MPa (porosity =70–77%) [30], while HA constructs coated with apatite–wollastonite (A/W) glass ceramic had a compressive strength of .1 MPa (porosity = 93%) [49]. A higher compressive strength of 17 MPa (porosity = 73%) was obtained for HA constructs prepared by a gas foaming technique [50], whereas a much higher strength (30 ± 8 MPa) was obtained for HA constructs formed by a solid freeform fabrication (or rapid prototyping) technique but the porosity of the constructs was only 35% [51].

When compared to constructs prepared by the polymer foam replication technique, the higher strength achieved in the present work was attributed to two reasons: (1) the homogeneous particle packing in the as-formed constructs, which facilitated the densification of the particulate network during sintering, and (2) the ease of densifying the particulate network during sintering, due to the favorable viscous flow characteristics of 13–93 glass. In comparison, 45S5 glass suffers from limited viscous flow, and the glass crystallizes prior to densification, so full densification of the particulate network of the construct is difficult. In the polymer foam replication technique, decomposition of the polymer results in the formation of triangular voids in the particulate network [52]. In

glass-ceramics and crystalline ceramics such as HA, these triangular voids, much larger than the particle size of the material, are difficult to remove during the sintering stage because of the limited viscous flow or diffusion in these materials. This residual porosity in the solid network of the cellular structure leads to a reduction in strength. The triangular voids in the constructs fabricated in this work were filled by facile viscous flow of the 13–93 glass during sintering, giving a dense solid network with higher strength. The elastic modulus of the fabricated 13–93 glass scaffolds was 3.0 ± 0.5 GPa, approximately equal to the upper limit of values reported for human trabecular bone (0.1–5 GPa) [36]. The elastic modulus of cellular low-density solids is given by [35]:

$$\frac{E}{E_o} = C_2\left(\frac{\rho}{\rho_o}\right)^n = C_2(1-P)^n \qquad (3)$$

where E and E_o, are the elastic modulus of the porous cellular material and the fully dense solid, respectively, C_2 and n are constants that depend on the microstructure, where C_2 includes all geometric constants of proportionality. For cellular structures with a dense solid network, $C_2 = 1$, whereas in the case of a hollow ceramic network with a central void, $C_2 = 0.3$. The constant n has a value in the range $1 < n < 4$, with $n = 2$ for open-cell structures. Microstructural observations (Figure 4) indicated that the fabricated 13-93 constructs can be approximated as an open-cell structure in which the solid network was fully dense. In this case, $C_2 = 1$, and $n = 2$. The elastic modulus of dense silicate glass is 60–80 GPa [53]. Using these values, and the measured porosity of the fabricated glass constructs (P = 0.83–0.87), the elastic modulus E of the porous glass scaffold is predicted to be 1.0–2.3 GPa, which is within a factor of 2 of the measured value (3.0 ± 0.5 GPa). The formation of a biologically active HA layer, which is equivalent chemically and structurally to the main mineral constituent of bone, is a key requirement for developing a

strong interfacial bond between bioactive ceramics and tissues *in vivo* [9]. The formation of an HA surface layer *in vitro* is indicative of a material's bioactive potential *in vivo* [3]. In the present work, the formation of an HA surface layer was observed within 7 days for the 13-93 glass immersed in an SBF (Figure 7). The HA crystals were similar to those of human trabecular bone in terms of size, morphology, and chemical composition. In comparison, the formation of an amorphous calcium phosphate layer on the surface of porous 45S5 glass-ceramic constructs was observed after 28 days in an SBF [15]. More rapid formation of an HA layer is favorable for obtaining early biological fixation of a bioactive implant in bone repair and regeneration.

The MC3T3-E1 cells are a well-characterized mouse pre-ostoblastic cell line, and they have been used widely for *in vitro* cytotoxicity testing of biomaterials [36,37]. The M3T3-E1 cell morphology on the porous 13–93 glass scaffolds in this work was similar to that observed on 45S5 glass discs reported elsewhere [54]. The cells colonized the surfaces of the porous 13-93 glass scaffolds, and aggregated with each other. The cell morphology, coupled with the *in vitro* cell culture data, indicated the ability of the 13–93 glass scaffolds to support the attachment and proliferation of MC3T3-E1 osteoblastic cells, both on the surface and within the interior of the porous constructs (Figures 9 to 11). This, coupled with the favorable pore characteristics, microstructure, *in vitro* bioactivity, and compressive mechanical properties, indicates the potential of the fabricated 13-93 glass constructs for eventual application in bone repair and regeneration. Additional work is presently underway to assess the ability of the 13–93 glass scaffolds to support the production of extracellular matrix and bone mineralization *in vitro*.

5. CONCLUSIONS

Scaffolds of 13–93 bioactive glass, with a porosity of 85 ± 2% and pores of size 100–500 μm, were fabricated with a microstructure similar to that of trabecular bone using a polymer foam replication technique. The constructs had a compressive strength of 11 ± 1 MPa and an elastic modulus of 3.0 ± 0.5 GPa, equal to the highest values reported for human trabecular bone. Upon immersion in a simulated body fluid, a nanostructured hydroxyapatite layer formed on the surface of the porous scaffolds within 7 days, indicating the *in vitro* bioactivity of the scaffolds. *In vitro* cell culture and SEM observations showed that the scaffolds had an excellent ability to support the attachment and subsequent proliferation of MC3T3-E1 pre-osteoblastic cells, both on the surface and in the interior of the constructs. The results suggest that the fabricated 13-93 glass scaffolds could be applied as biological scaffolds for osseous repair and regeneration.

REFERENCES

[1] Goldstein SA, Patil PV, Moalli MR. Perspectives on tissue engineering of bone. Clin Orthop 1999;357S:S419–S423.

[2] Kneser U, Schaefer DJ, Munder B, Klemt C, Andree C, Stark GB. Tissue engineering of bone. Min Invas Ther Alllied Technol 2002;11:107–16.

[3] Griffith LG. Polymeric biomaterials. Acta Mater 2000;48:263–77.

[4] Borden M, El-Almin SF, Attawia M, Laurencin CT. Structural and human cellular assessment of a novel microsphere-based tissue engineered scaffold for bone repair. Biomaterials 2003;24:597–609.

[5] Zhang R, Ma PX. Poly(.-hydroxyl acids)/hydroxyapatite porous composites for bone-tissue engineering. I. Preparation and morphology. J Biomed Mater Res 1999;44:446–55.

[6] Thomson RC, Yaszemski MJ, Powers JM, Mikos AG. Hydroxyapatite fiber-reinforced poly(α-ydroxy ester) foams for bone regeneration. Biomaterials 1998;19:1935–43.

[7] Roether JA, Gough GE, Boccaccini AR, Hench LL, Maquet V, Jerôme R. Novel bioresorbable and bioactive composites based on bioactive glass and polylactide foams for bone tissue engineering. J Mater Sci: Mater Med 2002;13:1207–14.

[8] Hench LL, Wilson J. Surface active biomaterials. Science 1984;226:630–36.

[9] Hench LL. Bioceramics. J Am Ceram Soc 1998;81:1705–28 (1998).

[10] Huang W, Day DE, Kittiratanapiboon K, Rahaman MN. Kinetics and mechanisms of the conversion of silicate (45S5), borate, and borosilicate glasses to hydroxyapatite in dilute phosphate solutions. J Mater Sci: Mater Med 2006;17:583–96.

[11] Huang W, Rahaman MN, Day DE, Li Y. Mechanisms of converting silicate, borate, and borosilicate glasses to hydroxyapatite in dilute phosphate solution. Phys Chem Glasses: Europ J Glass Sci Technol B 2006;47:647–58.

[12] Rahaman MN, Brown RF, Bal BS, Day DE. Bioactive glasses for nonbearing applications in total joint replacement. Semin Arthroplasty 2007;17:102–12.

[13] Fu Q, Rahaman MN, Bal BS, Huang W. Day DE. Preparation and bioactive characteristics of a porous 13–93 glass, and fabrication into the articulating surface of a proximal tibia. J Biomed Mater Res 2007;82A:222–29.

[14] Filho OP, LaTorr GP, Hench LL. Effect of crystallization on apatite-layer formation on bioactive glass 45S5. J Biomed Mater Res 1996;30:509–14.

[15] Chen ZQ, Thompson ID, Boccaccini AR. 45S5 Bioglass®-derived glass–ceramic scaffold for bone tissue engineering. Biomaterials 2006;27:2414–25.

[16] Brink M. The influence of alkali and alkali earths on the working range for bioactive glasses. J Biomed Mater Res 1997;36:109–17.

[17] Brink M, Turunen T, Happonen R, Yli-Urppo A. Compositional dependence of bioactivity of glasses in the system Na2O-K2O-MgO-CaO-B2O3-P2O5-SiO2. J Biomed Mater Res 1997;37:114–21.

[18] Brown RF, Day DE, Day TE, Jung S, Rahaman MN, Fu Q. Growth and differentiation of osteoblastic cells on 13–93 bioactive glass fibers and scaffolds. Acta Biomater 2008;4:387–96.

[19] Maquet V, Boccaccini AR, Pravata L, Notingher I, Jérôme R. Preparation, characterization, and *in vitro* degradation of bioresorbable and bioactive composites based on Bioglass-filled polylactide foams. J Biomed Mater Res A 2003;66A:335–46.

[20] Ma PX, Zhang R. Microtubular architecture of biodegradable polymer scaffolds. J Biomed Mater Res 2001;56:469–77.
[21] Dellinger JG, Cesarano III J, Jamison RD. Robotic deposition of model hydroxyapatite scaffolds with multiple architectures and multiscale porosity for bone tissue engineering. J Biomed Mater Res A 2007;82A:383–394.
[22] Lin CY, Wirtz T, LaMarca F, Hollister SJ. Structural and mechanical evaluations of a topology optimized titanium interbody fusion cage fabricated by selective laser melting process. J Biomed Mater Res A 2007;83A:272–279.
[23] Lu HH, El-Amin SF, Scott KD, Laurencin CT. Three-dimensional, bioactive, biodegradable, polymer-bioactive glass composite scaffolds with improved mechanical properties support collagen synthesis and mineralization of human osteoblast-like cells *in vitro*. J Biomed Mater Res A 2003;64A:465–74.
[24] Kim SS, Ahn KM, Park MS, Lee JH, Choi CY, Kim BS. A poly(lactide-coglycolide)/hydroxyapatite composite scaffold with enhanced osteoconductivity. J Biomed Mater Res A 2007;80A:206–15.
[25] Deville S, Saiz E, Tomsia A. Freeze casting of hydroxyapatite scaffolds for bone tissue engineering. Biomaterials 2006;27:5480–9.
[26] Deville S, Saiz E, Nalla RK, Tomsia A. Freezing as a path to build complex composites. Science 2006;311:515–8.
[27] Fu Q, Rahaman MN, Dogan F, Bal BS. Freeze casting of porous hydroxyapatite scaffolds – I. Processing and general microstructure. J Biomed Mater Res B: Appl Biomater 2008; [in press].
[28] Fu Q, Rahaman MN, Dogan F, Bal BS. Freeze casting of porous hydroxyapatite scaffolds – II. Sintering, microstructure, and mechanical properties. J Biomed Mater Res B: Appl Biomater 2008; [in press].
[29] Callcut S, Knowles JC. Correlation between structure and compressive strength in a reticulate glass-reinforced hydroxyapatite foam. J Mater Sci Mater Med 2002;13:485–9.
[30] Ramay HRR, Zhang M. Preparation of porous hydroxyapatite scaffolds by combination of the gelcasting and polymer sponge methods. Biomaterials 2003;24:3293–302.
[31] Ramay HRR, Zhang M. Biphasic calcium phosphate nanocomposite porous scaffolds for loadbearing bone tissue engineering. Biomaterials 2004;25:5171–80.
[32] Wu C, Chang J, Zhai W, Ni S, Wang J. Porous akermanite scaffolds for bone tissue engineering: preparation, characterization, and *in vitro* studies. J Biomed Mater Res B: Appl Biomater 2006;78B:47–55.
[33] Hulbert SF, Young FA, Mathews RS, Klawitter JJ, Talbert CD, Stelling FH. Potential of ceramic materials as permanently implantable skeletal prostheses. J Biomed Mater Res 1970;4:433–56.
[34] Hollinger JO, Brekke J, Gruskin E, Lee D. Role of bone substitutes. Clin Orthop Relat Res. 1996;324:55–65.
[35] Gibson LJ, Ashby MF. Cellular solids: structure and properties. 2nd ed. Cambridge: Cambridge University Press; 1997.
[36] Foppiano S, Marshall SJ, Marshall GW, Saiz E, Tomsia AP. The influence of novel bioactive glasses on *in vitro* osteoblast behavior. J Biomed Mater Res A 2004;71A:242–249.

[37] Inoue M, LeGeros RZ, Inoue M, Tsujigiwa H, Nagatsuka H. *In vitro* response of osteoblast-like and odontoblast-like cells to unsubstituted and substituted apatites. J Biomed Mate Res A 2004;70A:585–593.
[38] Rahaman, MN. Ceramic Processing. Taylor & Francis/CRC Press, Boca Raton, FL, 2006.
[39] Kokubo T, Kushitani H, Sakka S, Kitsugi T, Yamamuro T. Solutions able to reproduce *in vivo* surface-structure changes in bioactive glass-ceramic A-W. J Biomed Mater Res 1990;24:721–34.
[40] Krieger IM, Dougherty M. A mechanism for non-newtonian flow in suspensions of rigid spheres. Trans Soc Rheol 1959;3:137–52.
[41] Bergström L. Shear thinning and shear thickening of concentrated ceramic suspensions. Colloids Surf A: Physicochem Eng Aspects 1998;133:151–5.
[42] Carter DR, Hayes WC. Bone compressive strength: the influence of density and strain rate. Science 1976;194:1174–6.
[43] Fung YC. Biomechanics: Mechanical Properties of Living Tissues. New York: Springer; 1993.
[44] Pirhonen E, Niirannen H, Niemelä, Brink M, Törmälä P. Manufacturing, mechanical characterization, and *in vitro* performance of bioactive glass 13-93 fibers. J Biomed Mater Res B: Appl Biomat 2006;77B:227–33.
[45] Yang F, Qu X, Cui W, Bei J, Yu F, Lu S, Wang S. Manufacturing and morphology structure of polylactide-type microtubular orientation-structure scaffolds. Biomaterials 2006;27:4923–33.
[46] Cyster LA, Grang DM, Howdle SM, Rose FRAJ, Irvine DJ, Freeman D, Scotchfor CA, Shakesheff KM. The influence of dispersant concentration on the pore morphology of hydroxyapatite ceramics for bone tissue engineering. Biomaterials 2005;26:697–702.
[47] Park Y-S, Kim K-N, Kim K-M, Choi S-H, Kim C-K, Legeros RZ, Lee Y-K. Feasibility of threedimensional macroporous scaffold using calcium phosphate glass and polyurethane sponge. J Mater Sci 2006;41:4357–64.
[48] Kim HW, Knowles JC, Kim HE. Hydroxyapatite porous scaffold engineered with biological polymer hybrid coating for antibiotic vancomycin release. J Mater Sci Mater Med 2005;16:189–95.
[49] Jun I-K, Song J-H, Choi W-Y, Koh Y-H, Kim H-E. Porous hydroxyapatite scaffolds coated with bioactive apatite–wollastonite glass–ceramics. J Am Ceram Soc 2007;90:2703–2708.
[50] Dong J, Kojima H, Uemura T, Kikuchi M, Tateishi T, Tanaka J. *In vivo* evaluation of a novel porous hydroxyapatite to sustain osteogenesis of transplanted bone marrow-derived osteoblastic cells. J Biomed Mater Res 2001;57:208–16.
[51] Chu T-MG, Orton DG, Hollister SJ, Feinberg SE, Halloran JW. Mechanical and *in vivo* performance of hydroxyapatite implants with controlled architectures. Biomaterials 2003;23:1283– 93.
[52] Studart AR, Gonzenbach UT, Tervoort E, Gauckler LJ. Processing routes to macroporous ceramics: a review. J Am Ceram Soc 2006;89:1771–89.
[53] Rouxel T. Elastic properties of glasses: a multiscale approach. C R Mecanique 2006;334:743–53.
[54] Levy S, Dalen MV, Agonafer S, Soboyejo WO. Cell/surface interactions and adhesion on bioactive glass 45S5. J Mater Sci Mater Med 2007;18:89–102.

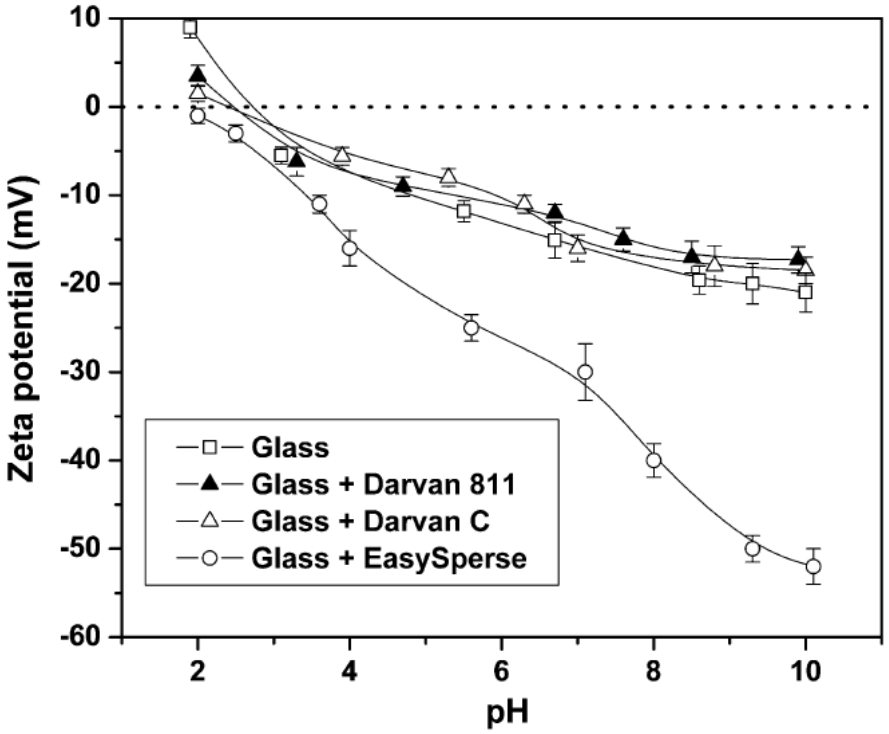

Figure 1. Zeta-potential of 13-93 glass particles versus pH, for suspensions without dispersant, and for suspensions containing 1 wt.% Darvan 811, Darvan C, or EasySperse.

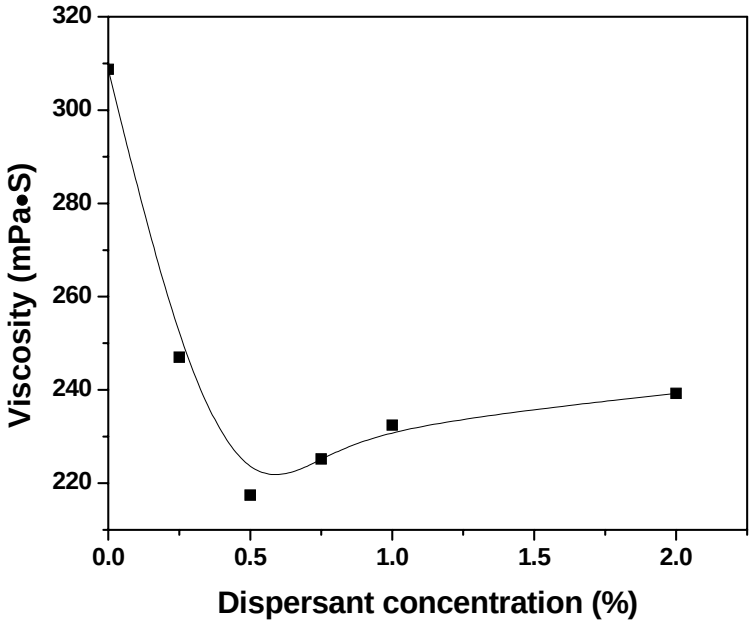

Figure 2. Viscosity of aqueous suspensions containing 35 vol% 13-93 glass particles versus dispersant concentration (shear rate = 100 s^{-1}).

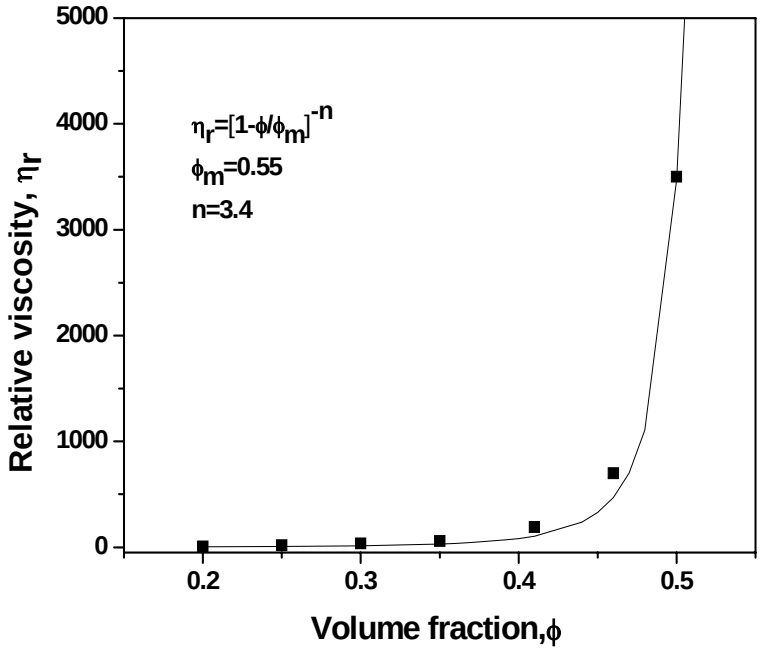

Figure 3. Relative viscosity versus volume fraction of glass particles in aqueous suspensions stabilized with 0.5 wt% EasySperse (shear rate = 100 s^{-1}).

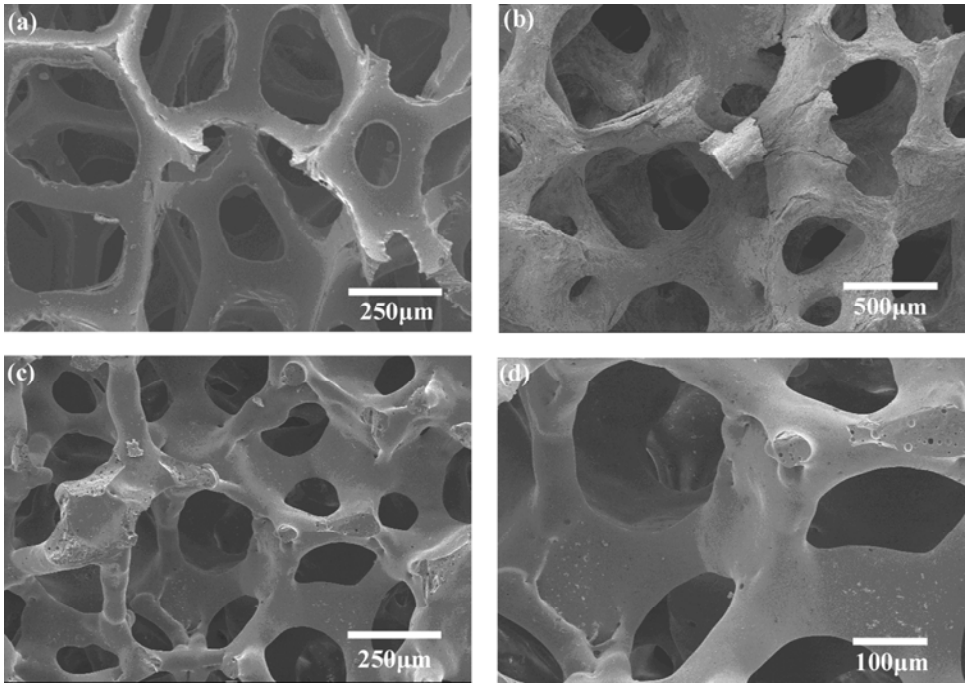

Figure 4. Microstructures of: (a) polyurethane foam used in the experiments; (b) dry human trabecular bone; and (c, d) 13–93 glass scaffolds fabricated by a polymer foam replication technique.

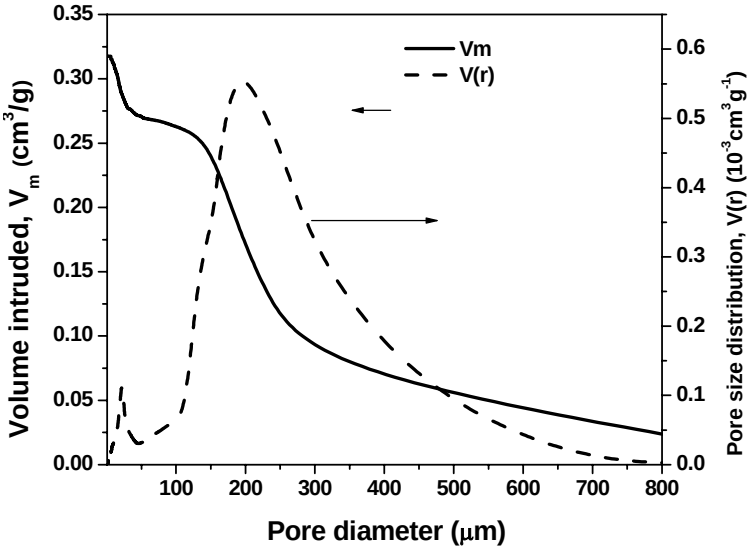

Figure 5. Mercury porosimetry data for the pore volume and pore size distribution versus pore radius, for the fabricated 13-93 glass scaffolds.

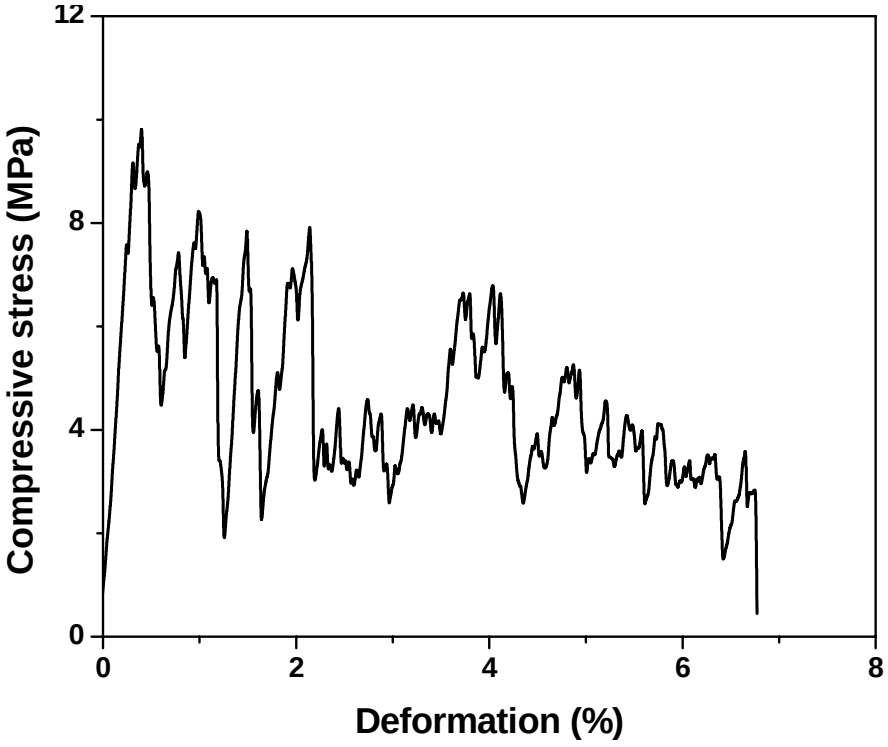

Figure 6. Stress-strain response of porous 13-93 glass constructs in compression.

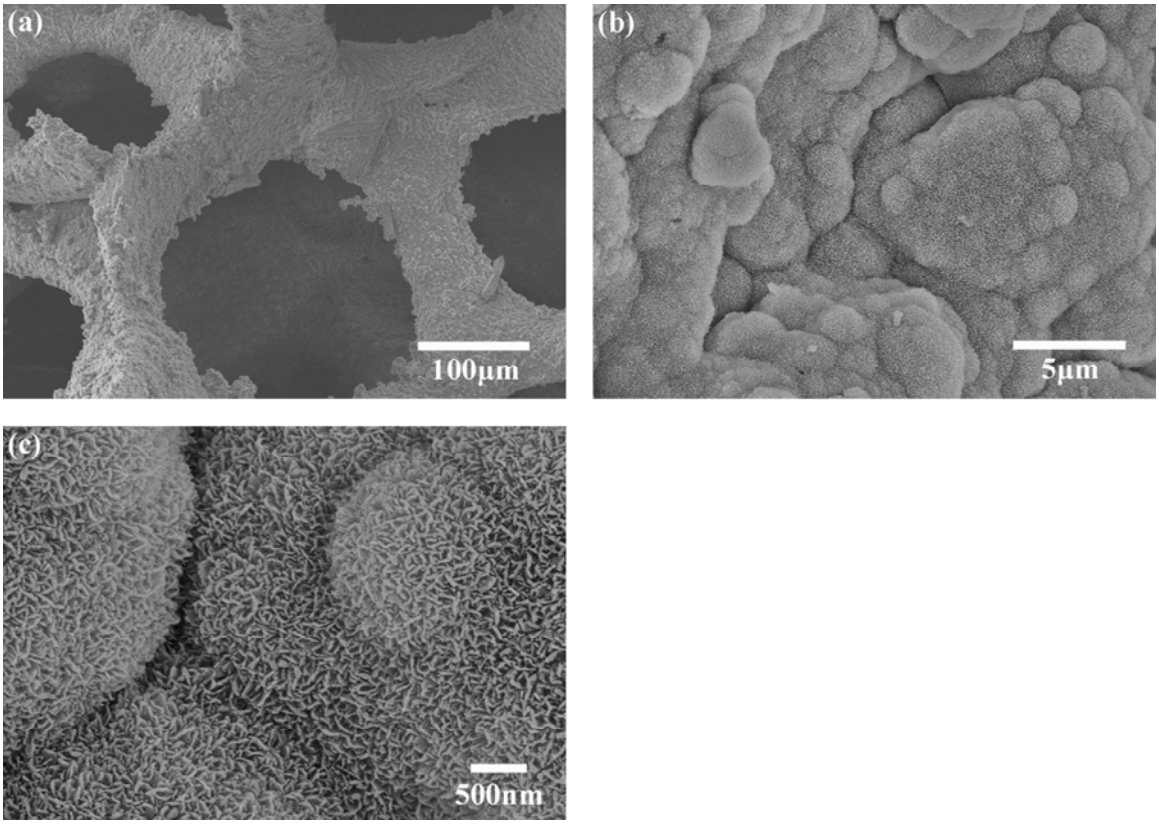

Figure 7. SEM images of the surface of 13-93 glass construct after immersion for 7 days in SBF: (a) lower magnification image; (b, c) higher magnification image showing fine needle-like hydroxyapatite crystals.

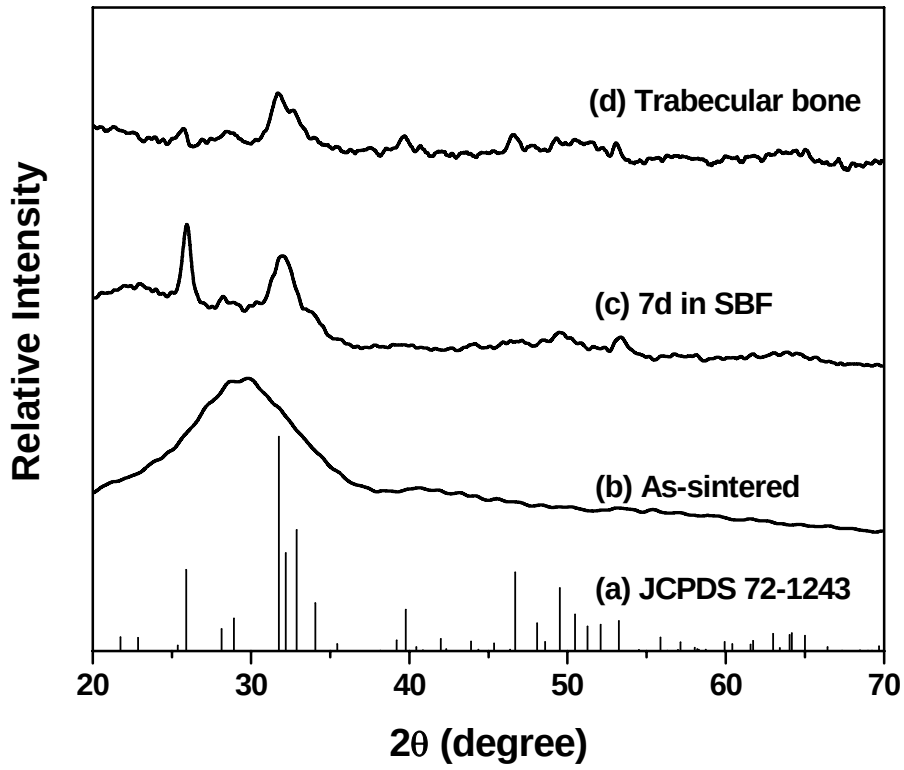

Figure 8. X-ray diffraction patterns of: (a) reference hydroxyapatite (JCPDS 72-1243); (b) porous 13–93 glass scaffold in the as-sintered condition; (c) sintered 13–93 glass scaffold after immersion in a simulated body fluid for 7 days; and (d) human trabecular bone.

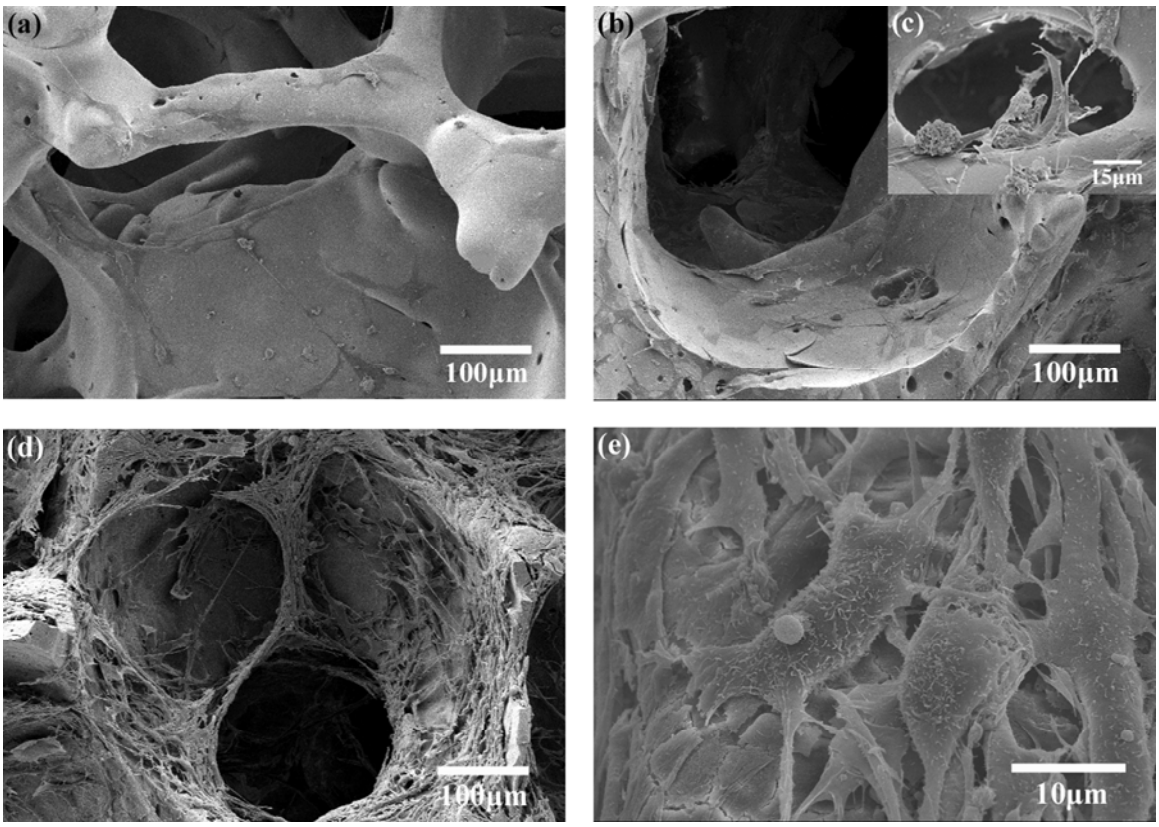

Figure 9. SEM images of 13-93 glass constructs seeded with MC3T3-E1 cells and cultured for (a) 2 days; (b,c) 4 days; (d,e) 6 days.

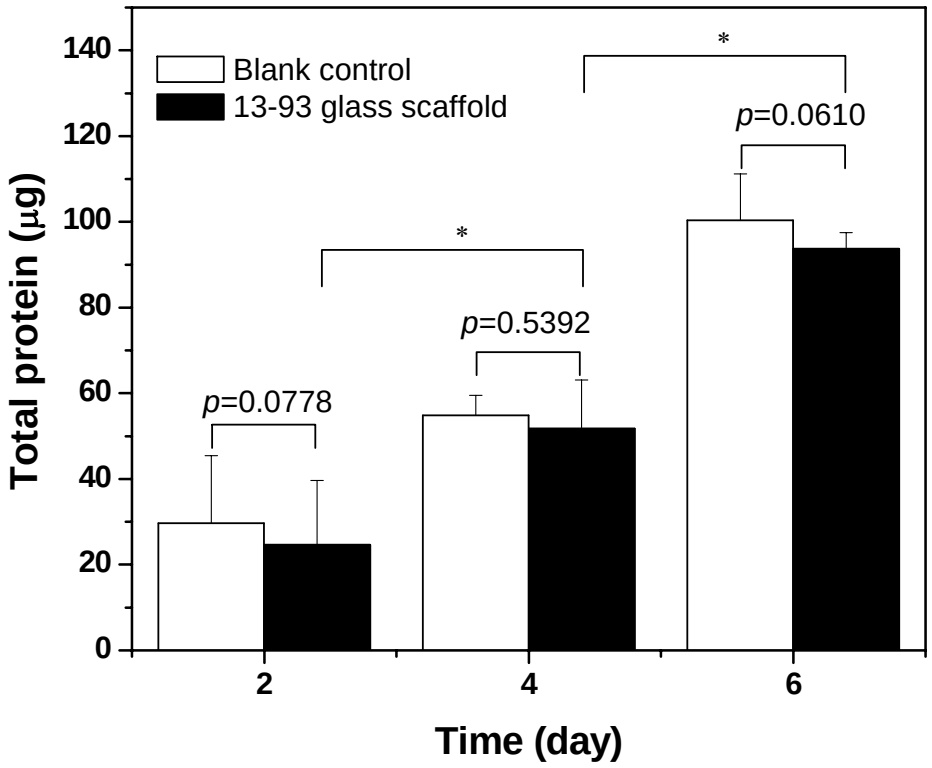

Figure 10. Quantitative measurement of total protein content per scaffold or well in MC3T3-E1 cell cultures incubated for 2, 4, and 6 d on porous 13-93 constructs prepared by the polymer foam replication method, and in control wells. Mean ± sd; n = 4. *Significantly increase in total amount of protein on the porous 13-93 glass constructs with increasing culture duration ($p<0.05$).

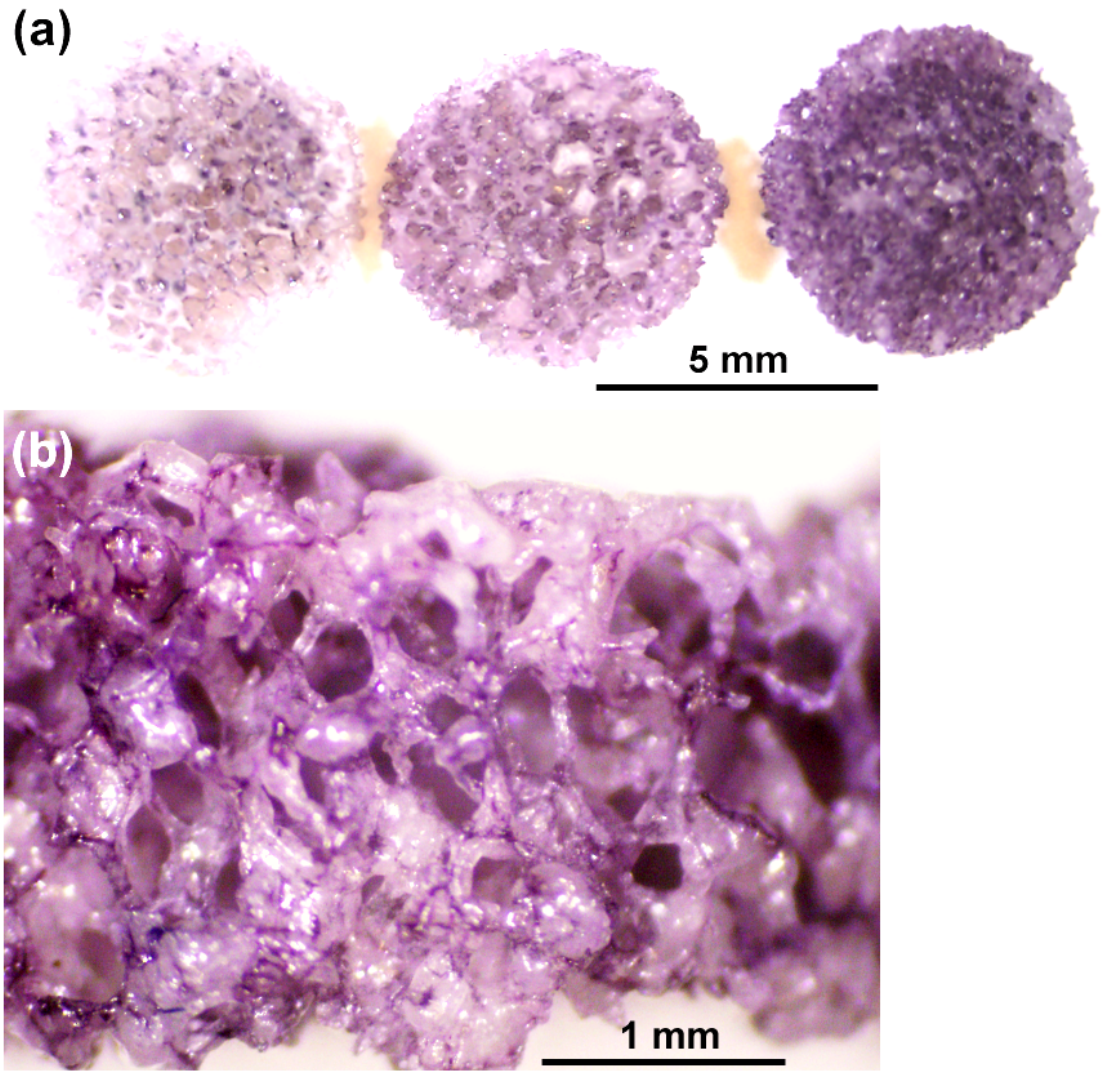

Figure 11. Cell-seeded 13–93 glass scaffolds treated with MTT: (a) surface of scaffolds after culture intervals of 2, 4 and 6 days (left to right, respectively); and (b) freeze-fracture section of scaffold cultured for 6 days, showing clusters of MTT-labeled cells within the interior.

VITA

Qiang Fu was born on January 1, 1980 in Zoucheng, Shandong Province, P.R. China. Until 1997, Qiang resided in Zoucheng and spent most of his spare time working on his family's farms. In September 1997, he started his undergraduate education at Tongji University in Shanghai. By chance, he was chosen into the Materials Science major and he found a lot fun there. After receiving his Bachelor's degree in 2001, Qiang continued his graduate study in Tongji University and got his Master's degree in Materials Science and Engineering in 2004. He then worked as a process engineer in Semiconductor Manufacturing International Corporation (SMIC) in Shanghai and did research on wafer-related defects in photolitho process. He gained invaluable industry work experience in SMIC and spent some happy time there. Driven by his curiosity on the biomedical materials research, Qiang started his doctoral study in Ceramic Engineering in Rolla after working for one year in SMIC.

In August 2005, Qiang started his Ph.D. study under the supervision of Dr. Mohamed N. Rahaman. His doctoral work has led to 20 journal papers, 12 in which he is the first author, and 5 presentations given across the United States. After completion of his Ph.D. requirements, Qiang will continue his work in the biomedical materials area at the Lawrence Berkeley National Laboratory (LBL) at Berkeley, CA, as a postdoctoral fellow in the Materials Science Division.